B 03409-000

THE NIMBUS III USER'S GUIDE

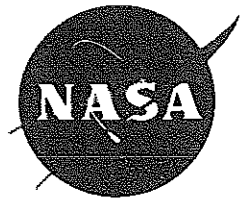

GODDARD SPACE FLIGHT CENTER
GREENBELT, MARYLAND

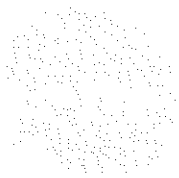

THE NIMBUS III USER'S GUIDE

Prepared by

The NIMBUS Project
Goddard Space Flight Center
National Aeronautics and Space Administration

Edited by

Romeo R. Sabatini
Allied Research Associates, Inc.
Concord, Mass.

TABLE OF CONTENTS

TABLE OF CONTENTS (Continued)

TABLE OF CONTENTS (Continued)

TABLE OF CONTENTS (Continued)

TABLE OF CONTENTS (Continued)

LIST OF FIGURES

LIST OF FIGURES (Continued)

LIST OF FIGURES (Continued)

LIST OF TABLES

LIST OF TABLES (Continued)

THE NIMBUS III USER'S GUIDE

FOREWORD

This document has been prepared to provide potential data users with background information on the Nimbus III Spacecraft System as a basis for selecting, obtaining and utilizing Nimbus III data in research studies.

The basic spacecraft system operation is outlined, followed by a detailed discussion of each of the meteorological experiments. The format, archiving and access to the data are also described. Finally, the contents and format of the Nimbus III Data Catalogs are described. These catalogs will be issued at approximately monthly intervals. They will contain IDCS, HRIR, and MRIR pictorial data obtained during each period as well as information on the collection and availability of all Nimbus III data.

The individual sections on The Meteorological Experiments were prepared by the respective Experimenters. The assembly and editing of this publication was accomplished by the Geophysics and Aerospace Division of Allied Research Associates, Inc. (ARA), Concord, Massachusetts under Contract No. NAS 5-10343 with the Goddard Space Flight Center, NASA, Greenbelt, Maryland.

Harry Press
Nimbus Project Manager
Goddard Space Flight Center

SECTION I

THE NIMBUS III SPACECRAFT SYSTEM

by
Staff Members, Nimbus Project
National Aeronautics and Space Administration
Goddard Space Flight Center

The purpose of this section is to outline the salient features of the Nimbus Spacecraft Systems as they relate to the performance and character of the Nimbus sensory systems.

1.1 The Nimbus III Spacecraft

The Nimbus III spacecraft, Figure 1-1, represents a major upgrading of the Nimbus I and II spacecraft with the following significant differences:

1. An increase in the number of meteorological experiments to seven (from 3 and 4 previously) including 3 new experiments, two of which are directed at atmospheric spectrometric sounding. The complement of experiments is listed in Table 1-1.
2. An expanded data system capable of handling diverse sensor requirements as well as additional storage capability which permits full global coverage.
3. An expanded power supply capability and the addition of a 50 watt Radioisotope Thermoelectric Generator (RTG).

The expansion of both the data system and power supply has provided the desired capability of continuous and concurrent operation of all experiments and the collection of all data on a daily, global basis.

1.2 Orbit

The Nimbus III orbit was selected to satisfy the diverse experiment power and data retrieval requirements. Nimbus III is intended to be placed in an orbit which is circular at 600 nautical miles, sun synchronous, having a local high noon equator crossing, and an 81 degree retrograde inclination. Successive

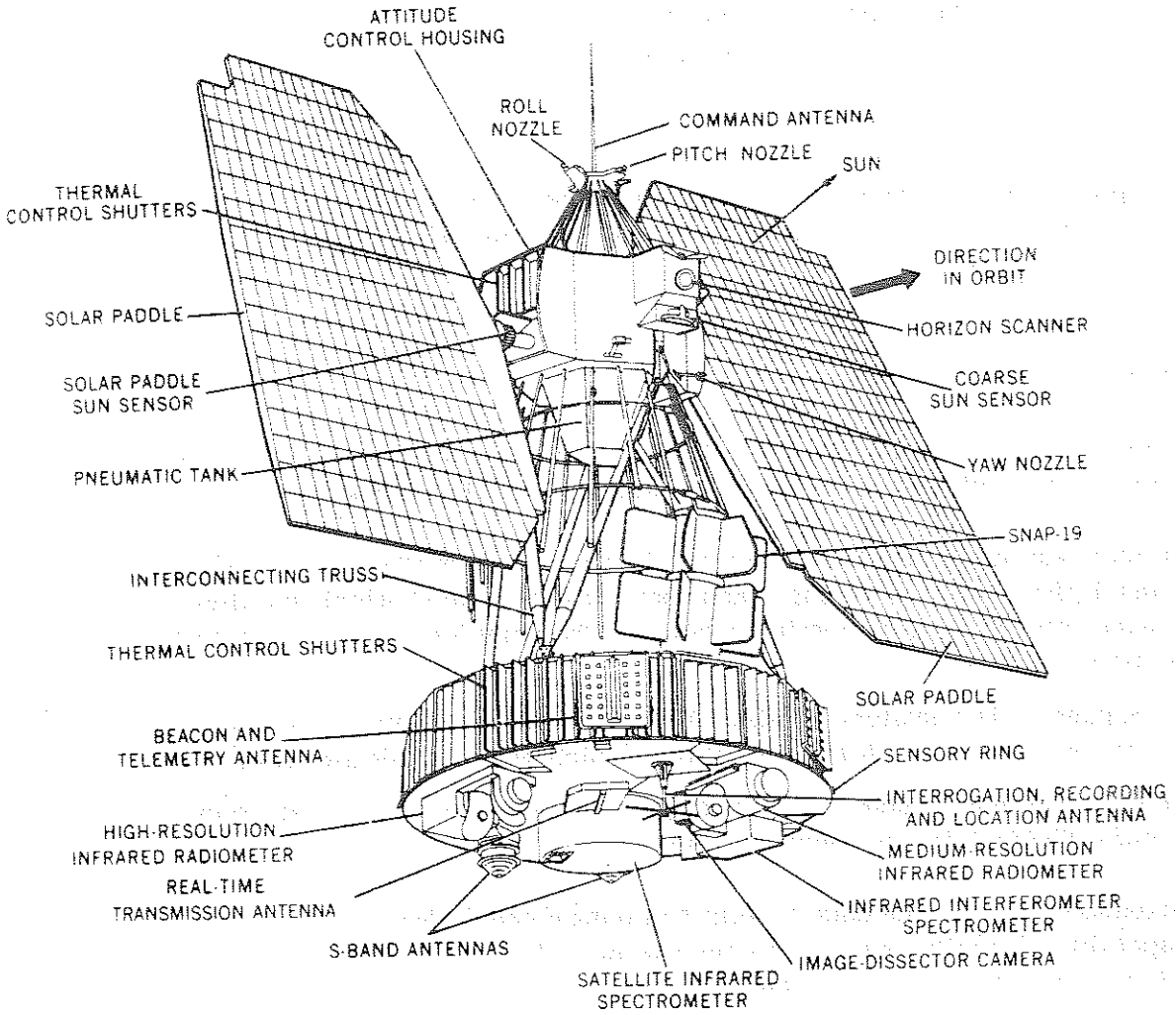

Figure 1-1– Basic Configuration of Spacecraft

Table 1-1
Nimbus III Meteorological Experiments

Experiment	Spectral Bands Microns	Main Purpose
High Resolution Infrared Radiometer (HRIR)+	3.4-4.2	Nighttime surface and cloud top temperatures, and cloud mapping
	0.7-1.3*	Daytime cloud mapping
Medium Resolution Infrared Radiometer (MRIR)	6.5-7.0 } 20-23* }	Atmospheric water vapor and cirrus cloud mapping
	10-11	Surface and cloud top temperatures
	14.5-15.5	Stratospheric temperatures
	0.2-4.0	Daytime cloud mapping, albedo
Infrared Interferometer Spectrometer (IRIS)*	5-20	Atmospheric temperature profile, 0_3, water vapor, surface temperature and minor atmospheric gases
Satellite Infrared Spectrometer (SIRS)*	11-15	Multilevel atmospheric temperature
Monitor of Ultraviolet Solar Energy (MUSE)*	0.12 } 0.16 } 0.18 } 0.20 } 0.26 }	Monitors changes in solar radiation
Image Dissector Camera System (IDCS)*+	0.45-0.65	Daytime cloud mapping
Interrogation, Recording and Location System (IRLS)*	—	Data collection from platforms

*Experiment or spectral band was not flown on previous Nimbus satellites.
+IDCS and HRIR data, besides being recorded for transmission to the DAF, are also broadcast to Automatic Picture Transmission (APT) ground stations throughout the world.

orbits cross the equator at 26° of longitude separation. The period for this orbit is about 107 minutes. Nimbus III is scheduled to be launched in the second quarter of 1969 from the Western Test Range in California. The launch vehicle is a Thorad-Agena D.

1.3 Spacecraft Attitude

The Nimbus spacecraft contains an active 3 axis stabilization system designed to maintain the spacecraft body axes earth-stabilized, with the yaw axis pointing normal to the earth, and the roll axis aligned to the spacecraft velocity vector (see Figure 1-2). From past experience, the attitude is closely maintained to the intended pointing directions. Pointing errors seldom exceed 1° in pitch, 2° in roll, and 5° in yaw. Larger excursions are normally associated with cold clouds. All the data obtained are geographically located by using the orbit ephemeris data. In view of the high pointing accuracy and the lack of more precise orientation data, attitude corrections are not utilized in the geographic location procedures.

1.4 Spacecraft Data System

Data are stored and transmitted via four independent data systems on the Nimbus III Spacecraft. They are the High Data Rate Storage System (HDRSS), the Pulse Code Modulation Telemetry System (PCM), the Real Time Transmission System (RTTS), and the Interrogation, Recording and Location System (IRLS). The individual data systems are described below. A summary of how the meteorological experiments are handled is provided in Table 1-2.

Table 1-2
Data Systems Summary

Experiment	Stored Data System	Real Time Backup Data System
IRIS	HDRSS	PCM*
MRIR	HDRSS	PCM*
HRIR	HDRSS	RTTS
IDCS	HDRSS	RTTS
IRLS	SELF CONTAINED	NONE
MUSE	PCM**	PCM
SIRS	PCM**	PCM

*In case of HDRSS failures, provision exists for real time data for IRIS and MRIR by time sharing with the normal PCM data.

**In case of PCM recorder failures, provision exists for recording the PCM data which includes MUSE and SIRS data in place of MRIR in the HDRSS system.

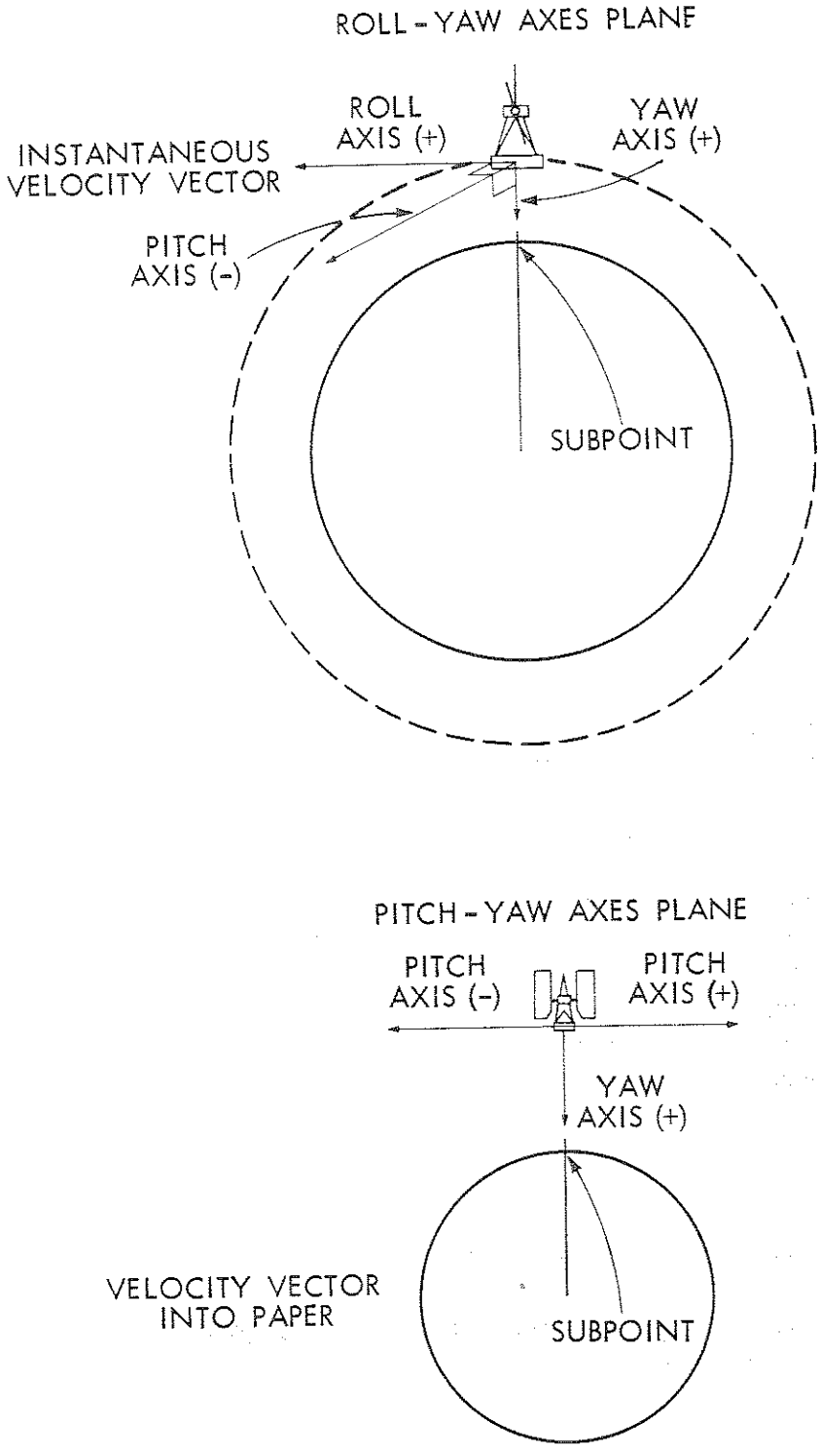

Figure 1-2– Nimbus Attitude Axes.

1.4.1 High Data Rate Storage System (HDRSS)

There are two identical HDRSS systems. Each system includes a five channel reel to reel tape recorder, a frequency multiplexing system and a 2 watt S-band transmitter. The tape recorder is a five channel analog tape recorder running at 1-3/8" per second and playing back 32 times that speed. The S-Band frequencies are 1702.5 and 1707.5 MHz and the multiplexed spectrum is from 10 to 700 Khz.

This system is used for the high data rate experiments: IDCS, MRIR, IRIS and HRIR. The fifth track contains the spacecraft time code which is also used for flutter and wow compensation. Each recorder can record approximately 150 minutes of data.

There is also provision for substituting the Telemetry (PCM) data for the MRIR experiment data on this tape recorder.

1.4.2 Pulse Code Modulation Telemetry System (PCM)

The PCM system includes an analog to digital encoder, a multiplexer, two endless loop tape recorders recording serial data and a 1/4-watt 136.5 MHz transmitter. The system can also accept digital data. In the PCM system each major frame consists of the data from 798 input channels, some are digital and some are analog depending on their position in the data format. Each major frame contains 16 subframes sampled at the rate of one per second. Each subframe consists of 60 7-bit data words plus appropriate sync and subframe identification words. Data include spacecraft subsystem and experiment housekeeping telemetry such as temperature of components, calibration signals and voltages plus the output of two experiments: SIRS and MUSE. The data are transmitted over the beacon transmitter in real time while being recorded on the spacecraft. The recorders run at 0.4" per second and playback is speeded up at a ratio of 30:1. Each recorder has the capacity for one orbit of data.

1.4.3 Real Time Transmission System (RTTS)

The RTTS system transmits IDCS or HRIR data over a 136.950 MHz, 5 watt transmitter, in real time. The IDCS data format is compatible with existing APT stations around the world; the HRIR data are available to APT stations modified to receive 48 RPM HRIR data.

1.4.4 Interrogation, Recording and Location System (IRLS)

This system consists of a 10 K bit memory device and a transceiver system. The 400.5 MHz downlink system is used to initiate interrogations with ground based or airborne IRLS platforms and to transmit data received from the platforms and stored in the memory to the Data Acquisition Facilities. The 466 MHz uplink is utilized to transmit data from the IRLS platforms to the spacecraft and also to transmit commands to the IRLS System for programming interrogations of the IRLS platforms.

1.5 Ground Station Complex

Data from the HDRSS are received at the two STADAN Data Acquisition Facilities (DAF) located near Fairbanks, Alaska and Rosman, North Carolina. Data transmitted over the PCM system are received at these two sites as well as at the Orroral Australia STADAN Station. Data from the IRLS system are received at the Alaska DAF station and at the Goddard Space Flight Center, Greenbelt, Maryland. The HDRSS data acquired at Alaska are recorded on pass and then transmitted over a microwave link at reduced rates to the Nimbus Data Handling Facility (NDHF) at GSFC. The PCM data are relayed to GSFC as they are received from the spacecraft. Raw data are relayed directly from the Rosman DAF to GSFC over a wideband data link. PCM recorded data received at Orroral are transmitted at reduced rates over a hardwire link.

Alaska acquires the spacecraft 10 orbits each day (of the 13 to 14 orbits per day). Rosman acquires two orbits per day missed by Alaska. Orroral acquires the PCM data for the remaining orbits missed by Rosman and Alaska.

All spacecraft data are processed in the Nimbus Data Handling Facility at GSFC. Photographic images of IDCS, HRIR and MRIR data are processed through the Nimbus Data Utilization Center. Digitized magnetic tape recordings of the IRIS, MRIR, HRIR, SIRS and MUSE experiment data are distributed to the respective experimenters for further data reduction.

1.6 Nimbus Data Utilization Center

The Nimbus Data Utilization Center (NDUC) performs the following functions:

1. Accountability for and distribution of all experiment data processed by the NDHF.

2. Processing and reproduction of photographic data until they have been archived.

3. Generation of periodic data catalogs in a format as outlined in Section 10 to provide information on IDCS, HRIR, MRIR, IRIS, SIRS and MUSE data collection and availability.

4. Special technical services concerning data processing to the experimenters and data users, including maintenance of a complete photographic data reference file.

1.7 Archival and Dissemination of Nimbus III Data

The nature and format of the data to be available from each experiment are explained in detail in the respective sections of this guide. The data will be archived and available as described below.

1. IDCS photographic data will be archived and available through the National Weather Records Center (NWRC), Environmental Sciences Service Administration, Federal Building, Asheville, North Carolina 28801.

2. HRIR and MRIR photographic data will be archived and available through the National Space Science Data Center (NSSDC), Goddard Space Flight Center, Code 601, Greenbelt, Maryland 20771.

3. HRIR, MRIR, IRIS and MUSE digital data tabulated as radiance values will be archived and available through the NSSDC.

4. SIRS digital data will be archived and available from two sources:
   Digital data tapes containing radiance values will be archived in the NSSDC.
   Digital data tapes containing temperature profiles and the radiance values from which they were derived will be archived in the NWRC.

IDCS photographic data and SIRS digital data will be available from the NWRC at cost. Limited quantities of all other data will be furnished to qualified investigators, by the NSSDC, without charge. A charge for production and dissemination costs may be established by NSSDC if a large volume of data is requested. Whenever it is determined that a charge is required, a cost estimate will be provided to the user prior to filling his data request.

All requests from non-United States researchers for HRIR, MRIR, IRIS, SIRS or MUSE data, in either film or digital output format, archived and available through NSSDC must be specifically addressed to: Director, World Data Center A for Rockets and Satellites, Code 601, Goddard Space Flight Center, Greenbelt, Maryland, 20771, U.S.A.

SECTION 2

THE IMAGE DISSECTOR CAMERA SYSTEM (IDCS) EXPERIMENT

by
Gilbert A. Branchflower, NASA, GSFC
and
Leon Goldshlak, Allied Research Associates, Inc.

2.1 Introduction

Nimbus III will carry one daytime camera system known as the Image Dissector Camera System (IDCS). Pictorial information will be recorded on video tape and stored in the satellite until commanded to playback at the prime Nimbus Data Acquisition Facilities near Rosman, North Carolina, and Fairbanks, Alaska. A second mode of data transmission is the real time transmission, which enables APT users worldwide to acquire directly from the satellite pictorial meteorological coverage of their immediate areas. The broadcasts in the real time transmission mode are essentially identical to those recorded on the video tape for subsequent transmission to the Data Acquisition Facility. Section 9 of this Guide and Reference 1 of Section 9 provide information on the IDCS Real Time Transmission mode.

The IDCS is mounted on the bottom of the sensory ring of the earth stabilized Nimbus III satellite. The "optic axis" of the camera system is aligned with the positive yaw axis (see Figure 1-2) of the satellite. The image dissector is a shutterless electronic scan and step tube mounted behind a wide angle lens. Scanning and stepping functions occur continuously while the satellite is progressing along its orbital path, i.e., the earth scene contained in a single frame is not exposed instantaneously from a fixed location in space. The image dissector scanning and stepping cycles in conjunction with the satellite orbital motion have been designed to achieve an image with a nearly 1:1 aspect ratio for the Nimbus III 600 nautical mile circular orbit. Successive IDCS frames are initiated at intervals of 208 seconds. An interval of 208 seconds is the complete timing cycle for a IDCS frame and associated electronic functions.

Advantages of the experimental IDCS over the more conventional vidicon camera systems are: the ability to sense a greater dynamic range (about 100:1), high signal to noise ratios, direct relationship between light flux input and electron current output, and the avoidance of a mechanical shutter.

2.2 Description

2.2.1 Optics

The optical system of the IDCS consists of a wide angle Tegea lens. The lens has a nominal focal length of 5.7 millimeters and a nominal diagonal field of view of 108 degrees. A minus blue filter in front of the lens is employed for enhancement of cloud images. The image dissector tube (sensor) is mounted directly behind the optical system.

Ground resolution obtained from the IDCS at an altitude of 600 nautical miles is approximately 1.75 nautical miles at the instantaneous satellite subpoint, decreasing to about 5 nautical miles at the north-south limits of view and to 6.65 nautical miles at the east-west limits of the field of view. The average picture resolution within the field of view is approximately 2.2 nautical miles.

2.2.2 Sensor

The image dissector tube is a non-storing, scanning detector of the photomultiplier class (see Figure 2-1). Basic components of the tube are a photocathode, an accelerating screen, a drift tube, an aperture and an electron multiplier. Excitation of the photocathode by light causes electrons to be emitted in direct proportion to the light level applied. The emitted electrons are accelerated from the photocathode and pass through a fine mesh screen into a unipotential drift space. A magnetic focus field (the focus coil is a long solenoid enclosing both the photocathode and aperture plane) is applied such that the electrons spiral, arriving at the aperture plane with the same spatial relationship as the original optical image on the photocathode. Thus, the optical image has been translated into an electron image and transferred to the single aperture plane within the image dissector tube.

At the center of the aperture plane is a small hole (the aperture). The aperture diameter is chosen to admit electrons from a selected area of the photocathode. Size and shape of the aperture may be chosen, within limits, as a function of the required sampling technique and resolution. The Nimbus III image dissector tube has a circular aperture of 0.001 inches diameter with an S11 photocathode of 0.7 inches diameter. The effective instantaneous field of view of the sensor is 0.166 degrees.

To generate a proper scan sequence for a normal raster, it is necessary to apply a transverse magnetic field in the drift space. Deflection coils, which are similar to vidicon deflection coils, develop the transverse field which causes the complete electron image to shift orthogonal to the direction of the magnetic

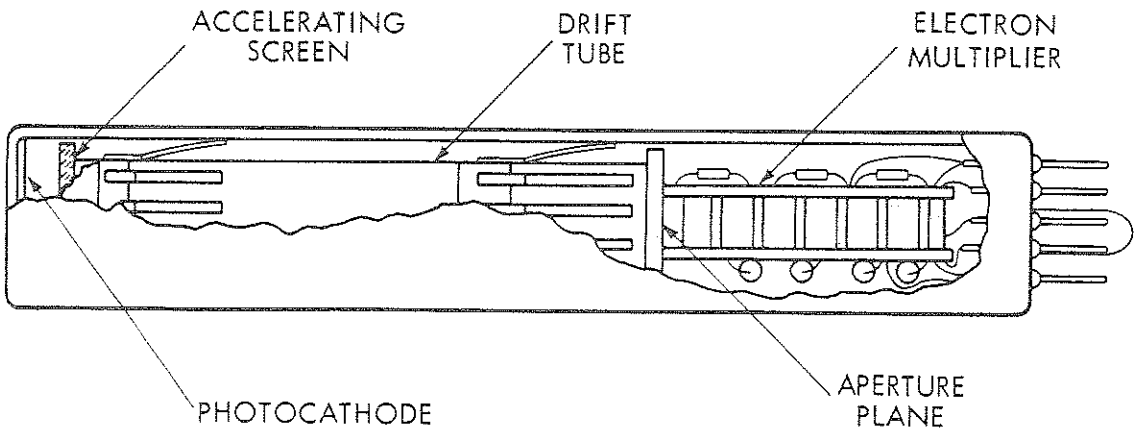

Figure 2-1 – Components of Image Dissector Tube

field. Thus, selected areas of the complete electron image can be scanned past the aperture centered in the aperture plane. Horizontal deflection generates scan lines and vertical deflection generates the scan step.

As the electron image is moved past the aperture, that spot of information passed through the aperture is detected as an electrical signal and is multiplied over a million times by the electron multiplier assembly located behind the aperture plane. After electron multiplication, the signal current is fed to the electronic circuits that enable the signal to be transmitted directly to the ground in real time (DRID) and/or to be stored on magnetic tape for subsequent playback at the Data Acquisition Facilities.

2.2.3 Sensor Operation

An entire image dissector video frame consists of 800 scan lines and requires 200 seconds of cycling time (Figure 2-2). The elapsed time for one complete scan line is 250 milliseconds (0.25 seconds). A complete scan line is composed of two parts: a 225 millisecond active scan following a 25 millisecond blanked scan. Video data are collected during the active portion of the scan. The blanked portion of the scan occurs during scan reorientation to the new start position. A scan line corresponds to a nominal viewing angle of 98.2 degrees in the image dissector tube. The stepping cycle (800 steps), which is perpendicular to the scan line direction, corresponds to a nominal 73.6 degrees viewing angle in the image dissector tube. These angles are not the actual angles of the field of view because they do not at this point include lens distortion, blanking, or satellite movement during the 200 second picture taking time. The stepping sequence is linear in time, thus, each step starts at 250 millisecond intervals.

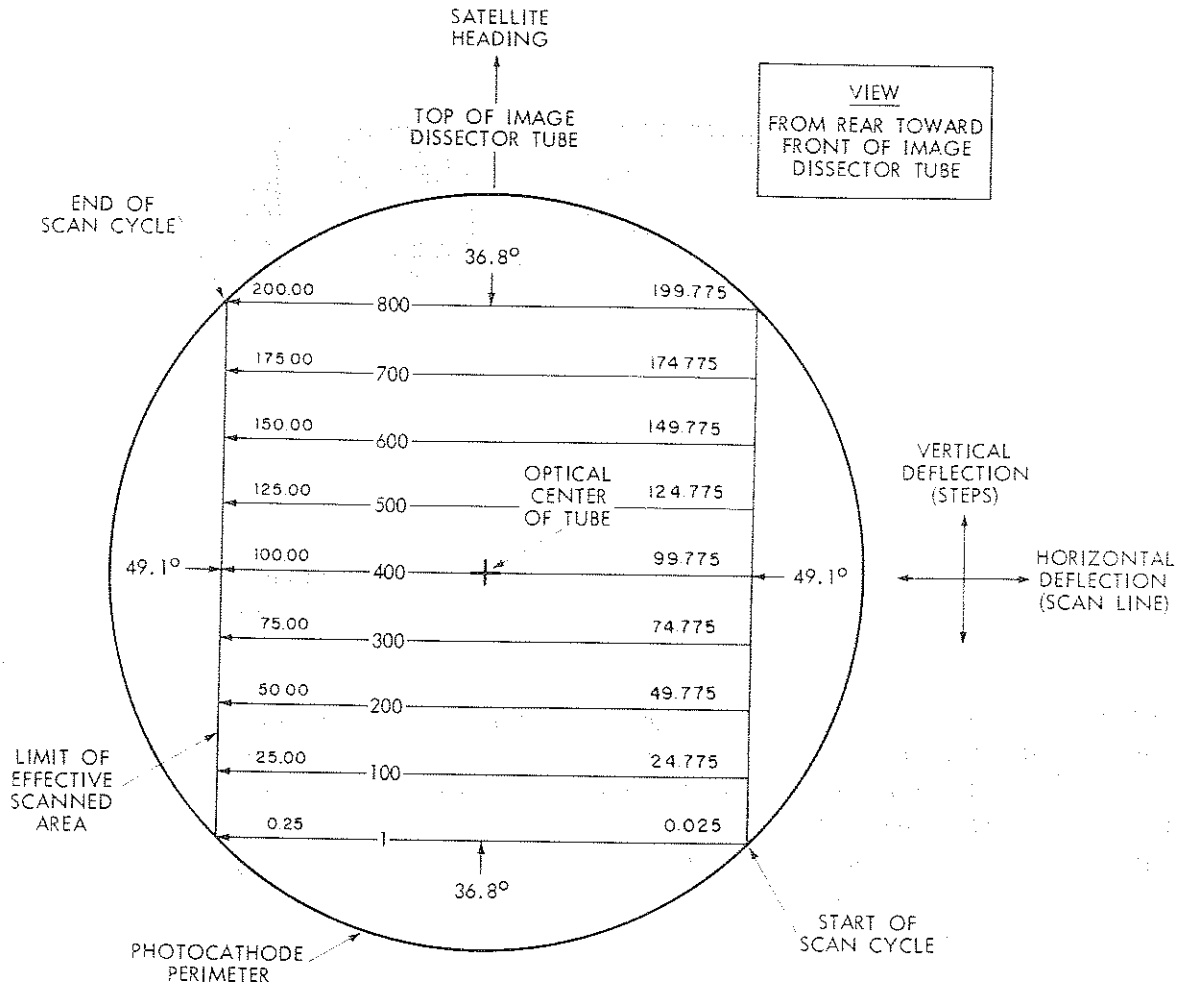

Figure 2-2–Schematic Representation of Image Dissector Scanning Cycle

In Figure 2-2 the column of numbers near the right hand limit of the scanned area is the start time (seconds) for active segments of selected scan lines. End times (seconds) of the same scan lines are shown near the left limit.

The scanned area or raster shown as a square in Figure 2-2 is in reality a rectangle on the photocathode. The rectangle has a height to base ratio of approximately 1.0 to 1.5. Successive scan lines are geometrically overlapped by about 33 percent on the photocathode. However, during the IDCS operational cycle this overlap is effectively removed by the forward motion of the satellite relative to the earth and the final display is nominally square.

The first video scan line commences below (36.8 degrees) and to the right (49.1 degrees) of the optical center of the image dissector tube (Figure 2-2).

Scan lines are generated from right to left, whereas the stepping sequence is from the bottom to top of the image dissector tube. The top of the tube is oriented on the spacecraft in the heading direction.

2.3 Calibration Results

Figure 2-3 is a IDCS calibration picture showing the field of view of the camera system including simulated satellite motion for a circular orbit at a height of 600 nautical miles. The nodal point of the lens was at a measured distance of 59.844 inches from the plane of the calibrated target shown in the figure. The black grid network shown in Figure 2-3 should theoretically consist of squares. Deviations from a square grid network represent a combination of lens distortion, internal sensor alignments, and known mechanical and electronic distortions introduced during the calibration procedures. Henceforth, the combined distortions resulting from the camera lens and the internal sensor alignments will be referred to, simply as lens distortion.

The "pin-cushion" distortion pattern exhibited by the black grid network in the calibration picture is, however, indicative of the true camera system distortions.

2.3.1 Image Principal Point

At one instant during the scanning sequence of a complete IDCS frame the image dissector sensor will be aligned with the local vertical. The instantaneous satellite subpoint, at that time, is defined to be the object principal point. The corresponding location of this instantaneous subpoint in the final IDCS display is defined to be the image principal point.

As determined from the calibration picture (Figure 2-3) the image principal point is not located at the geometric center of the IDCS display but is offset slightly toward the left and above the center of the display. Location of the image principal point is shown at the intersection of the two diagonals in the calibration picture in Figure 2-3. The image principal point is located 51.6 percent of the horizontal distance from the right hand edge of the display and 48.8 percent of the vertical distance from the top of the display (step 410 from the bottom of the IDCS display).

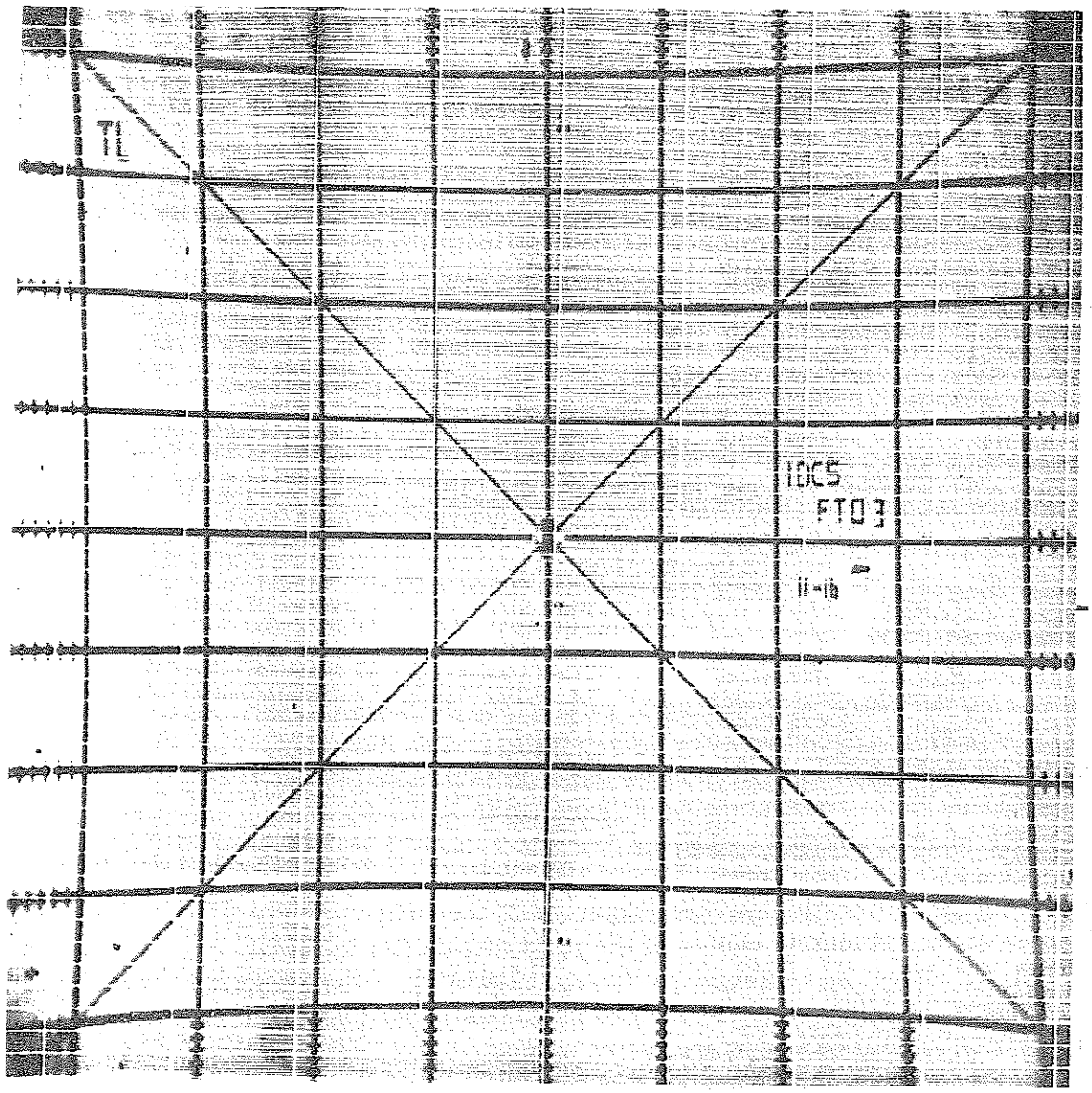

Figure 2-3–IDCS Target Calibration Picture

2.3.2 Lens Distortion

The wide angle Tegea lens coupled with the image dissector tube results in a low distortion optical system in the central portion of the field of view. Distortion effects are zero in the center of the field of view and become more noticeable near the sides and corners of the picture. Figure 2-4 shows the location errors, in nautical miles, of points in the IDCS picture resulting from lens distortion. Location errors shown in the figure are for a satellite height of 600 nautical miles. Data points are referenced to the image principal point and values are shown only for the upper right hand quadrant of the display since the distortion is symmetrical about the axes through the image principal point. Isolines are drawn for 1, 6, 30 and 60 nautical mile location errors within the entire IDCS picture area.

Figure 2-5 shows the lens distortion vectorially. Only the upper right hand quadrant of the IDCS display is shown. The origin of the vector represents the location of points as seen through an ideally perfect nondistorting lens. Termination of the vector represents the relocated position of the same points caused by the lens distortion and presented in the final IDCS image. Vectors are properly scaled relative to the shown format except that the scalar values at those points containing coordinate values of 0.9 and/or 1.0 are approximate. Units are arbitrary, rendering the diagram useful for Nimbus III IDCS application regardless of satellite height or size of the final display.

2.3.3 Field of View

The coverage presented in a IDCS frame results from a composite of the fixed scan and step modes of the image dissector tube, blanking, plus the satellite motion and lens distortion. Figure 2-6 and Table 2-1 indicate, respectively, the IDCS field of view in terms of angular measurements at the spacecraft and earth coverage in nautical miles as displayed in the IDCS picture. Earth coverage measured from the image principal point to the picture boundaries are given in Table 2-1 for satellite heights at and near the nominal 600 nautical miles. All data in Table 2-1 are referenced from the image principal point, not from the geometric center of the IDCS display, and contain the lens distortions mentioned in Section 2.3.2 (shown in Figure 2-6) and the contribution of the satellite motion.

2.3.4 Shading Characteristics

When a constant light intensity impinges on the sensitized surface of the image dissector tube, the resultant output shows slight shading characteristics.

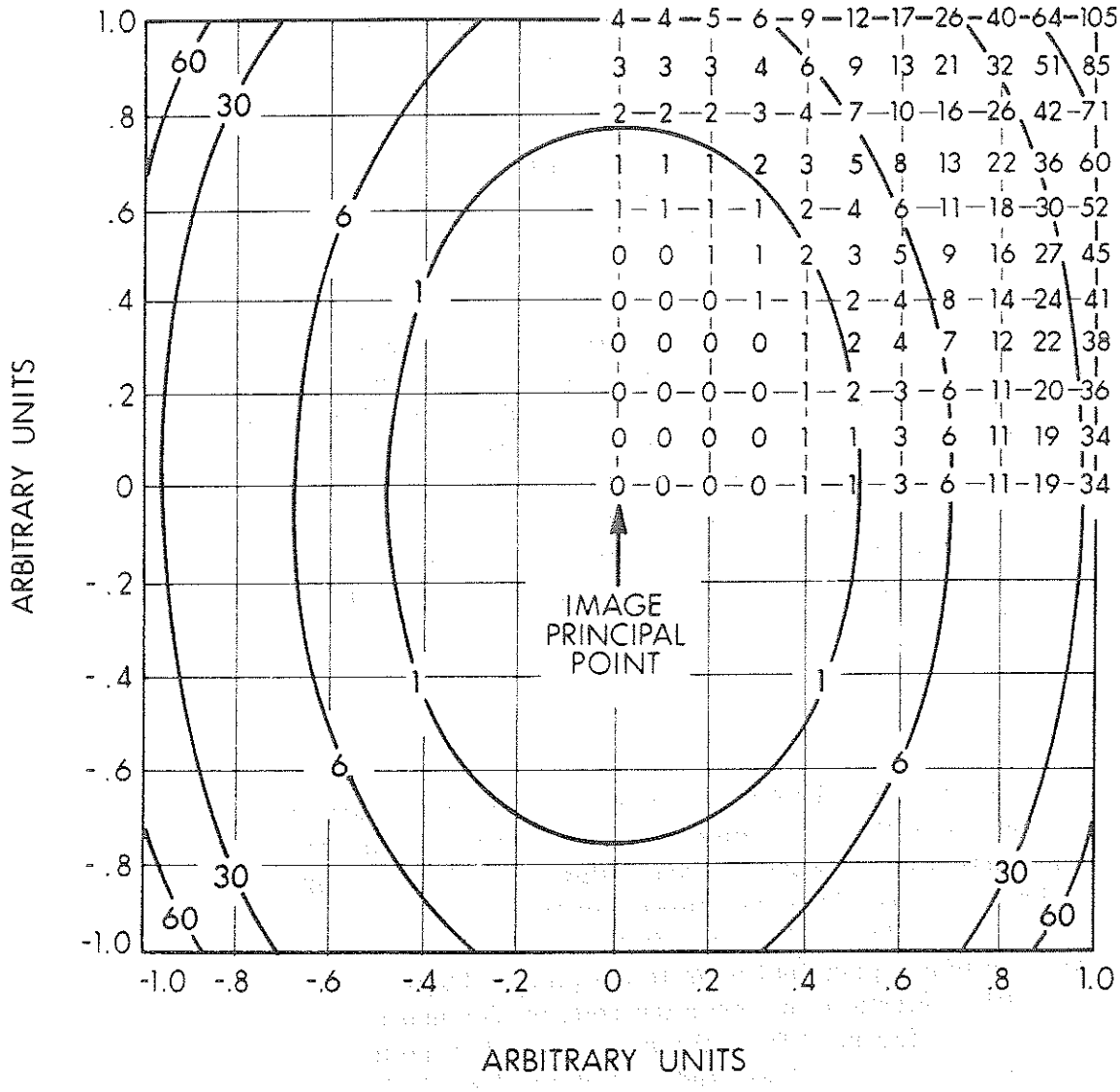

Figure 2-4—Location Errors Caused by Lens Distortion

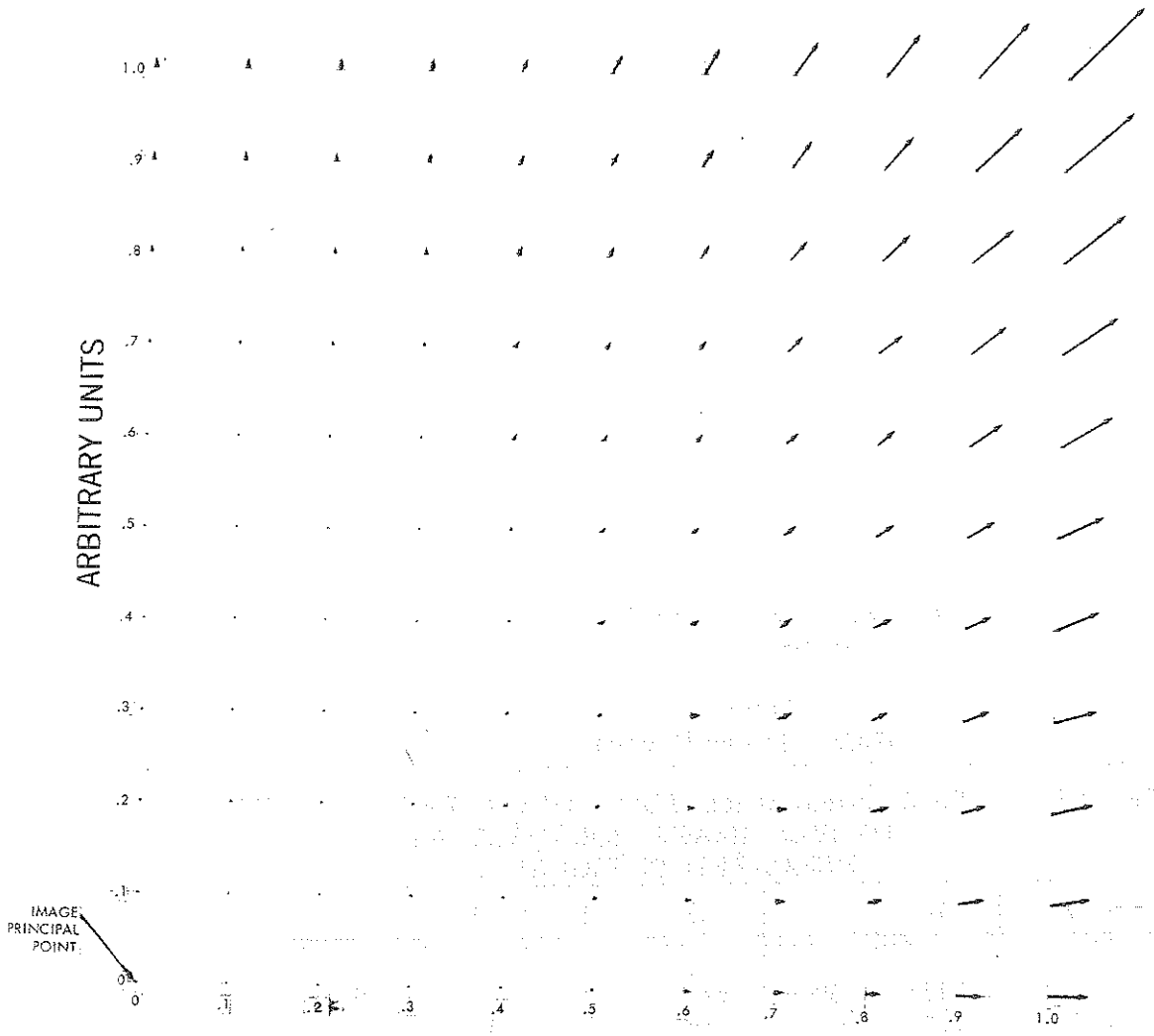

Figure 2-5–Vectorial Lens Distortion Errors - One Quadrant

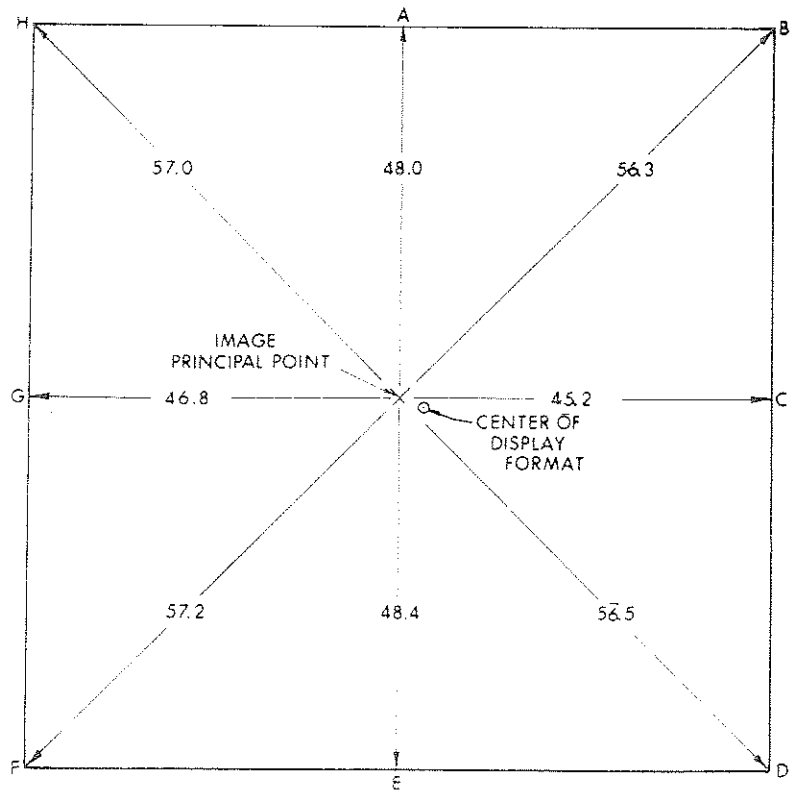

Figure 2-6–Angular Picture Limits of IDCS Display for Satellite Height of 600 N. Miles

Table 2-1
IDCS Picture Coverage

SATELLITE HEIGHT Nautical Miles	DISTANCES (Nautical Miles) FROM IMAGE PRINCIPAL POINT TO IDCS IMAGE BOUNDARY AS INDICATED IN FIGURE 2-6							
	A	B	C	D	E	F	G	H
540	730	1153	599	1173	743	1246	643	1224
550	737	1175	612	1195	750	1273	657	1250
560	742	1194	624	1217	756	1299	671	1273
570	749	1217	637	1238	762	1325	684	1300
580	754	1237	649	1261	768	1353	698	1325
590	761	1261	662	1285	775	1383	712	1354
600	766	1283	675	1309	781	1413	727	1382
610	773	1308	688	1335	788	1446	741	1412
620	779	1332	701	1362	795	1482	755	1443
630	786	1359	714	1390	802	1519	769	1478
640	793	1386	727	1418	809	1559	784	1514
650	799	1413	740	1448	816	1603	798	1551

Figure 2-7 is an enhanced calibration test picture which displays the shading pattern for a 10,000 foot lambert input over the full field of view of the camera. This response pattern is essentially the same for all light inputs below 10,000 foot lamberts. The arbitrary gray levels in Figure 2-7 are used only to delineate the different shading characteristics of the camera for a given input.

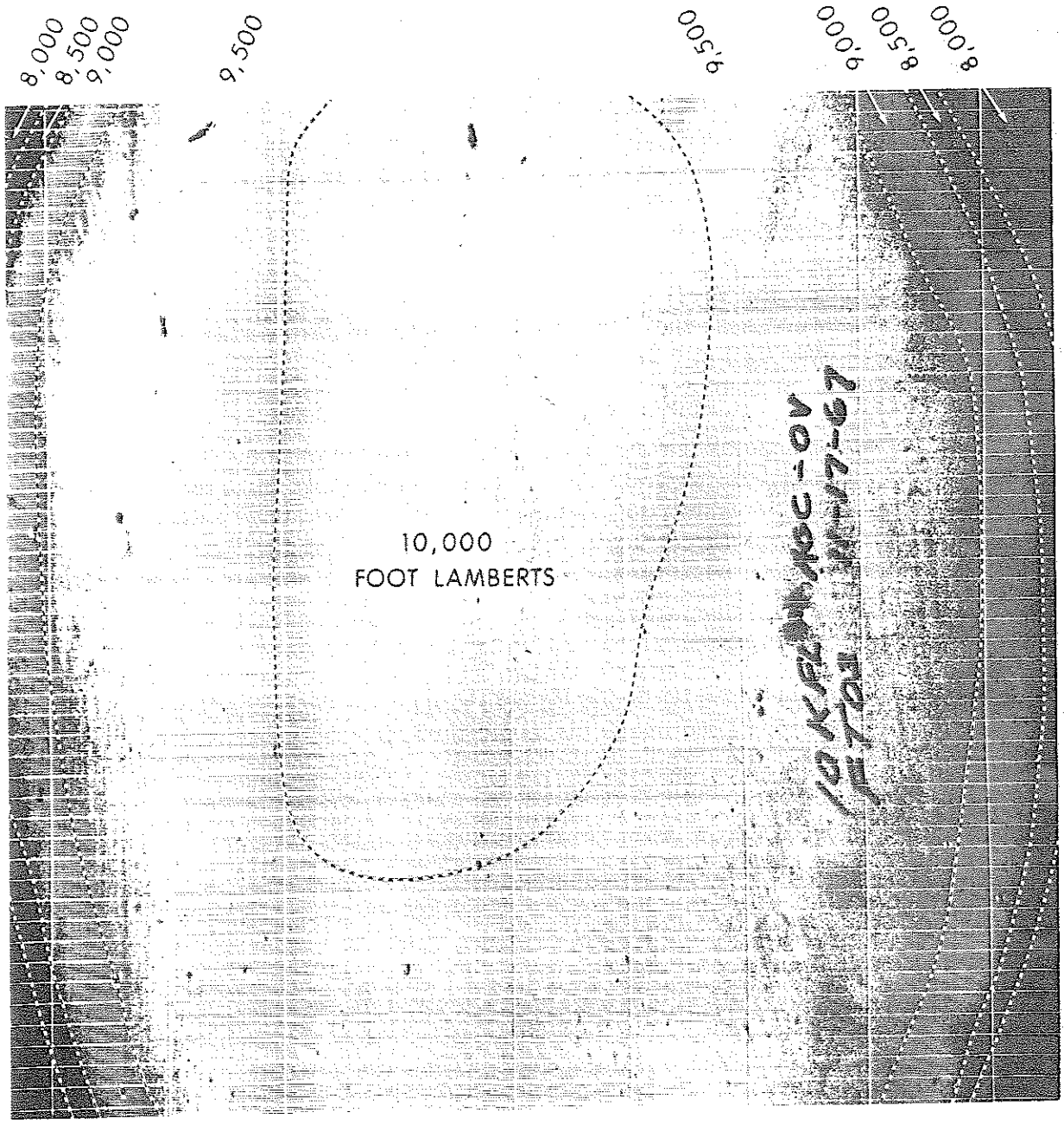

Figure 2-7—IDCS Shading Characteristics

Correct boundaries between different shading areas are closely approximated by the contours superimposed on the calibration picture. Striated patterns within the picture result from interference in the test equipment and should be ignored.

The left and central area of the picture labeled 10,000 foot lamberts is the brightest response and is very near or at saturation. The two adjacent areas delineated and labeled 9,500 foot lamberts represents a five percent drop in camera output for the same 10,000 foot lambert input. Differences between the 10,000 and 9,500 foot lambert areas, or any two adjacent areas, may not be noticeable in the IDCS pictures played back on the ground equipment.

In fact, the camera response deviation may barely be noticeable throughout the entire frame.

At the four corners and near the right hand edge of the picture additional areas of camera response "fall off" are delineated and appear at 9,000, 8,500 and 8,000 foot lamberts.

Interpretation of the shading phenomenon, from the user standpoint, is that he be aware that a given albedo, when observed in the central portion of the picture will appear slightly brighter than the identical albedo observed toward the edges or corners of the picture.

2.4 Picture Formulation

As previously mentioned, the IDCS display is a composite resulting from the fixed scan and step mode of the image dissector tube plus the contribution provided by the satellite motion. The satellite motion, as it affects the IDCS display, may be thought of as being composed of two classes of phenomena:

(i) Satellite Location – the position of the satellite in space, relative to the earth, as a function of time, and
(ii) Satellite Attitude – the direction toward which the satellite, or camera "optic axis," is facing at any instant of time.

Only the location of the satellite as function of time is used as the satellite motion contribution for the final composition of the IDCS frame. Attitude deviations, which are also a component of the satellite motion are assumed to be zero.

2.4.1 Scan Component

An active IDCS scan line samples data that are perpendicular to the instantaneous spatial heading of the satellite. Due to the electronic stepping, or "pitching" sequence of the sensor, the instantaneous satellite subpoint is not contained in the sampled data of a scan line, except for data sampled during scan line 410 (t_0 +102 seconds). The user should note that the scan direction is not perpendicular to the subpoint track of the satellite.

Facing the direction of motion of the satellite, an active scan is generated by observing the earth from right to left relative to the satellite location (Figure 2-8).

The field of view represented by a single active scan line, as determined from calibration data, is 92.0 degrees from side to side.

2.4.2 Step Component

During the framed picture-taking interval the electronic stepping component continuously varies the sensor look angle in the roll-yaw plane from behind the satellite, through the yaw axis to a point ahead of the satellite. For clarity of illustration we temporarily assume that the satellite is fixed in space. Figure 2-9 shows schematically the stepping mode of the image dissector tube for one complete video frame.

At the start of the picture-taking interval the sensor look angle is 35.3 degrees behind the satellite. Approximately midway during the picture taking interval, at step number 410, the sensor look angle is aligned with the yaw axis. At the end of the picture taking interval, the sensor look angle is 34.4 degrees ahead of the satellite. Thus, the total field of view in the roll-yaw plane accounted for by the electronic stepping sequence (excluding satellite motion) is 69.7 degrees.

The sensor varies linearly through 69.7 degrees in 800 steps. A composite picture resulting from the scanning and stepping cycles requires 200 seconds for completion (800 successive steps or scan lines at 0.25 seconds per scan line).

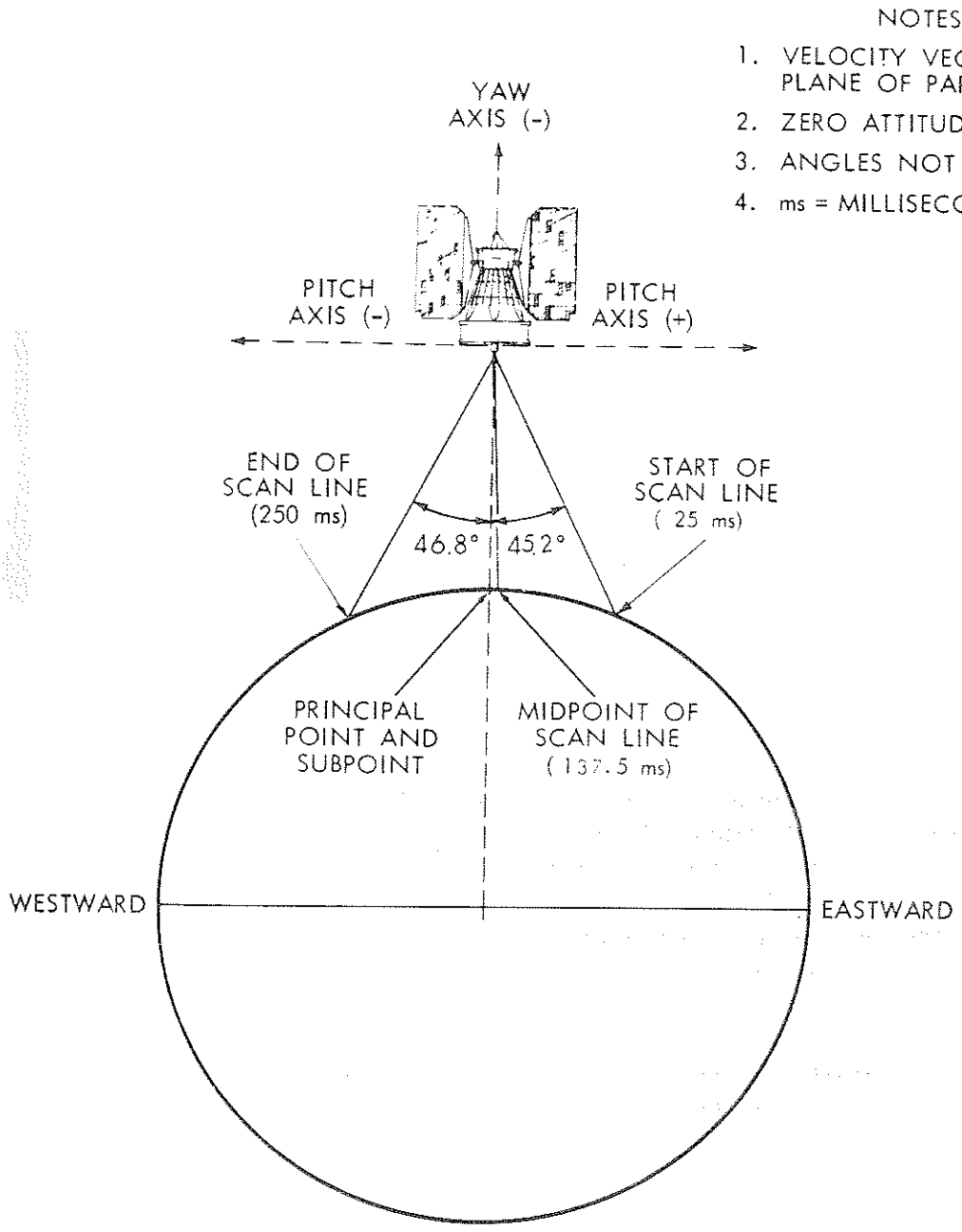

Figure 2-8–IDCS Scan in Pitch-Yaw Plane

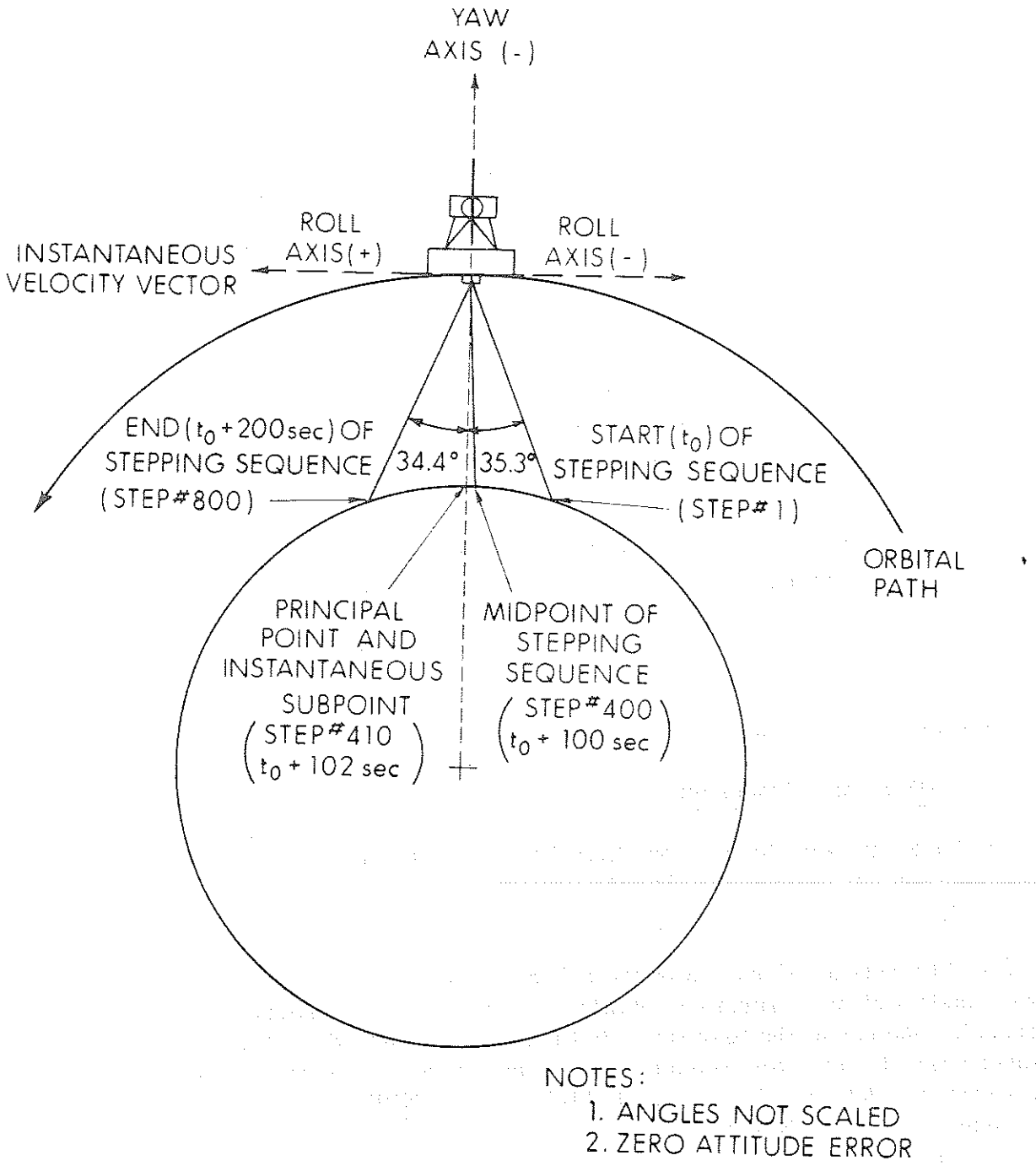

Figure 2-9—Stepping Mode of Image Dissector Tube

2.4.3 Satellite Motion Component

The image dissector camera is in continuous operation for 200 seconds. During this time interval the satellite is constantly progressing along its orbit. The motion of the satellite, relative to the earth, contributes significantly to the image aspect ratio, resolution, and area viewed during the 200 second camera cycle.

Angular and timing specifications for the image dissector tube were pre-selected so that when integrated with the satellite motion, the resultant image would be in a nearly 1:1 aspect ratio. The most significant contribution made by the satellite motion is to expand the viewed image in the direction of motion of the satellite (along the heading line) so that the aspect ratio approaches 1:1.

A true aspect ratio of 1:1 cannot be achieved by the image dissector camera system since another variable, the rotation of the earth during the 200 second picture taking cycle, is not compensated. However, the image distortion resulting from earth rotation is a second order effect.

Figure 2-10 shows schematically the integration of the satellite motion with the limits of the stepping motion of the image dissector camera. The 600 nautical mile circular orbit causes the Nimbus III satellite to traverse 11.11 degrees of great circle arc during the 200 seconds of the picture taking cycle.

2.5 IDCS Data Processing, Archiving and Access

2.5.1 IDCS Data Processing

The IDCS data are stored in the High Data-Rate Storage Subsystem (HDRSS) and transmitted on command to the DAF station, in reverse at 32 times the record rate.

The IDCS data are received on the S-band frequency at the DAF. The S-band signal consists of five channels of multiplexed data, four on separate subcarrier frequencies and one at the baseband. At the ALASKA DAF, the composite group of subcarriers is demultiplexed and the subcarriers are recorded on magnetic tape so that the data may be transmitted to the GSFC NDHF. The Video Data processing system for Nimbus III is the modified AVCS subsystem used on Nimbus I and II.

At the NDHS the photographic processing of the IDCS kinescope pictures is accomplished by a rapid BIMAT system which includes a develop, fix, wash, and

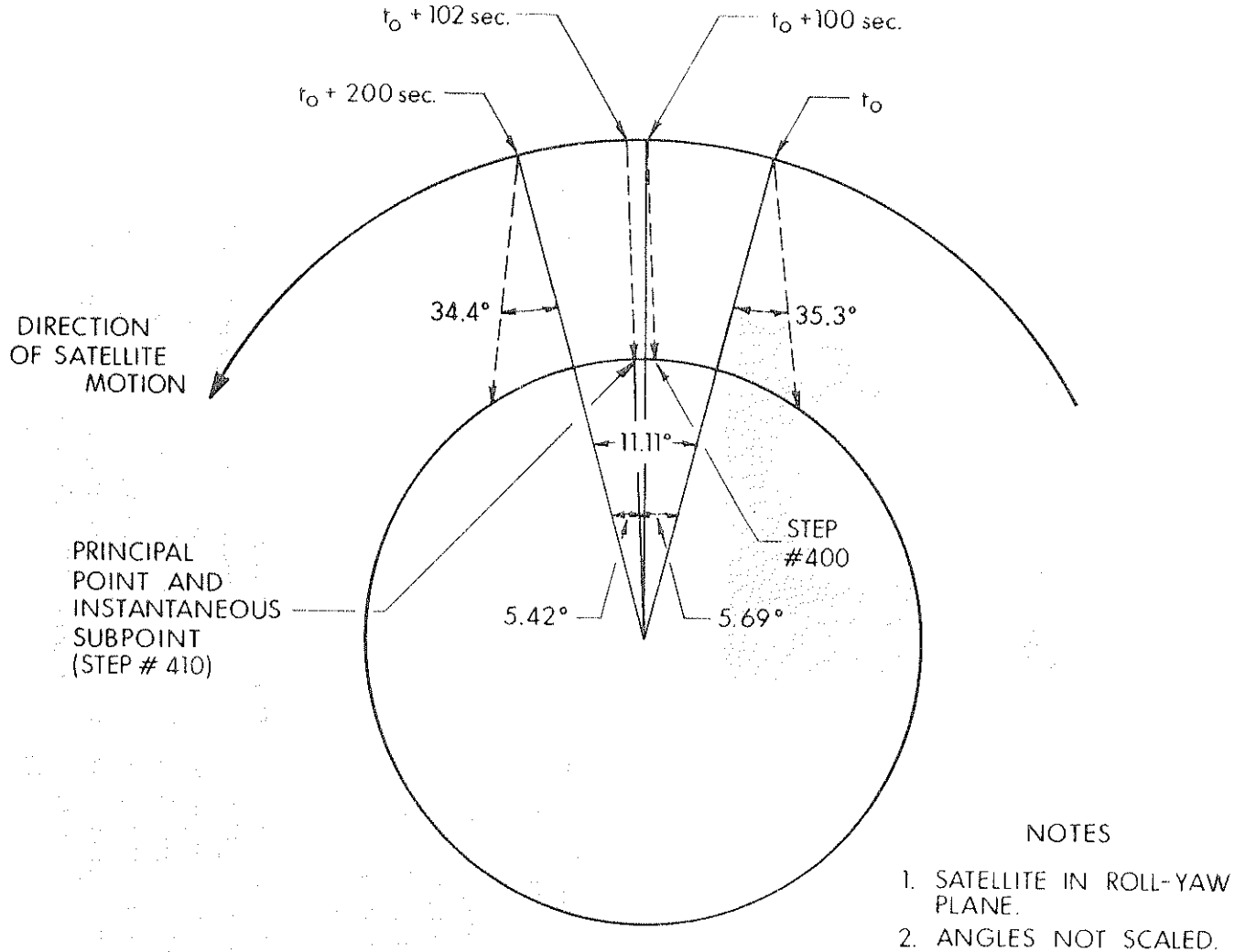

Figure 2-10–IDCS Satellite Motion Compensation

dry cycle. This system produces a 70 mm negative and positive transparency simultaneously, the negative being of archival quality.

Each IDCS frame, approximately 2 × 2 inches, has a computer produced latitude-longitude grid and time of the first scan line (top) of the video display. Figure 2-11 is an illustrative example of the IDCS picture format with time and latitude-longitude grids.

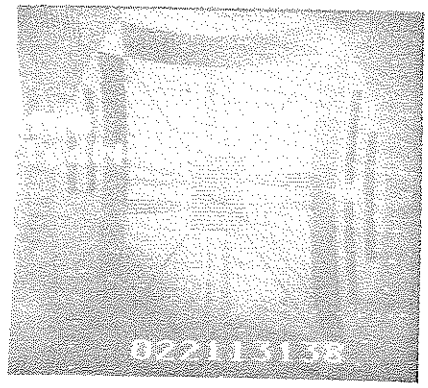

Figure 2-11—Sample IDCS Picture Format

The latitude-longitude grid points are computed by a CDC 924 computer and electronically integrated with the video signal at the ground station. The grid points form latitude grid lines at 10° intervals and are composed of grid points at two degree intervals. The longitude grid lines are formed at ten degree intervals between 60°S to 60°N and are composed of grid points at two degree intervals. The longitude grid lines from 60°S and 60°N to the Poles are formed at 20 degree intervals and are composed of grid points at 5° intervals from 60° to 80° Colatitude.

An arrowhead pointing to the north appears near the vertical center of the picture at a latitude-longitude intersection. The latitude and longitude of the intersection appears at the left side of the picture. Latitude is indicated by the two upper digits followed by an "N" for north or "S" for south. Longitude is given by the three digits below followed by "E" for east or "W" for west. The longitude display does not appear at the Poles. Three tick marks are located at the center right of the picture. The longer tick mark in the middle positions the four hundredth line of the frame which is midway during the picture-taking interval. For all practical purposes this corresponds to the sensor scan through the subsatellite point. The time annotation at the bottom of the display is the time of the first scan line (top line) of the video display. The time of the 400th

scan line (defined by the longer tick mark) is obtained by adding 100 seconds to the time given at the bottom of the display. In the example shown (Figure 2-11) the arrowhead is located at 40°N and 166°W and the time (Universal) is 022 days (January 22), 11 hours, 31 minutes, 38 seconds.

2.5.2 IDCS Data Archiving and Access

The original 70 mm negatives are arranged in data orbit or swath format, i.e., sequential pictures of a single swath from pole to pole. The individual swaths, labeled by appropriate data orbit number are spliced together in orbit sequence. These negatives are reproduced under strict quality control standards on 70 mm roll film stock as both positive and negative transparencies. The transparencies, in 500-foot reels, will be forwarded to the National Weather Records Center (NWRC) in Asheville, North Carolina, for archiving. A 500-foot reel of film will contain approximately one week's IDCS coverage. Film data can be ordered from NWRC at cost of reproduction.

Reference to the Nimbus III monthly catalog containing daily IDCS montages and coverage will enable the user to determine his data requirements as to time and geographical location and in turn the particular swaths of data he requires. Orders and inquiries should be addressed to:

National Weather Records Center
ESSA
Federal Building
Asheville, North Carolina 28801

The following information should be included in correspondence or on orders:

1. Satellite, i.e., Nimbus III
2. Sensor, i.e., IDCS
3. Date
4. Swath Number
5. Positive or Negative Transparency

For the interim period between launch of Nimbus III and the issuance of the first Nimbus III Monthly Catalog, the GSFC, upon request, can make available Nimbus III IDCS film data in 70-mm copies on a limited and time available basis. As resources permit, limited quantities of data will be furnished to qualified investigators without charge.

Special requests for Nimbus III IDCS data during the interim period should be addressed to:

National Aeronautics & Space Administration
Goddard Space Flight Center
Nimbus Project, Code 450
Greenbelt, Maryland 20771

It is sufficient to indicate the date and specific geographical area of coverage for these special interim requests. 70-mm IDCS data can be made available in the following formats by swath:

Negative Transparencies
Positive Transparencies
Positive Contact Prints

SECTION 3

THE HIGH RESOLUTION INFRARED RADIOMETER (HRIR) EXPERIMENT

by
G. Thomas Cherrix and Lewis J. Allison
National Aeronautics and Space Administration
Goddard Space Flight Center

3.1 Introduction

The Nimbus High Resolution Infrared Radiometer (HRIR) was designed to perform two major functions: first, to map the Earth's cloud cover at night to complement the television coverage during the daytime portion of the orbit, and second, to measure the temperatures of cloud tops and terrain features. It is recommended that the user read the descriptions of previous HRIR Experiments in the Nimbus I and II User's Guides (References 1,2,3) and in the NASA Special Publication SP-89 titled "Observations From the Nimbus I Meteorological Satellite." (1966) (Reference 4).

The Nimbus III HRIR has been modified to allow nighttime and daytime cloud cover mapping by use of a dual band-pass filter which transmits 0.7 to 1.3 micron, as well as, 3.4 to 4.2 micron radiation. The improvement of detector temperature control and electronics compensation has eliminated the multiple calibrations of previous instruments.

A new tape recorder system provides play back only in the reverse direction, simplifying data reduction. More reliable time identification of data film strips is an important improvement. Nimbus III HRIR data users can order two types of film strips; Variable Density Exposure Film Strips as before, and Uniform Density Exposure Film Strips which were not available to Nimbus I and II data users.

3.2 Instrumentation

3.2.1 Radiometer

The single-channel dual band-pass scanning radiometer is shown in Figure 3-1. The detector is a lead selenide (PbSe) photoconductive cell which is radiatively cooled to, and controlled at 196°K (-77°C).

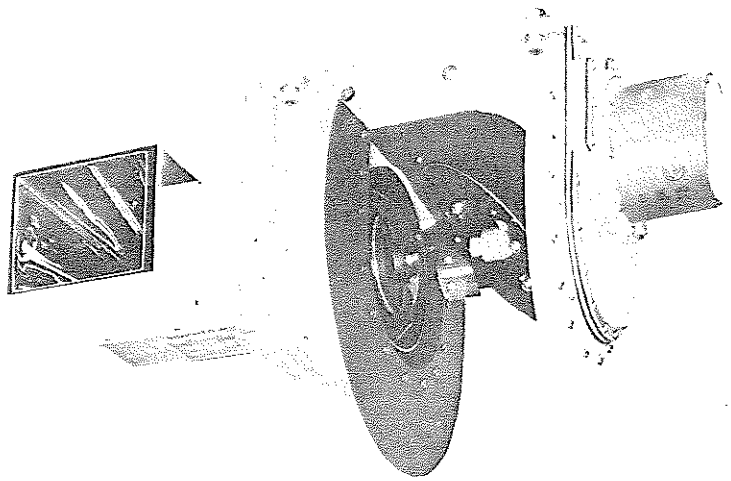

(a) The HRIR Scanner (4.8 kg)

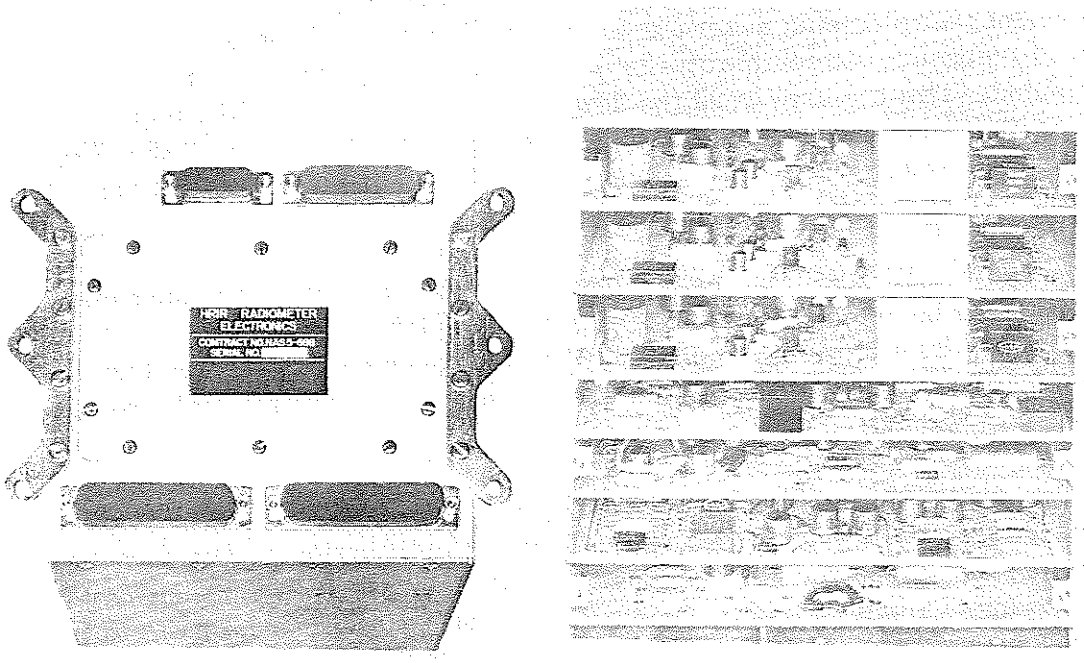

SEALED EXPOSED

(b) The HRIR Electronics Module (3.3 kg)

Figure 3-1—The High Resolution Infrared Radiometer

Nighttime operation is, as before, in the 3.4 to 4.2 micron near infrared "window" region. Daytime operation is based on the predominance of reflected solar energy in the 0.7 to 1.3 micron region. Change-over from nighttime to daytime operation (and vice versa) is accomplished automatically (or by a ground station command), by actuating a relay in the early stages of the radiometer electronics. The system gain is reduced in the daytime mode to compensate for the higher energy levels present. Separate calibrations are made for the two (2) modes of operation. (Section 3.3).

The white collars shown in Figure 3-1a are sunshields to prevent solar radiation from entering the radiometer during spacecraft sunrise and sunset. The scan mirror is located between the sunshields. The cylinder projecting from the end of the scanner contains the motor which drives both the scan mirror and chopper. The front of the pyramidal horn, which is part of the radiative cooling assembly, can be seen. The early stages of the electronics are located around this horn.

The radiometer, which weighs slightly over 8 kg (17.8 lbs.) and consumes 8 watts of electrical power, measures radiance temperatures between 210°K and 330°K with a noise equivalent temperature difference of 1°K for a 260°K background. The radiative cooling system is shown in Figure 3-2. Cooling is accomplished by means of a blackened cooling patch at the bottom of a highly reflective gold-coated pyramidal horn. The horn is oriented to view space during the entire orbit. The patch is thermally isolated from the housing and horn assembly by a 0.012 inch diameter wire suspension system. The detector is connected to the cooling patch by a high thermal conductance transfer bar.

Figure 3-3 illustrates the HRIR optical system. The scan mirror is inclined 45 degrees to the axis of rotation which is coincident with the spacecraft velocity vector (assuming no yaw or pitch attitude error). The optical scan path thus lies in a plane perpendicular to the orbital motion. Scan mirror rotation is such that, when combined with the velocity vector of the satellite, a right-hand spiral results. Therefore, the field of view scans across the earth from east to west in daytime and west to east at night, when the satellite is traveling northward and southward, respectively.

The radiation reflected from the scan mirror is chopped at the focus of a 4-inch f/1 modified Cassegrainian telescope. It is then refocused at the detector by a reflective relay system containing the dual band-pass filter.

The instantaneous field of view of the HRIR is approximately a square of 1/2 degree on a side. At an altitude of 1112 kilometers (600 nautical miles) this results in a subsatellite ground resolution of 8.5 kilometers (4.6 nautical

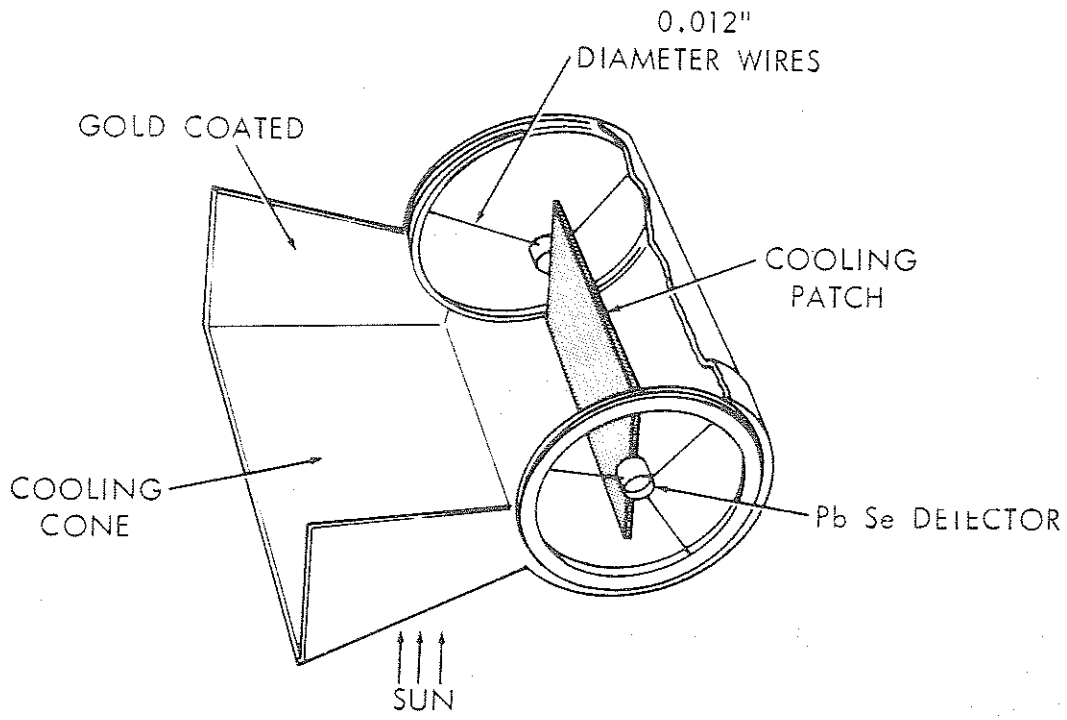

Figure 3-2–The HRIR Detector Cell Radiative Cooling System

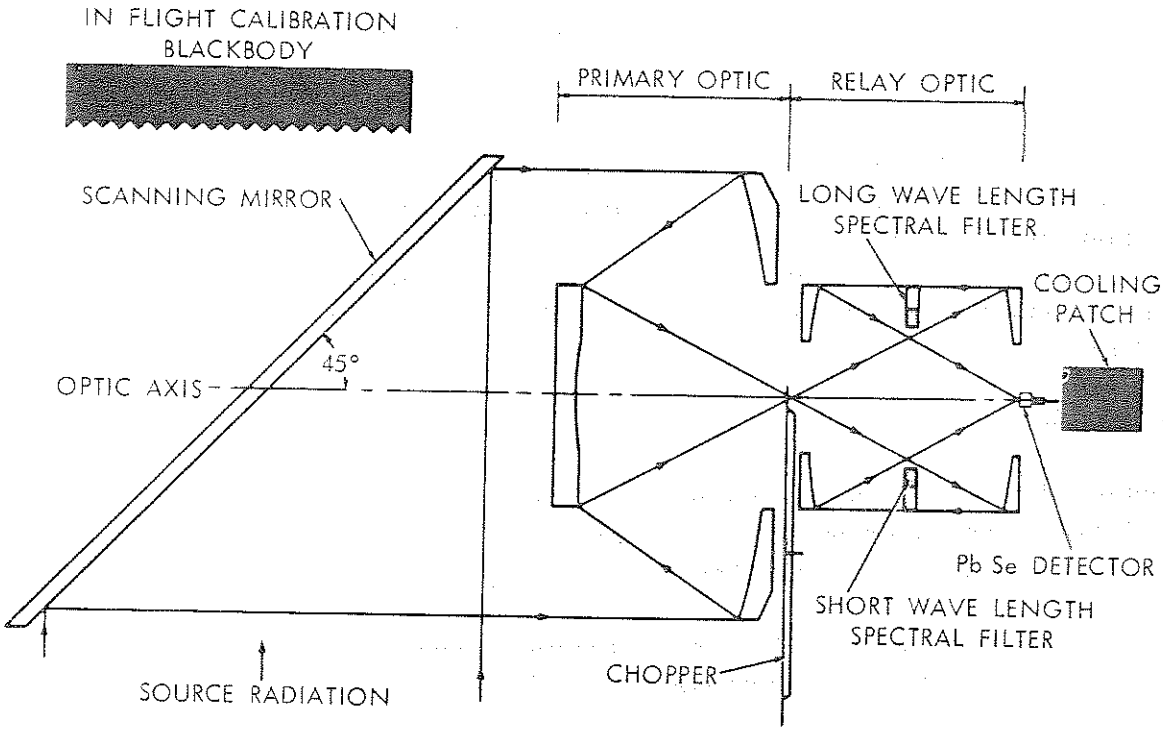

Figure 3-3–The Optical System of the Nimbus III HRIR

miles). The scan rate of 48 RPM produces contiguous coverage along the sub-satellite track. Due to the earth-scan geometry of the HRIR, as nadir angle increases, overlapping occurs between consecutive scans, reaching 350 percent overlap at the horizons, resulting in a loss of ground resolution in the direction of the satellite motion. Even greater loss of resolution occurs along the scan line (perpendicular to the line of motion of the satellite) because of the expansion, with increasing nadir angle, of the target area viewed.

Figure 3-4b gives graphically the relationship between nadir angle and ground resolution element size along the path of the satellite and perpendicular to it. Pictorially this is represented in Figure 3-4a. The numbers under each resolution element are nadir angle (in degrees), resolution along the scan line (in kilometer), and resolution parallel to the satellite line of motion (in kilometer). For example, at 50° nadir angle, the ground resolution element of the HRIR is a rectangle 35.2 kilometers long (approx. east and west) by 15.3 kilometers wide (approx. north and south).

In contrast to television, no image is formed within the radiometer: the HRIR sensor merely transforms the received radiation into an electrical (voltage) output with an information bandwidth of 0 to 350 cycles per second. The radiometer scan mirror continuously rotates the field of view of the detector through 360 degrees in a plane normal to the spacecraft velocity vector. The detector views in sequence the in-flight blackbody calibration target (which is a part of the radiometer housing), outer space, Earth, outer space, and returns again to intercept the calibration target. The space and housing-viewed parts of the scan, which can be identified without difficulty, serve as part of the in-flight check of calibration. Information on housing temperatures, which are monitored by thermistors, are telemetered to the ground stations and for calibration purposes are constantly compared with the temperatures obtained from the radiometer housing scan. The space scan serves as the zero reference point. During the first space sweep of each scan, a permanent magnet on the scan mirror gear triggers an electronic gate and a multivibrator so that seven pulses are generated. These pulses are used to synchronize automatic display equipment on the ground. During a portion of the housing scan, a series of voltage steps are substituted for the radiometer signal as a check of the telemetry system. A Visicorder oscillograph trace of a portion of a previous Nimbus analog record with a simulated Nimbus III stairstep calibration included, is shown in Figure 3-5.

3.2.2 Subsystem

A simplified block diagram of the HRIR Subsystem is given in Figure 3-6. The radiometer produces three (3) identical outputs (0 to -6 V.D.C.). Two (2)

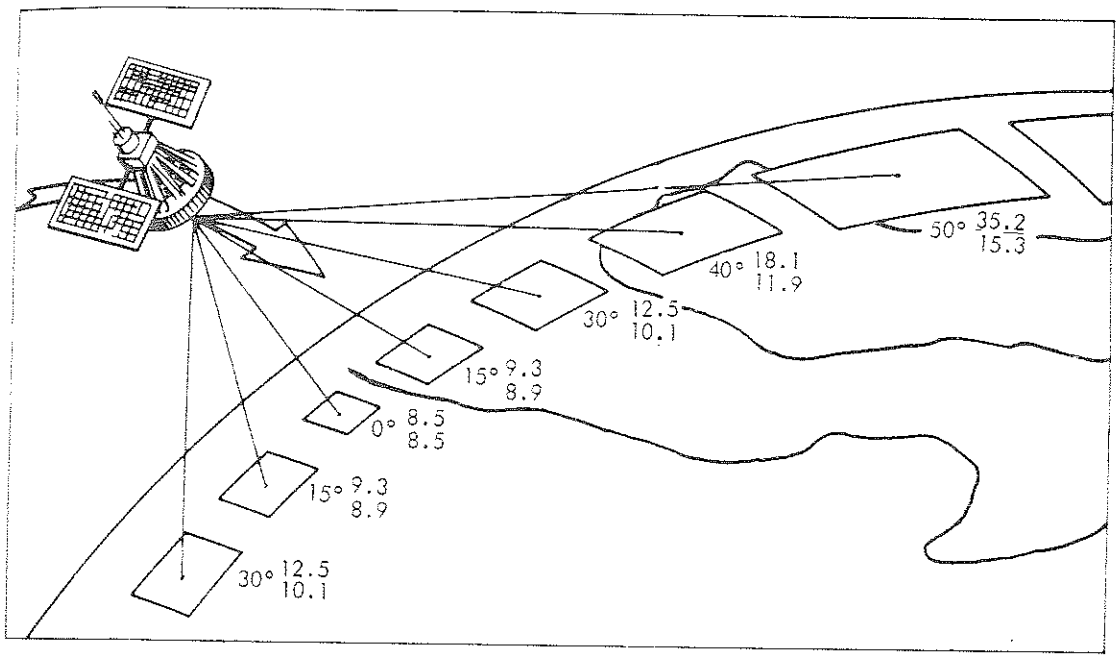

(a)

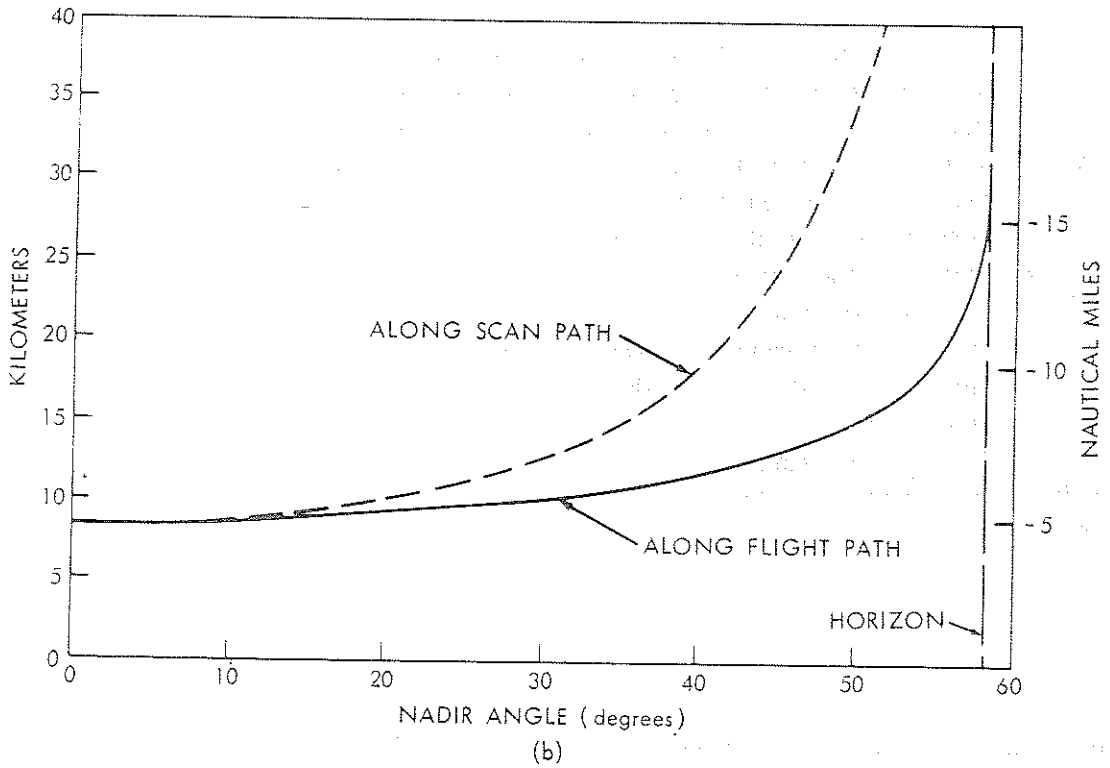

(b)

Figure 3-4–Relationship between Nadir Angle and Ground Resolution for the HRIR at 600 N. Miles a) Pictorial b) Graphical

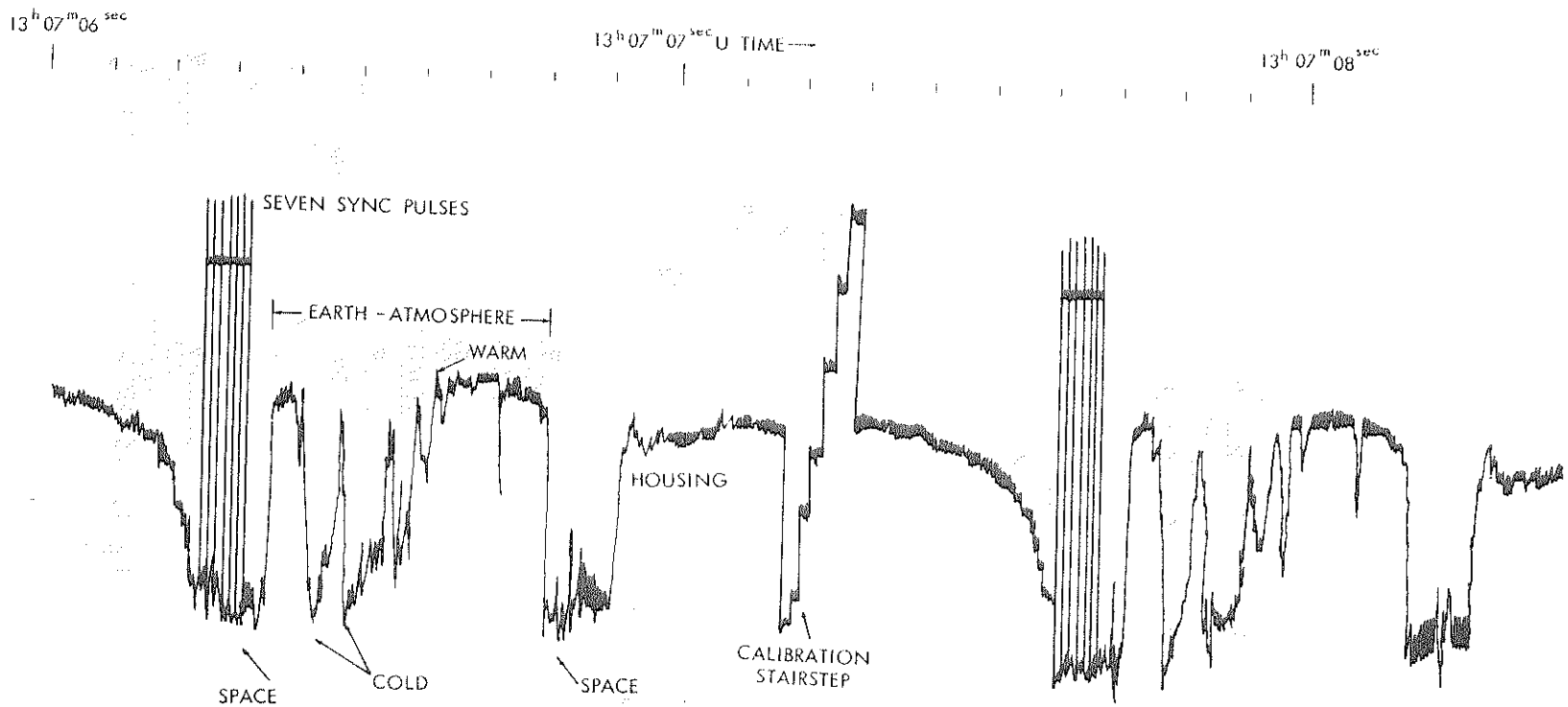

Figure 3-5–HRIR Visicorder Oscillograph Trace

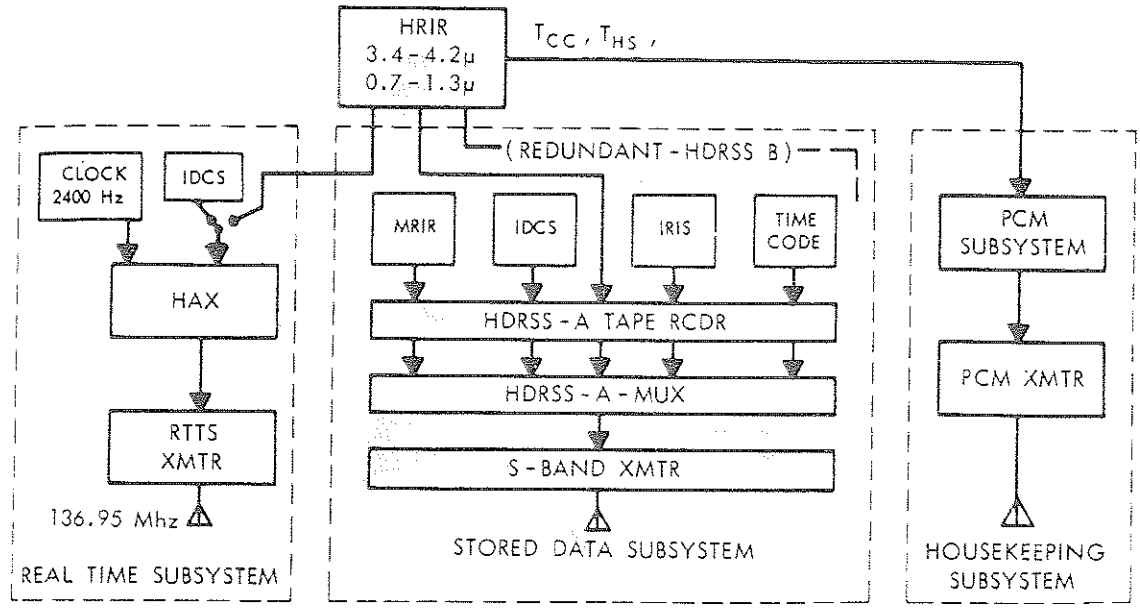

(a) Spacecraft Data Flow

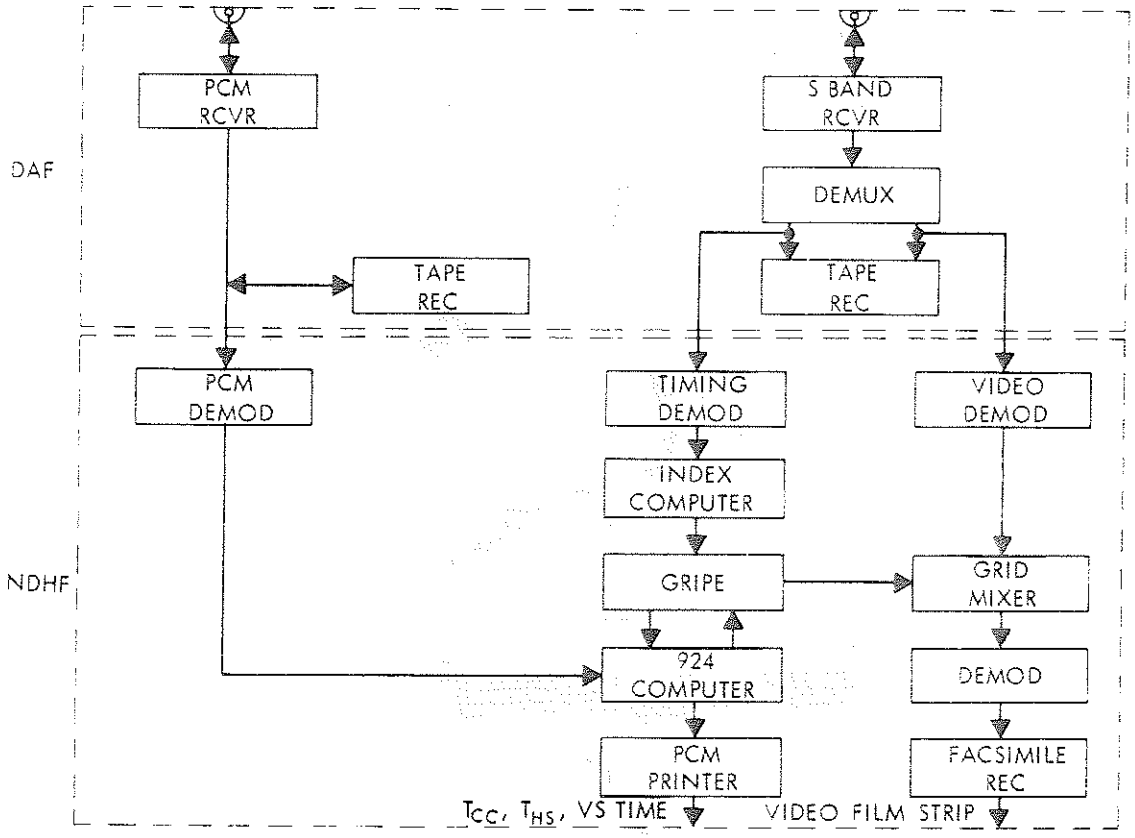

(b) Ground Data Flow

Figure 3-6–Simplified Block Diagram of the HRIR Subsystem

of these are routed to separate tape-recorder subsystems (High Data Rate Storage Subsystems HDRSS "A" and "B") and the third called Direct Readout Infrared Radiometer (DRIR) is broadcast in real time through the Real Time Transmission System.

3.2.2.1 Stored Data

The HRIR records on one track of the 5 track HDRSS tape recorder subsystem along with IDCS, MRIR, IRIS, and the time code. There are two (2) similar HDRSS's in the spacecraft for increased reliability and data coverage.

The varying D.C. voltage from the HRIR modulates a VCO (voltage controlled oscillator) between 2.3 kHz and 3.16 kHz and is recorded on the HDRSS tape recorder. Upon command the recorder plays back (in reverse) thirty-two (32) times faster into one channel of the multiplexer (MUX). The signal is doubled and beat against an 850 kHz local oscillator, producing a 702.8 kHz to 647.76 kHz FM signal. This is directed into the S-Band transmitter and broadcast to the Data Acquisition Facility (DAF) along with the Time Code, MRIR, IDCS, and IRIS frequencies.

3.2.2.2 Direct Readout Infrared Radiometer (DRIR)

The HRIR Real-time Transmission Subsystem (RTTS) is shared with IDCS (Section 9). Generally Real Time IDCS (DRID) data will be broadcast in daytime and DRIR data in nighttime. On a few selected occasions Real Time DRIR data will be transmitted in daytime to evaluate the daytime HRIR (0.7-1.3 micron) experiment.

The HRIR output is channeled into a mixer-modulator (HAX) where it amplitude modulates a 2400 Hz signal from the spacecraft clock. This subcarrier in turn frequency modulates a 136.95 MHz transmitter which broadcasts continuously.

3.3 Calibrations

The operation of the Nimbus III HRIR at night is similar to previous instruments since only negligible quantities of short wavelength radiation are detected and the response of the instrument is essentially limited to the 3.4 to 4.2 micron region. Section 3.3.1 covers the nighttime calibration procedures and results for the Nimbus III flight instrument.

In daytime, radiation is sensed in three discrete spectral intervals (see Figure 3-7 following), and a single calibration curve of albedo vs. output cannot be obtained directly. However, cloud-cover maps of high reliability are produced. Section 3.3.2 covers the daytime calibration procedures and results for the Nimbus III flight instrument.

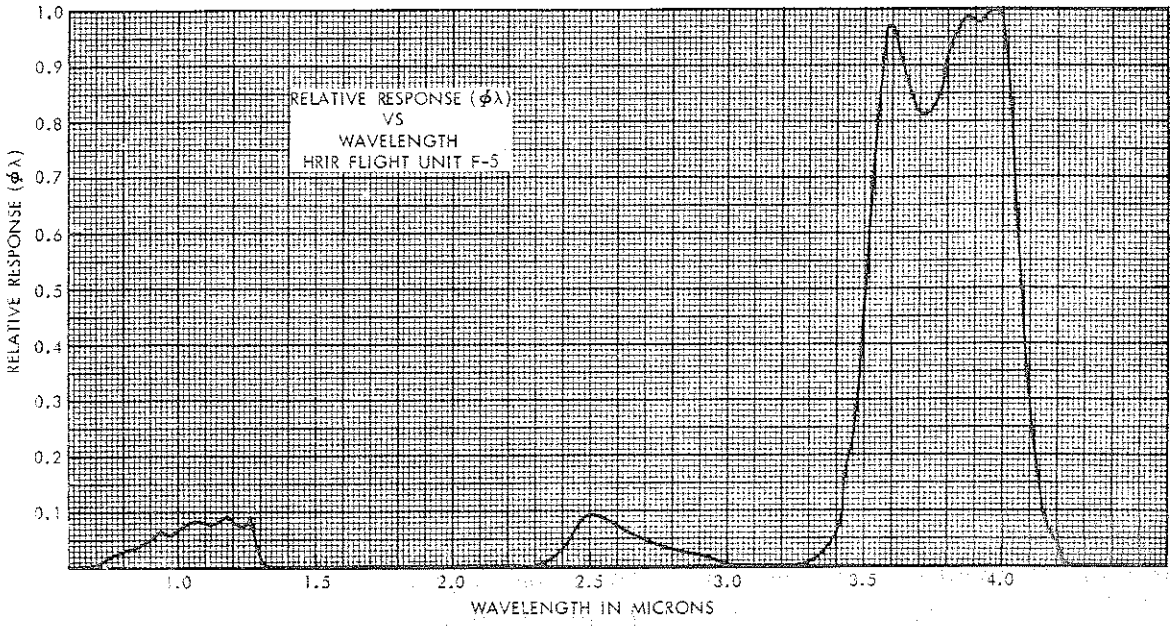

Figure 3-7—Effective HRIR Spectral Response of the Radiometer

3.3.1 Nighttime Calibration (3.4-4.2 microns)

In discussing the calibrations, three fundamental quantities must be defined: the effective spectral response, ϕ_λ; the effective radiance, $\bar{N}$; and the equivalent blackbody temperature, T_{BB}.

3.3.1.1 Effective Spectral Response

The radiation received by the radiometer is reflected by three frontsurface aluminized mirrors, two frontsurface gold-coated mirrors, and transmitted through a filter before reaching the coated PbSe detector. The effective spectral response, ϕ_λ, is defined as $\phi_\lambda = R_\lambda f_\lambda D_\lambda$ where R_λ is the combined spectral reflectivity of all five frontsurface mirrors, f_λ is the spectral transmittance of the filter and D_λ is the relative spectral response of the detector.

The materials used in the optics are given in Table 3-1. The function f_λ was calculated from laboratory measurements of the components used in HRIR unit F-5, the Nimbus III instrument. The functions D_λ and R_λ were calculated from typical laboratory curves. The effective spectral response is given in Figure 3-7.

Table 3-1
Nimbus III HRIR Optical Components

Filter
- Nighttime Section (3.4 to 4.2 microns)
  - Type: Multilayer wide band-pass interference
  - Substrate: Germanium
  - Area: 85% of aperture
- Daytime Section (0.7 to 1.3 and 2.5 microns)
  - Type: Multilayer wide band-pass interference
  - Substrate: Glass
  - Area: 15% of aperture

Scan Mirror
- Type: Evaporated SiO over hard-coated aluminum
- Substrate: Aluminum

Cassegrainian Telescope (Primary and Secondary)
- Type: Front-surface Al with SiO over-coating
- Substrate: Glass

Relay Optics
- Type: Front-surface Au with SiO over-coating (two surfaces)
- Substrate: Glass

Detector
- Type: Evaporated Lead Selenide (PbSe)
- Sensitive Area: 0.695 mm × 0.695 mm

3.3.1.2 Effective Radiance

Because of its narrow field of view, the HRIR essentially measures beam radiation or radiance toward the satellite along the optical axis. In the preflight laboratory calibration, the field of view of the radiometer was filled by a blackbody target whose temperature could be varied and accurately measured over a range of 190°K to 340°K. From the temperature of the blackbody target, T_{BB}

the spectral radiance of the target is determined by the Planck function, B_λ. The integration of this function over the effective spectral response, ϕ_λ, yields that portion of the radiance of the target to which the radiometer responds, the "effective radiance, $\overline{N}$," given by

$$\overline{N} = \int_0^\infty B_\lambda (T_{BB})\ \phi_\lambda d\lambda \tag{3}$$

3.3.1.3 Equivalent Blackbody Temperature

The effective radiance to which the orbiting radiometer responds may be expressed by

$$\overline{N} = \int_0^\infty N_\lambda \phi_\lambda d\lambda \tag{4}$$

where N_λ is the spectral radiance in the direction of the satellite from the Earth and its atmosphere. It is convenient to express the measurement from orbit in terms of an equivalent temperature of a blackbody filling the field of view which would cause the same response from the radiometer. From Equations 3 and 4 it is seen that this "equivalent blackbody temperature" corresponds to the target temperature, T_{BB}, of the blackbody used in the laboratory calibration. This relationship is expressed schematically in Figure 3-8. Therefore, the radiometer measurements can be expressed either as values of effective radiance, $\overline{N}$, or as equivalent blackbody temperatures, T_{BB}. The $\overline{N}$ versus T_{BB} function from Equation 3 is given in Figure 3-9 and Table 3-2.

Figures 3-10 through 3-12 are the calibration curves for the HDRSS "A", HDRSS "B", and DRIR subsystems. Each graph contains curves for 10°C, 25°C, and 35°C electronic module temperatures. The D.C. volts scales refer to the "stair step" levels (section 3.2.1) inserted in the backscan portion of each scan, and data samples should be interpolated between the appropriate pair of these steps. However the zero step is affected by conditions on the spacecraft and the true zero step should be estimated by extrapolating beyond the two-volt and one-volt steps. This method is more accurate than using the "demodulated output frequency" scale (right-hand axes).

3.3.2 Daytime Calibration

A diffuser is placed in front of a lamp and filter system and the light level is varied from zero to the equivalent of that from a "bright" cloud (approx. 75% albedo). Several neutral filters are inserted to reduce the intensity of the energy

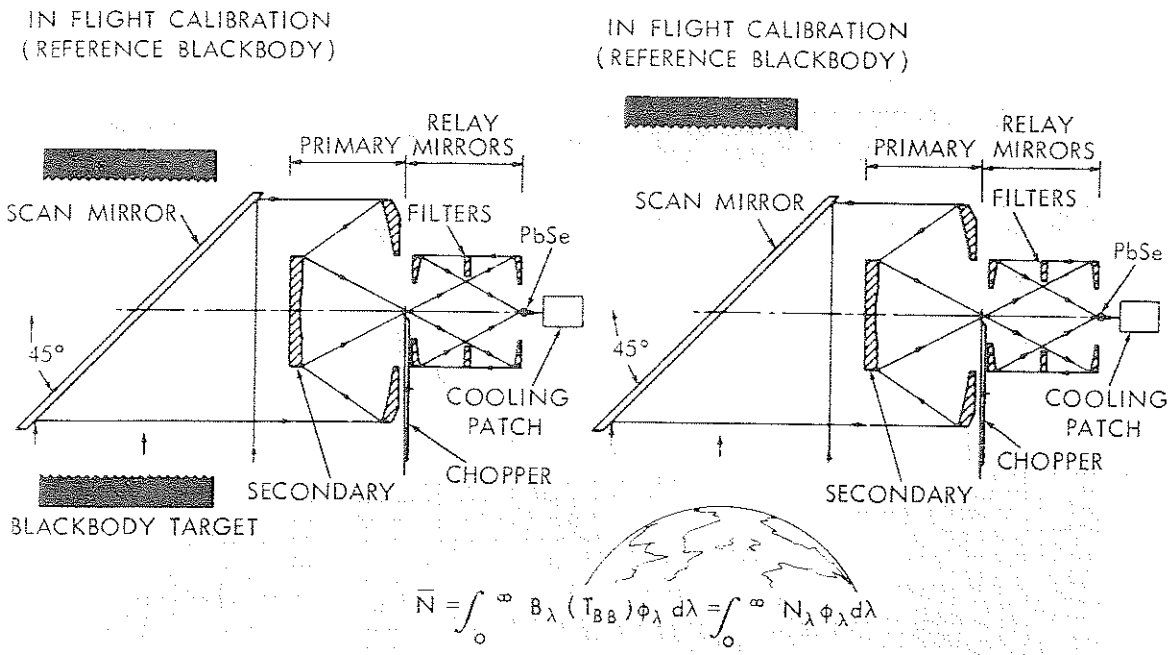

Figure 3-8—Schematic Illustration of the Relationship between Laboratory Calibration and T_{BB} Measurements made in Orbit at Night

Table 3-2
Effective Radiance ($\bar{N}$) vs Equivalent Blackbody Temperature (T_{BB})
for HRIR Flight Unit F-5

T_{BB} Degrees Kelvin	$\bar{N}$ Watts/Meter^2·Ster	T_{BB} Degrees Kelvin	$\bar{N}$ Watts/Meter^2·Ster
180	7.230×10^{-5}	270	6.950×10^{-2}
190	2.126×10^{-4}	280	1.139×10^{-1}
200	5.624×10^{-3}	290	1.806×10^{-1}
210	1.358×10^{-3}	300	2.776×10^{-1}
220	3.030×10^{-3}	310	4.154×10^{-1}
230	6.311×10^{-3}	320	6.063×10^{-1}
240	1.238×10^{-2}	330	8.650×10^{-1}
250	2.302×10^{-2}	340	1.209
260	4.085×10^{-2}	350	1.658

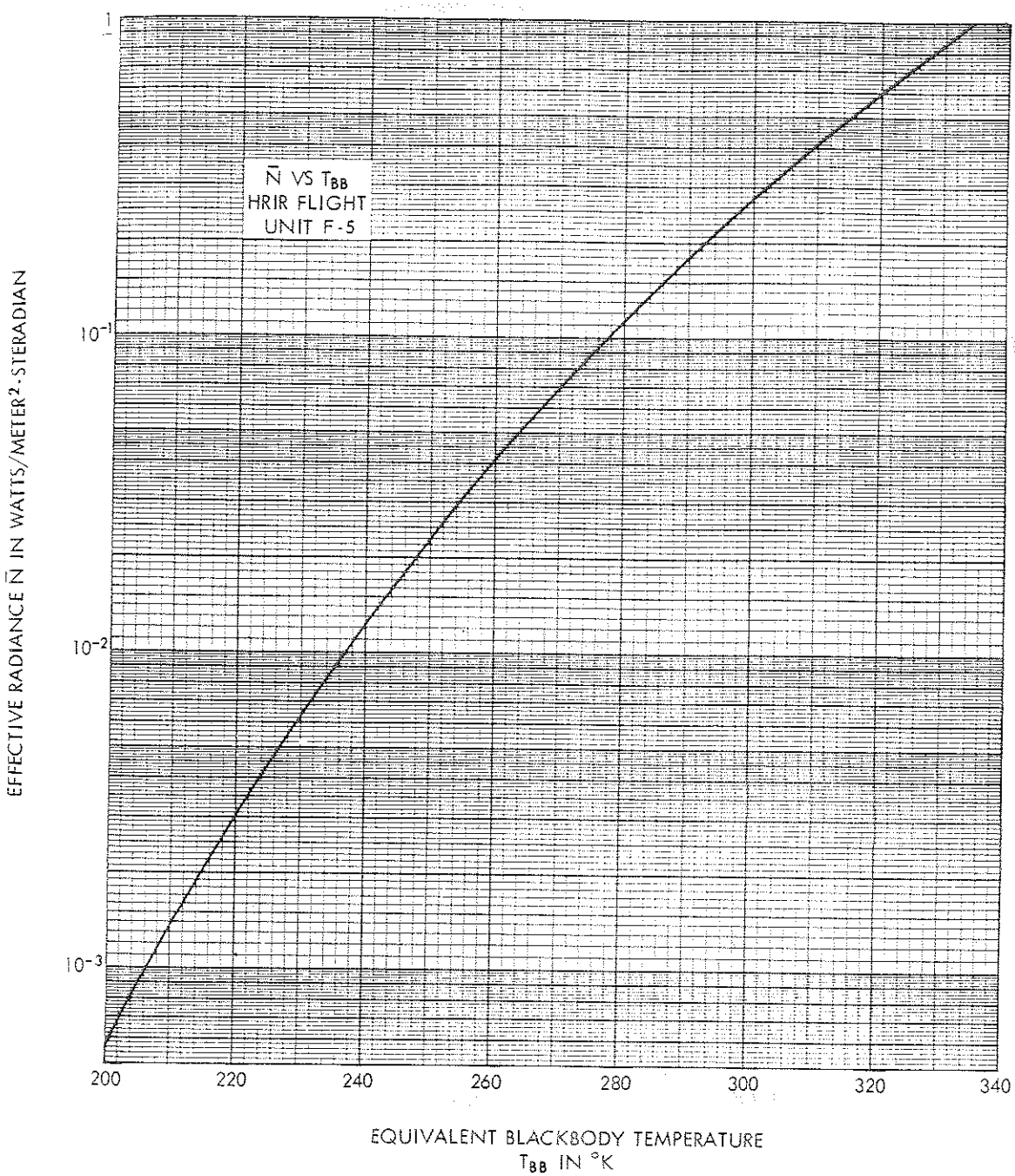

Figure 3-9–Effective Radiance $\bar{N}$ versus the Blackbody Temperature T_{BB}

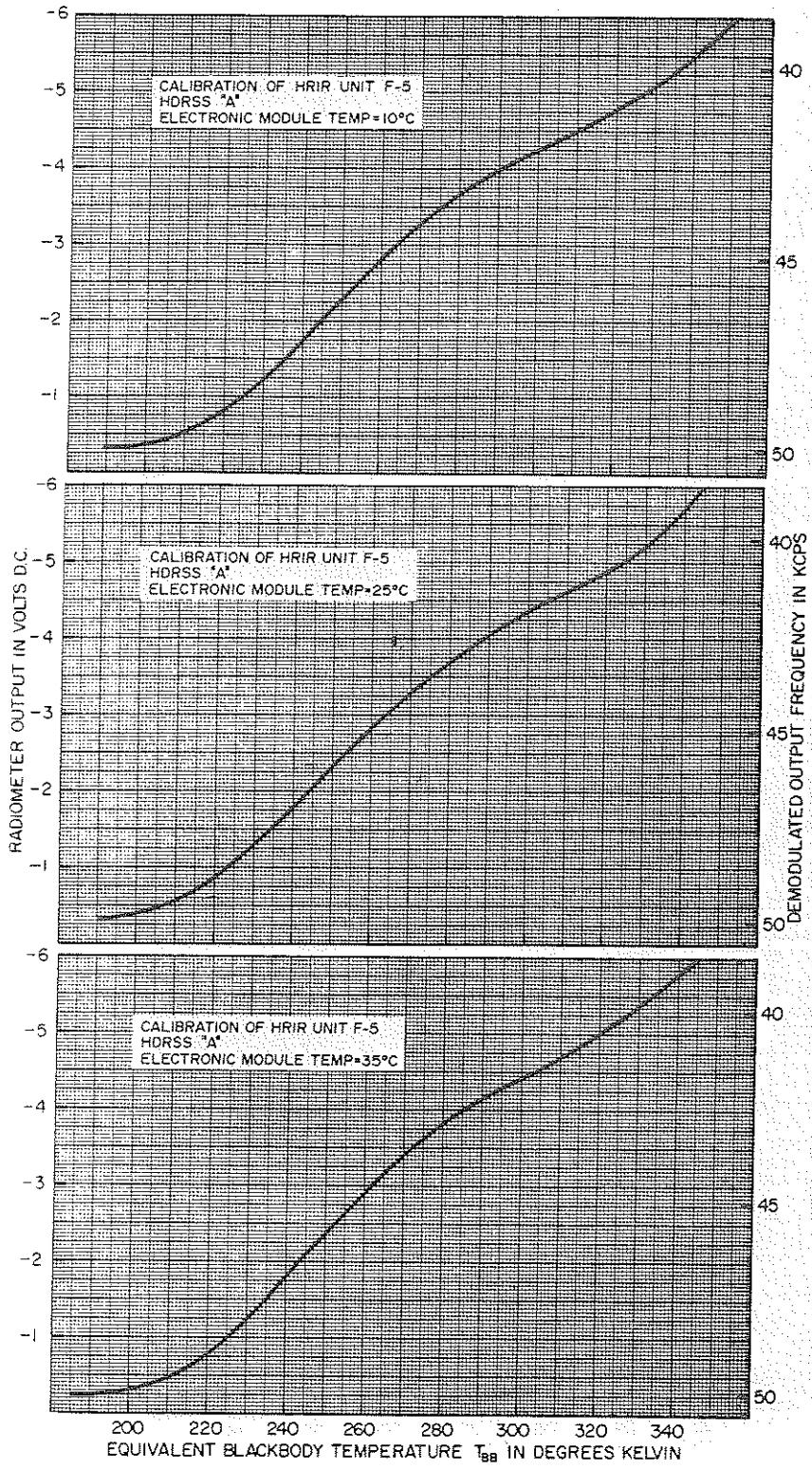

Figure 3-10–Calibration Data for the HRIR Unit F-5 Valid for Data Recorded by HDRSS "A" at 10°C, 25°C, 35°C Electronic Module Temperatures.

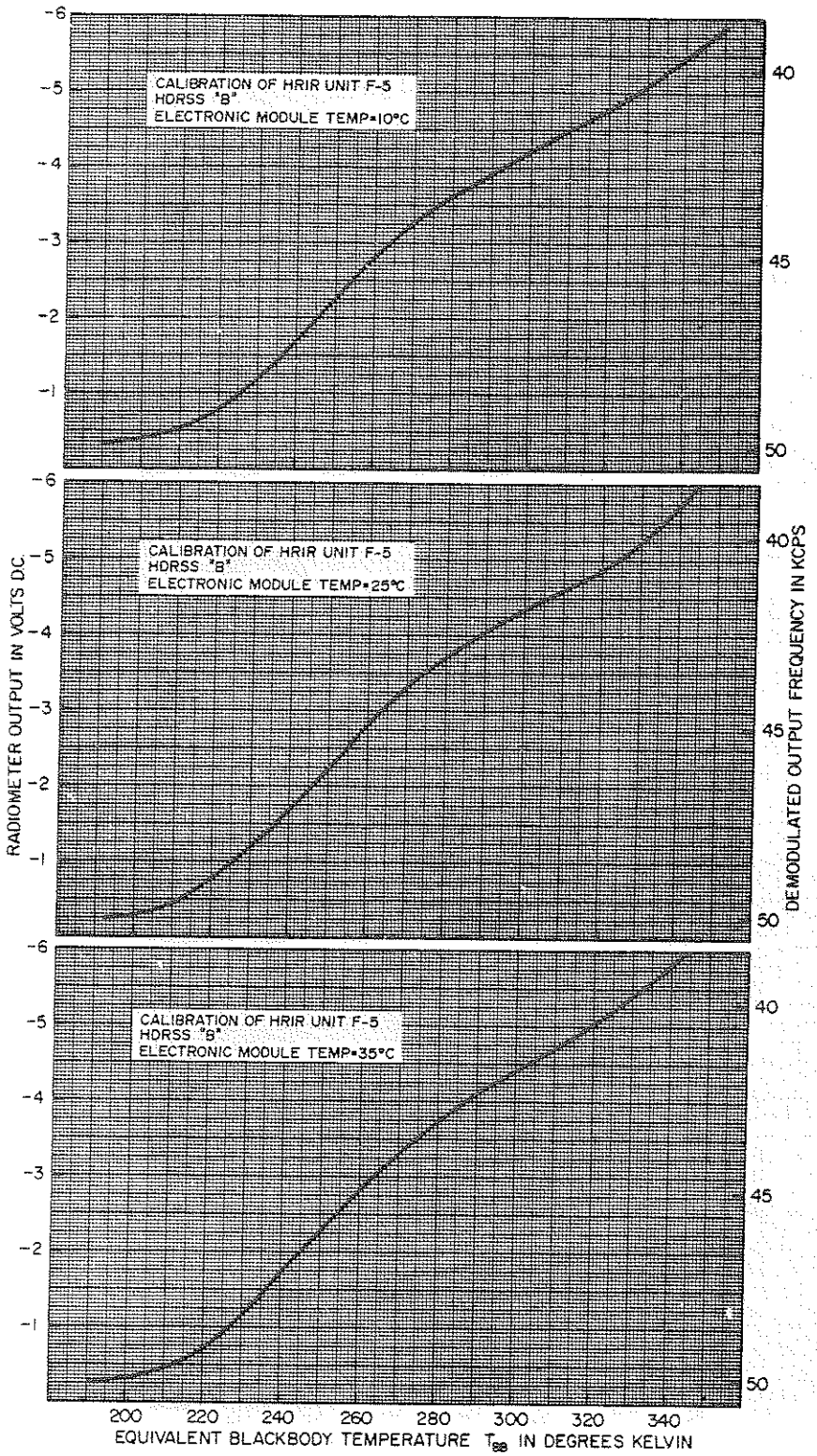

Figure 3-11–Calibration Data for the HRIR Unit F-5 Valid for Data Recorded by HDRSS "B" at 10°C, 25°C, 35°C Electronic Module Temperatures.

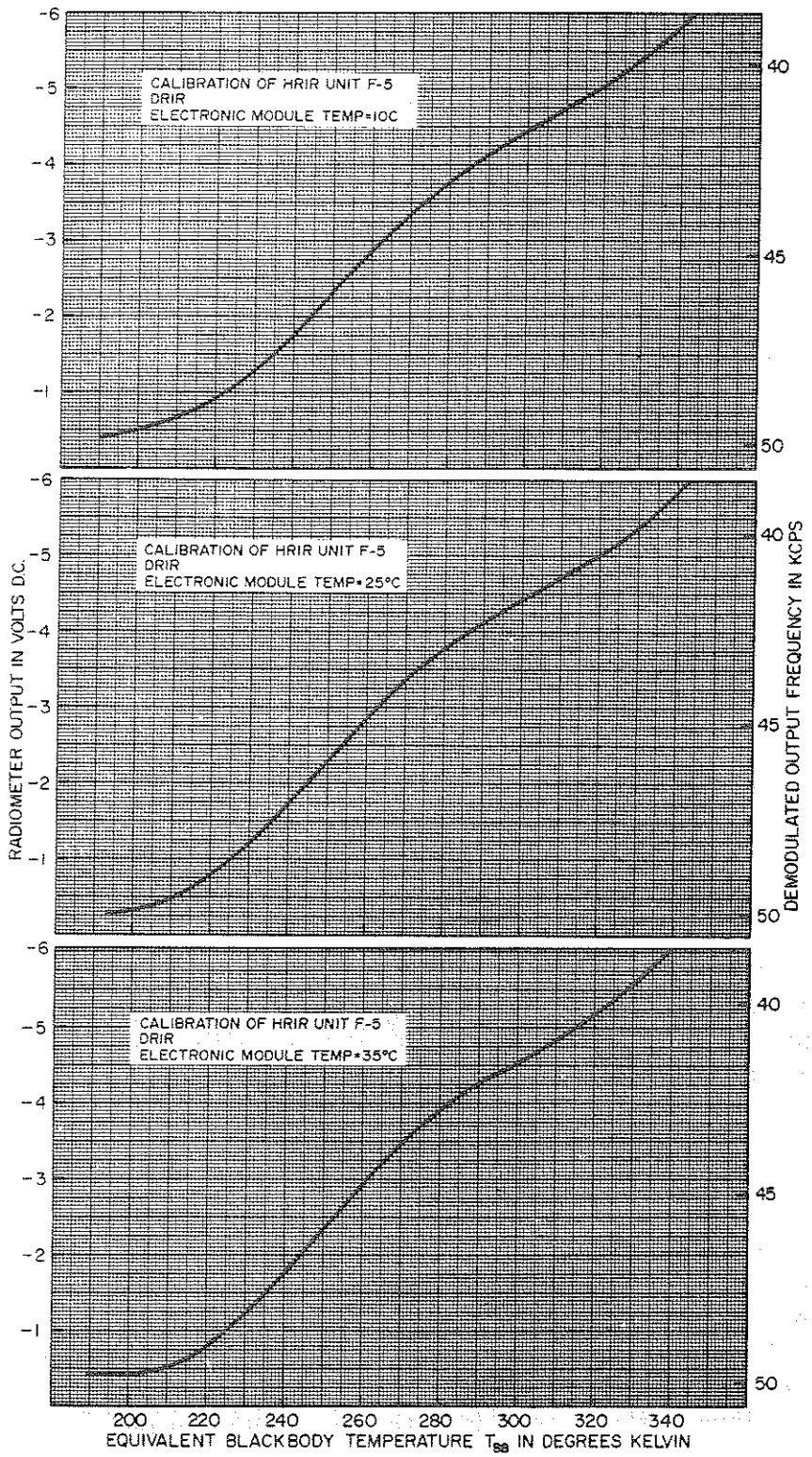

Figure 3-12–Calibration Data for the HRIR Unit F-5 Valid for Data Recorded by the DRIR at 10°C, 25°C, 35°C Electronic Module Temperatures.

reaching the radiometer. The diffuser is made of glass, which is opaque in the 3 to 4 micron region. Hence, it emits nearly blackbody radiation in the long wavelength portion of the HRIR's response. This signal is added into that from the lamp and filter system producing a compounded output.

A similar situation exists at the satellite. The solar radiation reflected from a cloud produces a signal primarily in the short wavelength band-pass of the instrument, while the thermal emission of the cloud produces an additional signal in the long wavelength band-pass of the instrument. Figure 3-13 depicts schematically the relationship between the laboratory calibration and measurements in orbit. The combination of these two components produces a given output signal from the radiometer. This is expressed mathematically by

$$\overline{N} = \int_0^\infty N_s(\lambda)\,\phi(\lambda)\,d\lambda + \int_0^\infty N_E(\lambda)\,\phi(\lambda)\,d\lambda \qquad (5)$$

where $N_s(\lambda)$ = spectral radiance due to reflected and backscattered solar radiation at the top of the atmosphere in the direction of the satellite.

$N_E(\lambda)$ = spectral radiance due to thermal emission from the earth-atmosphere system emerging at the top of the atmosphere in the direction of the satellite.

and $\phi(\lambda)$ = the effective spectral response of the instrument.

The filters of the HRIR were designed to cause the reflected solar radiation component (the first term in Equation (5)) to be larger than the thermal emission component (the second term in Equation (5)) by more than an order of magnitude under the expected conditions of the earth-atmosphere system. Therefore, except for situations involving very warm emitting surfaces having low reflectances, the daytime measurement can be interpreted approximately in terms of reflected short-wavelength radiation alone, within an accuracy of 10% or less.

For example, from a warm surface having a temperature slightly greater than 300°K and a relatively low reflectance (such that the equivalent blackbody temperature due to emission measured at the satellite through clear skies in an atmospheric window is 300°K and the reflectance of solar radiation measured at the satellite corresponds to a surface illuminated by the solar constant at normal incidence and having a diffuse reflectance of 20%) the contribution of the first term in Equation (5) would be

$$N_S = 2.06\ W \cdot M^{-2} \cdot Ster^{-1}.$$

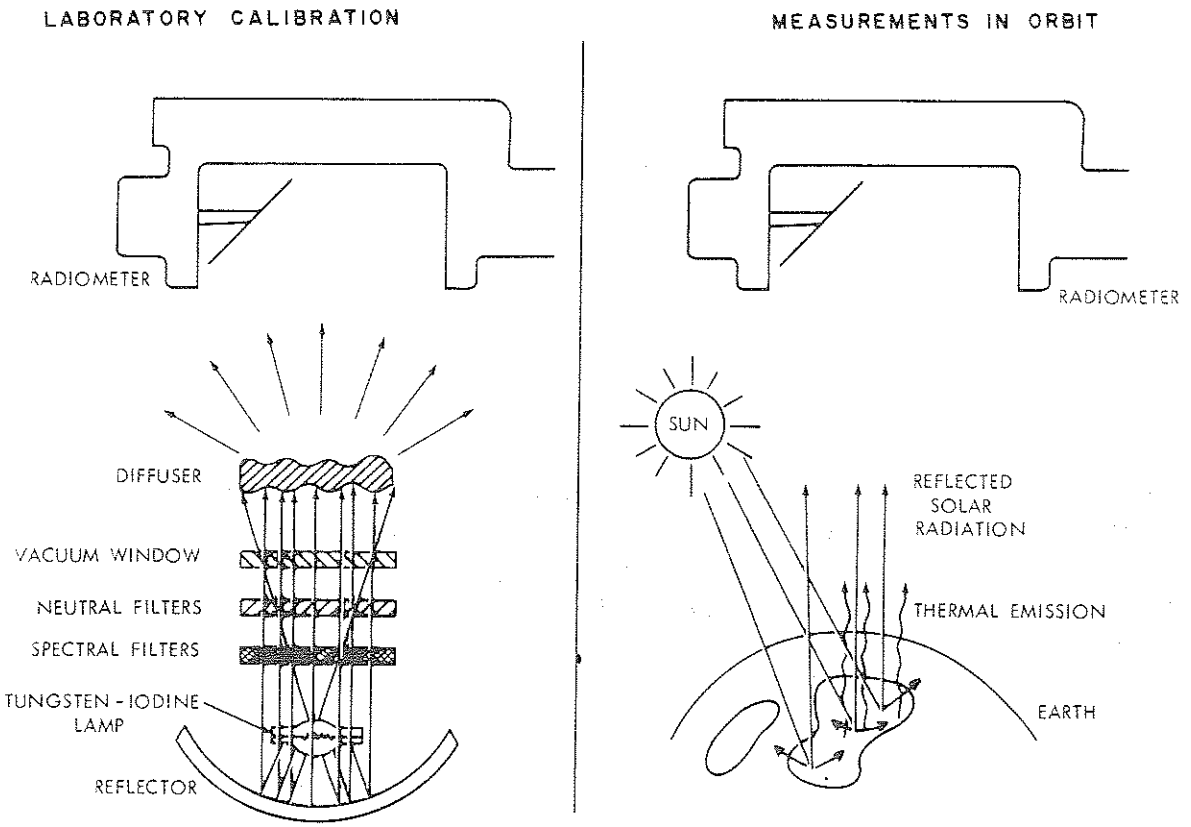

Figure 3-13—Schematic Illustration of Relationship Between Laboratory Calibration and Daytime Measurements in Orbit

whereas the contribution of the second term (emission) would be about 14% of N_s, or

$$N_E = 0.28\ W \cdot M^{-2} \cdot Ster^{-1}.$$

On the other hand, for a diffusely reflecting cloud under similar atmospheric conditions and normal incidence of the sun (such that the corresponding equivalent blackbody temperature and reflectance values are 275°K and 50% respectively), the contribution of the first term in equation (5) would be

$$N_s = 5.14\ W \cdot M^{-2} \cdot Ster^{-1}.$$

whereas the contribution of the second term would be less than 2% of N_s or

$$N_E = 0.089\ W \cdot M^{-2} \cdot Ster^{-1}.$$

The daytime calibration data have not been fully evaluated as of the printing of this guide, and will be presented in a forthcoming Nimbus III data catalog.

It must be emphasized that the primary purpose in modifying the spectral response of the HRIR was to improve its daytime cloud-cover mapping capabilities by producing measurement primarily of reflected solar radiation, thus eliminating the ambiguities that sometimes arose in attempting to distinguish between highly reflecting clouds and warm land and water surfaces sensed solely in the 3.4 to 4.2 micron region with the Nimbus I and II HRIR experiments.

3.4 Data Processing, Archiving and Availability

Nimbus III HRIR data are available from the NSSDC in three (3) general forms: Photofacsimile film strips (Figure 3-14a); computer processed digital data shown in Figure 3-17, and raw analog records (Figure 3-14b). The film strips are separated into two (2) files, one for daytime data swaths, and one for nighttime data swaths. The user has the choice of ordering these film strips as Uniform or Variable density exposure, positive or negative copies in either a transparency or paper print.

The form of data most readily available to the user is the film strip.

Computer processing of the complex and voluminous data however, will be accomplished whenever requested by a user, as indicated in Section 3.4.2. The analog data records require a comprehensive knowledge of the HRIR subsystem for interpretation and reduction. The format of the analog data display makes it practical only for studies requiring extreme accuracy and detail over small areas.

Nimbus III HRIR data are always produced in the reverse mode, i.e., the data are read out with the tape traveling in the opposite direction from that in which it traveled while data were recorded. This is a departure from previous Nimbus HRIR data which were produced in both forward and reverse direction.

3.4.1 Photofacsimile Film Strips

At the Data Acquisition Facility (DAF), the HRIR information is demultiplexed and recorded on magnetic tape. It is then transmitted to the Goddard Space Flight Center, where the FM signal is demodulated, synchronized, and displayed by a photofacsimile recorder. The facsimile recorder converts the radiometer output signals into a continuous strip picture, line by line, on 70 mm

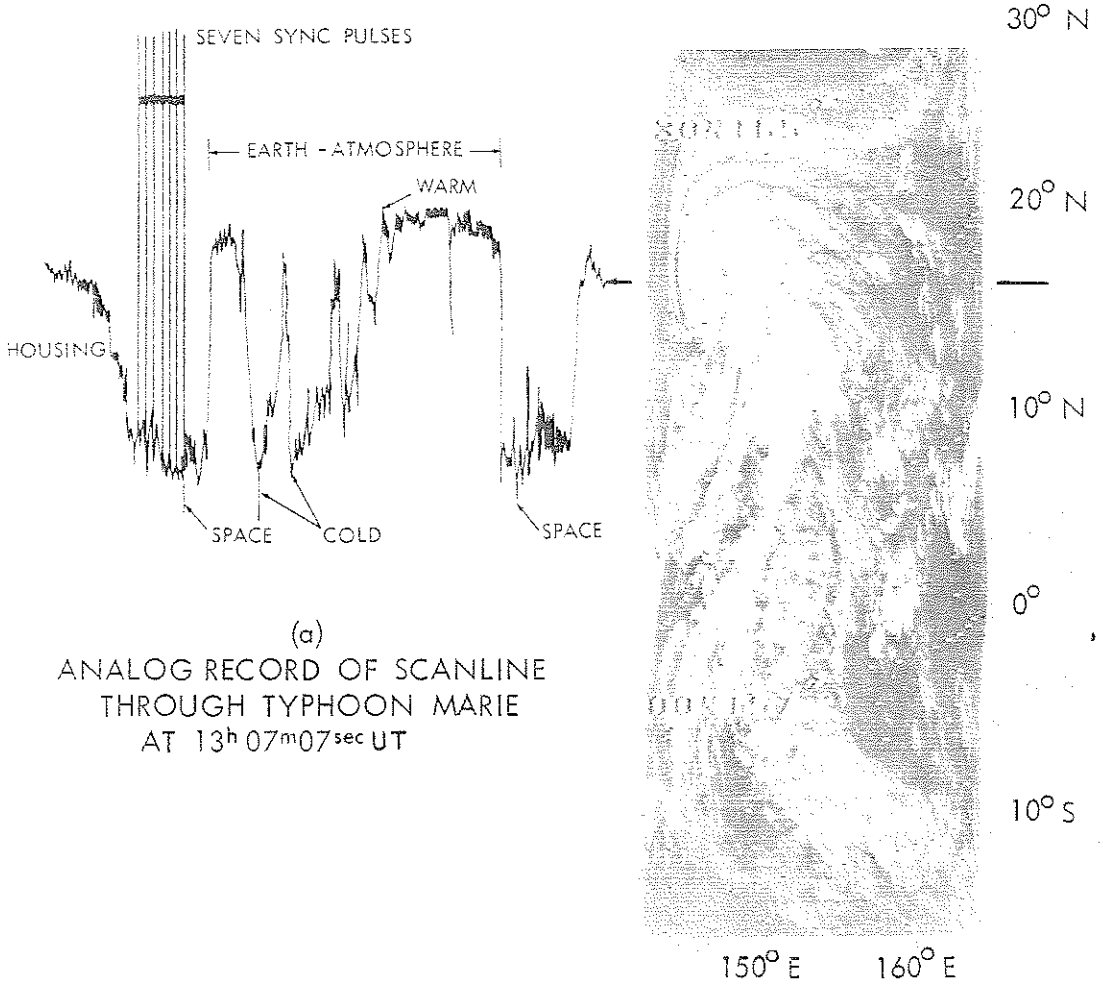

(a)
ANALOG RECORD OF SCANLINE
THROUGH TYPHOON MARIE
AT $13^h\ 07^m07^{sec}$ UT

(b)
FILM STRIP OF
TYPHOON MARIE
NIMBUS II HRIR
D/O 2266
Nov. 1, 1966

Figure 3-14– Nimbus II HRIR Visicorder Analog Record and Photofacsimile Film Strip

film. Blanking circuits in the recorder reject unwanted sections of each scan line. Only the Earth scan and, for calibration purposes, very small portions of the space scan are recorded on the film strip. Daytime and nighttime data will be split and separate files compiled for user convenience. All of the HRIR data are available on photofacsimile film strips.

Figure 3-14b is a typical example of a portion of an orbital film strip exhibiting the fully developed typhoon "Marie" of 1966. The vortex center (located near 22°N 152°E) is marked by a cirrus canopy which obscures the eye. The convective inflow spiral bands are well pronounced and can be distinguished from the thinner and more diffuse cirrus outflow streamers. A large number of structural details can be seen in this photo display, but the distortions at the sides of the film strip obscure part of the storm.

3.4.1.1 Photographic Processing of Film Strips

The original photofacsimile film strips are processed and reproduced by the NDUC photographic laboratory and archived at the NSSDC for safe and permanent storage. The copy is then used as a master for producing all film strips requested by the user.

Two (2) types of film strips are available to the Nimbus III HRIR data user: Uniform Density Exposure Film Strips (Section 3.4.1.1.1), and Variable Density Exposure Film Strips (Section 3.4.1.1.2). Variable Density Exposure film strips are produced with enhanced contrast and a nearly uniform average density, while uniform density exposure film strips are true copies of the archived HRIR film strip. Therefore, EQUIVALENT BLACKBODY TEMPERATURES CAN ONLY BE OBTAINED FROM UNIFORM DENSITY EXPOSURE FILM STRIPS. Be sure to request the proper type of film strips for the intended use. Nimbus I and II HRIR film strips released to the users were all Variable Density Exposure type.

3.4.1.1.1 Uniform Density Exposure Film Strips

The un-altered master film strip copies are used for making true reproductions of the HRIR data. No photographic exposure altering techniques are employed in producing these film strips. Therefore, using the included grey scales (Section 3.4.1.1.4), a good quality densitometer, and proper care, equivalent blackbody temperatures can be obtained from this type of film strip.

3.4.1.1.2 Variable Density Exposure Film Strips

Because of the wide range of average surface temperatures over various regions of the earth, small temperature differences are not prominent in the

HRIR film strips. The polar areas appear overexposed, while the equatorial areas appear underexposed (for positive film strips). Therefore, the contrast between warm and cool surfaces within a given area is small. In order to produce high contrast, e.g. between low clouds and ocean surface, exposure controlling techniques can be used in reproducing the film strips. The Variable Density Exposure process darkens the cold regions and lightens the warm regions so that the average film density over the entire orbit is held nearly constant. This allows increased contrast over small temperature ranges. Hence, clouds, ocean currents, coastlines, mountain peaks, etc., "stand out" producing a better "picture." Experience has shown that prints produced by this process are far superior to those produced in the Uniform Density Exposure mode for all uses except where actual temperatures are to be derived from film strip density measurements. (Section 3.4.1.1.1).

3.4.1.1.3 Positive and Negative Film Strips

The film strips are available in positive and negative copies. In the positive copy of nighttime data, higher temperatures are indicated by darker areas. Hence the colder clouds appear white as in television pictures. The opposite is true of the negative copies. The daytime response of the HRIR is, in effect, opposite the nighttime response – that is, higher energy levels are received from clouds in daytime and from land and water in nighttime. Hence, negative film strip copies of daytime data resemble television pictures as do positive film strip copies of nighttime data.

3.4.1.1.4 Daytime and Nighttime Data Swaths

The orbital film strips are separated into daytime and nighttime swaths. Each swath is indexed appropriately and separately archived. Hence, the user must order both a daytime swath and a nighttime swath to obtain one entire orbit of data.

Due to the conditions explained in Section 3.4.1.1.3, the user who wishes to obtain film strips in which clouds appear white and land and water appear black must order positive copies of nighttime data and negative copies of daytime data.

3.4.1.1.5 Grey Scale Calibration

The photofacsimile recorder is provided with the means for automatically producing a ten-step calibration gray scale wedge (Figure 3-15). Progressive voltage levels, from a manually adjusted ten-step potentiometer network, are sequentially selected by a ten-step motor driven cam operated by a timed program selector switch and are recorded on the film. The ten voltage levels

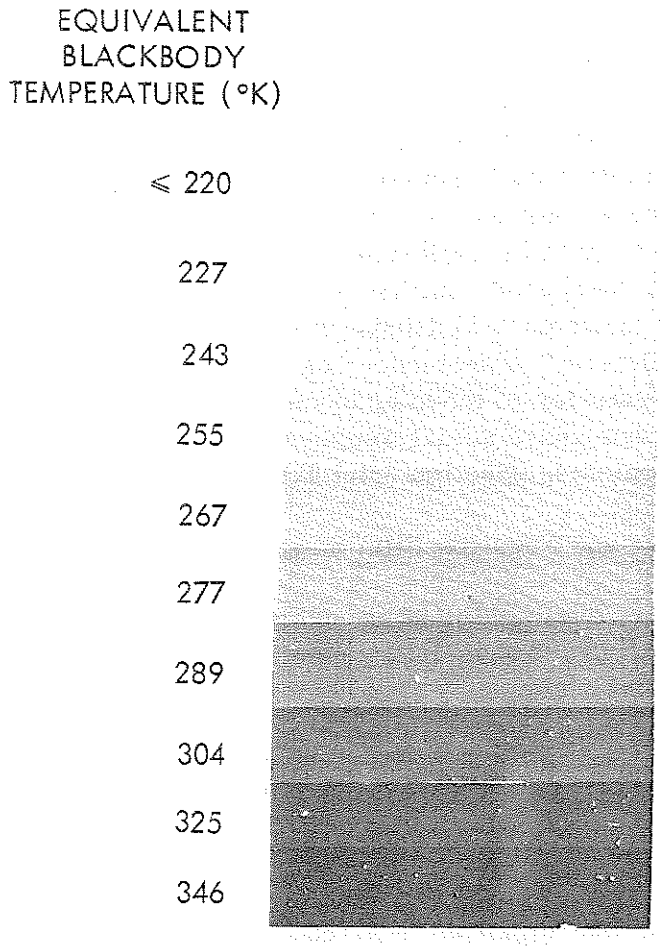

Figure 3-15–HRIR Calibration Gray Scale

correspond to ten equivalent blackbody temperatures on nighttime film strips and ten reflected energy levels on daytime film strips. The levels indicated in the figure were set before launch of the spacecraft and are likely to be re-set after the first few orbits of data have been received and evaluated. The daytime levels will be given along with the calibration curve (Section 3.3.2) in a forthcoming data catalog.

Variations in photographic reproduction and printing make it impossible to calibrate absolutely all data with one gray scale wedge. However, these gray scales are produced and exposed on the film strips immediately before or after the associated data are recorded. Thus, any variation in photographic processing should affect the gray scales and the data equally.

Naturally, the gray scales have no function on the specifically requested Variable Density Exposure film strips. The gray scale calibration described has application only to the Uniform Density Exposure mode film strips.

3.4.1.2 Film Strip Identification

HRIR data are archived in separate nighttime and daytime swaths. A swath therefore covers a distance approximately pole to pole and may include in rare cases more than one block of data. Each swath is identified by a label with the data orbit number. The nighttime swath is labeled with the orbit number followed by N. The daytime swath crossing the ascending node is identified by the higher orbit number followed by D. Each block is provided with a label showing the correct universal time of the first data scan nearest the label.

Figure 3-16 shows a film strip containing sample Nimbus III label formats, and computer produced grids with no sensory data. The film strip has been gridded for nighttime data. The affixed label gives the data orbit number 25. The end time is given in the affixed label and is 10:28:45 UT.

A series of time marks in increments of two minutes are found on the left side of the film (Figure 3-16). The first time mark represents the first even minute before the end time given in the affixed label (for daytime data it would represent the first even minute after the time given in the affixed label). In this case the first time mark is 10:28:00 UT, the second is 10:26:00 UT, etc. The time identifies the data to have been recorded during orbit 25. The data are properly oriented when the film is held (shiny side toward the viewer) with the label at the bottom as shown in Figure 3-16.

3.4.1.3 Film Strip Gridding

The geographical location of each picture element scanned by the radiometer depends on the stability of spacecraft. The Nimbus II control system demonstrated a pointing accuracy of about ±1 degree in pitch, roll, and yaw. A pointing error of 1 degree corresponds to a subsatellite error of 20 km (11 nm) in the location of a picture element from an altitude of 1100 km (600 nm). On a global basis, this is an acceptable error for most meteorological analyses.

Automatic gridding of the data is accomplished by utilizing a CDC 924 Computer to compute geographic coordinates, and a grid mixer which generates the grid points and adds them to the HRIR data in analog form. These grid points are electronically superimposed on the film and manually checked to maintain an accuracy of better than ±1 degree of great circle arc at the subsatellite point. Referring still to Figure 3-16 the grid point array makes up lines for every 10°

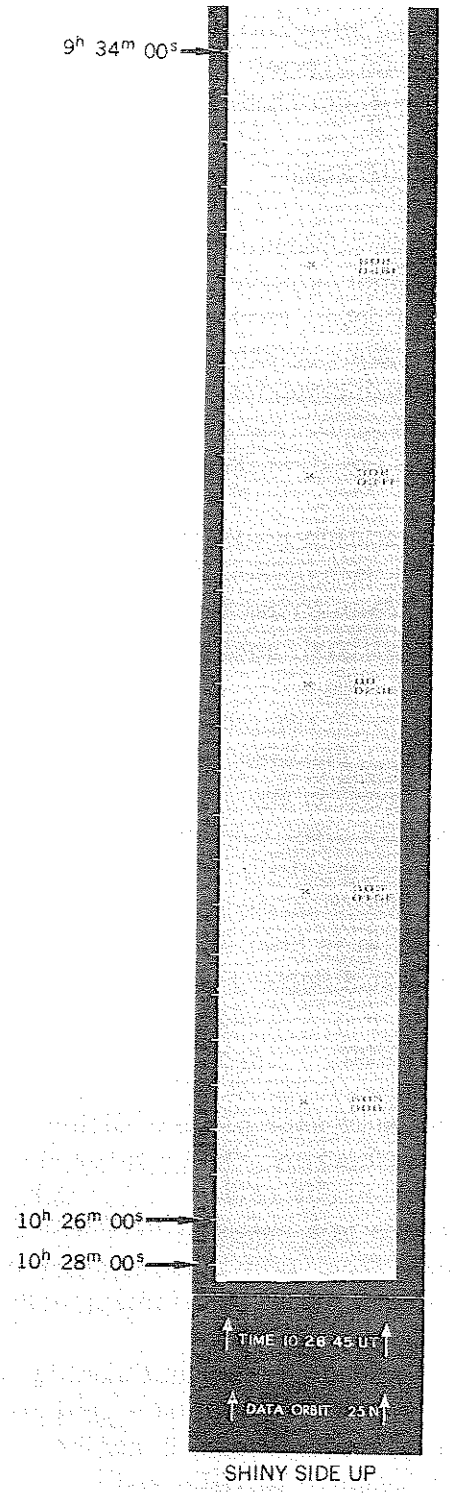

Figure 3-16—Nimbus III Format of Computer Produced Grid

of latitude and longitude, with points spaced at 2° intervals along each line between 60°N and 60°S latitude. Outside of 60°N and 60°S latitude, there are latitude lines each 10° and longitude lines each 20°, and latitude points each 2° and longitude points each 5°.

A small cross is placed at the intersections of the 60°N, 30°N, 0°, 30°S, and 60°S latitude lines with the subsatellite track. The first cross from the bottom of Figure 3-15 marks the intersection of the subsatellite track and 60°S at 80°E latitude. The full subsatellite track is not gridded. The longitude and latitude of each cross (rounded to the nearest degree) is displayed at the extreme right hand edge of the picture opposite that cross (latitude above longitude). The latitude format is XXY where $00 \leq XX \leq 90°$, and Y is N or S. The longitude format is XXXY where $000 \leq XXX \leq 180°$, and Y is E or W.

3.4.1.4 Ordering HRIR Film Strips

When requesting HRIR film strip data from NSSDC the following information should be given.

1. Satellite (e.g., Nimbus III)
2. Date
3. Data orbit number and whether daytime or nighttime
4. Data format, i.e., positive, negative, transparencies or prints
5. Uniform or Variable Density exposure

3.4.2 Digital Data

A much more quantitative picture results when the original analog signals are digitized with full fidelity and the digital data are processed by an IBM 360 computer where calibration and geographic referencing is applied automatically.

A simplified block diagram of the A/D processing system is shown in Figure 3-19. The analog magnetic tape is fed to an A/D converter which utilizes a CDC 924 computer to prepare a digital tape. This tape is then operated upon by the IBM 360 which prepares a reduced radiation data tape called the Nimbus Meteorological Radiation Tape-HRIR (NMRT-HRIR). The NMRT archived at NSSDC can be used to generate grid print maps or to accomplish special scientific analyses. The format of this tape, nearly the same as for Nimbus II HRIR, is given in Section 3.5.

An example of a grid print map presentation is shown in Figure 3-17, where the central portion of Typhoon "Marie," (see Figure 3-14) is displayed. The advantages of this form of presentation are the display of absolute values

(temperatures for nighttime, radiances for daytime) in their approximate location, geographical rectification of the data, and the possibility of automatically composing measurements from consecutive orbits into quasi-synoptic aerial maps. However, due to the scanning geometry, either a loss of detail will result from smoothing in the center portions of each swath or data gaps (being larger than the grid interval) will occur at some distance from the subsatellite point. Figure 3-17 shows a portion of the rectified composite of three (3) consecutive orbits (including that of Figure 3-14) giving equivalent blackbody temperatures. The lowest temperatures shown over typhoon "Marie" in this map indicate cloud top heights above 11 kilometers. The printed values are averages of up to 200 data points within areas of up to 140 kilometers by 140 kilometers. Figure 3-18 shows an analysis of the typhoon developed using several forms of HRIR data. An example of some methods of HRIR data interpretation is contained in Reference 5.

From the calibration curves (Figures 3-10 to 3-12) it can be seen that the response of the instrument cuts off at some low temperature around 210°K. Below this cut-off, data in the computer processing are usually set to 190°K and are not to be considered as real data. They have to be eliminated when interpreting the measurements, particularly before map production. The actual cut-off temperature will be evaluated during the satellite experiment. The user of Nimbus III HRIR data must therefore check the periodic data catalogs (to be published monthly) for information concerning the actual cut-off temperature.

3.4.2.1 Availability of Processed Digital HRIR Data

Due to the large volume of data (both day and night full time coverage) and the long computer running time required for processing it into NMRT's, Nimbus III HRIR digital data are not routinely reduced to final NMRT Format. Only those data which are specifically requested by the user will be processed. Requests should be made through NSSDC. It is anticipated that requested HRIR-NMR tapes will begin to be available through NSSDC six months after launch. The user is urged to make full use of the film strips which are abundantly available in nearly real-time from the NSSDC.

A series of programs produce printed and contoured data referenced to a square mesh grid on polar stereographic or Mercator map bases. Grid print maps may be produced for either a single orbit or a composite of several orbits. The following standard options are available and should be specified when requesting grid print maps from NSSDC:

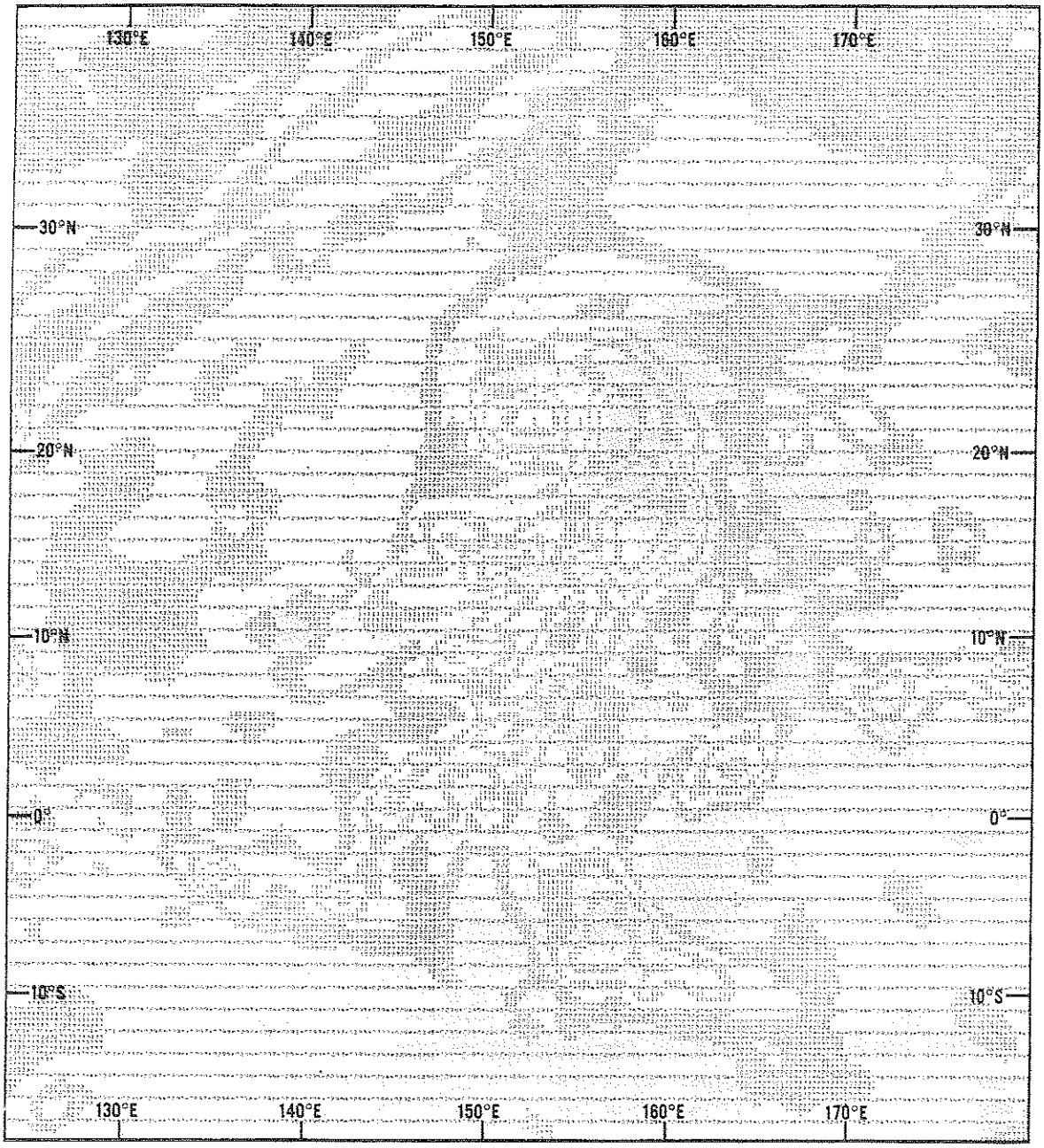

Figure 3-17– Computer Produced Grid Print Map of Typhoon "Marie" of 1966 Utilizing Nimbus II HRIR Data

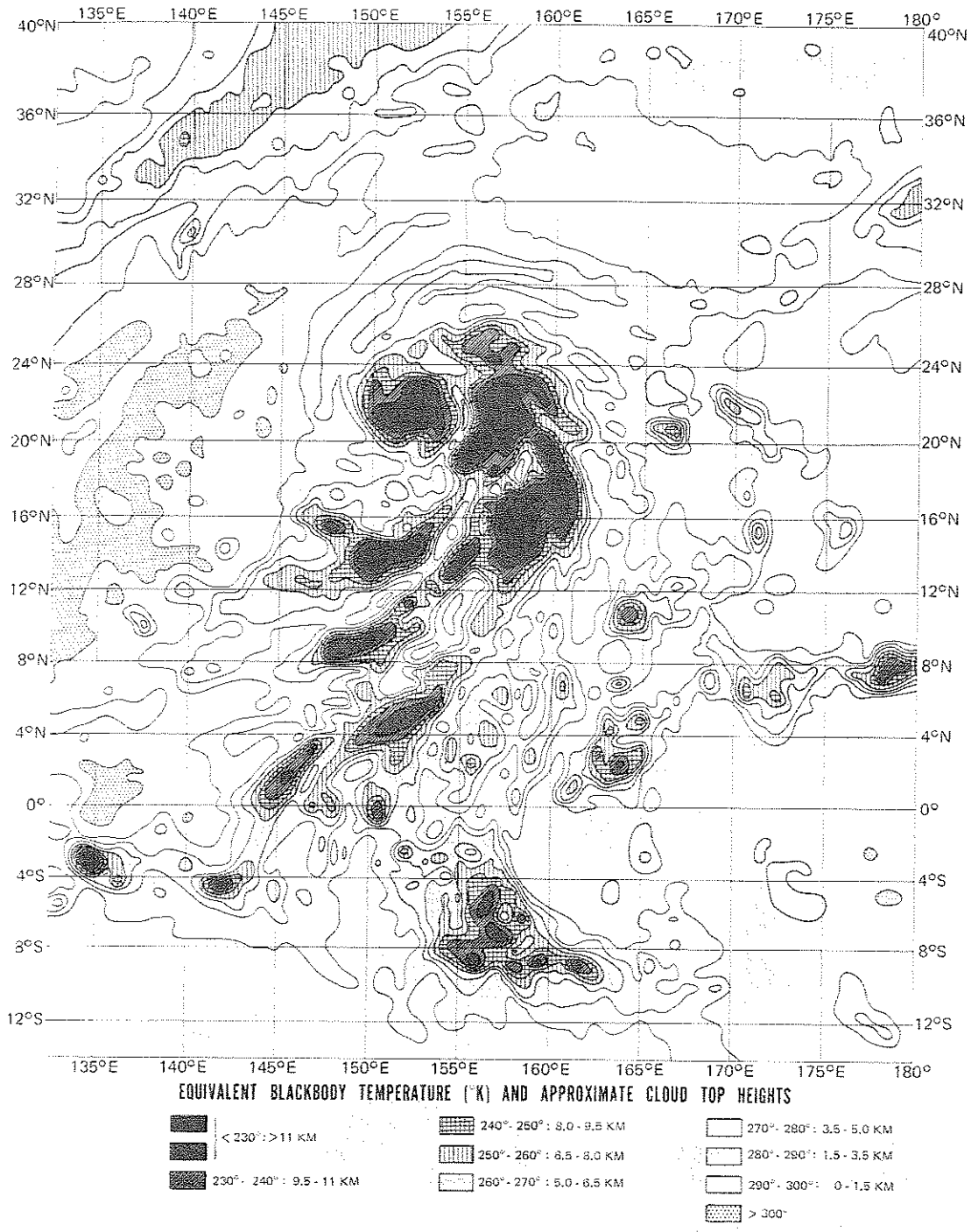

Figure 3-18– Analysis of Typhoon Marie Using Several Forms of HRIR Data

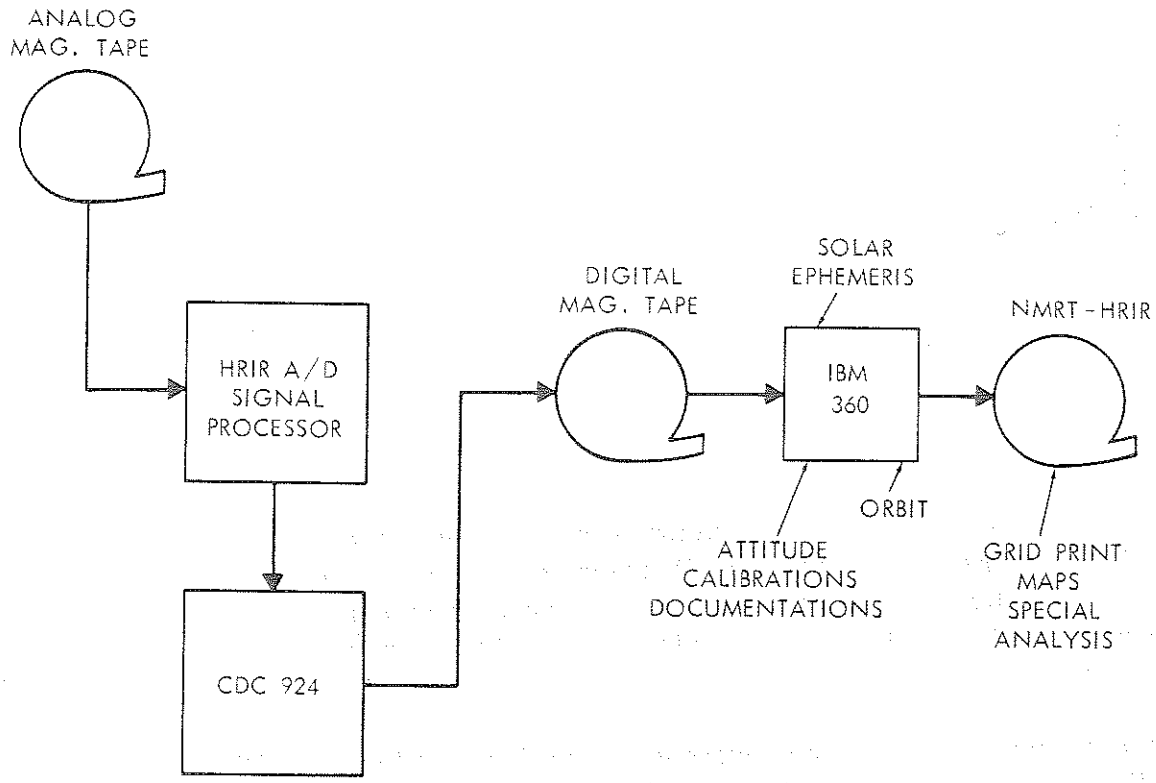

Figure 3-19–Simplified Block Diagram of the A/D Processing System

1. Map and Approximate Scale

   a. Polar Stereographic, 1/30 million (approx.)
   b. Polar Stereographic, 1/10 million (approx.)
   c. Multi-Resolution Mercator maps are available down to 1/1 million scale.

2. Maximum Sensor Nadir Angle

3. Field Values and Contouring. Unless otherwise specified, all maps will include field values and contouring except Mercator Maps of scales larger than 1/20 million. A data population map, indicating the number of individual measurements contained in each grid point average, as well as a latitude-longitude description for geographically locating the data, will ordinarily be provided along with each grid print map.

When ordering "hard copy" data, the following identifying information should also be given:

1. Satellite (e.g. Nimbus III)
2. Sensor (HRIR)
3. Data Orbit No.
4. Calendar Date of Equator Crossing
5. Beginning and Ending Times of Data in GMT
6. Format Desired (see 3.4.2.1, items 1; 2; 3)

When ordering NMR Tapes, only items 1, 2, 3 and 5 above need to be given.

3.4.3 Analog Data

Analog records can be made from the original spacecraft interrogation record (Figure 3-14b). These Visicorder oscillograph records permit accurate measurement of temperature as a function of time and sensor scan angle as long as the user has adequate knowledge of the workings of the instrument and all parameters involved.

However, the requirements for a comprehensive knowledge of the total HRIR subsystem and the sheer volume of the data prohibits the use of this method except for special cases.

3.5 Format of the NMRT-HRIR Tape

The Nimbus Meteorological Radiation Tape-HRIR will be a basic repository for radiation data from the Nimbus High Resolution Infrared Radiometer. This tape will contain data in binary mode at a density of 800 bits per inch.

The first file on this tape contains a BCD label. The label consists of fourteen words of BCD information followed by an end-of-file. The remaining files on this tape contain formatted HRIR data in the format described on the following pages. The first record in this data file is a documentation record which describes the data to be found in the succeeding records. This first record contains seventeen words (see Table 3-3). The remaining records in the file will be of variable length, but this length will be consistent within the file (see Table 3-4). The length (L) of the data record can be computed as follows:

$$L = (\text{SWATHS PER RECORD}) \times (\text{WORDS PER SWATH}) + (\text{NUMBER OF NADIR ANGLES}) + 7$$

Table 3-3
NMRT-HRIR Documentation Record Format

Word No.	Quantity	Units	Scaling	Remarks
1	Dref	–	B=35	Number of days between 0 hours on 9/1/57 and zero hour on day of launch
2	Date	MMDDYY	B=35	Date of interrogation for this orbit, i.e., 2/5/64 would be $(020504)_8$. Only the last digit of year is used.
3	Nimbus Day	–	B=35	Start time for this file of data
4	Hour	Z Hour	B=35	
5	Minute	Z minute	B=35	
6	Seconds	Z seconds	B=35	
7	Nimbus Day	–	B=35	End time for this file of data
8	Hour	Z hour	B=35	
9	Minute	Z minute	B=35	
10	Seconds	Z seconds	B=35	
11	Mirror Rotation Rate	Deg/Sec	B=26	Rotation rate of radiometer mirror
12	Sampling Frequency	Samples/Sec	B=35	Digital sampling of frequency per second of vehicle time
13	Orbit Number	–	B=35	Orbit Number
14	Station Code	–	B=35	DAF Station identification code
15	Swath Block Size	–	B=35	Number of 35-bit words per swath
16	Swaths/Record	–	B=35	Number of swaths per record
17	Number of Locator Points	–	B=35	Number of anchor points per swath for which latitudes and longitudes are computed.

Table 3-4
NMRT-HRIR Data Record Format

Word No.	Quantity	Units	Scaling	Remarks
1D	Nimbus Day	–	B= 17	Start time for this record of data
1A	Hour	Z hour	B= 35	
2D	Minutes	Z minute	B= 17	
2A	Seconds	Z seconds	B= 35	
3D	Roll Error	Degrees	B= 14	Roll error at time specified in words one and two.
3A	Pitch Error	Degrees	B= 32	Pitch error at time specified in words one and two.
4D	Yaw Error	Degrees	B= 14	Yaw error at time specified in words one and two.
4A	Height	Kilometers	B= 35	Height of spacecraft at time specified in words one and two.
5D	Detector cell Temperature	Degrees K	B= 17	Measured temperature of detector cell at time specified in words one and two.
5A	Electronics Temperature	Degrees K	B= 35	Measured temperature of electronics at time specified in words one and two.
6D	24V Supply	Volts	B= 14	Measured voltage at time specified in words one and two.
6A	20V Supply	Volts	B= 32	Measured voltage at time specified in words one and two
7D	Reference Temperature A	Degrees K	B= 17	Measured temperature of housing at time specified in words one and two.
7A	Reference Temperature B	Degrees K	B= 35	

Table 3-4 (Continued)

Word No.	Quantity	Units	Scaling	Remarks
8 . . . N	Nadir Angle Nadir Angle	Degrees Degrees	B=29 B=29	Nadir angles corresponding to each locator point, and measured in the plane of the radiometer
(N+1)D	Seconds	Z Seconds	B=8	Seconds past time in words 1A & 2D for beginning of this swath.
(N+1)A	Data Population	–	B=35	Number of data points in this swath.
(N+2)D	Latitude	Degrees	B=11	Latitudes of subsatellite point for this swath
(N+2)A	Longitude	Degrees	B=29	Longitude of subsatellite point for this swath, positive westward 0 to 360°.
N+3	Flags	–	–	Reserved for flags describing this swath
(N+4)D	Latitude	Degrees	B=11	Latitude of viewed point for the first anchor spot
(N+4)A . . . MD MA	Longitude Latitude Longitude	Degrees Degrees Degrees	B=29 B=11 B=29	Longitude of viewed point for first anchor spot, positive westward 0 to 360°. Latitude and longitude for Mth anchor spot
(M+1)D (M+1)A . . . K(A or D)	HRIR Data HRIR Data HRIR Data	– – –	B=14 B=32 B=32 -14	HRIR measurements. Tag and prefix reserved for flags. Last HRIR data measurement

The above data constitute what is essentially the documentation portion of a data record. These data will be followed by several blocks of data with each block representing a swath. The number of these blocks in a record as well as the size of each block is specified in the documentation record represented on the previous page.

All remaining or unused portions of a swath data block are set to zero, giving a swath block size as specified in the documentation record. The above data on this page is repeated for the number of swaths in each record.

Ninety degrees are added to all latitudes and attitude data to eliminate negative signs.

Table 3-5 defines the flags which appear in the data records.

Table 3-5
Definition of Flags Describing Each HRIR Swath

Flag	Bit	Definition	Yes	No
1	35	Summary flag. All checks defined by flags 2 thru 12 are satisfactory. (each flag is zero)	0	1
2	34	Consistency check between sampling rate and vehicle time is satisfactory	0	1
3	33	Vehicle time is satisfactory	0	1
4	32	Vehicle time has been inserted by flywheel	1	0
5	31	Vehicle time carrier is present	0	1
6	30	Vehicle time has skipped	1	0
7	29	Unassigned		
8	28	Sync pulse recognition was satisfactory	0	1
9	27	Dropout of data signal was detected	1	0
10	26	Unassigned		
11	25	Unassigned		
12	24	Swath size is satisfactory when compared with the theoretical swath size	0	1
13	23	Unassigned		

Flags For Individual Measurements

Prefix	Tag	Definition	Yes	No
S	18	The particular measurement is below the earth-space threshold	1	0
1	19	Unassigned		
2	20	Unassigned		

REFERENCES

1. Aeronomy and Meteorology Division, 1965: Nimbus I High Resolution Radiation Data Catalog and User's Manual, NASA, Goddard Space Flight Center, Greenbelt, Maryland

2. Nimbus Project, 1966: Nimbus II User's Guide, NASA, Goddard Space Flight Center, Greenbelt, Maryland.

3. Nimbus Project, 1966: Nimbus II HRIR Montage Catalog, NASA, Goddard Space Flight Center, Greenbelt, Maryland.

4. NASA Special Publication SP-89, Observations from the Nimbus I Meteorological Satellite, 1966.

5. Warnecke, G., Allison, L., Kreins, E., and McMillin, L., A Typical Cyclone Development as Revealed by Nimbus II High Resolution Infrared and ESSA-3 Television Data, NASA X-622-68-39, January 1968.

6. Nordberg, W., A. W. McCulloch, L. L. Foshee, W. R. Bandeen, Preliminary Results from Nimbus II, NASA X-620-66-349, August 1966.

SECTION 4

THE MEDIUM RESOLUTION INFRARED RADIOMETER (MRIR) EXPERIMENT

by
Andrew W. McCulloch
National Aeronautics and Space Administration
Goddard Space Flight Center

4.1 Description of the Experiment

The Medium Resolution Infrared Radiometer (MRIR) experiment is designed to measure electromagnetic radiation emitted and reflected from the earth and its atmosphere in five selected wavelength intervals. The scientific basis for the experiment and the results from earlier measurements of this type acquired from the TIROS series have been well documented (References 1-34). For this reason the objectives will be only summarized here. Since the radiometer includes one channel having a response extending into the visible, the term Medium Resolution Infrared Radiometer is somewhat inaccurate. However, because the use of the term "MRIR" has historically become so firmly entrenched, this familiar designation will be used to identify the experiment discussed below.

For meteorological purposes, data for heat balance of the earth-atmosphere system will be obtained as well as water vapor distribution, (in the lower, middle and upper troposphere), surface or near surface temperatures, and seasonal changes of stratospheric temperature distribution. The Nimbus circular, polar orbit is ideally suited to this experiment since global coverage is necessary to accomplish the stated objectives. In addition, the three-axis stabilization of the Nimbus spacecraft permits the acquisition of data in a systematic way at continuously varying angles of view in a simple geometrical pattern.

The five wavelength regions, each with a brief description of its purpose, are as follows:

6.5 to 7.0 microns – This channel covers the 6.7 micron water vapor absorption band. Its purpose is to provide information on water vapor distribution in the upper troposphere and, in conjunction with the other channels to provide data concerning relative humidities at these altitudes.

10 to 11 microns – Operating in an atmospheric "window," this channel measures surface or near-surface temperatures over clear portions of the atmosphere. It also provides cloud cover and cloud height information (day and night).

14.5 to 15.5 microns – This channel, centered about the strong absorption band of CO_2 at 15 microns, measures radiation which emanates primarily from the stratosphere. The information gained here is of primary importance in following seasonal stratospheric temperature changes.

20 to 23 microns – This channel yields data from the spectral region containing the broad rotational absorption bands of water vapor. It will provide information similar to that of the 6.5 to 7.0 micron channel except that the flux will largely be radiated from lower in the atmosphere.

0.2 to 4.0 microns – This channel covers more than 99% of the solar spectrum and yields information on the intensity of reflected solar energy from the earth and its atmosphere.

The instrument devised for this experiment is shown in Figure 4-1. It has a nominal spatial resolution (angular field of view) of 0.050 radians. The actual measured horizontal and vertical fields of view for each channel are shown in Figures 4-2 to 4-6.

For clarification, the "vertical" direction was measured on a line parallel to the velocity vector of the spacecraft and through the optical axis. Horizontal refers to the direction at 90° to the vertical and also including the optical axis.

Radiant energy from the earth is collected by a flat scanning mirror inclined at 45° to the optical axis. The mirror rotates at 8 rpm and scans in a plane perpendicular to the direction of motion of the satellite. Hence, in every 360° scan it samples the earth from horizon to horizon, views space twice, and "looks" at its own housing once. Figure 4-7 shows a typical earth scan as presented on a strip chart recorder. The portions of the scan labelled "Space, Spacecraft, Scanner Housing, Space" yield in-flight calibration data (discussed in detail below). The incident flux is then focused onto a thermistor bolometer detector through appropriate optical filtering which limits the radiation to the desired wavelengths. The energy is modulated by a mechanical chopper to produce an a.c. signal from the detector. Figure 4-8 shows an optical diagram of the system. Used in this manner, the chopper becomes the reference temperature for the radiometer. Since the chopper temperature can reasonably be expected to vary during orbit, and because the detector signal represents the difference in energy between the target and the chopper, some method of determining the absolute temperature of

the target as the chopper changes temperature is necessary. This is accomplished by introducing an electronic offset which is controlled by thermistors monitoring the chopper temperature. This offset voltage is added to or subtracted from the signal in direct proportion to the chopper temperature so that a target of a given temperature will always produce the same absolute voltage output.

The electrical signal from the detector is then amplified and synchronously demodulated to yield an analog output of 0 to -6.4 volts to cover the desired range of target temperatures (or of radiance in the 0.2-4.0 micron interval) for each channel. These analog signals are sampled 33-1/3 times per second and converted to 8-bit digital data.

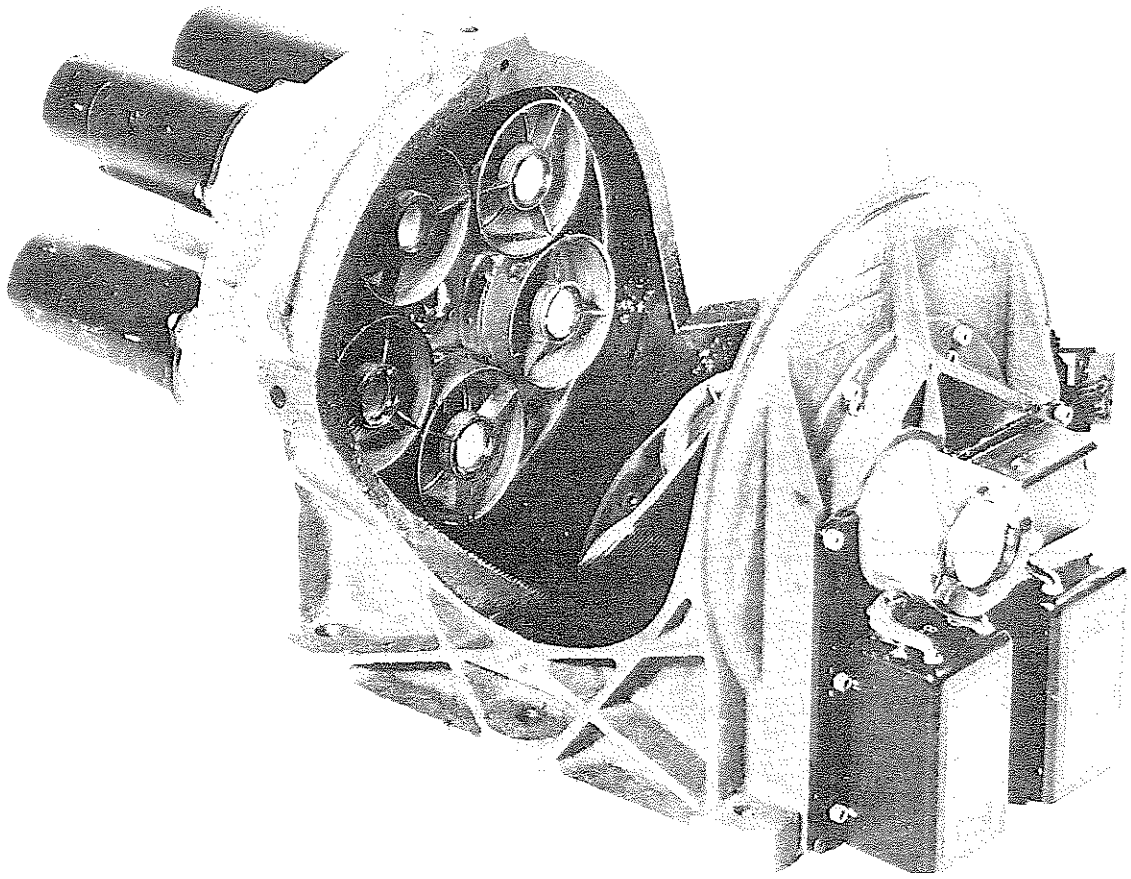

Figure 4-1– The Medium Resolution Infrared Radiometer

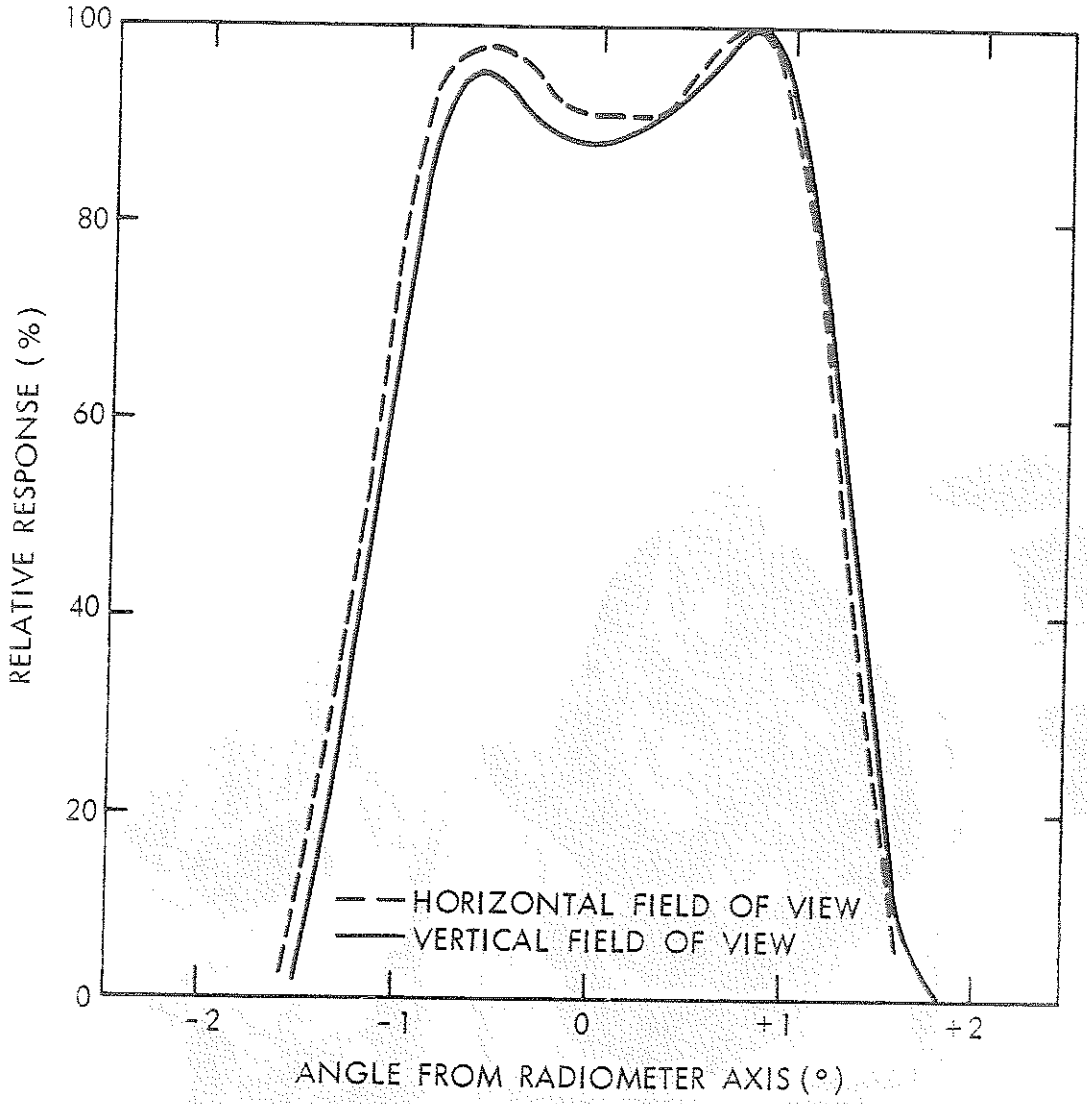

Figure 4-2– Angular Field of View of the 6.5 to 7.0 Micron Channel

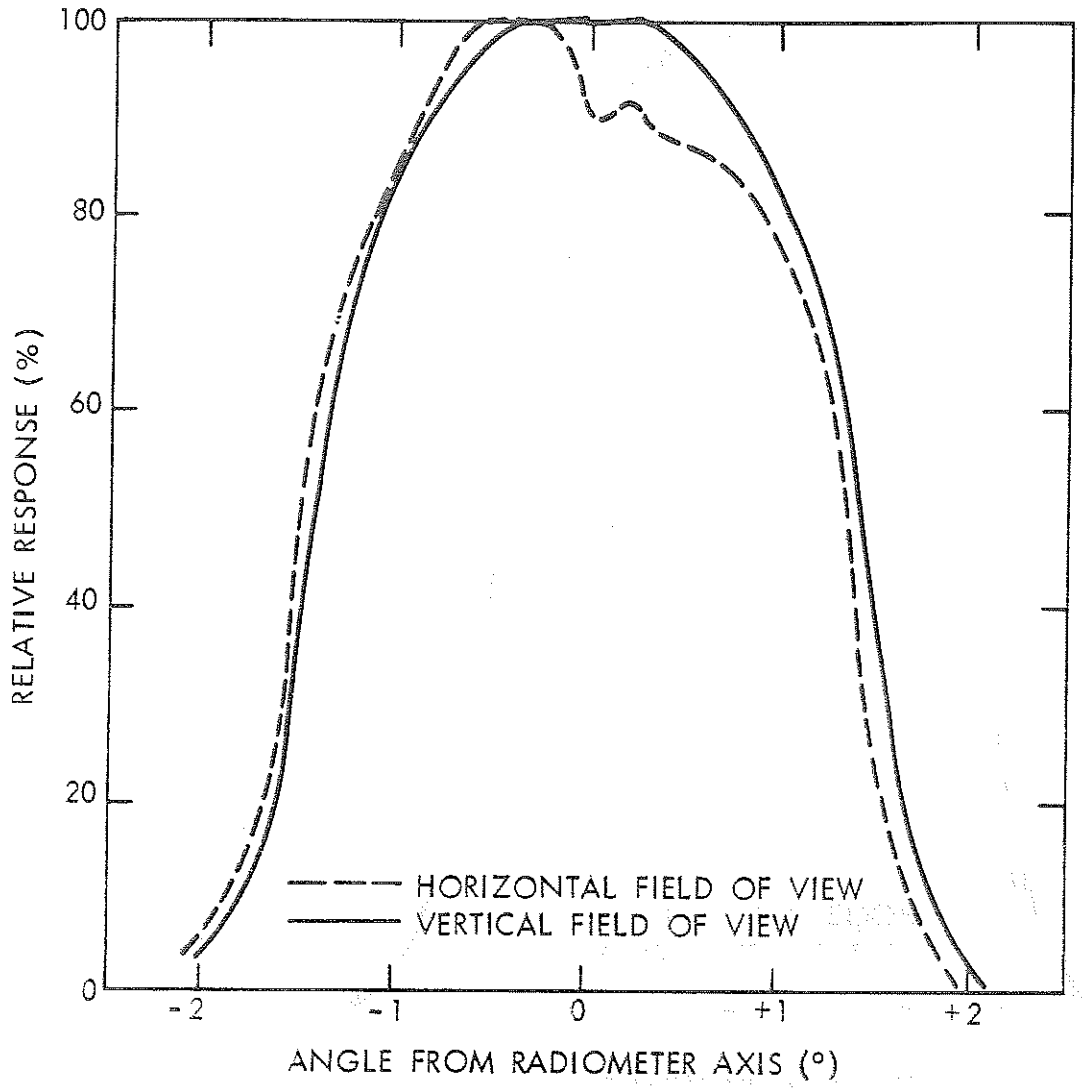

Figure 4-3– Angular Field of View of the 10 to 11 Micron Channel

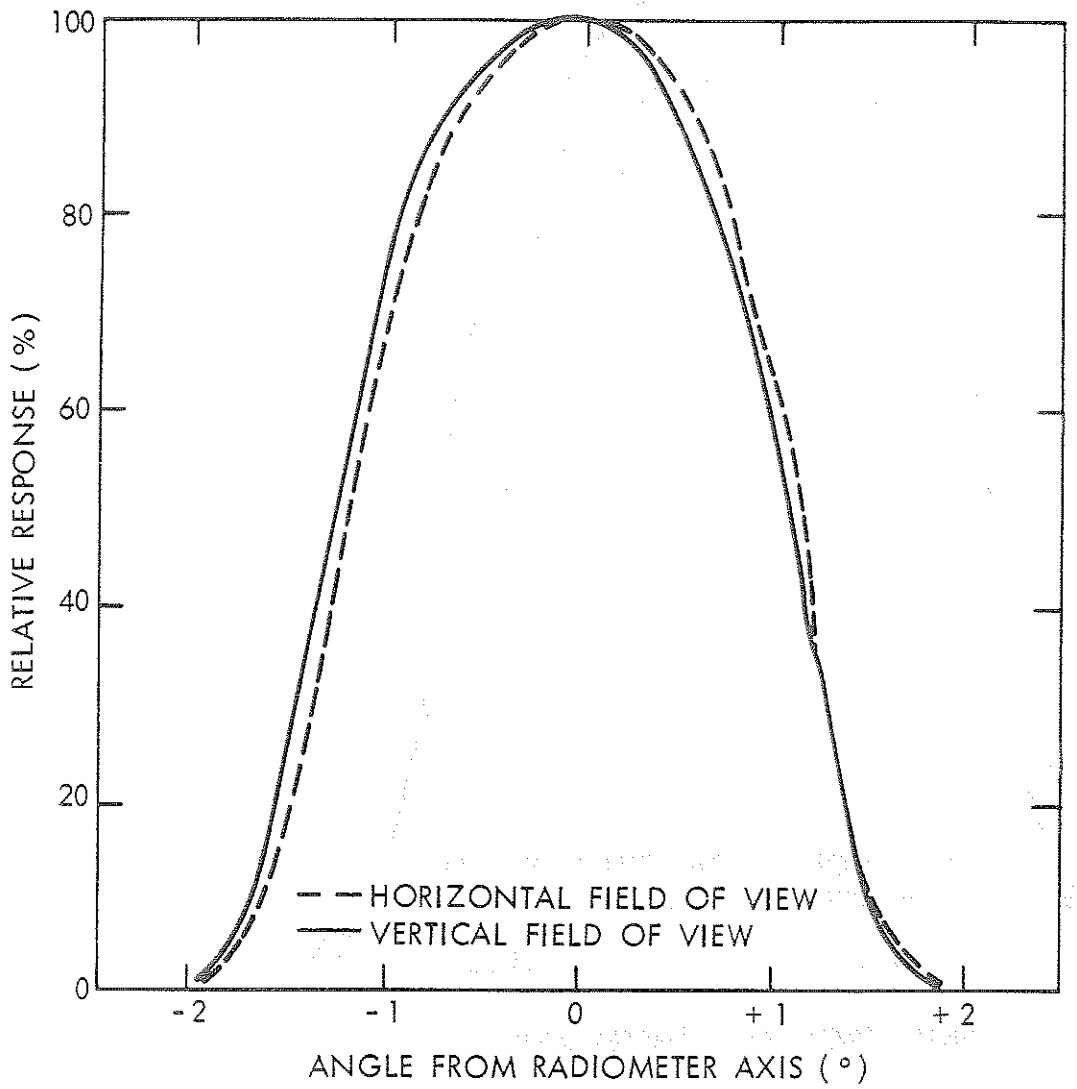

Figure 4-4–Angular Field of View of the 14.5 to 15.5 Micron Channel

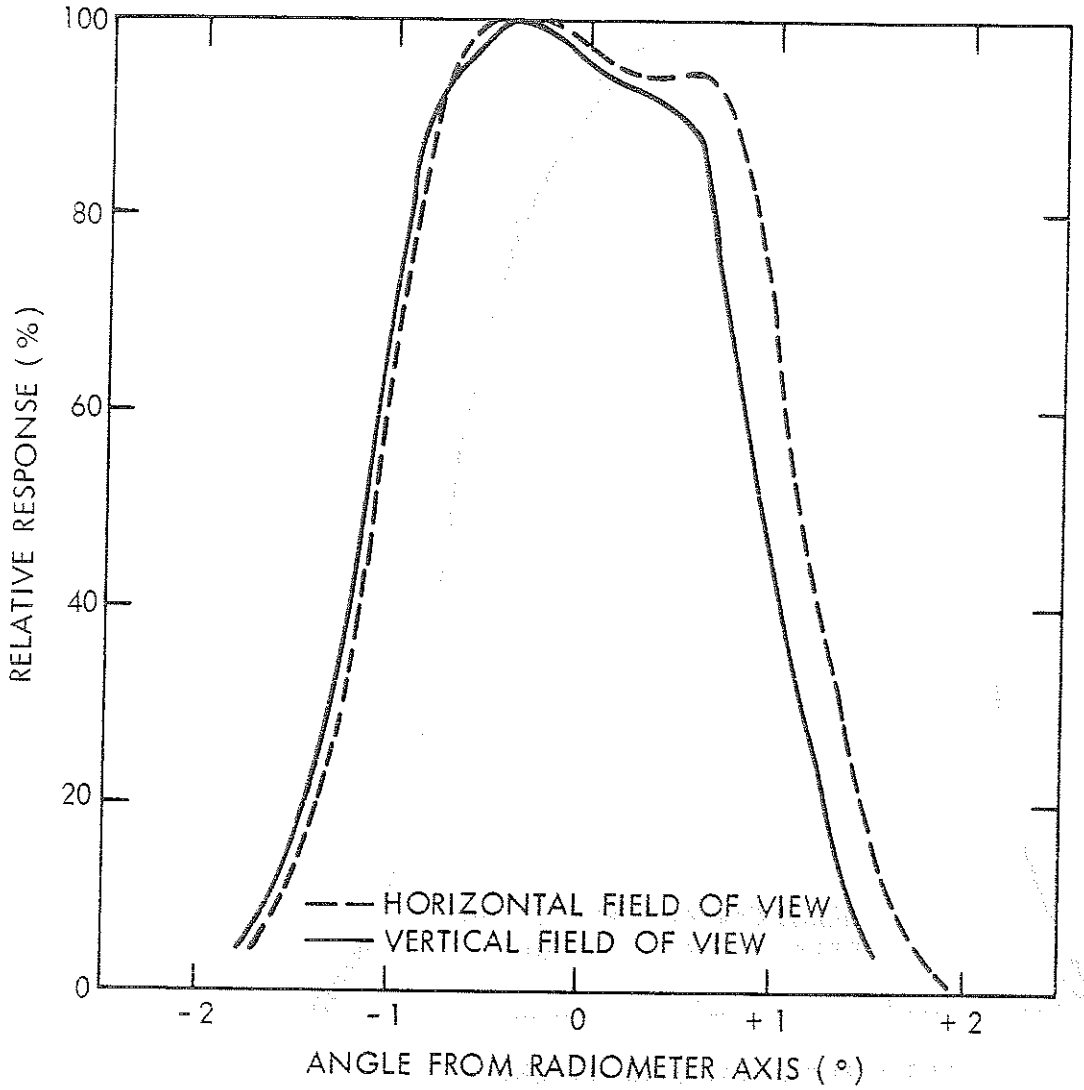

Figure 4-5– Angular Field of View of the 20 to 23 Micron Channel

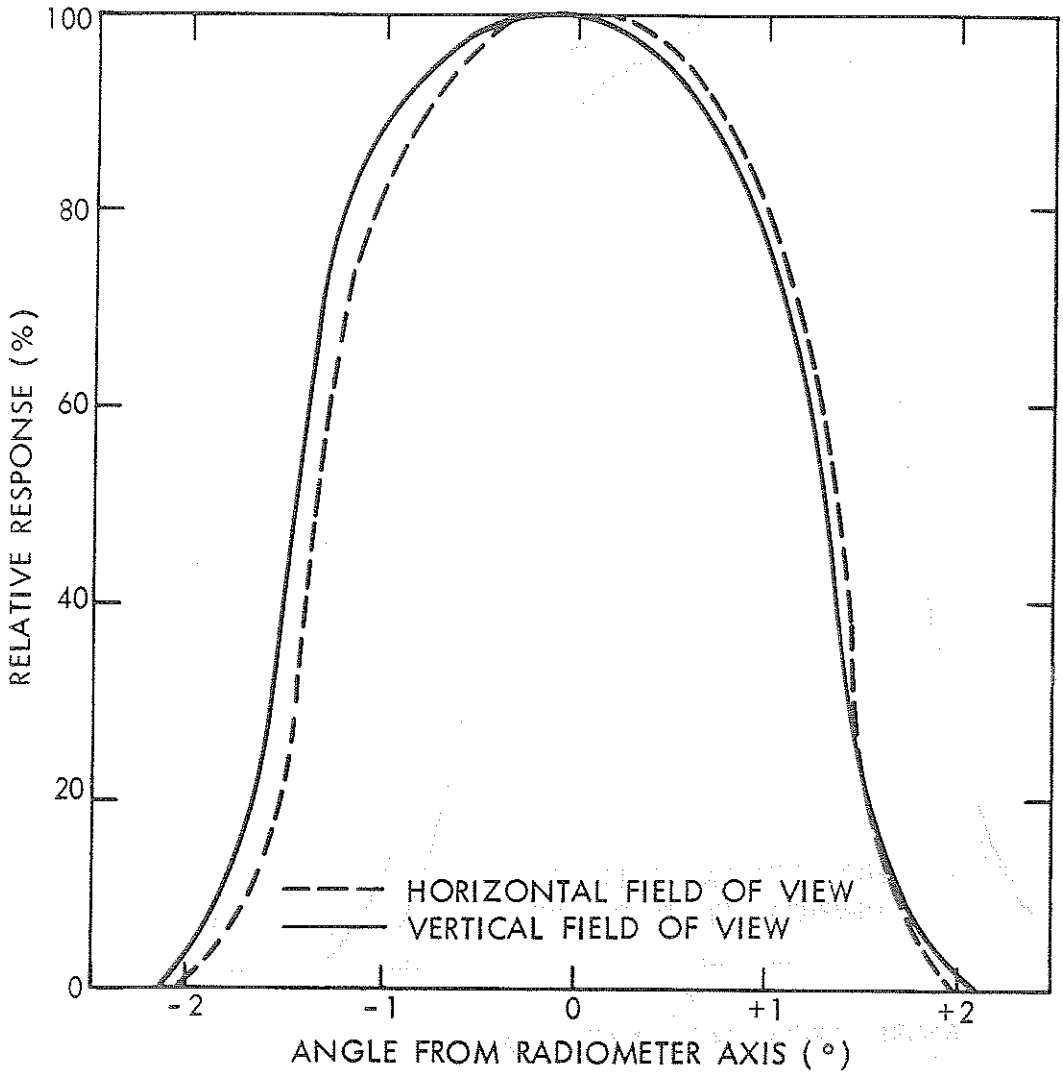

Figure 4-6– Angular Field of View of the 0.2 to 4 Micron Channel

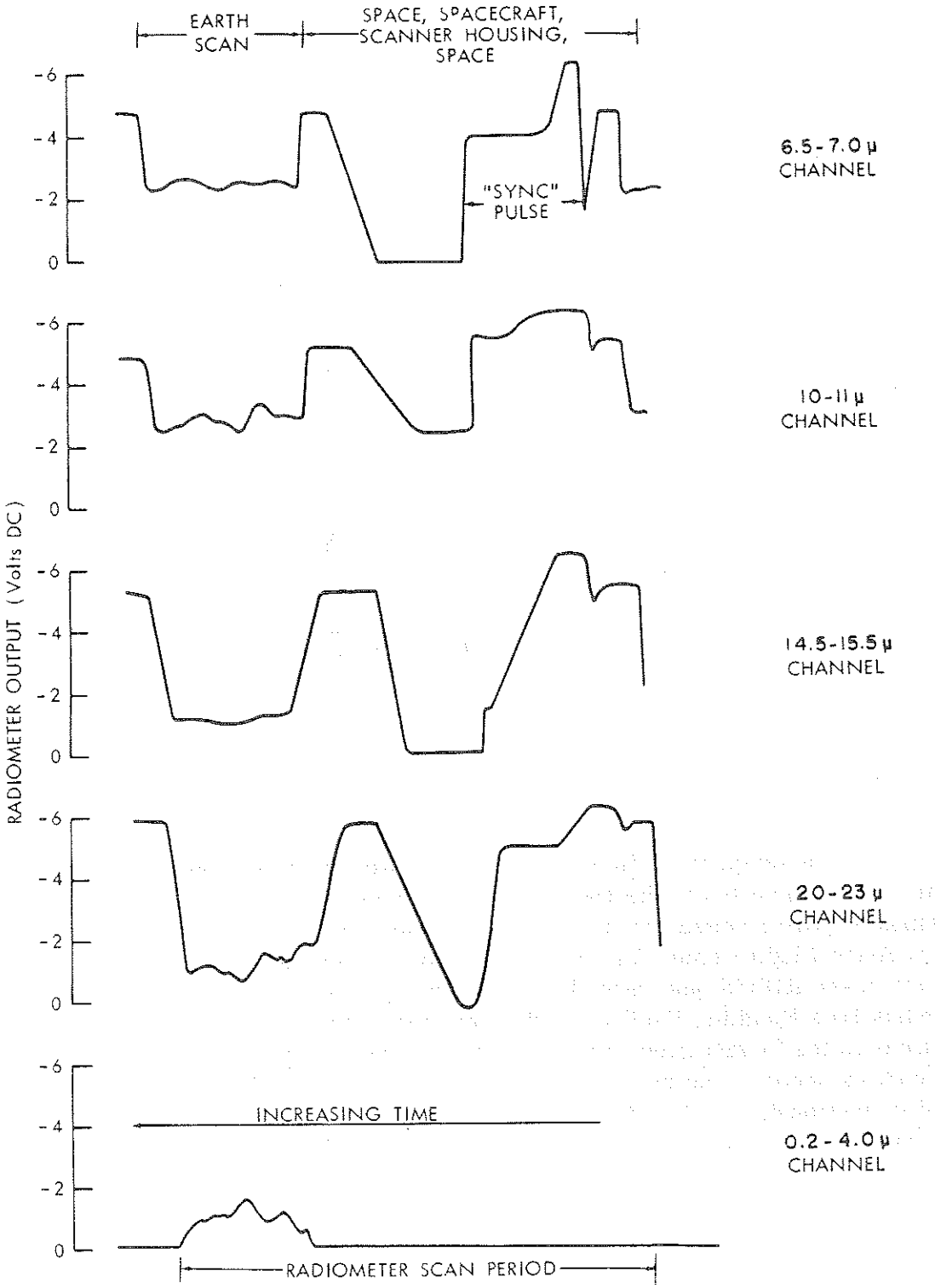

Figure 4-7—Typical Scan Pattern for MRIR in Orbit

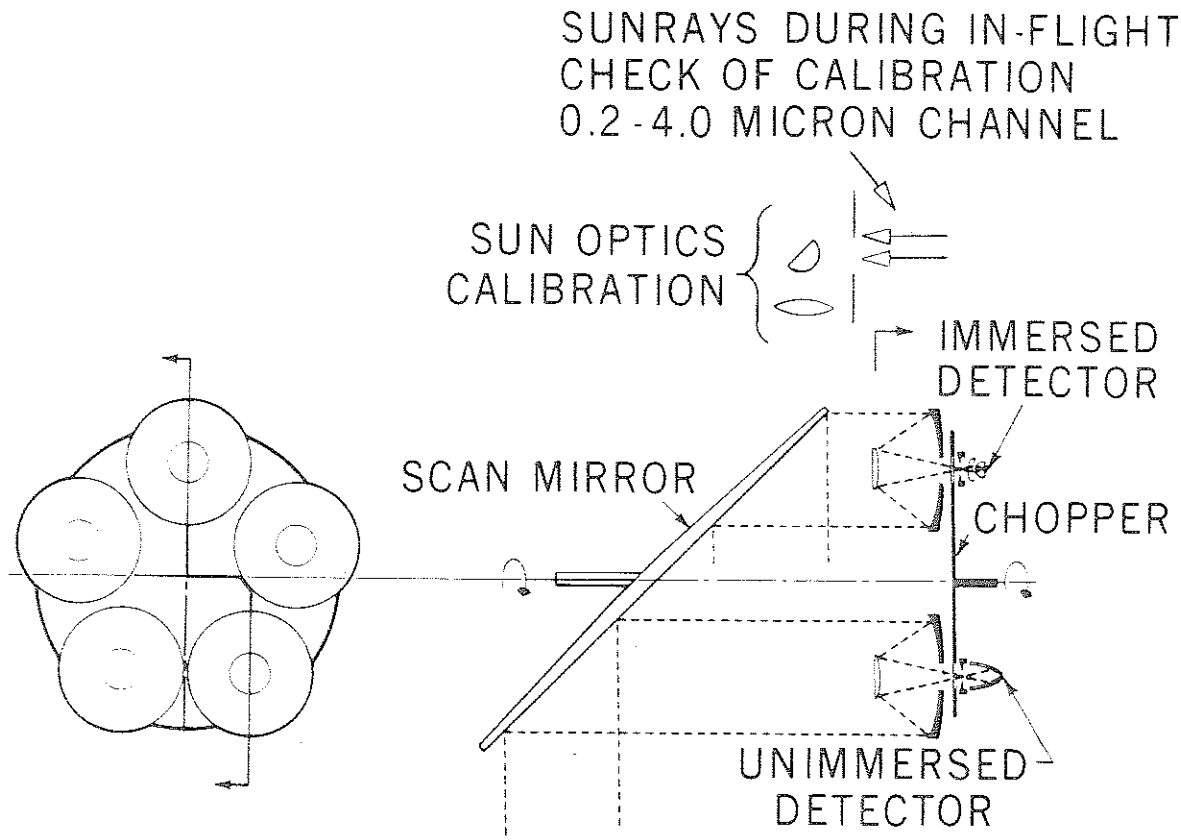

Figure 4-8– Optical Arrangement of Nimbus Five-Channel Medium Resolution Infrared Radiometer

The data are stored in serial form on one track of a HDRSS tape recorder. On command, data are transmitted to the Data Acquisition Facility (DAF) using the S-band transmitter. After receipt at the ground, the information is transmitted to Goddard Space Flight Center for final processing. Time code is stored on a separate track of the HDRSS tape recorder. The timing information is received at the Nimbus Data Handling Facility (NDHF) and furnished to all experiment ground stations in the format generated on the spacecraft. At the ground station the time code is decoded and displayed on the analog record. This display is described in section 4.3.2. Simultaneously the time information is formatted in IBM compatible language and included on the digital tape output (section 4.3.3) for computer processing. Figure 4-9 shows a block diagram of the system. (See Reference 35.)

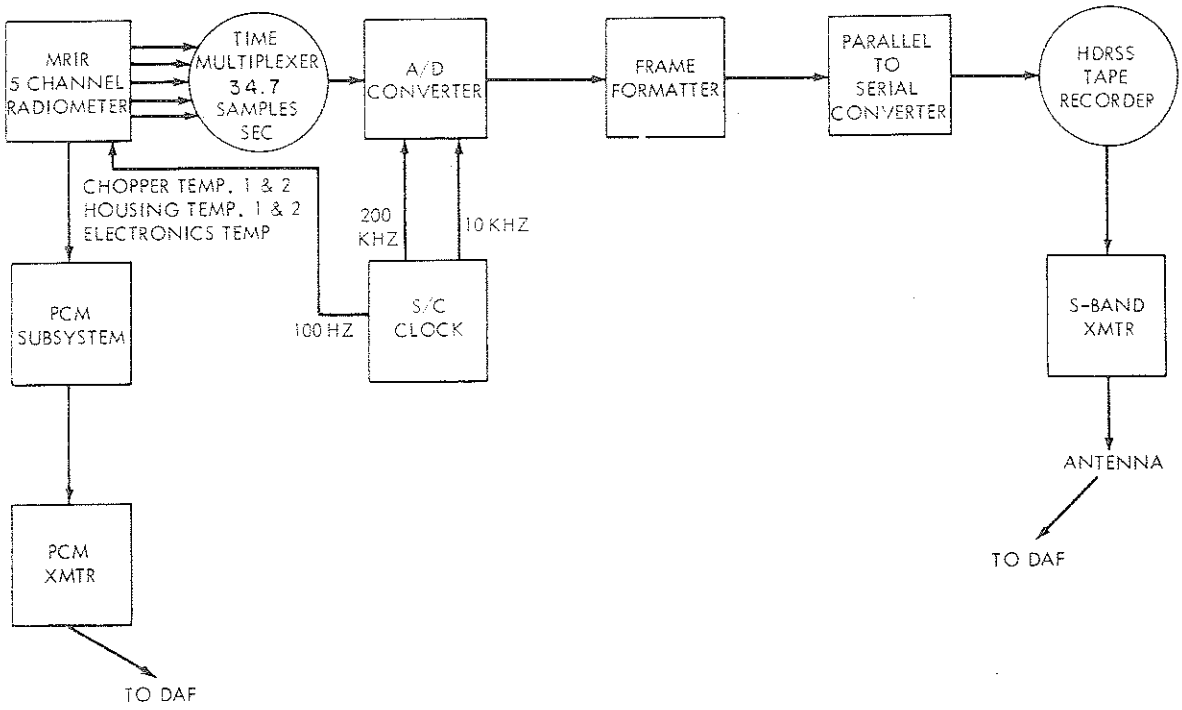

Figure 4-9– Block Diagram of Spacecraft Portion of MRIR System

4.2 Calibration

The main parameters for calibration of all electromagnetic radiation detection devices are essentially the same. These parameters have been defined in Section 3.3.1. Briefly, they are the quantities, $\bar{N}$, T_{BB} and ϕ_λ. Here ϕ_λ is a composite function involving all of the factors which contribute to the spectral response of the instrument, such as filter transmission, mirror reflectances, and the spectral responsivity of the detector. The effective radiance, $\bar{N}$, is defined as

$$\bar{N} = \int_0^\infty N_\lambda \, \phi_\lambda \, d\lambda \qquad (1)$$

where N_λ represents the generally non-Planckian radiation from the earth and its atmosphere. For the infrared channels, T_{BB} then becomes the equivalent blackbody temperature as defined in Section 3.3.1.3, and used in the laboratory calibration. Table I gives values of $\bar{N}$ vs T_{BB} for all five channels. Figure 4-10 is a typical $\bar{N}$ vs. T_{BB} curve. Table 4-2 through 4-6 list values of the spectral response, ϕ_λ, of each channel. The total instrument spectral response function

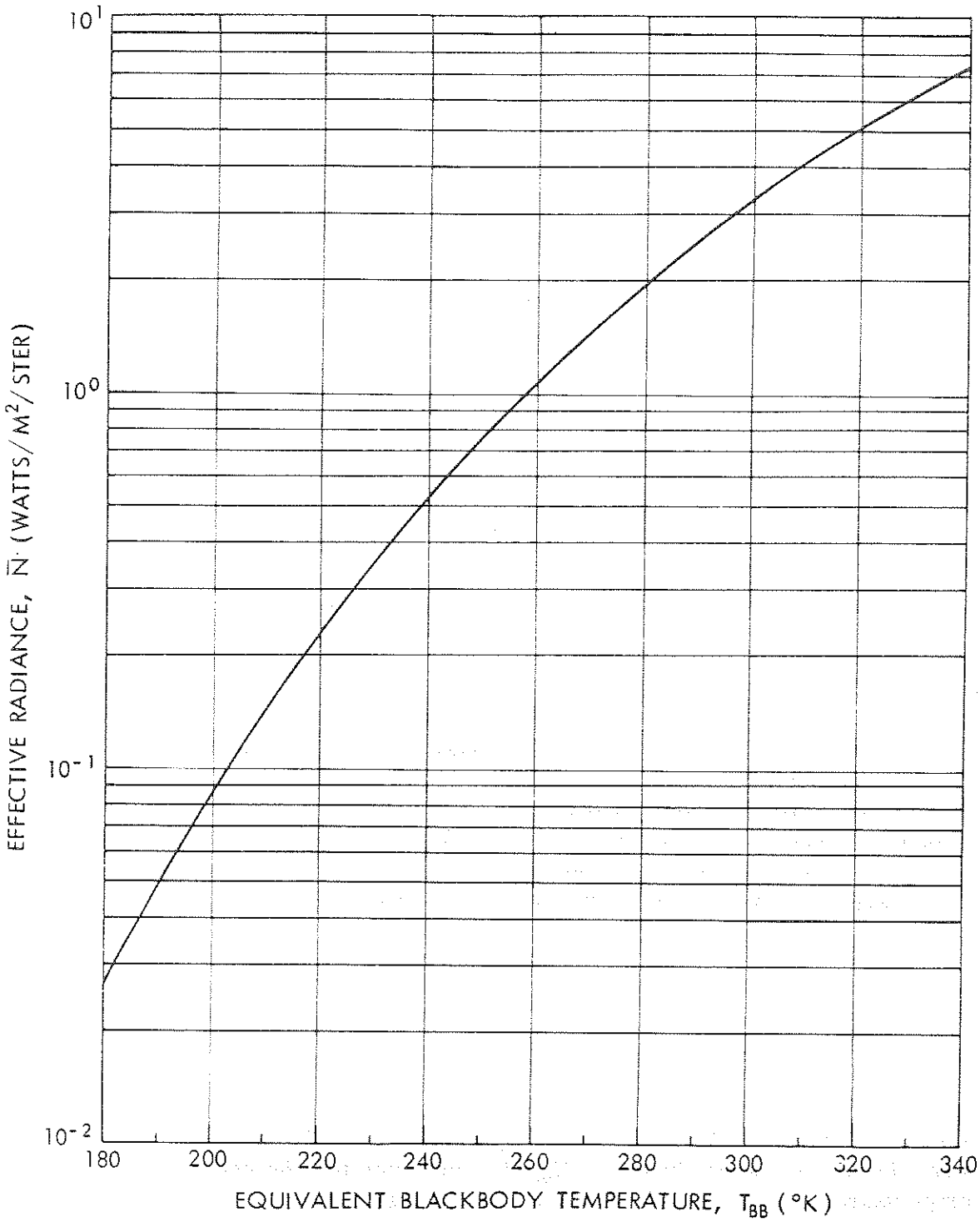

Figure 4-10– Typical $\bar{N}$ T_{BB} Curve

for each channel was measured utilizing a Perkin-Elmer model 112U spectrometer with a radiation thermocouple as a reference. Because of low signal-to-noise ratios, especially at the longer wavelengths, some error was introduced into these measurements. However, departures from the spectral characteristics of the filter are, in general, small and upon integration to obtain $\bar{N}$, errors of no more than 1-2% are encountered.

Table 4-1
Effective Radiance, $\bar{N}$, for the Thermal Channels of the MRIR
$\bar{N}$ (watts M^{-2} ster $^{-1}$)

Channel (μ)	6.5 - 7.00	10 - 11	14.5 - 15.5	20 - 23
T_{BB} (°K)				
150	.00158	.1257	.3369	.6625
160	.00395	.2201	.5011	.8742
170	.00885	.3611	.7118	1.118
180	.01813	.5610	.9727	1.392
190	.03446	.8323	1.287	1.697
200	.06143	1.187	1.657	2.029
210	.1036	1.638	2.083	2.388
220	.1668	2.196	2.566	2.773
230	.2575	2.869	3.106	3.181
240	.3835	3.668	3.702	3.611
250	.5532	4.600	4.354	4.061
260	.7760	5.670	5.059	4.531
270	1.062	6.883	5.817	5.081
280	1.420	8.244	6.626	5.522
290	1.862	9.754	7.483	6.042
300	2.398	11.42	8.387	6.576
310	3.039	13.23	9.336	7.123
320	3.794	15.19	10.33	7.683
330	4.675	17.31	11.36	8.254
340	5.690	19.57	12.43	8.837
350	6.848	21.99	13.54	9.430

Table 4-2
Effective Spectral Response, φ_λ 6.5 - 7.0 Micron Channel

λ, Microns	Relative Response	λ, Microns	Relative Response
6.0	0.0	6.55	1.00
6.05	.002	6.60	.958
6.10	.004	6.65	.765
6.15	.009	6.70	.572
6.20	.014	6.75	.361
6.25	.117	6.80	.150
6.30	.220	6.85	.080
6.35	.501	6.90	.011
6.40	.782	6.95	.006
6.45	.880	7.00	0.0
6.50	.958		

Table 4-3
Effective Spectral Response, φ_λ 10 - 11 Micron Channel

λ, Microns	Relative Response	λ, Microns	Relative Response
9.1	0.0	10.7	.998
9.2	.010	10.8	.991
9.3	.020	10.9	.958
9.4	.020	11.0	.839
9.5	.037	11.1	.696
9.6	.055	11.2	.515
9.7	.090	11.3	.357
9.8	.129	11.4	.224
9.9	.240	11.5	.119
10.0	.372	11.6	.088
10.1	.539	11.7	.052
10.2	.679	11.8	.035
10.3	.803	11.9	.030
10.4	.887	12.0	.018
10.5	.967	12.1	0.0
10.6	1.00		

Table 4-4
Effective Spectral Response, ϕ_λ, 14.5 - 15.5 Micron Channel

λ, Microns	Relative Response	λ, Microns	Relative Response
14.0	0.0	15.2	1.00
14.1	.022	15.3	.974
14.2	.053	15.4	.919
14.3	.143	15.5	.870
14.4	.270	15.6	.761
14.5	.538	15.7	.615
14.6	.787	15.8	.410
14.7	.917	15.9	.261
14.8	.976	16.0	.134
14.9	.990	16.1	.058
15.0	.996	16.2	.026
15.1	1.00	16.3	0.0

Table 4-5
Effective Spectral Response, ϕ_λ, 20 - 23 Micron Channel

λ, Microns	Relative Response	λ, Microns	Relative Response
20.2	0.0	22.1	.782
20.3	.034	22.2	.711
20.4	.061	22.3	.669
20.5	.138	22.4	.664
20.6	.244	22.5	.703
20.7	.404	22.6	.758
20.8	.599	22.7	.807
20.9	.765	22.8	.826
21.0	.829	22.9	.810
21.1	.847	23.0	.760
21.2	.860	23.1	.675
21.3	.880	23.2	.574
21.4	.906	23.3	.455
21.5	.924	23.4	.324
21.6	1.00	23.5	.218
21.7	1.00	23.6	.130
21.8	.980	23.7	.065
21.9	.916	23.8	.030
22.0	.844	23.9	0.0

Table 4-6
Effective Spectral Response, ϕ_λ 0.2 - 4 Micron Channel

λ, Microns	Relative Response	λ, Microns	Relative Response
0.2	0.0	2.4	0.87
0.3	0.20	2.5	0.86
0.4	0.40	2.6	0.88
0.5	0.64	2.7	0.89
0.6	0.58	2.8	0.90
0.65	0.545	2.9	0.995
0.7	0.53	3.0	1.00
0.75	0.47	3.1	1.00
0.8	0.45	3.2	0.98
0.85	0.465	3.3	0.91
0.9	0.55	3.4	0.928
1.0	0.74	3.5	0.94
1.1	0.86	3.6	0.70
1.2	0.92	3.7	0.60
1.3	0.97	3.8	0.53
1.4	0.97	3.9	0.51
1.5	1.00	4.0	0.40
1.6	0.96	4.1	0.36
1.7	0.98	4.2	0.28
1.8	0.96	4.3	0.21
1.9	0.92	4.4	0.11
2.0	0.92	4.5	0.135
2.1	0.92	4.6	0.15
2.2	0.89	4.7	0.085
2.3	0.90	4.8	0.0

For laboratory calibrations a blackbody target whose surface was treated with a diffuse black paint of high emissivity was used. To further improve the emissivity, the target was machined with a series of parallel V shaped grooves of approximately 15° wedge angle. The target assembly is shown in Figure 4-11.

The blackbody can be cooled by liquid nitrogen to 100°K or below and then heated with nichrome wire to any temperature within the overall dynamic range of the radiometer. The heater coil is designed so that during the warming cycle thermal gradients across the surface are maintained within ±1/2°C.

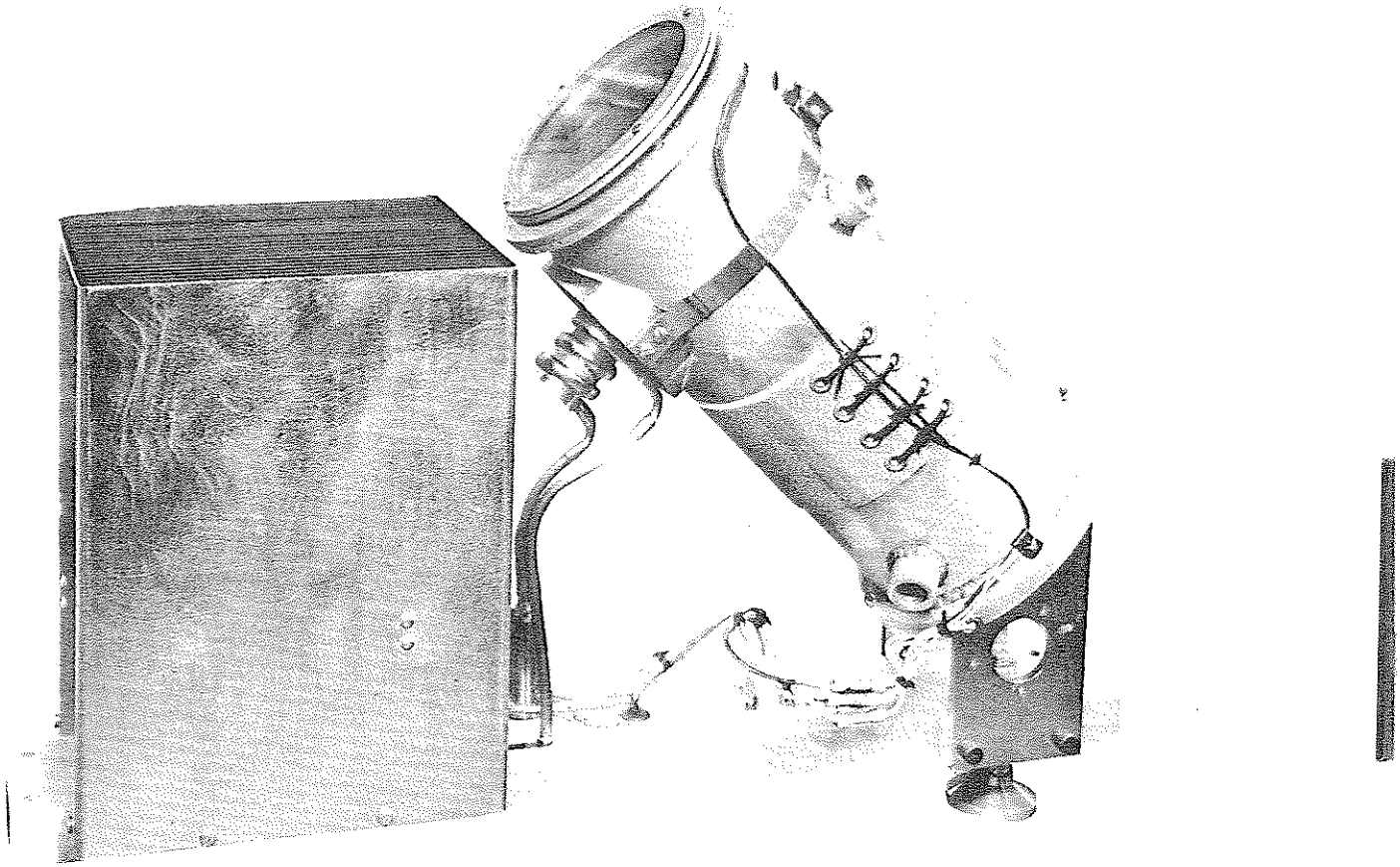

Figure 4-11– Calibration Targets for the MRIR

The radiometer is mounted such that the blackbody and the short wave radiation targets fill the fields of view of the appropriate channels. The output of the radiometer is recorded on a strip chart recorder, and a calibration curve, such as that shown in Figure 4-12, is constructed.

The short wave channel is calibrated by means of a diffuse target whose absolute calibration was determined by comparison with a standard of spectral radiance furnished by the National Bureau of Standards. The calibration of the diffuse target was carried out at a number of color temperatures and given in terms of spectral radiance, N vs. input voltage to the target lamp. By varying the input voltage, a calibration curve of radiometer output voltage (0 to -6.4v) vs. $\bar{N}$, is generated with the aid of Equation (1). A typical calibration curve for this channel is given in Figure 4-13. In order to calculate the reflectance of incident

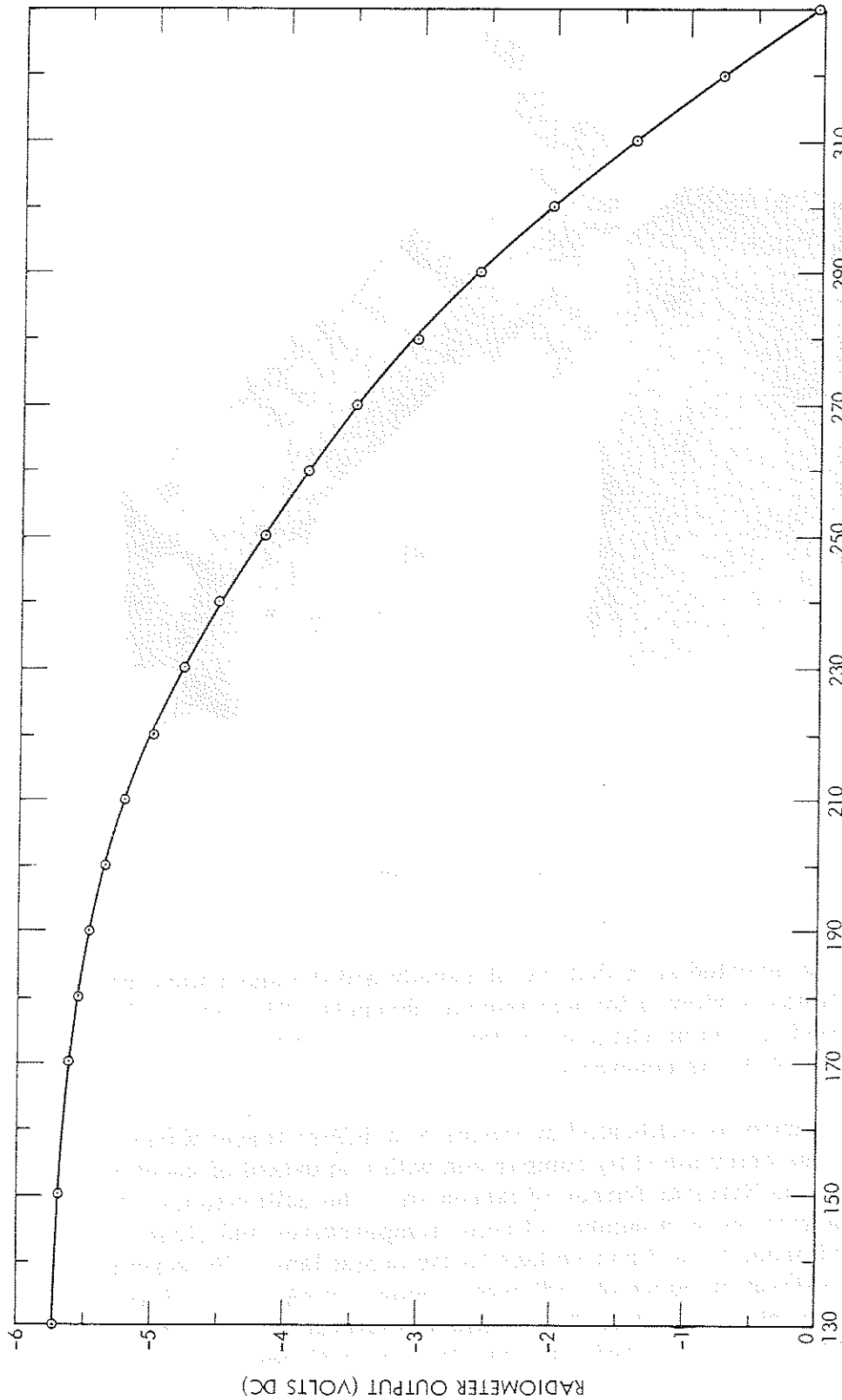

Figure 4-12–Typical Calibration Curve for an IR Channel

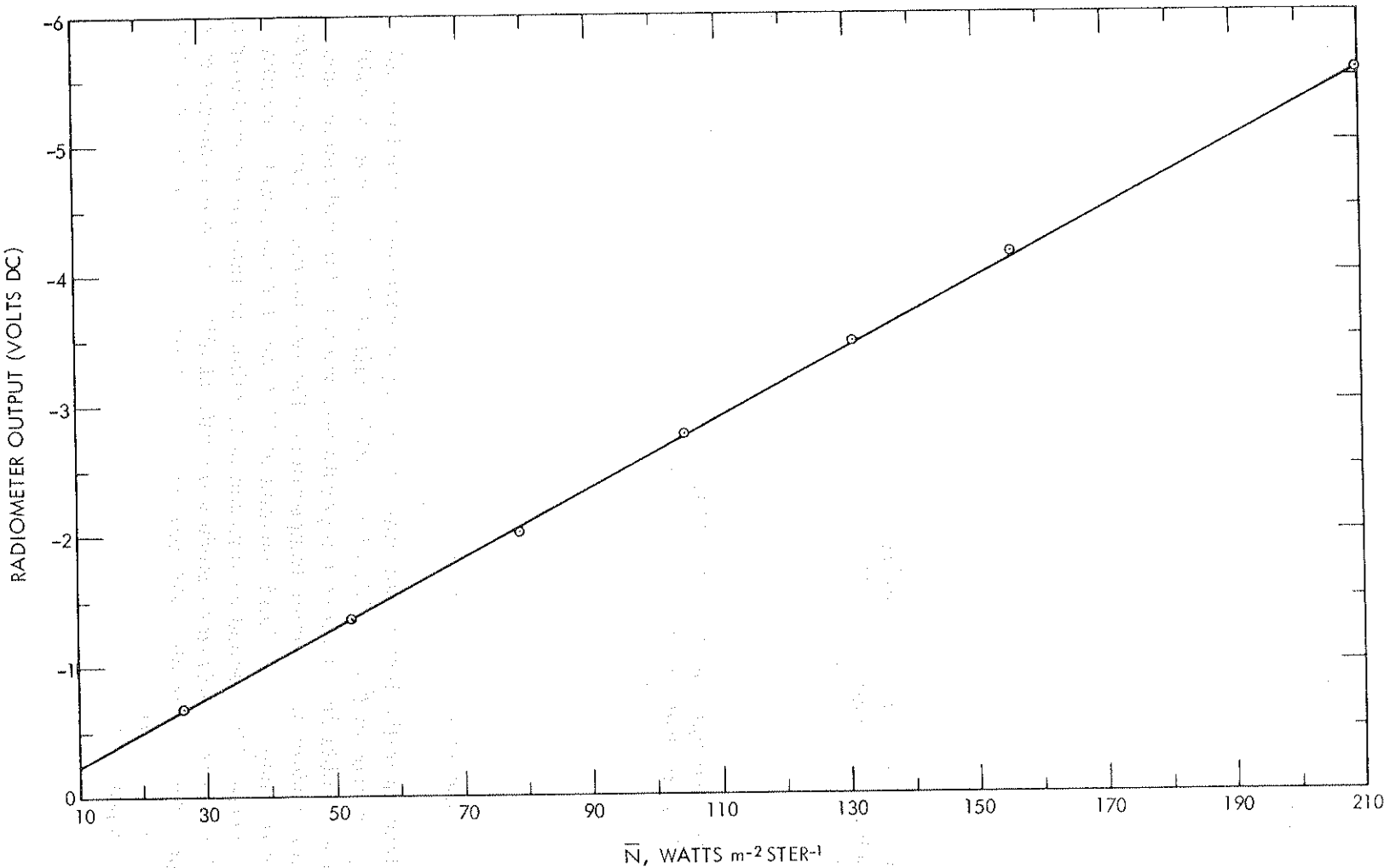

Figure 4-13– Typical Calibration Curve for 0.2–4.0 Micron Channel

solar radiation of a spot on earth viewed by the radiometer, one must know the effective solar constant, $\bar{H}^*$, i.e., the integral over all wavelengths of the solar spectral irradiance at the top of the atmosphere, $\bar{H}^*$, multiplied by the effective spectral response of the channel, given by

$$\bar{H}^* = \int_0^\infty H_\lambda^* \, \phi_\lambda \, d\lambda \tag{2}$$

where

$$\int_0^\infty H_\lambda^* \, d\lambda = 2.0 \text{ g-cal cm}^{-2} \text{ min}^{-1} = 1395 \text{ watts m}^{-2} \tag{3}$$

A calculation of $\bar{H}^*$ was made using the solar spectral irradiance data given in "The Handbook of Geophysics" (Reference 36), and the effective spectral response given in Table 4-7, resulting in the value

$$\bar{H}^* = 870.2 \text{ watts m}^{-2} \tag{4}$$

The effective average radiant reflectance in the direction of the satellite, $\bar{r}$, of a surface filling the field of view of the radiometer and illuminated by unattenuated solar radiation can be defined by

$$\bar{r} = \frac{\pi \bar{N}}{\bar{H}^* \cos \zeta^*} \tag{5}$$

where ζ^* is the solar zenith angle.

Calibration of the instrument was performed in vacuum at nominal radiometer temperatures of 0°C, 10°C, 17.5°C, 25°C, and 40°C. Two sets of calibration data were obtained at these temperatures, one with the radiometer and its electronics module at the same temperature; the second set of data was obtained with the electronic module held constant at 25°C and the radiometer cycled through the same range. The second calibration is to allow for interpolation should the radiometer and its electronics module operate at different temperatures on the spacecraft. The values obtained from these calibrations are tabulated in Tables 4-7 and 4-8. The tables refer to radiometer serial number P-2 which is installed on Nimbus III.

TABLE 4-7

CALIBRATION DATA FOR MRIR RADIOMETER P-2, CHOPPER AT TEMPERATURE INDICATED, ELECTRONICS AT 25°C

CHANNEL →	6.5–7.0 MICRONS					10–11 MICRONS					14.5–15.5 MICRONS					20–23 MICRONS					0.2–4.0 MICRONS					
	OUTPUT SIGNAL (VOLTS DC)					OUTPUT SIGNAL (VOLTS DC)					OUTPUT SIGNAL (VOLTS DC)					OUTPUT SIGNAL (VOLTS DC)					OUTPUT SIGNAL (VOLTS DC)					
RADIOMETER TEMP °C →	0	10	17.5	25	40	0	10	17.5	25	40	0	10	17.5	25	40	0	10	17.5	25	40	0	10	17.5	25	40	
TARGET TEMP °K ↓																										Ñ FOR SOLAR CHANNEL
0	-4.75	-4.75	-4.75	-4.72	-4.72	-5.75	-5.80	-5.77	-5.70	-5.47	-5.70	-5.60	-5.57	-5.50	-5.15	-5.50	-5.12	-4.87	-4.57	-3.90	0	0	0	0	0	27.70
110	-4.75	-4.75	-4.75	-4.72	-4.72	-5.72	-5.77	-5.75	-5.70	-5.45	-5.67	-5.60	-5.55	-5.45	-5.15	-5.40	-5.02	-4.80	-4.50	-3.82	-0.80	-0.80	-0.80	-0.78	-0.77	55.40
130	-4.72	-4.72	-4.72	-4.72	-4.70	-5.72	-5.76	-5.75	-5.70	-5.45	-5.60	-5.50	-5.45	-5.37	-5.02	-5.20	-4.82	-4.62	-4.35	-3.65	-1.62	-1.50	-1.50	-1.47	-1.47	83.10
150	-4.72	-4.72	-4.70	-4.72	-4.70	-5.72	-5.72	-5.74	-5.67	-5.45	-5.40	-5.30	-5.25	-5.17	-4.85	-4.97	-4.57	-4.40	-4.10	-3.45	-2.20	-2.20	-2.22	-2.20	-2.17	110.80
170	-4.67	-4.69	-4.69	-4.68	-4.67	-5.66	-5.64	-5.66	-5.60	-5.39	-5.00	-4.97	-4.87	-4.80	-4.52	-4.57	-4.20	-4.00	-3.75	-3.12	-3.00	-2.95	-3.00	-2.97	-2.95	138.50
180	-4.62	-4.65	-4.65	-4.65	-4.62	-5.57	-5.60	-5.60	-5.52	-5.32	-4.77	-4.70	-4.62	-4.50	-4.30	-4.30	-4.00	-3.80	-3.52	-2.97	-3.72	-3.67	-3.75	-3.72	-3.72	166.20
190	-4.55	-4.55	-4.57	-4.57	-4.57	-5.46	-5.50	-5.47	-5.42	-5.20	-4.55	-4.40	-4.30	-4.25	-4.02	-4.00	-3.77	-3.55	-3.27	-2.77	-4.47	-4.47	-4.50	-4.52	-4.50	193.90
200	-4.42	-4.42	-4.50	-4.45	-4.42	-5.37	-5.40	-5.40	-5.32	-5.10	-4.10	-4.02	-3.97	-3.90	-3.70	-3.72	-3.47	-3.30	-3.02	-2.55	-5.22	-5.20	-5.30	-5.32	-5.32	221.60
210	-4.25	-4.27	-4.25	-4.25	-4.25	-5.20	-5.22	-5.20	-5.17	-5.00	-3.72	-3.62	-3.65	-3.50	-3.35	-3.40	-3.20	-2.97	-2.77	-2.30	-5.95	-5.95	-6.00	-6.02	-6.00	
220	-4.00	-3.97	-4.00	-4.00	-4.00	-5.00	-5.02	-5.02	-5.00	-4.80	-3.27	-3.17	-3.10	-3.02	-2.90	-3.07	-2.85	-2.67	-2.45	-2.02						
230	-3.60	-3.60	-3.62	-3.62	-3.60	-4.80	-4.80	-4.80	-4.80	-4.60	-2.77	-2.65	-2.60	-2.52	-2.45	-2.75	-2.52	-2.35	-2.15	-1.80						
240	-3.06	-3.07	-3.10	-3.12	-3.15	-4.57	-4.55	-4.50	-4.52	-4.37	-2.20	-2.07	-2.00	-1.92	-1.90	-2.35	-2.17	-2.00	-1.80	-1.50						
250	-2.45	-2.42	-2.40	-2.45	-2.50	-4.22	-4.22	-4.20	-4.22	-4.05	-1.60	-1.47	-1.40	-1.32	-1.35	-1.97	-1.80	-1.60	-1.42	-1.22						
260	-1.45	-1.50	-1.55	-1.55	-1.60	-3.90	-3.90	-3.87	-3.90	-3.77	-0.92	-0.82	-0.75	-0.62	-0.65	-1.57	-1.40	-1.22	-1.05	-0.85						
270	-0.35	-0.40	-0.40	-0.40	-0.45	-3.52	-3.55	-3.47	-3.52	-3.37	-0.20	-0.12	-0.00		-0.02	-1.10	-1.00	-0.82	-0.67	-0.50						
280						-3.05	-3.15	-3.02	-3.12	-2.95						-0.65	-0.60	-0.45	-0.30	-0.10						
290						-2.60	-2.67	-2.60	-2.65	-2.50						-0.25	-0.17	-0.05								
300						-2.05	-2.17	-2.10	-2.15	-2.00																
310						-1.52	-1.57	-1.55	-1.60	-1.47																
320						-0.80	-0.97	-1.00	-1.02	-0.90																
330						-0.27	-0.37	-0.37	-0.40	-0.30																

TABLE 4.8

CALIBRATION DATA FOR MRIR S/N P-2 RADIOMETER, CHOPPER AND ELECTRONICS AT INDICATED TEMPERATURE

CHANNEL →	6.5–7.0 MICRONS					10–11 MICRONS					14.5–15.5 MICRONS					20–23 MICRONS					0.2–4.0 MICRONS					
	OUTPUT SIGNAL (VOLTS DC)					OUTPUT SIGNAL (VOLTS DC)					OUTPUT SIGNAL (VOLTS DC)					OUTPUT SIGNAL (VOLTS DC)					OUTPUT SIGNAL (VOLTS DC)					
RAD. AND ELECT TEMP °C →	0	10	17.5	25	40	0	10	17.5	25	40	0	10	17.5	25	40	0	10	17.5	25	40	0	10	17.5	25	40	
TARGET TEMP °K ↓																										$\bar{N}$ FOR SOLAR CHANNEL
0	-4.55	-4.55	-4.72	-4.72	-4.80	-5.72	-5.60	-5.70	-5.70	-5.57	-5.37	-5.42	-5.50	5.50	-5.32	-5.30	-5.10	-4.82	-4.55	-3.85	0	0	0	0	0	0
110	-4.55	-4.55	-4.72	-4.72	-4.80	-5.45	-5.60	-5.70	-5.70	-5.55	-5.35	-5.40	-5.47	-5.45	-5.32	-5.20	-5.07	-4.72	-4.50	-3.80	-0.72	-0.75	-0.77	-0.78	-0.78	27.70
130	-4.55	-4.55	-4.70	-4.72	-4.78	-5.45	-5.55	-5.68	-5.68	-5.54	-5.27	-5.32	-5.37	-5.37	-5.20	-5.05	-4.85	-4.60	-4.35	-3.62	-1.40	-1.42	-1.47	-1.50	-1.47	55.40
150	-4.55	-4.54	-4.69	-4.72	-4.77	-5.40	-5.50	-5.64	-5.64	-5.50	-5.10	-5.15	-5.20	-5.17	-5.00	-4.80	-4.60	-4.30	-4.10	-3.42	-2.07	-2.12	-2.20	-2.20	-2.20	83.10
170	-4.53	-4.52	-4.66	-4.67	-4.70	-5.32	-5.42	-5.56	-5.56	-5.43	-4.75	-4.80	-4.82	-4.80	-4.62	-4.40	-4.20	-3.95	-3.75	-3.10	-2.80	-2.85	-2.95	-2.97	-2.95	110.80
180	-4.50	-4.45	-4.62	-4.65	-4.67	-5.30	-5.40	-5.50	-5.52	-5.40	-4.50	-4.52	-4.60	-4.50	-4.40	-4.20	-3.97	-3.72	-3.52	-2.90	-3.55	-3.60	-3.72	-3.75	-3.75	138.50
190	-4.40	-4.37	-4.57	-4.57	-4.60	-5.20	-5.30	-5.42	-5.42	-5.30	-4.22	-4.22	-4.27	-4.25	-4.10	-3.95	-3.70	-3.50	-3.27	-2.75	-4.30	-4.35	-4.50	-4.52	-4.52	166.20
200	-4.30	-4.30	-4.42	-4.45	-4.50	-5.07	-5.20	-5.30	-5.32	-5.20	-3.90	-3.90	-3.95	-3.90	-3.75	-3.62	-3.45	-3.22	-3.02	-2.47	-5.02	-5.15	-5.27	-5.30	-5.32	193.90
210	-4.07	-4.10	-4.27	-4.25	-4.30	-4.97	-5.02	-5.17	-5.17	-5.02	-3.52	-3.47	-3.57	-3.50	-3.35	-3.37	-3.10	-3.00	-2.77	-2.20	-5.72	-5.85	-6.00	-6.02	-6.05	221.60
220	-3.80	-3.85	-4.00	-4.00	-4.07	-4.80	-4.90	-5.00	-5.00	-4.87	-3.10	-3.05	-3.07	-3.02	-2.87	-3.02	-2.82	-2.62	-2.45	-1.97						
230	-3.50	-3.47	-3.62	-3.62	-3.70	-4.60	-4.70	-4.80	-4.80	-4.70	-2.62	-2.57	-2.60	-2.52	-2.40	-2.67	-2.50	-2.30	-2.15	-1.65						
240	-3.00	-3.00	-3.07	-3.12	-3.20	-4.35	-4.42	-4.52	-4.52	-4.40	-2.07	-2.00	-2.00	-1.92	-1.82	-2.30	-2.15	-1.97	-1.80	-1.35						
250	-2.35	-2.30	-2.42	-2.45	-2.50	-4.05	-4.17	-4.22	-4.22	-4.15	-1.50	-1.40	-1.40	-1.32	-1.25	-1.97	-1.77	-1.60	-1.42	-1.00						
260	-1.42	-1.45	-1.55	-1.55	-1.60	-3.75	-3.80	-3.90	-3.90	-3.80	-0.85	-0.75	-0.70	-0.62	-0.60	-1.55	-1.40	-1.22	-1.05	-0.70						
270	-0.35	-0.35	-0.45	-0.40	-0.47	-3.40	-3.45	-3.55	-3.52	-3.40	-0.20	-0.02	-0.00			-1.15	-1.00	-0.82	-0.67	-0.40						
280						-3.00	-3.05	-3.15	-3.12	-3.02						-0.72	-0.60	-0.45	-0.30	-0.10						
290						-2.57	-2.62	-2.62	-2.65	-2.57						-0.30	-0.20	-0.05								
300						-2.05	-2.12	-2.17	-2.15	-2.05																
310						-1.50	-1.60	-1.62	-1.60	-1.55																
320						-0.92	-1.00	-1.02	-1.02	-0.95																
330						-0.30	-0.40	-0.40	-0.40	-0.32																

The points tabulated in Tables 4-7 and 4-8 are actual measured values. There is some scatter due to experimental error, therefore some smoothing of the data is desirable. For example, utilizing the $\bar{N}$ vs. T_{BB} values (Table 4-1), a linear least squares fit of the points may be readily obtained and then converted to Voltage vs. T_{BB} curves if desired.

During flight the calibration of the instrument can be checked by two measurements in each channel.

In the infrared channels these points occur when the scanner is viewing cold space and when it is "looking" at the radiometer housing. Two housekeeping telemetry points monitor the housing temperature and these may be compared to the radiation temperature as indicated by the radiometer output during that portion of the scan. The expected response to deep space is known (see 0°K points in Tables 4-7 and 4-8), so the two measurements should be sufficient to reconstruct the calibration curve if any instrumental degradation should occur in the space environment.

Three of the infrared channels (those centered at 6.6, 15 and 22 microns) are not expected to record the expected housing temperatures. Signals that otherwise would be positive voltages from these three channels while viewing the relatively warm housing are electronically clamped at 0 volts (Figure 4-7) and, hence, cannot be used for calibration purposes. To obtain a check of calibration in these two channels an electronic input ("sync" pulse) which is present in all of the thermal channels is utilized. This voltage consists of a pulse added to the signal and to the offset voltage once per scan just as the scan mirror enters the housing (Figure 4-7). This pulse is a precise voltage primarily designed to calibrate the electronic gain of the system, but since it is added to the signal its height above the zero volt level will be proportional to the housing temperature. Figures 4-14, 4-15 and 4-16 are curves of the "sync" pulse amplitude vs. housing temperature for these three channels. Also, these values are listed in Table 4-9.

In addition to the housing temperature monitors, the temperature of two locations in the chopper housing and one in the electronics module are monitored. The housekeeping telemetry values are tabulated in Table 4-10.

4.3 Data Processing, Archiving and Access

4.3.1 General

The spacecraft tape recorder has a capacity for recording data for more than one complete orbit. The tape recorder is not of the endless loop type. It records

Table 4-9
Output of Radiometer when Field of View is Filled by the Housing and the "Sync" Pulse is Applied

Rad. Temp. (°C)	6.7 Micron	14.5-15.5 Micron	20-23 Micron
0	-4.47	-4.29	-3.38
5	-4.43	-3.93	-3.17
10	-4.34	-3.55	-2.93
15	-4.25	-3.12	-2.66
20	-4.09	-2.66	-2.35
25	-3.94	-2.21	-2.08
30	-3.77	-1.77	-1.82
35	-3.60	-1.35	-1.56
40	-3.41	-0.97	-1.34

Table 4-10
Temperature Telemetry Values For MRIR Radiometer

Temp. (°C)	Chopper #1	Chopper #2	Housing #1	Housing #2	Electronics Modules
0	-4.56	-4.50	-4.55	-4.44	-4.47
5	-3.87	-3.82	-3.85	-3.83	-3.82
10	-3.25	-3.22	-3.24	-3.25	-3.21
15	-2.71	-2.69	-2.72	-2.73	-2.71
20	-2.25	-2.25	-2.29	-2.30	-2.27
25	-1.90	-1.89	-1.93	-1.92	-1.90
30	-1.61	-1.60	-1.64	-1.61	-1.61
35	-1.36	-1.36	-1.39	-1.36	-1.36
40	-1.15	-1.14	-1.16	-1.15	-1.16

in one direction and plays back in the reverse direction. This direction reversal is taken into account when the data are processed in the ground station. Upon the command to playback, the tape speed is increased 32 times and the data are transmitted in approximately 4 minutes. Because of the capacity of the recorder at least one full orbit of data can be received at each interrogation.

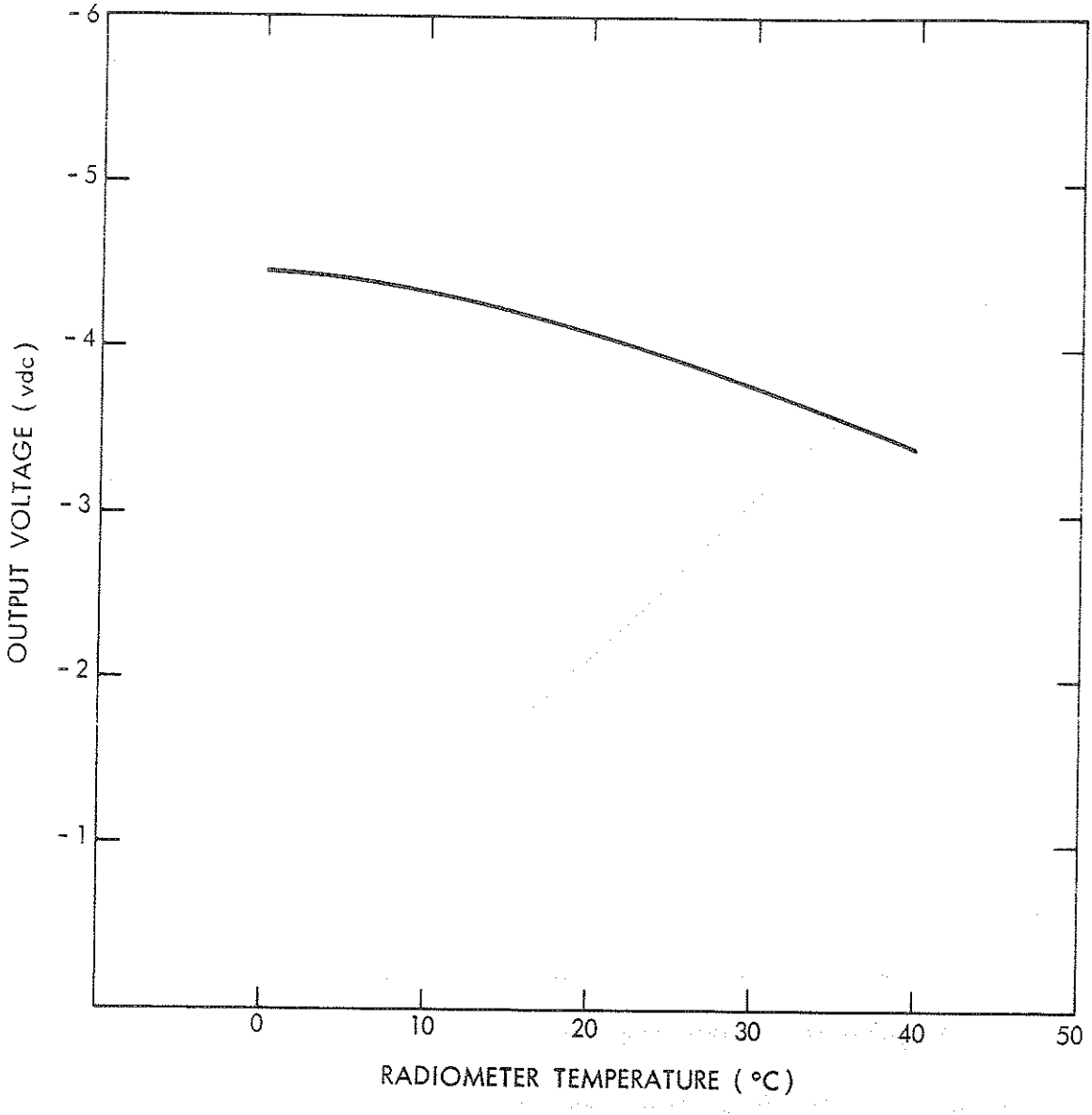

Figure 4-14– Output of 6.5–7.0 Micron Channel When the Field of View is Filled by the Housing Scan and the Sync Pulse is applied

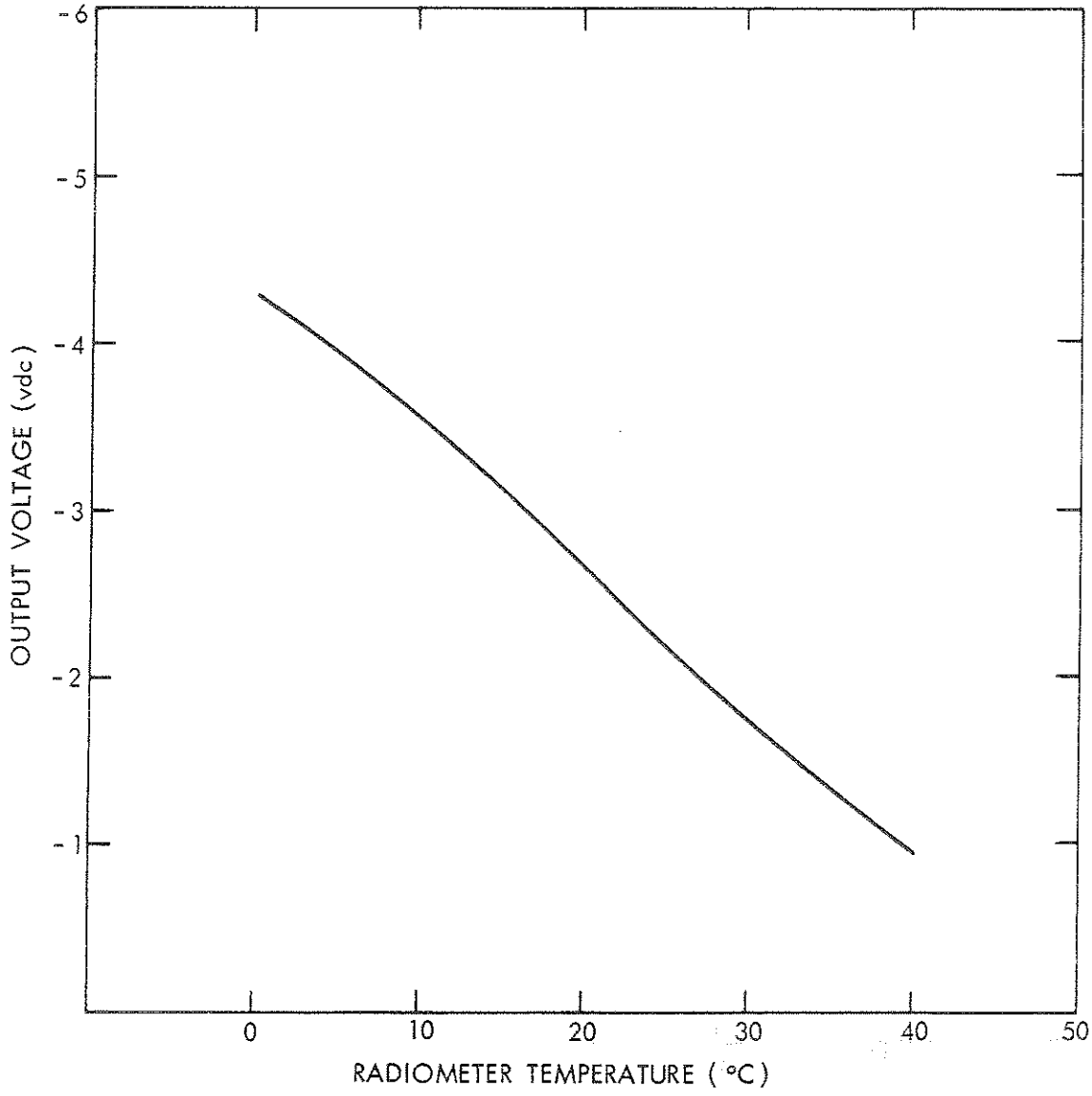

Figure 4-15–Output Voltage of14.5–15.5 Micron Channel When the Field of View is Filled by the Housing Scan and the Sync Pulse is Applied

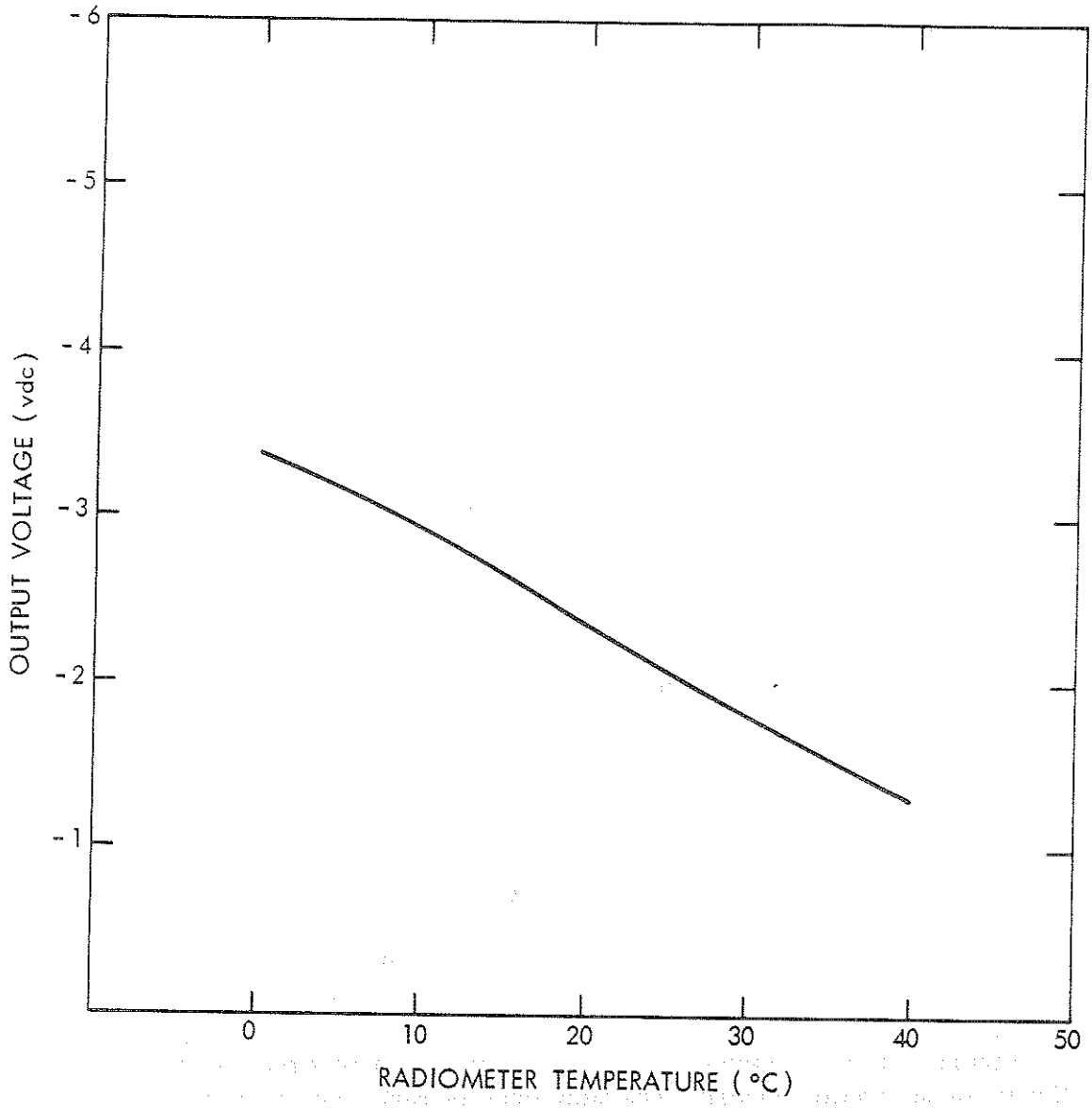

Figure 4-16–Output Voltage of 20–23 Micron Channel When the Field of View is Filled by the Housing Scan and the Sync Pulse is Applied

After data from the spacecraft are transmitted to GSFC, they are processed by a Telemetrics 670 computer. The Telemetrics 670 has three distinct outputs for data analysis which will be discussed in the following sections: (1) a strip chart recording of analog output as a function of time for detailed study of specific phenomena; (2) a digital tape compatible with the IBM 360 for automatic mapping and analysis; and (3) a photo display of each channel for each orbit.

All three data formats are available to the scientific community through the NSSDC.

4.3.2 Analog Outputs

These will be in the form of strip charts from an eight-channel Brush Mark 200 recorder. Each chart will contain an entire orbit of data from each channel with timing information recorded on the eighth channel (see Figure 4-17). The data will be recorded as voltage from 0 to -6.35 volts d.c. and the calibration data shown in Tables 4-7 and 4-8 will apply.

The arrangement of information is as follows:

Recorder Channel	Information
1	6.5-7.0 micron data
2	10-11 micron data
3	14.5-15.5 micron data
4	20-23 micron data
5	0.2 - 4.0 micron data
6	Blank
7	Earth scan boundaries
8	Time code display

Figure 4-17 is a sample of the time information recorded on the eighth channel of the analog record. The time code is read from right to left. It consists of two short pulses of full amplitude (-6.35 volts), followed by day, hour, minute, second frames, each separated by one full amplitude pulse. Units of time within each frame are represented by pulses of proportional amplitude. The full amplitude (-6.35 volts) is divided into tenths: one tenth (-0.6 volts) represents one, two tenths (-1.3 volts) represents two, etc. Zero is represented by a 0.2 volts pulse. Small narrow pulses of 1 volt amplitude are at the beginning and end of the hour and minute frames, and at the beginning (right) of the day, and second frames.

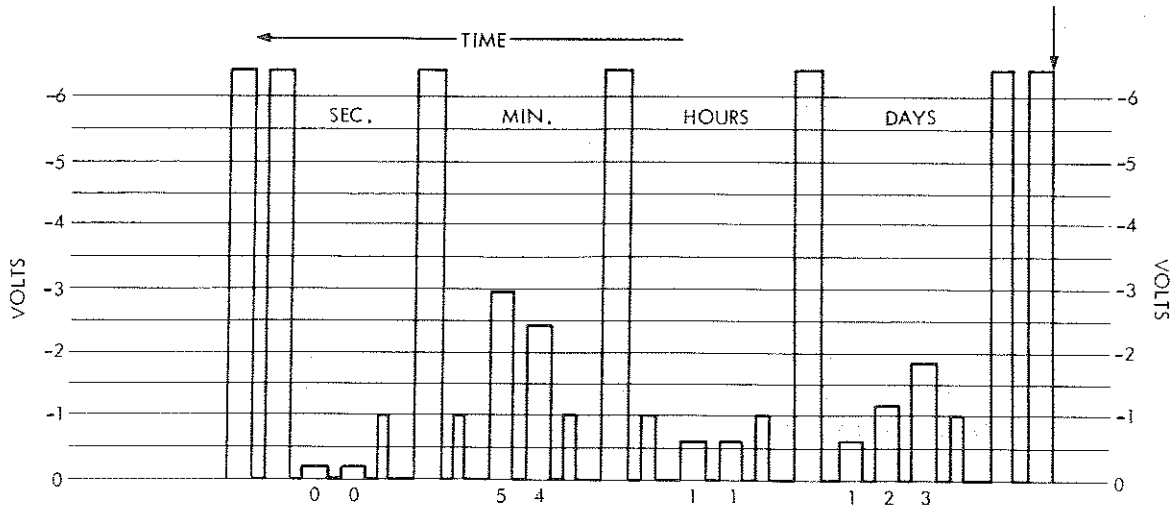

Figure 4-17– MRIR Analog Record Time Display. Time Shown Occurs at the Vertical Arrow and is Day 321, 11h 45m 00 sec

Temperature fluctuations of the instrument throughout the orbit require that data from the infrared channels be corrected by means of in-flight calibration points (Sec. 4-2). To facilitate data analysis, a copy of the Selected Data Tape listing will be furnished with each analog record. This listing includes the two housing thermistor readings, the two chopper thermistor readings and the electronics Module Temperature. The column headings are in terms of a "function number" which are identified as follows:

Telemetry Function	Function Number
Housing Temperature 1	1102
Housing Temperature 2	1108
Chopper Temperature 1	1103
Chopper Temperature 2	1107
Electronics Module Temperature	1105

4.3.3 Digital MRIR Data Processing

4.3.3.1 The Nimbus Meteorological Radiation Tape – MRIR (NMRT-MRIR)

The digital magnetic tape output of the Telemetrics 670 computer represents a primary source of raw experimental data from the MRIR radiometer. Radiation data from this tape, calibration data, and orbital data are combined by an IBM 360 to produce a reduced radiation data tape called the Nimbus Meteorological

Radiation Tape – MRIR (NMRT-MRIR). The NMRT archived at NSSDC can be used to generate grid print maps or to accomplish special scientific analyses. It is anticipated that MRIR-NMR Tapes will begin to be available through NSSDC within 6 months after launch. The format of this tape is the same as for the Nimbus II NMRT-MRIR and is given in Section 4.4.

4.3.3.2 Grid Print Maps

A series of programs produce printed and contoured data referenced to a square mesh grid on polar stereographic Mercator map bases. Grid print maps may be produced for either a single orbit or a composite of several orbits. The following standard options are available and should be specified when requesting grid print maps:

1. Map and Approximate Scale

    a. Polar Stereographic, 1/30 million (approx.)
    b. Polar Stereographic, 1/10 million (approx.)
    c. Multi-Resolution Mercator

        1. 5.0 degrees long. per mesh interval – 1/40 million (approx.)
        2. 2.5 degrees long. per mesh interval – 1/20 million (approx.)
        3. 1.25 degrees long. per mesh interval – 1/10 million (approx.)

2. Maximum Sensor Nadir Angle

3. Field Values and Contouring (unless otherwise specified, all maps will include field values and contouring).

A data population map, indicating the number of individual measurements contained in each grid point average, as well as a sample latitude-longitude overlay for geographically locating the data, will ordinarily be provided along with each grid print map.

When ordering NMRT output data from NSSDC, the following identifying information should be given:

1. Satellite (e.g. Nimbus III)
2. Sensor (e.g. MRIR)
3. Read-Out Orbit No.
4. MRIR Channel No. (e.g. MRIR Channel 2, 10 - 11 Microns)
5. Calendar Data of Equator Crossing
6. Beginning and Ending Times of Data in GMT
7. Format Desired (see 4.3.3.2, items 1; 2; 3)
8. Address to which data are to be mailed.

4.3.4 Photo Display

As part of the "on-line" processing, the digital output of each channel will be transmitted to a cathode ray tube photo display which will index each data word as to its X-Y coordinates by synchronizing with spacecraft time and the radiometer "sync" pulse described in Section 4-2. The "Z" axis modulation is determined by the amplitude of the radiometer output. The format of this photo display is shown in Figure 4-18. The annotation, time bench marks, and gridding are produced prior to interrogation by a CDC 924 computer, punched on paper tape, and fed to the Telemetrics 670. The calibration gray scale is generated within the Telemetrics computer and displayed on the CRT coincidentally with the data. Because the same shades of gray represent different target temperatures (or effective radiance for the 0.2-4 channel) for different channels, they are labeled only by arbitrary intensity levels. Table 4-11 gives the correlation between these levels and T_{BB} (or $\bar{N}$) for each channel. Figure 4-18 is actually a print of Nimbus II data; however, only minor changes have been made between this format and that of Nimbus III.

The CRT display is rigidly controlled electronically by monitoring the phosphor intensity of each spot as the picture is generated on the screen. Because of this the main errors to be expected in an attempt to analyze the photo display quantitatively will occur in the picture development itself. The picture will be made by photographing the CRT face with a Polaroid camera using 4" × 5" film pack which provides both a positive print and negative transparency.

Positive and negative transparencies will be stored at the National Space Science Data Center, code 601, GSFC, Greenbelt, Maryland 20771, to fulfill users requests. Reproductions of these data can be made as positive and negative film transparencies and enlarged prints.

The basic unit for furnishing photographic data will be the Readout Orbit number, which normally contains data recorded in the spacecraft during the orbital period immediately prior to the interrogation.

When ordering MRIR photographic data the following information should be furnished:

1. Satellite (e.g. Nimbus III)
2. Sensor (e.g. MRIR)
3. Readout Orbit number
4. Beginning and end data and time of data desired for confirmation of readout orbit number.
5. Format desired (e.g. positive or negative film transparencies or positive paper prints and size (4" × 5", 8" × 10")
6. Address to which data are to be mailed.

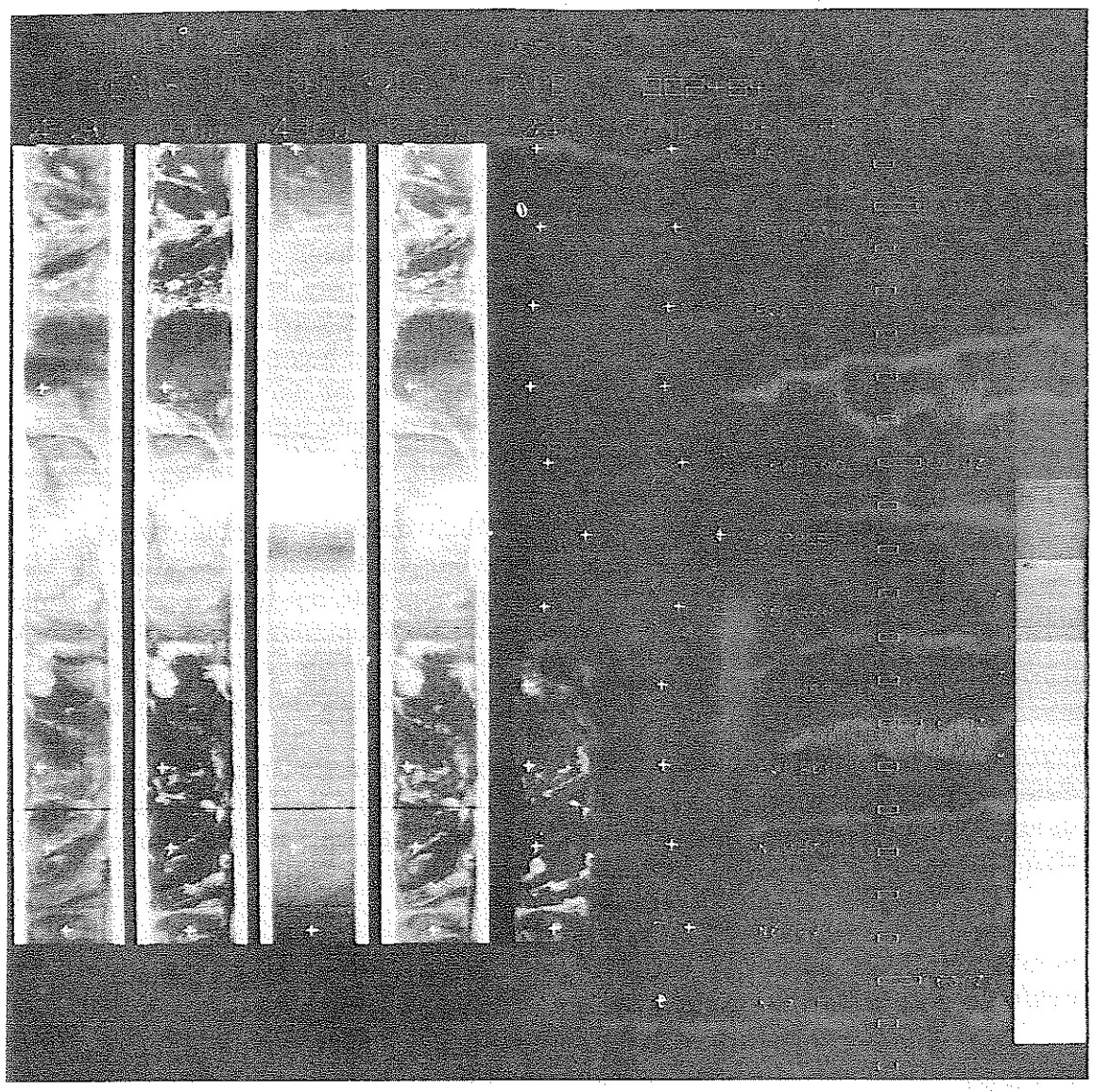

Figure 4-18– Format of CRT Display

Table 4-11
Gray Level Values for Pictorial Display

Grey Level	Channel Target Values				
	6.4-6.8μ	10-11μ	14.5-15.5μ	20-23μ	0.2-4.0μ
	°K	°K	°K	°K	$\bar{N}(Wm^{-2}\,Ster^{-1})$
1	264-270	309-320	239-245	282-290	199-210
2	257-263	297-308	234-239	273-281	169-189
3	250-257	285-296	228-233	264-272	148-168
4	243-249	273-284	222-227	255-263	127-147
5	236-242	261-272	216-221	246-254	106-126
6	229-235	249-260	210-215	237-245	85-105
7	222-228	237-248	204-209	228-236	64-84
8	215-221	225-236	198-203	219-227	43-63
9	208-214	213-224	192-197	210-218	22-42
10	201-207	201-212	186-191	201-209	1-21
11	200 & below	200 & below	185	200 & below	0

4.4 Format of the NMRT-MRIR Tape

The MRIR digital magnetic tape (output of the Telemetrics 670 Computer) is formatted for compatibility with the IBM 360 computer system. The digital response from each radiometer sensor is stripped of sync bits and all five simultaneous responses are placed in one 36-bit IBM word with 7 bits for each data measurement and a one in the least significant bit. The time code is also stripped of all unnecessary bits and formatted into one 36-bit word expressing time to the nearest second. The following special code words are inserted to identify the various conditions described below:

1. $(666666666666)_8$ – Identifies the next word as the Minitrack time word.
2. $(777777777777)_8$ – Identifies end of data.
3. $(525252525252)_8$ – Identifies data dropout. This code word is used when all five measurements are simultaneously bad. When an individual measurement is bad, the data for that measurement is set equal to the previous measurement.

The magnetic tape containing the formatted MRIR radiation data represents the primary source of radiometer data for further processing and archiving. The first step in this procedure is to examine the formatted radiometer output and create an intermediate tape which contains (1) the response from each radiometer channel for every earth-viewed scan, (2) the associated response from each channel of the radiometer while viewing space, (3) the associated response from each channel of the radiometer while viewing spacecraft housing, and (4) the time associated with each earth scan. The intermediate tape will be the basic repository for raw radiation data from the Nimbus Medium Resolution Infrared Radiometer, and also represents the primary input source of radiometer data for the second step in the data processing plan.

The Nimbus Meteorological Radiation Tape (NMRT-MRIR) for the Medium Resolution Infrared Radiometer is the output from the second step of the data processing plan. The inputs to this program are (1) the intermediate MRIR data tape, (2) pertinent telemetry data transmitted from the spacecraft, (3) the Minute Vector Tape (MVT) containing position vectors of the spacecraft at one minute intervals, and (4) miscellaneous documentation data.

During this second phase, each data measurement is converted to equivalent units of energy, latitudes and longitudes are computed for locator points, and orbital and telemetry data are computed as a function of time. These data are formatted as described below, and the Nimbus Meteorological Radiation Tape for medium resolution infrared data is produced.

The NMRT-MRIR is the basic repository for calibrated radiation data from the medium resolution infrared radiometer. This tape contains data in binary mode and a density of 800 bits per inch. The first file on each tape contains a BCD label consisting of fourteen words of BCD information followed by an end-of-file. The remaining files on this tape contain the MRIR data in the format described below. There will be one file for each orbit of data. The first record in a data file is a documentation record containing 15 words which describe the data to be found in each succeeding record (see Table 4-12). The remaining data records in each file will be of variable length, but this length will be consistent within the file (see Table 4-13). The length of a data record (L) can be determined as follows:

$$L = (\text{SWATHS PER RECORD}) \times (\text{WORDS PER SWATH}) + (\text{NUMBER OF NADIR ANGLES}) + 8$$

Ninety degrees are added to all latitudes and attitude errors to eliminate negative signs.

Table 4-12
NMRT-MRIR Documentation Record Format

Word No.	Quantity	Units	Scaling	Remarks
1	Nimbus Day	–	B = 35	Start time for this file of data.
2	Hour	Z Hour	B = 35	
3	Minute	Z Minute	B = 35	
4	Seconds	Z Seconds	B = 35	
5	Nimbus Day	–	B = 35	End time for this file of data.
6	Hour	Z Hour	B = 35	
7	Minute	Z Minute	B = 35	
8	Seconds	Z seconds	B = 35	
9	Mirror Rotation Rate	Deg/sec	B = 26	Rotation rate of radiometer mirror.
10	Sampling Frequency	Samples/sec	B = 23	Digital sampling frequency per second of vehicle time.
11	Orbit Number	–	B = 35	Orbit Number.
12	Station Code	–	B = 35	Station code for DAF ground station.
13	Swath Block Size	–	B = 35	Number of 35-bit words per swath.
14	Swaths Per Record	–	B = 35	Number of swaths per record.
15	Number of Locator Points	–	B = 35	Number of anchor points per swath for which latitudes and longitudes are computed

Table 4-13
NMRT-MRIR Data Record Format

Word No.	Quantity	Units	Scaling	Remarks
1D	Nimbus Day	–	B = 17	Start time for this record of data.
1A	Hour	Z Hour	B = 35	
2D	Minutes	Z Minute	B = 17	
2A	Seconds	Z Second	B = 35	
3D	Roll Error	Degrees	B = 14	Roll error at time specified in words one and two.
3A	Pitch Error	Degrees	B = 32	Pitch error at time specified in words one and two.
4D	Yaw Error	Degrees	B = 14	Yaw error at time specified in words one and two.
4A	Height	Kilometers	B = 35	Height of Spacecraft at time specified in words one and two.
5A	Housing one Temperature	Degrees K	B = 32	Measured temperature of housing one at time specified in words one and two.
6D	Housing two Temperature	Degrees K	B = 14	Measured temperature of housing two at time specified in words one and two.
6A	Electronics Temperature	Degrees K	B = 32	Measured temperature of electronics at time specified in words one and two.
7D	Chopper one Temperature	Degrees K	B = 14	Measured temperature of chopper at time specified in words one and two.
7A	Chopper two Temperature	Degrees K	B = 32	Measured temperature of chopper at time specified in words one and two.
8D	GHA of SUN	Degrees	B = 14	GHA of sun at time specified in words 1 and 2.
8A	Decl. of Sun	Degrees	B = 32	Declination of sun at time specified in words 1 and 2. Ninety degrees added to eliminate negative sign.
9 . . . N	Nadir Angle	Degrees	B = 29	Nadir angles corresponding to each locator point and measured in the plane of the scanning radiometer. Last nadir angle.

Table 4-13
NMRT-MRIR Data Record Format (Continued)

Word No.	Quantity	Units	Scaling	Remarks
(N+1)D	Seconds	Z Seconds	B = 8	Seconds past time in words 1A & 2D for beginning of this swath.
(N+1)A	Data Population	–	B = 35	Number of data points in this swath.
(N+2)D	Latitude	Degrees	B = 11	Latitude of subsatellite point for this swath.
(N+2)A	Longitude	Degrees	B = 29	Longitude of subsatellite point for this swath.
(N+3)D	Latitude	Degrees	B = 11	Latitude of viewed point for the first anchor spot.
(N+3)A	Longitude	Degrees	B = 29	Longitude of viewed points for the first anchor spot. Measured positive westward, 0 - 360 degrees.
(M)D	Latitude	Degrees	B = 11	Latitude and longitude of last anchor spot.
(M)A	Longitude	Degrees	B = 29	Latitude and longitude of last anchor spot.
(M+1)D	MRIR Data	–	B = 14	MRIR Data Measurement, channel one.
(M+1)A	MRIR Data	–	B = 32	MRIR Data Measurement, channel one.
K(A or D)	MRIR Data	–	B = 14 - 42	Last MRIR Data Measurement, channel one.

The data on preceeding page constitute what is essentially the documentation portion of a data record. These data will be followed by several blocks of data with each block representing a swath. The number of these blocks in a record as well as the size of each block is specified in the documentation record represented on the previous page.

Words M+1 through K are repeated for channels two through five respectively. All remaining or unused portions of a swath data block are set to zero, giving a swath block size as specified in the documentation record. The above data on this page are repeated for the number of swaths in each record.

REFERENCES

1. "TIROS VII Radiation Data Catalog and Users' Manual." Goddard Space Flight Center, Greenbelt, Maryland, Volume 1 thru 4.

2. "TIROS IV Radiation Data Catalog and Users' Manual." Goddard Space Flight Center, Greenbelt, Maryland, 15 December 1963. 250 pp.

3. "TIROS II Radiation Data Users' Manual." Goddard Space Flight Center, Greenbelt, Maryland, 15 August 1961. 57 pp.

4. "TIROS III Radiation Data Users' Manual." Goddard Space Flight Center, August 1962. 71 pp.

5. Bandeen, W. R., R. A. Hanel, John Licht, R. A. Stampfl, and W. G. Stroud. "Infrared and Reflected Solar Radiation Measurements from the TIROS II Meteorological Satellite." J. of Geophys. Res., 66, 3169-3185, October 1961.

6. Hanel, R. A., W. R. Bandeen, and B. J. Conrath. "The Infrared Horizon of the Planet Earth." J. of the Atmos. Sciences, 20, 73-86, March 1963.

7. Bandeen, W. R., B. J. Conrath and R. A. Hanel. "Experimental Confirmation from TIROS VII Meteorological Satellite of the Theoretically Calculated Radiance of the Earth Within the 15 Micron Band of Carbon Dioxide." J. of the Atmos. Sciences, 20, 609-614, November 1963.

8. Nordberg, W., W. R. Bandeen, G. Warnecke, and V. Kunde. "Stratospheric Temperature Patterns Based on Radiometric Measurements from the TIROS VII Satellite." Space Research V, North-Holland Publishing Co., 1964.

9. Bandeen, W. R., V. Kunde, W. Nordberg, and H. P. Thompson. "TIROS III Meteorological Satellite Radiation Observations of a Tropical Hurricane." TELLUS, XVI, 1964.

10. Deacon, E. L., "Water Vapor over the Sahara and TIROS III Observation." J. of Atmos. Sciences, 20, 614-615, November 1963.

11. Fritz, Sigmund, and Jay S. Winston. "Synoptic Use of Radiation Measurements from Satellite TIROS II." Monthly Weather Review, 90, 1-9 January 1962.

12. Fritz, S., P. Krishna Rao, and M. Weinstein. "Satellite Measurements of Reflected Solar Energy and the Energy Received at the Ground." J. of Atmos. Sciences, 21, 141-151, March 1964.

13. Furukawa, P. M., P. A. Davis, and W. Viezee. "An Examination of Some TIROS II Radiation Data and Related Studies." Final Report, Contract No. AF 19(628)-322, Stanford Research Institute, Menlo Park, California, July 1962.

14. Greenfield, S. M., and W. W. Kellogg. "Calculations of Atmospheric Infrared Radiation as seen from a Meteorological Satellite." J. of Meteor., 17, 283-289, June 1960.

15. Hanel, R. A., and D. Q. Wark. "TIROS II Radiation Experiment and Its Physical Significance." J. Opt. Soc. Am., 51, 1394-1399, December 1961.

16. King, Jean I. F., "Meteorological Inferences from Satellite Radiometer." J. of Atmos. Sciences, 20, 245-250, July 1963.

17. Larsen, S. H. H., T. Fujita, and W. L. Fletcher. "Evaluations of Limb Darkening from TIROS III Radiation Data." Research Paper No. 18, Mesometeorology Project, Department of Geophysical Sciences, The University of Chicago, August 1963.

18. Pederson, Finn, and Tetsuya Fujita. "Synoptic Interpretation of TIROS III Measurements of Infrared Radiation." Research Paper No. 19, Mesometeorology Project, Department of Geophysical Sciences, The University of Chicago, October 1963.

19. Larsen, S. H. H., T. Fujita, and W. L. Fletcher. "TIROS III Measurements of Terrestrial Radiation and Reflected and Scattered Solar Radiation." Research Paper No. 20, Mesometeorology Project, Department of the Geophysical Sciences, The University of Chicago, October 1963.

20. London, Julius, "Satellite Observations of Infrared Radiation." Scientific Report No. 1, Contract No. AF 19(604)-5955, College of Engineering, New York University, New York 53, N. Y., December 1959.

21. London, Julius, Katsuyuki Ooyama, and Herbert Viebrock. "Satellite Observations of Infrared Radiation." Report No. 2, Contract No. AF 19(604)-5955, College of Engineering, New York University, New York 53, N. Y., July 1960.

22. London, Julius, Katsuyuki Ooyama, and Herbert Viebrock. "Satellite Observations of Infrared Radiation." Final Report, Contract No. AF 19(604)-5955, College of Engineering, New York University, New York 53, N. Y., October 1961.

23. Möller Fritz, and Ehrhard Raschke. "Evaluation of TIROS III Radiation Data." Interim Report No. 1 (July 1963) and Final Report (March 1964) NASA Research Grant Ns G-305, Ludwig-Maximilians-Universtät, Meteorologisches Institut, Munchen, Germany.

24. Nordberg, W., W. R. Bandeen, B. J. Conrath, V. Kunde, and I. Persano. "Preliminary Results of Radiation Measurements from the TIROS III Meteorological Satellite." J. of the Atmos. Sciences, 19, 20-30, January 1962.

25. Prabhakara, C., and S. I. Rasool. "Evaluation of TIROS Infrared Data." 234-246 in Proceedings of the First International Symposium on Rocket and Satellite Meteorology, Washington, D.C., April 1962, edited by H. Wexler and J. E. Caskey, Jr., North-Holland Publishing Co., Amsterdam, 1963.

26. Rasool, S. I., "Cloud Heights and Nighttime Cloud Cover from TIROS Radiation Data." J. of the Atmos. Sciences, 21, 152-156, March 1964.

27. Wark, D. Q., G. Yamamoto, and J. H. Lienesch. "Methods of Estimating Infrared Flux and Surface Temperatures from Meteorological Satellites." J. of the Atmos. Sciences, 19, 369-384, September 1962. (Also "Infrared Flux and Surface Temperature Determinations from TIROS Radiometer Measurements." Meteorological Satellite Laboratory Report No. 10 (1962) and Supplement thereto (1963), U. S. Weather Bureau, Washington, D.C.).

28. Wexler, R., "Satellite Observations of Infrared Radiation." First Semi-annual Technical Summary Report, Contract No. AF 19(604)-5968, Allied Research Associates, Inc., Boston, Mass., December 24, 1959.

29. Wexler, R., "Satellite Observations of Infrared Radiation." Second Semi-annual Technical Summary Report, Contract No. AF 19(604)-5968, Allied Research Associates, Inc., Boston, Mass. June 30, 1960.

30. Wexler, R., "Interpretation of Satellite Observations of Infrared Radiation." Scientific Report No. 1, Contract No. AF 19(604)-5968, Allied Research Associates, Inc., Boston, Mass., April 20, 1961.

31. Wexler, R., "Interpretation of TIROS II Radiation Measurements." Final Report, Contract No. AF 19(604)-5968, Allied Research Associates, Inc., Boston, Mass., May 31, 1962.

32. Wexler, Raymond and Paul Sherr. "Synoptic Analysis of TIROS III Radiation Measurements." Final Report, Contract No. AF 19(628)-429, ARACON Geophysics Co., Concord, Mass., January 31, 1964.

33. Bandeen, W. R., M. Haley, and I. Strange. "A Radiation Climatology in the Visible and Infrared from the TIROS Meteorological Satellites." Paper presented at the International Radiation Symposium, I.U.G.G., Leningrad, August, 1964 (available in Document X-651-64-218, Goddard Space Flight Center, Greenbelt, Maryland; also published as NASA TN D-2534).

34. Nordberg, W., McCulloch, A. W., Foshee, L. L., and Bandeen, W. R. "Preliminary Results from Nimbus II," Bulletin of the American Meteorological Society, Vol. 47, No. 11, Nov. 1966.

35. Feinberg, Paul, "The MRIR-PCM Telemetry System – A Practical Example of Microelectric Logic Design," NASA TN D-2311, Goddard Space Flight Center, Greenbelt, Maryland.

36. "Handbook of Geophysics." Revised Edition, The MacMillan Co., New York, 1960.

SECTION 5

THE INFRARED INTERFEROMETER SPECTROMETER (IRIS) EXPERIMENT

by
Rudolf A. Hanel
National Aeronautics and Space Administration
Goddard Space Flight Center

The purpose of this section is to describe the nature and format of the IRIS data so researchers in the field may be prepared to interpret and use the data as soon as they become available through the National Space Science Data Center.

5.1 Scientific Objectives

The IRIS experiment is to provide information on the vertical structure of the atmosphere and the emissive properties of the surface. In the spectral region covered, water vapor, carbon dioxide, and ozone bands are available in addition to spectral features associated with minor constituents as methane and nitrous oxide. The specific intensity measured in the absorption bands and in the more transparent "windows" may be used to derive vertical profiles of temperature, water vapor and ozone, in addition to other parameters of meteorological interest.

The techniques used to recover the temperature, and water vapor profiles are described, for example, by Wark and Fleming, 1966, and Conrath, 1967 (References 1, 2). The ozone interpretation and the evaluation of the infrared spectra for other purposes have not advanced as far as the temperature analysis but publications are under preparation.

For convenience, the objectives of IRIS may be divided into the following categories:

1. Derivation of atmospheric temperature and humidity structure on a global scale to be used in numerical studies of the general circulation.

2. Observation of temperature, water vapor, and ozone fields for synoptic meteorological studies.

3. Collection of spectra for research studies in meteorology, in radiative transfer, and for nonmeteorological purposes.

5.2 The IRIS Instrument

The instrument is a Michelson type interferometer constructed by Texas Instruments Inc. The optical and electronics module are shown in Figure 5-1. Table 5-1 summarizes the more important parameters and Figure 5-2 shows a simplified diagram of the instrument.

The essential part of the interferometer is the beam splitter which divides the incoming radiation into two approximately equal components. After reflection on the fixed and moving mirrors, respectively, the two beams interfere with each other with a phase difference proportional to the optical path difference between both beams. The recombined components are then focused onto the bolometer detector where the intensity is recorded as a function of path difference, δ. Since the mirror motion is phase locked to the spacecraft clock, the mirror path difference is also proportional to time. For quasi-monochromatic radiation, a circular fringe pattern appears at the focal plane of the condensing mirror. The detector size is chosen to cover just the smallest central fringe for the highest wave number of interest. The aperture at the detector and the interferometer mirrors constitute the limiting apertures and determine the 8° field of view of the instrument.

The central fringe may be light or dark depending on the path difference δ between the two beams. For polychromatic radiation and neglecting constant terms the signal at the detector, called the interferogram, is

$$i(\delta) = \int_0^\infty K_\nu (B_\nu - B_\nu(T_{instr})) \cos(2\pi\nu\delta - \phi_\nu)\, d\nu \qquad (1)$$

The amplitude is proportional to a responsivity factor $K(\nu)$ and the difference in radiance between the scene within the field of view B_ν and the instrument $B_\nu(T_{instr})$. The phase is defined with respect to a point chosen as close as possible to, but not necessarily at, the zero path difference point. Imperfect optical compensation and residual phase shift in the analog part of the data channel cause the angle ϕ to depend on the wave number. Reconstruction of the spectrum by a ground based computer will be discussed later. A detailed block diagram of the instrument is shown in Figure 5-3.

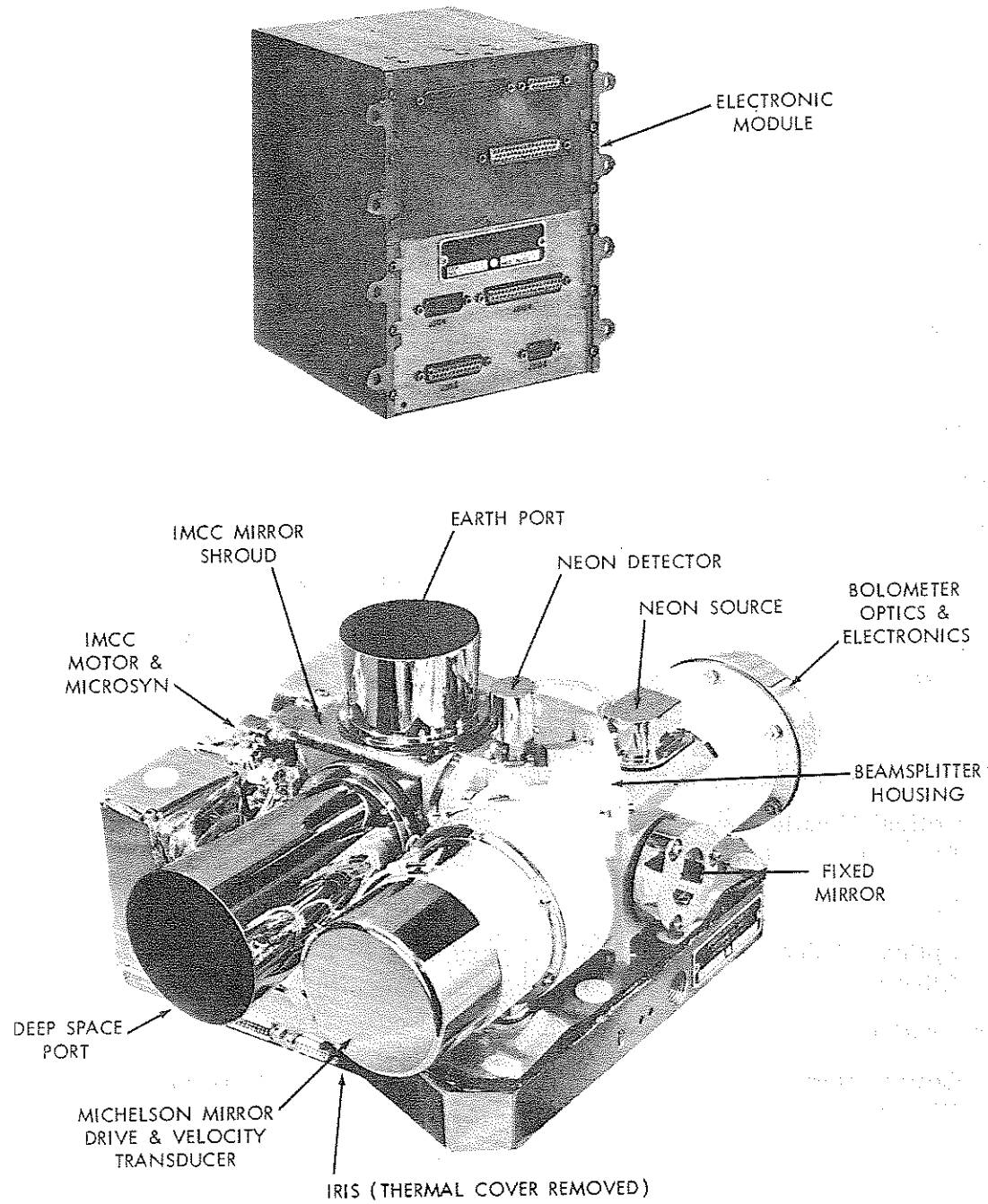

Figure 5-1–Electronic and Optical Module of the IRIS Instrument

Table 5-1
Summary of the More Important Parameters of the IRIS "B"

Nominal Spectral Range	500 to 2000 cm^{-1} (5 - 20μ)
Spectral Resolution Element	5 cm^{-1}
Field of view	Circular, 4° half angle
Diameter of view area from 1100 km altitude	Approx. 150 km
Motion of moving mirror	0.2 cm
Velocity of moving mirror	0.0183 cm/sec
Duration of interferogram	10.9 sec
Wavelength of fringe control	0.5852 μ
Data Words per interferogram	3408
Word Rate	312.5 Words/sec
Bits per Word	12 (2 Sync, 1 Gain, 8 Data, 1 Parity)
Bit rate	3.75 k bits/sec
IMCC rotation rate	0.4 deg/sec
Operating temperature of	
Optical Module	250±2.5°K
Electronic Module	298±25°K
Weight	
Optical Module	23.13 lbs.
Electronic Module	9.13 lbs.
Dimensions	
Optical Module	15.3 × 12.75 × 8.43 inches
Electronic Module	8 × 6.5 × 6.5 inches
Power consumption	16 Watt average

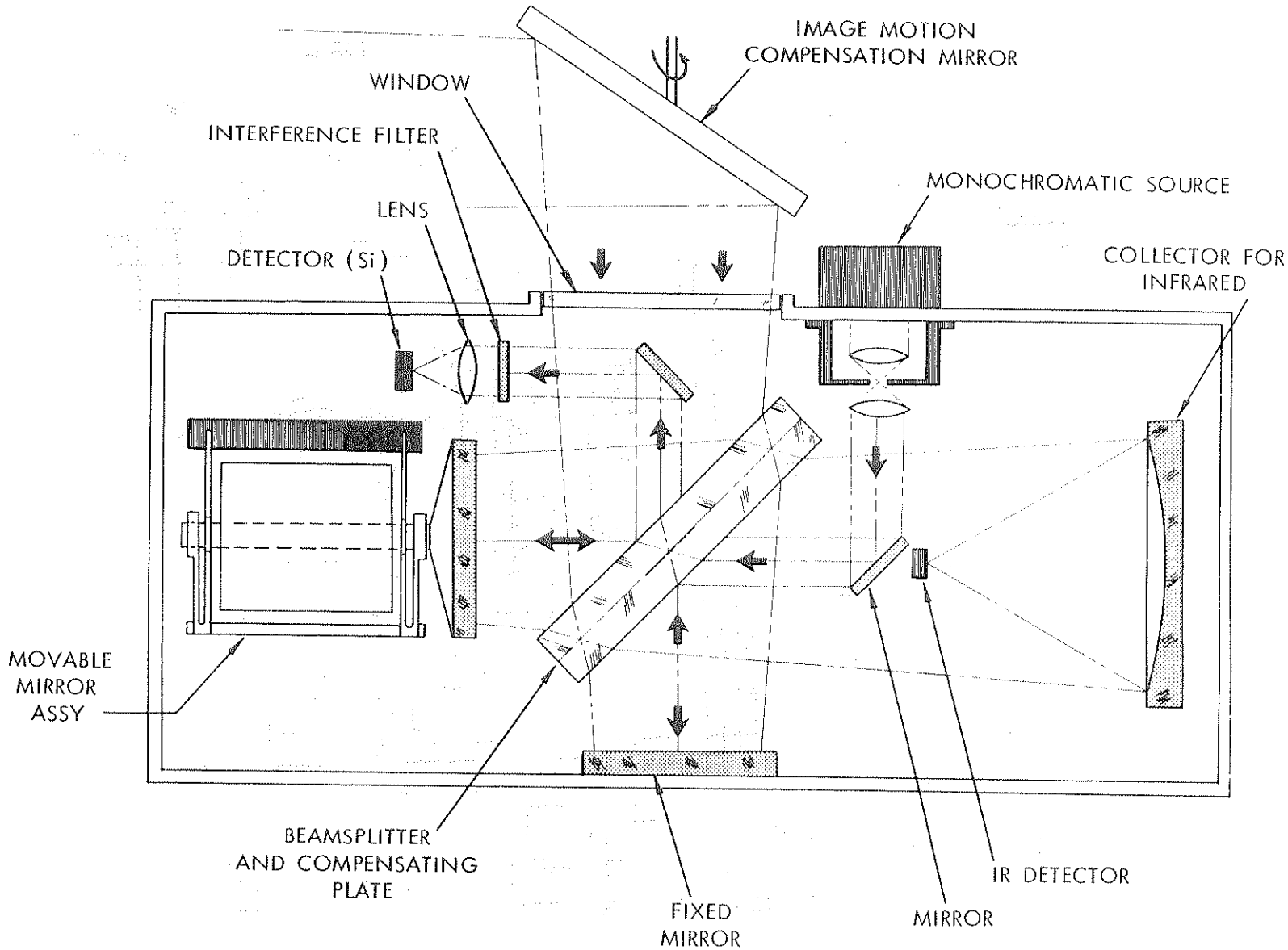

Figure 5-2–Schematic Diagram of Michelson Interferometer. The Monochromatic Source is a Neon Discharge Tube.

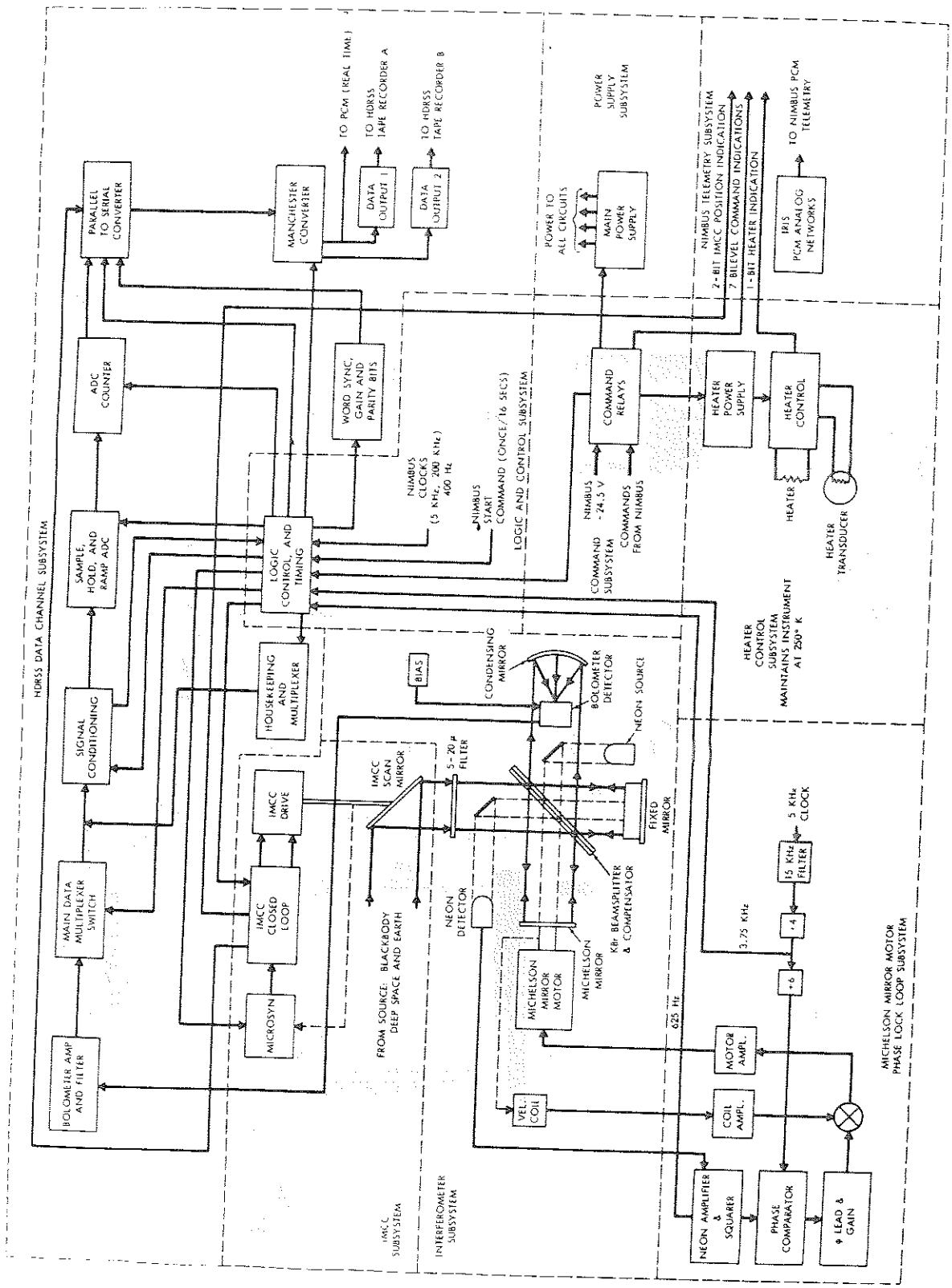

Figure 5-3—Block Diagram of the IRIS System

The beamsplitter, made of potassium bromide (KBr) and supplied by Perkin-Elmer, is polished optically flat to a fraction of a visible fringe. It has a multi-layer dielectric coating which is optimized to the 5-20μ region except for a small area in the center where it is coated to perform well in the visible. In this center region the fringe control interferometer operates. It utilizes not only the same beam-splitter but also the prime infrared interferometer mirrors. The fringe control interferometer generates a sine wave of 625 Hz at the silicon diode detector from a nearly monochromatic spectral line (0.5852μ) of a neon discharge lamp. The line is isolated by an interference filter. The 625 Hz signal serves two purposes. First, after being divided by two, it serves as a sample command and assures equal distance sampling. Secondly, it is compared in phase to a spacecraft clock derived frequency to provide the error signal for the phase locked loop.

The Michelson mirror assembly has an electromagnetic drive coil and also a pick-up coil to generate a voltage proportional to mirror velocity. The velocity signal is also used in a feedback arrangement to provide electrical damping and to make the system less sensitive to external vibration. The phase locked condition of the Michelson mirror provides a constant mirror velocity and permits a constant data rate; moreover the data stream is synchronized with the spacecraft clock.

The Image Motion Compensation and Calibration system channels radiation from several sources to the interferometer. After 14 interferograms are taken in the operating mode, one is taken from a built-in blackbody kept at spacecraft temperature followed by an interferogram from outer space which is considered a nearly zero degree sink. The interferograms from the hot blackbody and cold interstellar background serve calibration purposes. The inflight calibration will be discussed later. During the normal mode where the earth is in the field of view, the IMCC mirror rotates slowly at a rate of 0.4 degree/sec to assure image motion compensation. The calibration mode is prohibited near the north polar region where danger of viewing the sun exists.

A typical interferogram is shown in Figure 5-4 for a blackbody warmer than the instrument. The large central peak is reduced in a signal conditioner. The transfer function of the signal conditioner is shown in Figure 5-5. The inverse function must be applied in the computer. The purpose of the signal conditioner is to preserve dynamic range to 8 bits in the analog to digital converter without a great sacrifice in accuracy. A ninth bit, the gain bit, indicates that the signal exceeded ±0.07 volts input to the range standardization transfer curve.

The instrument generates main data and housekeeping data. Some of the housekeeping data are multiplexed with the main data and are then transmitted just before and just after an interferogram. This set of housekeeping data is

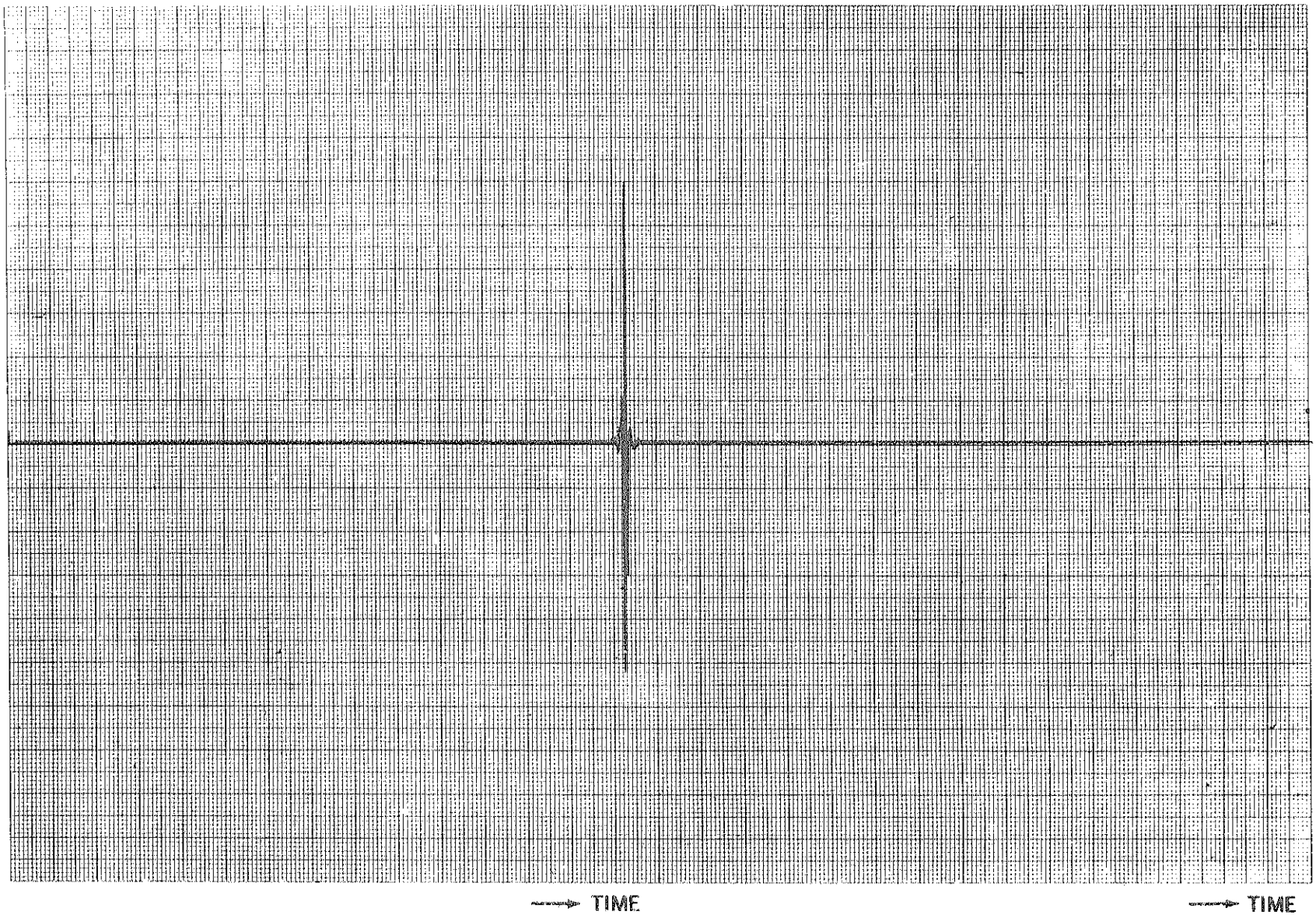

Figure 5-4--Interferogram of Warm Blackbody. Relative Amplitudes are Plotted versus Time.

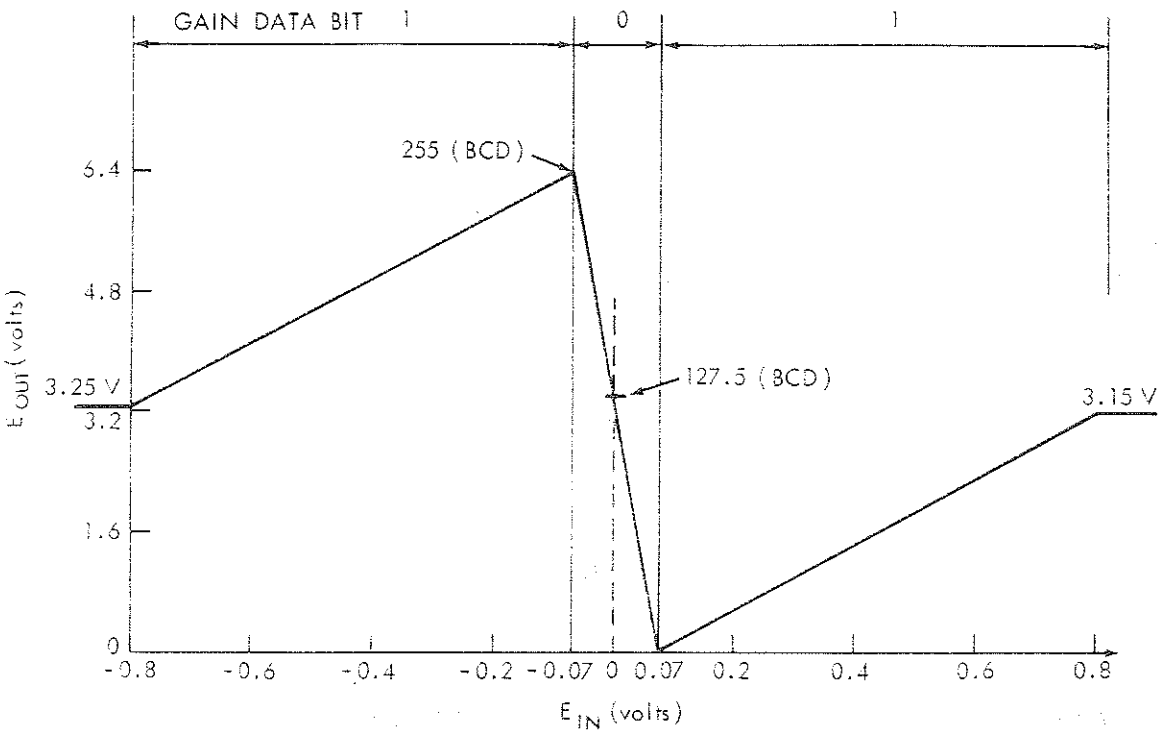

Figure 5-5—Transfer Function of the Range Standardization Circuit

required in the computer for the data reduction process. Another set of housekeeping data is transmitted via the Nimbus PCM system. It is needed for engineering evaluation. Table 5-2 lists the housekeeping information recorded together with the interferogram and Table 5-3, the housekeeping channel available for performance evaluations.

5.3 Data Flow

The main bit stream of data is recorded at one of the HRDSS recorders in the spacecraft. Real time transmission capability exists also via the PCM subsystem and the beacon transmitter. Another channel of the HRDSS recorder carries a time code signal. The data format and timing is shown in Figure 5-6. The data flow in the spacecraft is shown in Figure 5-7 and on the ground in Figure 5-8.

At STADAN Data Acquisition Facility, the receiver output is demultiplexed and recorded on tape. The IRIS data are transmitted from ALASKA by a landline data link to the Nimbus Data Handling System (NDHS) at GSFC. In some

Table 5-2
IRIS Telemetry (HDRSS)

Channel No.	Channel No.
0. Synch Word	8. +0.6 Volt Calibration
1. Bolometer temp.	9. 0 Volt Calibration
2. Blackbody temp.	10. -0.6 Volt Calibration
3. Beamsplitter temp.	11. IMCC Position (2 bit digital)
4. MMDA Housing temp.	12. Bolometer temp. (Redundant)
5. IMCC Drive temp.	13. Blackbody temp. (Redundant)
6. Radiating surface temp.	14. Calibration transducer
7. Spare	15. Sync word

Table 5-3
IRIS Telemetry (PCM Subsystem)

Analog	B1-Level
1. Reference Interferometer amplitude and Phase-Lock Condition	1. IMCC Stowage (Blackbody Position Command Relay Monitor)
2. IMCC Earth Scan Indicator	2. Heater Power Command Relay Monitor (on or off)
3. Bolometer Temperature	3. IRIS Power Command Relay Monitor (on or off)
4. Blackbody Temperature	4. Calibration Mode Command Relay Monitor (Manual or Auto)
5. Radiating Surface Temperature	5. Calibration Command Relay Monitor (Inhibit or Enable)
6. Electronics Module Temperature	6. Calibration Switch (Auto) Relay Monitor (Inhibit or Enable)
7. Optical Cube Support Plate Temperature	7. IMCC Mirror Position (2 Adjacent Channels coded for Positon)
8. 0.6 Volt Zener Reference	8. Heater Output (on or off)
	9. Neon Source A-Neon B-Clock

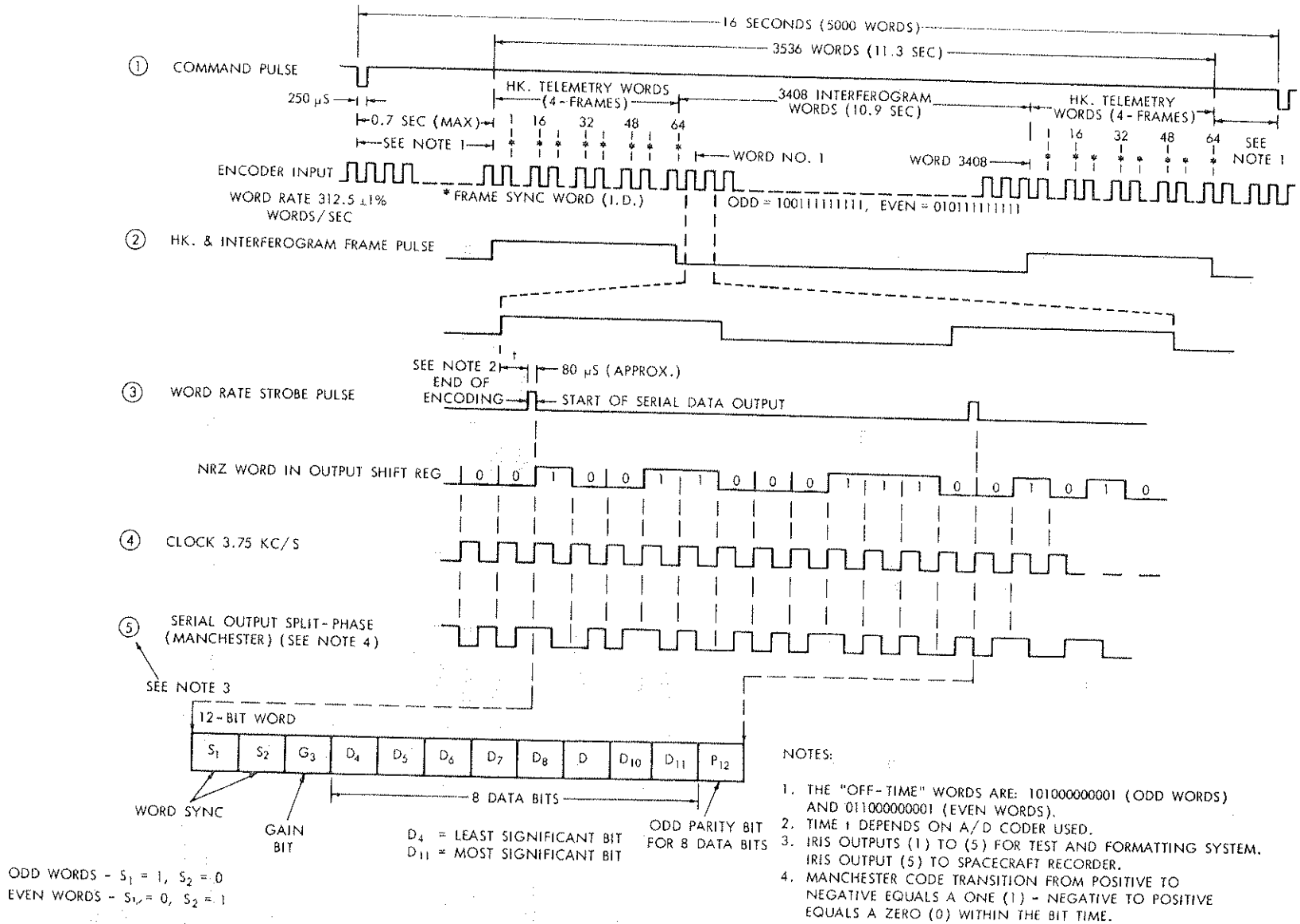

Figure 5-6–Timing Diagram of Single Frame of Data

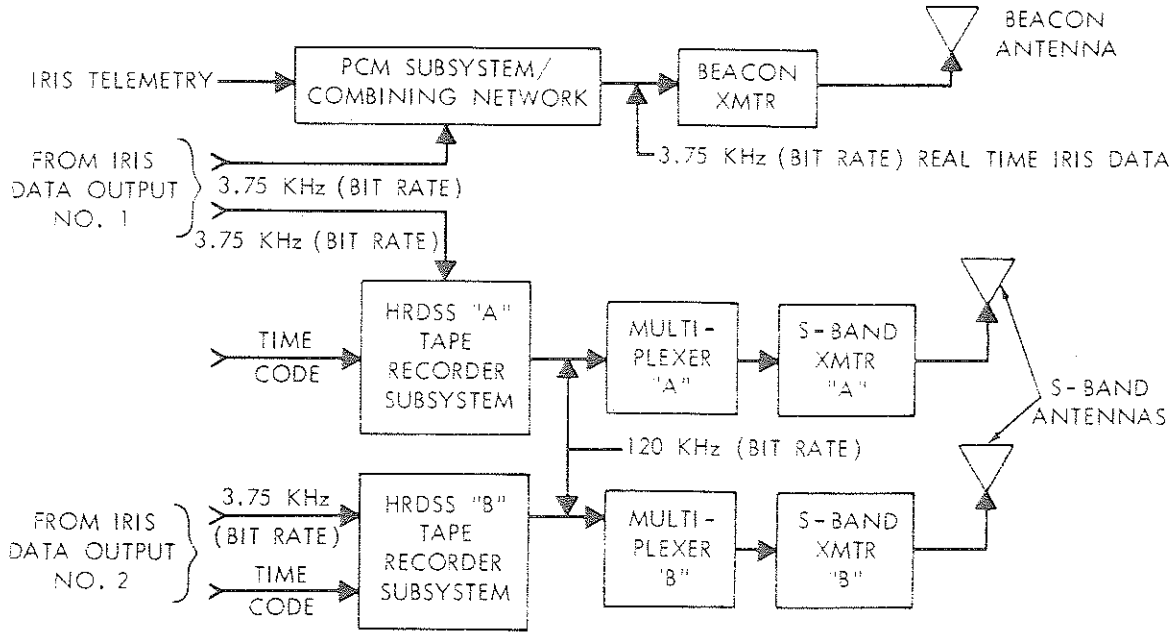

Figure 5-7–Flow Diagram of IRIS Data in the Nimbus Satellite

cases, a small fraction is transmitted from ROSMAN via the microwave links when transmission time is available. At the NDHS a Telemetrics 670 computer formats the data, performs several checks, such as parity checks etc., and produces an IBM 360 compatible digital tape.

The NDHF also displays the housekeeping data for engineering purposes and provides weekly plots of the on-off time of the IRIS experiment and tables of height and position of the spacecraft as well as a table of the ascending and descending nodes. The IBM compatible digital tape is then carried to the LABS IBM-360 computer where the actual data reduction takes place.

5.4 Data Reduction in the IBM-360 Computer

The data reduction process consists of four steps:

1. A check of consistency and completeness of input tape and processing of housekeeping information.

2. Fourier transformation of each interferogram including consideration of phase.

3. Application of calibration procedure.

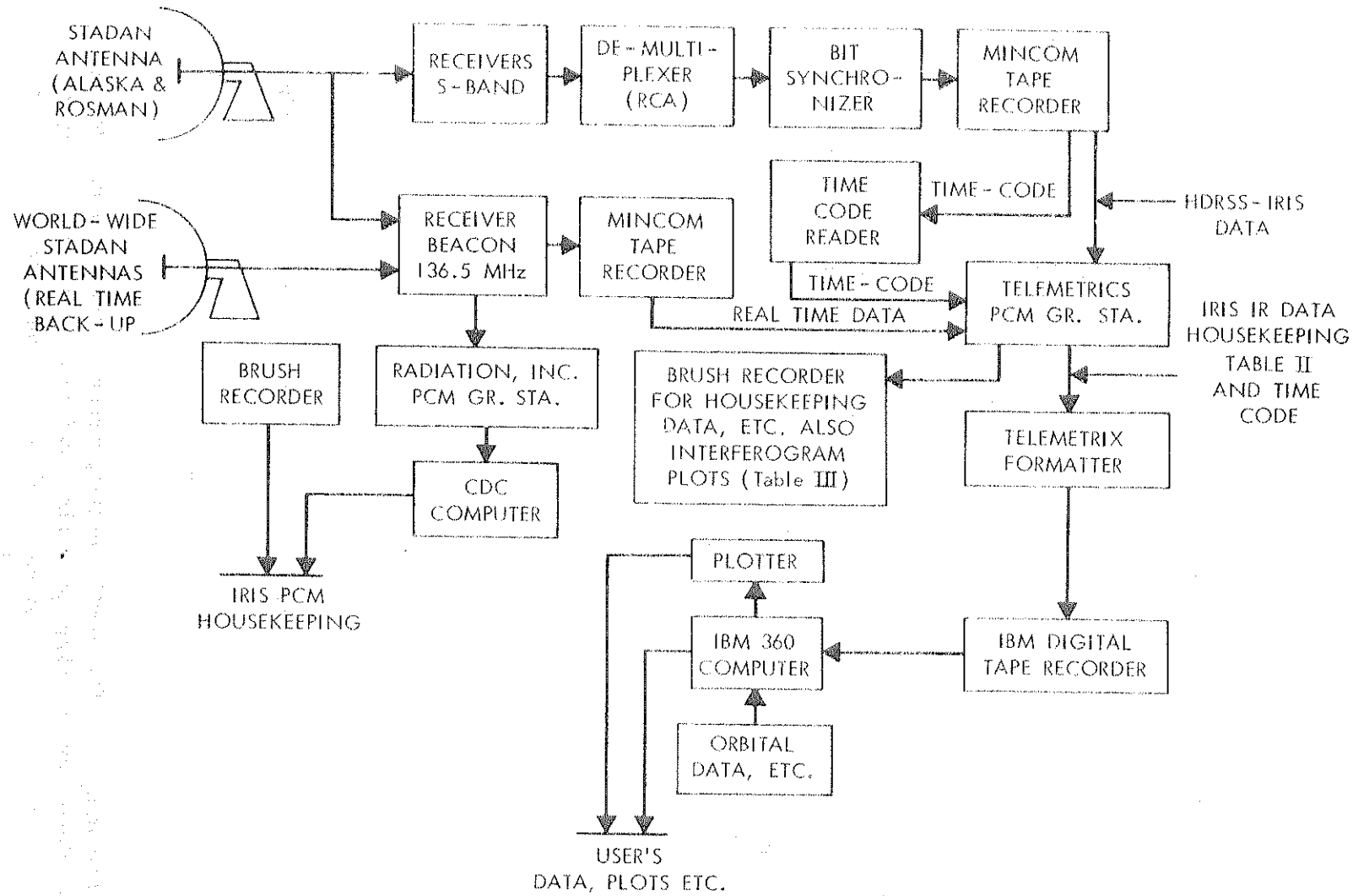

Figure 5-8--Flow Diagram of the Ground Station System and Computer Complex

4. Production of IRIS archival tape containing the calibrated spectra, housekeeping information and orbital parameters.

In the check of consistency and completeness, the total number of words per interferogram and the value, sign and position of the peak word in each interferogram are determined. Furthermore, a scan for gain switch pulses outside the central region of the interferogram, and a check on parity errors and errors in the word sync bits is performed and the results printed out. Only interferograms which show a number of parity and sync errors less than some upper limit will be processed further. This upper limit will be established in operation.

Housekeeping data are converted into engineering units such as temperatures by application of conversion tables established during preflight calibrations.

Interferograms which pass the screening procedure mentioned above will then be transformed by means of the Cooley-Tukey method (References 3, 7). A smoothing or apodisation function is applied to each interferogram prior to transformation in order to reduce side lobes of the instrument function. The particular apodisation function now planned is $(0.54 + 0.46 \cos 2\pi \tau/T)$ where τ is the distance from the center and T the total length of the interferogram. This function and its effects are discussed by Blackman and Tukey (1958) (Reference 4).

The Fourier transformation yields two amplitudes

$$a_\nu = \int_{-\infty}^{\infty} A(\delta)\, i(\delta) \cos 2\pi \nu \delta \, d\delta$$

and

$$b_\nu = \int_{-\infty}^{\infty} A(\delta)\, i(\delta) \sin 2\pi \nu \delta \, d\delta$$

where $A(\delta)$ is the apodisation function. From a_ν and b_ν a magnitude and phase is computed

$$c'_\nu = \sqrt{a_\nu^2 + b_\nu^2}$$

and $\phi_\nu = \arctan b_\nu / a_\nu$. The location of the pronounced central peak of the calibration interferograms is taken as the phase reference point. For atmospheric interferograms which may or may not have a strong central peak, the average phase reference point of several calibration interferograms is used.

The phase information is required to distinguish between a target radiance larger (warmer) or smaller (colder) than the radiance corresponding to the instrument temperature. Wherever the brightness temperature of the target changes from colder to warmer than 250°K or vice versa, a 180° change in phase of the particular frequency component takes place.

Between 640 cm^{-1} and 690 cm^{-1}, the strongest portion of the CO_2 band, only brightness temperatures colder than 250°K are to be expected. In that spectral interval the phase is therefore taken equal to 180° and the magnitude c_ν is assigned a negative sign; wherever the phase changes by ±90°, the sign is alternated.

The slope of the phase curve versus wave number between 640 and 690 cm^{-1} is also used as a check on the selection of the proper phase reference point. Should the slope exceed a certain limit, the phase reference point is shifted proportional to the slope and a new set of c_ν and ϕ_ν are computed. It is hoped that this iterative procedure will not be necessary.

A typical amplitude and phase spectrum for a blackbody are shown in Figure 5-9. The phase information is used for a second purpose. As apparent from Figure 5-9, the phase exhibits a certain amount of jitter caused by random fluctuations, primarily detector noise. The noise-free phase function is relatively smooth, only slowly varying with wave number. This a priori knowledge can be used to reduce the noise in the spectrum. The phase of the signal is supposed to be the average phase $\bar{\phi}_\nu$. The average is taken over 20 spectral intervals on each side of the spectral interval for which the average phase is to be computed. Then the magnitude c'_ν is multiplied by the cosine of the phase difference and a corrected amplitude is obtained, $c_\nu = c'_\nu \times \cos(\phi_\nu - \bar{\phi}_\nu)$. This procedure removes all noise components which are 90° out of phase with the expected signal phase. Where the signal-to-noise ratio is good, the phase jitter is small and the cosine term nearly one. Where the signal is weak, the cosine multiplication technique reduces the noise in the average by a factor $2^{1/2}$. This is the same improvement which is realized by synchronous over non-synchronous detection (Reference 5).

After the spectral amplitudes are corrected by the cosine multiplication and the proper sign of each amplitude is established, the calibration is performed. The instrument is exposed every 16th frame to a built-in calibration blackbody, and to the interstellar background, considered to be near zero, by rotation of the IMCC mirror. The calibration interferograms are processed in the same manner as the interferograms obtained while viewing the atmosphere. The amplitude c_ν in the spectrum is proportional to the difference in radiance between the instrument and the target.

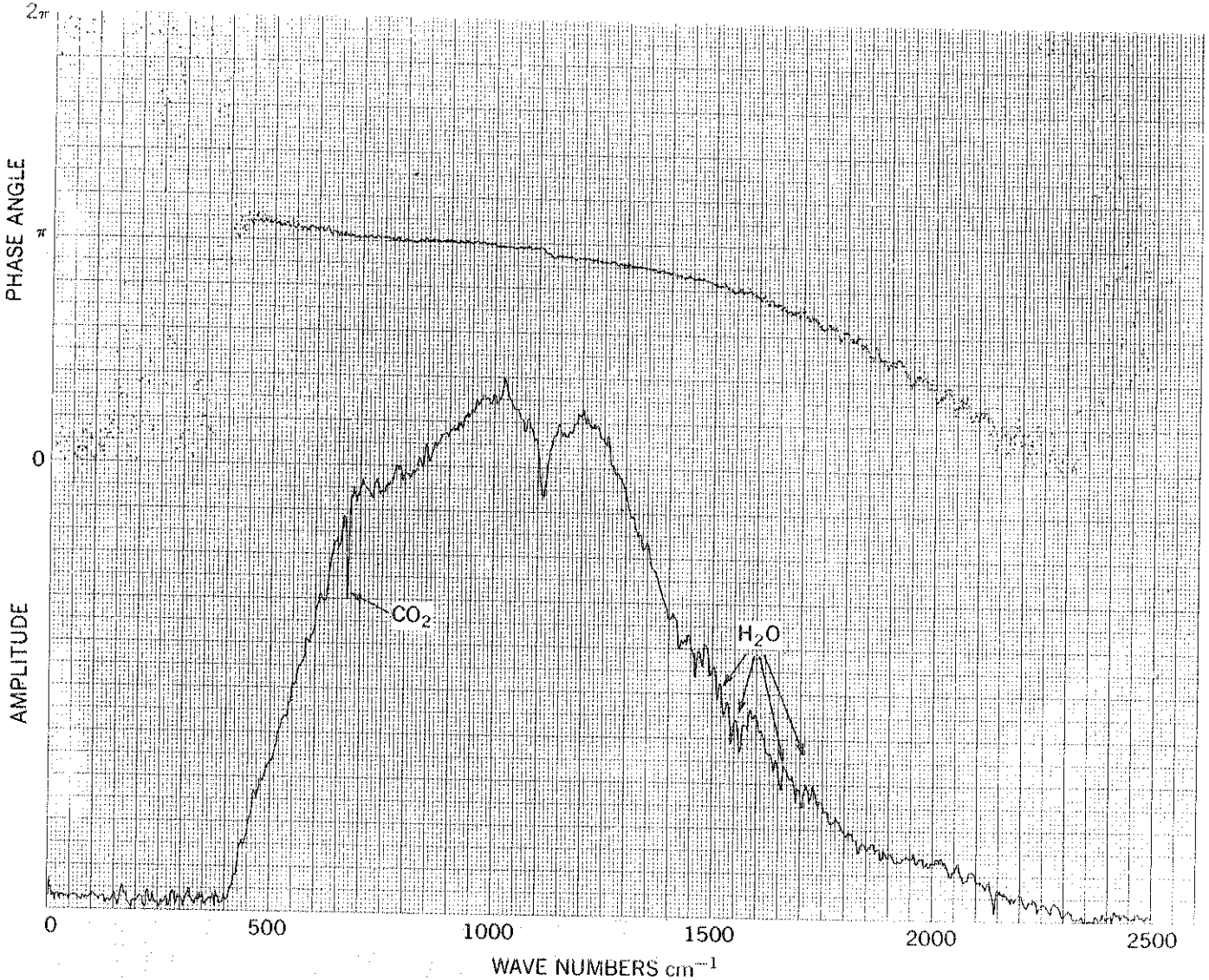

Figure 5-9--Amplitude and Phase Plot Derived From the Interferogram Shown in Figure 5-4

$$C_\nu = r_\nu \, (B_{target} - B_{instrument}).$$

The factor of proportionality is the responsivity of the instrument.

One obtains a set of three equations; one for the target (index 1), one for the cold blackbody (index 2), and one for the warm blackbody (index 3).

$$C_1 (\nu) = r_\nu \, (B_1 - B_i)$$

$$C_2 (\nu) = r_\nu \, (B_2 - B_i)$$

$$C_3 (\nu) = r_\nu \, (B_3 - B_i) \, .$$

Under the assumption that the responsivity, r_ν, is independent of the target brightness and that the detection and amplification is a linear process, the 3 equations may be solved to yield B_1 as well as r_ν and B_i. If one uses the interstellar background as the cold reference ($\sim 4°K$), then B_2 is for all practical purposes zero and the equations simplify to

$$B_1 = B_3 \frac{C_2 - C_1}{C_2 - C_3} \, ,$$

$$r_\nu = \frac{C_2 - C_3}{-B_3} \, ,$$

$$B_i = B_3 \frac{C_2}{C_2 - C_3} \, ,$$

The equation for B_1 is used to reduce the spectra. Neither the responsivity nor the instrument temperature are contained explicitly in this equation. The calibration spectra C_2 and C_3 are the average of about 25 individual spectra so that the random effects in these spectra are greatly reduced. Then the sample standard deviation s (cf. Wilson, 1952) of the responsivity is determined for each orbit.

$$s = \left(\frac{\sum_{i=1}^{k} (r_i - \bar{r})^2}{k - 1} \right)^{1/2}$$

The r_i are the responsivities computed from each calibration pair (hot and cold blackbody). The average responsivity per orbit is called $\bar{r}$ and k is the number of calibration pairs per orbit. Instead of tabulating the standard deviation of the responsivity the noise equivalent radiance (NER) calculated from the calibration spectra is included into the table. The NER is calculated from

$$NER = \frac{s\, B_3}{\bar{r}}$$

The same level of the NER may be expected to exist in the individual atmospheric spectra.

The NER gives the short time repeatability of the instrument and a comparison of the average orbital responsivity for each spectral interval from orbit to orbit, and from day to day yields the long term drift.

The instrument temperature, T_i, which is calculated from B_i and the instrument temperature measured by the thermistors imbedded in the housing should be in close agreement. A deviation from this agreement is used as a caution flag which calls for a special investigation if it should occur.

Figures 5-10 to 5-13 show the responsivity, the noise equivalent radiance, the instrument temperature, and a blackbody spectrum, all derived during the thermal vacuum tests of the Nimbus B2 spacecraft.

5.5 Format of the IRIS Archival Tape

The IRIS Archival Tape will be the basic repository for radiation data from the Nimbus Infrared Interferometer Spectrometer (IRIS). This tape will be generated on the IBM 360 System with 7 track recording in binary mode at 800 bytes per inch, and will be available to the scientific community through the NSSDC within 6 months after launch.

The IRIS Archival Tape contains one file for each readout orbit of data processed from the Nimbus spacecraft. Within each file there are several types of records. These are listed below and each type is described in detail in the following tables 5-4 through 5-12

Record Type	Description
1	Documentation information for each file (Table 5-4)
2	Average cold reference calibration spectrum (Table 5-5)
3	Average warm reference calibration spectrum (Table 5-6)
4	Average Responsivity, R_ν, calculated from the calibration spectra (Table 5-7)
5	Noise Equivalent Radiance (Table 5-8)
6	Average instrument temperature, T_i, calculated from calibration spectra (Table 5-9)
7	Standard Deviation of T_i (Table 5-10)
8	Calibrated Atmospheric Spectrum (Table 5-11)
9	Summary for each orbital pass (Tables 5-12)

The Type 1 documentation record will consist of 18 32 bit words. All other records in the data file will consist of 1080 32 bit words, or 960 36 bit words, or 576 60 bit words. The End of File Mark will be recorded at the end of each playback orbit, and will be repeated at least twice following the last readout orbit on any reel of tape.

Ninety degrees are added to all latitudes to eliminate negative signs.

Final formats of any computer printouts obtainable from the archival tapes cannot be defined at present, and will be included in a future Nimbus III data catalog.

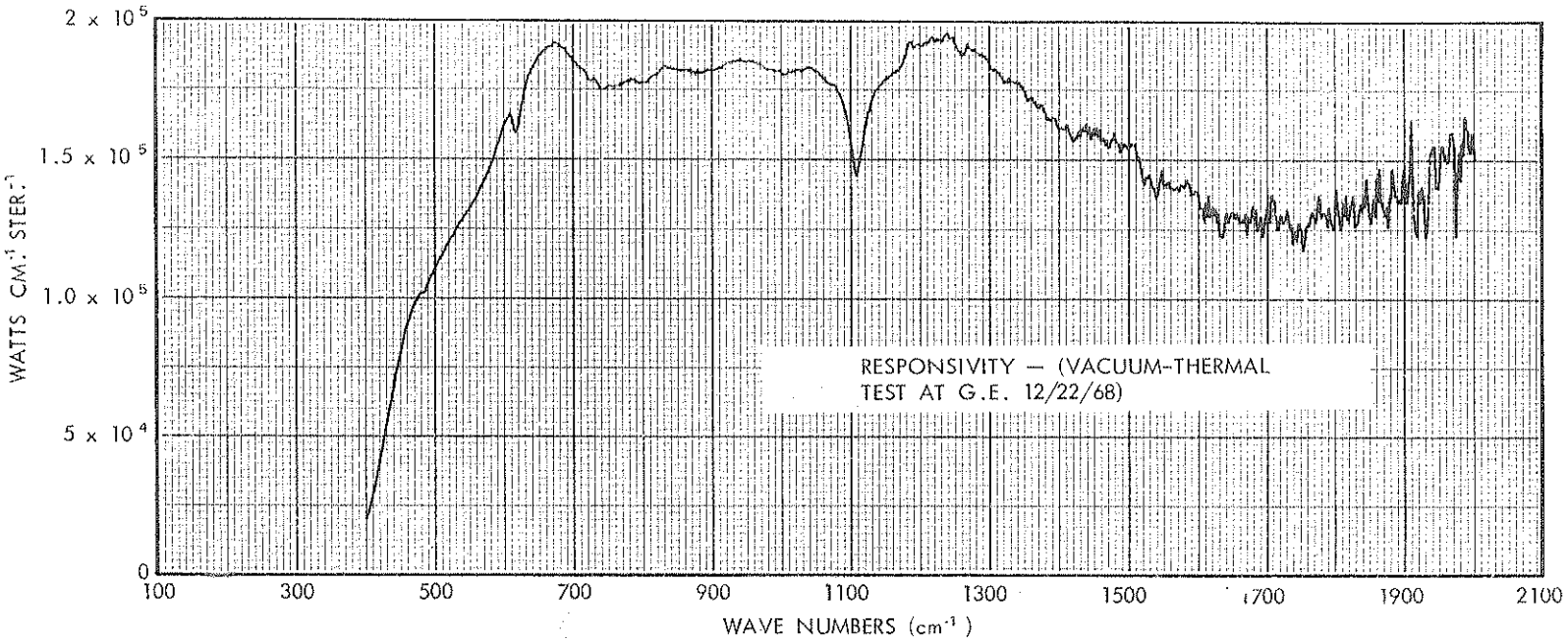

Figure 5-10—Responsivity of the IRIS

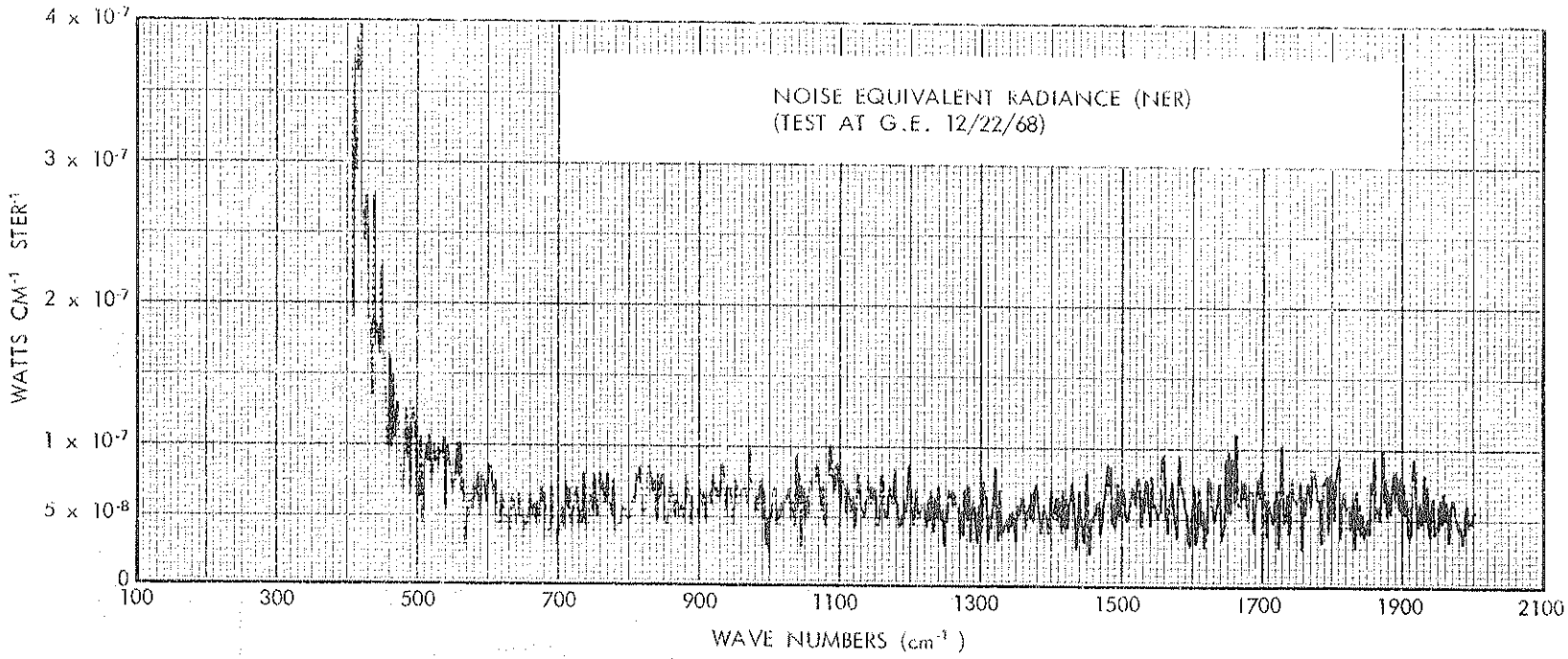

Figure 5-11—Noise Equivalent Radiance of the IRIS

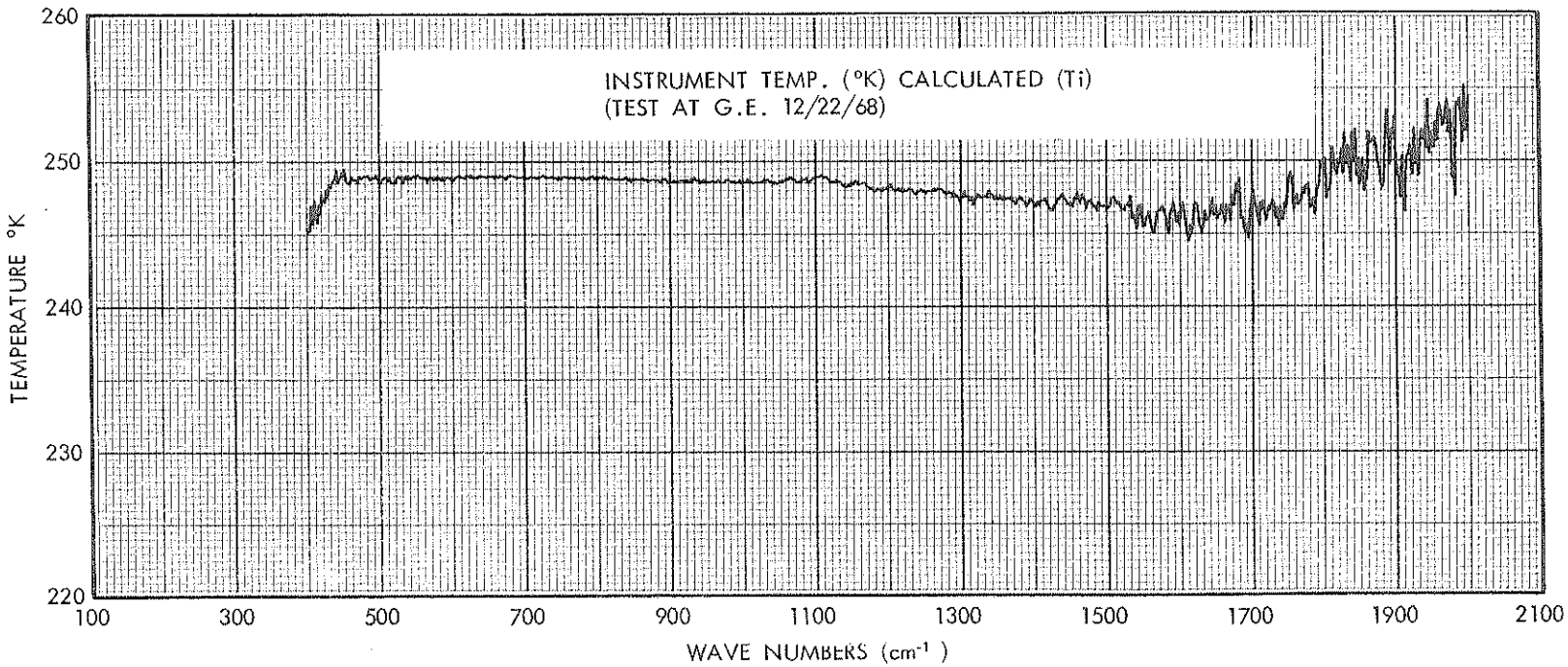

Figure 5-12–The IRIS Temperature

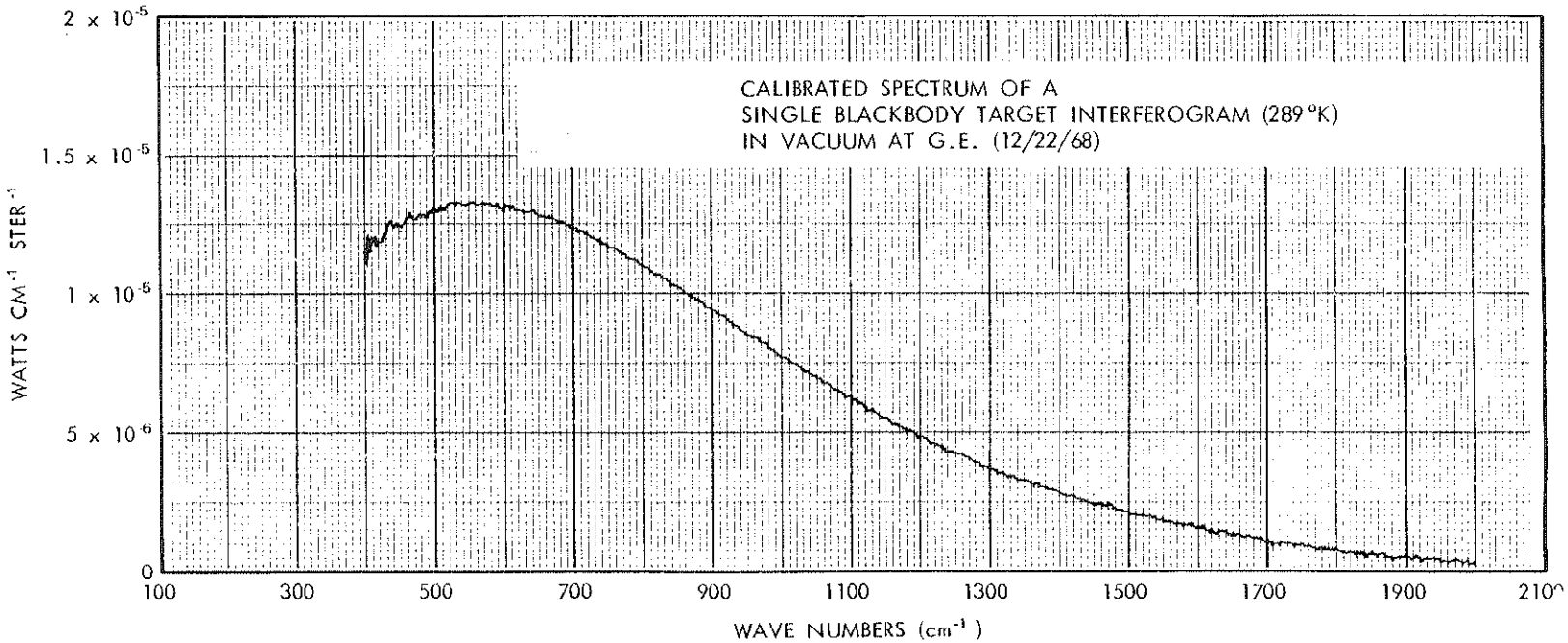

Figure 5-13–Calibrated Spectrum of a Single Blackbody Target Interferogram

Table 5-4
Documentation Record

Word No.	Quantity	Units	Scaling	Remarks
1	Record Type	–	B31	Type = 1 indicates this record contains documentation data for this file.
2	Satellite I.D.	–	B31	Nimbus III = 3
3	Orbit Number	–	B31	Readout Orbit No.
4	Day	Days	B31	Time for first calibrated spectrum in this orbit.
5	Hour	Z Hours	B31	
6	Minute	Z Minutes	B31	
7	Second	Z Seconds	B31	
8	Day	Days	B31	Time for last calibrated spectrum in this orbit.
9	Hour	Z Hours	B31	
10	Minute	Z Minutes	B31	
11	Second	Z Seconds	B31	
12	Initial Wave No.	cm^{-1}	Fl. Pt.	Initial wave number for each calibrated spectrum. Normally $\nu_1 \geq 250$ cm^{-1}
13	Final Wave No.	cm^{-1}	Fl. Pt.	Final wave number for each calibrated spectrum. Normally $\nu_{1951} \geq 2442$ cm^{-1}.
14	Wave No. Increment	cm^{-1}	Fl. Pt.	The wave number increment. Normally $\Delta\nu \geq 2.08578499$ cm^{-1}.
15	Spare			
16	Spare			
17	Spare			
18	Spare			

Table 5-5
Cold Reference Calibration Spectra

Word No.	Quantity	Units	Scaling	Remarks
1	Record Type	–	B31	Type = 2 indicates this record contains the average cold reference calibration spectrum.
2	Orbit No.	–	B31	Readout orbit over which the average cold reference calibration spectrum was computed.
3	Number of Cold reference calibration spectra	–	B31	Number of cold reference calibration spectrum averaged.
4	Average peak value	–	Fl. Pt.	Average peak value of the cold reference calibration interferograms.
5	Standard Deviation of Peak Value	–	Fl. Pt.	Standard deviation of peak values from the cold reference calibration interferograms.
6	Average Position of Peak Value	–	Fl. Pt.	Average location of peak values in the cold reference calibration interferograms.
7	Standard Deviation of Position of Peak Value	–	Fl. Pt.	Standard deviation of the location of peak values in the cold reference calibration interferograms.
8 . . . 29	Spares			
30	Averaged Cold Reference Calibration Spectrum Intensity Count	–	Fl. Pt.	Spectral intensity for the averaged cold reference calibration spectrum at $\nu_1 \simeq 250\ cm^{-1}$

Table 5-5
Cold Reference Calibration Spectra (Continued)

Word No.	Quantity	Units	Scaling	Remarks
31	Averaged Cold Reference Calibration Spectrum Intensity Count		Fl. Pt.	Spectral intensity for the Averaged cold reference calibration spectrum at $\nu_1 = 250\ cm^{-1}$. $\nu_2 = \nu_1 + \Delta\nu$.
.	"		"	"
.	"		"	"
.	"		"	"
.	"		"	"
1080	Averaged Cold Reference Calibration Spectrum Intensity Count	–	Fl. Pt.	Spectral intensity for the Averaged cold reference calibration spectrum at $\nu_{1051} \cong 2442\ cm^{-1}$.

Table 5-6
Warm Reference Calibration Spectra

Word No.	Quantity	Units	Scaling	Remarks
1	Record Type	–	B31	Type = 3 indicates this record contains the average warm reference calibration spectrum.
2	Orbit No.	–	B31	Readout orbit over which the average warm reference calibration spectrum was computed.
3	Number of warm reference calibration spectra	–	B31	Number of warm reference calibration spectrum averaged.
4	Averaged Peak Value	–	Fl. Pt.	Average Peak value of the warm reference calibration interferograms.
5	Standard Deviation of Peak Value	–	Fl. Pt.	Standard deviation of peak values from the warm reference calibration interferograms.
6	Average position of Peak Value	–	Fl. Pt.	Average location of peak values in warm reference calibration interferograms.
7	Standard deviation of the position of Peak Value	–	Fl. Pt.	Standard deviation of the location of peak values in the warm reference calibration interferograms.
8 . . . 29	Spares			
30	Average warm reference calibration spectrum intensity count	–	Fl. Pt.	Spectral Intensity for the Averaged warm reference calibration spectrum at $\nu_1 \simeq 250\ cm^{-1}$.
31	Average warm reference calibration spectrum intensity count			Spectral intensity for Averaged warm reference calibration spectrum $\nu_2 = \nu_1 + \Delta\nu$.

Table 5-6
Warm Reference Calibration Spectra (Continued)

Word No.	Quantity	Units	Scaling	Remarks
.	Average warm reference calibration spectrum intensity count		"	"
.	Average warm reference calibration spectrum intensity count		"	"
.	Average warm reference calibration spectrum intensity count		"	"
1080	Averaged warm reference calibration spectrum intensity count	–	Fl. Pt.	Spectral intensity for the averaged warm reference calibration spectrum at $\nu_{1051} \simeq 2442\ cm^{-1}$.

Table 5-7
Average Responsivity

Word No.	Quantity	Units	Scaling	Remarks
1	Record Type	–	B31	Type = 4 indicates this record contains the average responsivity for the orbit.
2	Orbit No.	–	B31	Readout orbit over which the average responsivity was calculated.
.	Spares			
.	Spares			
.	Spares			
.	Spares			
.	Spares			
.	Spares			
29				
30	Average responsivity for the orbit at a given ν.	watts cm^{-1} $ster.^{-1}$	Fl. Pt.	Average responsivity for the orbit at $\nu_1 \simeq 250$ cm^{-1}.
.	"	"	"	"
.	"	"	"	"
.	"	"	"	"
1080	Average responsivity for the orbit at a given ν.	watts cm^{-1} $ster.^{-1}$	Fl. Pt.	Average responsivity for the orbit at $\nu_{1051} \simeq$ 2442 cm^{-1}.

Table 5-8
Noise Equivalent Radiance

Word No.	Quantity	Units	Scaling	Remarks
1	Record Type	–	B31	Type = 5 indicates this record contains the standard deviation of the responsivity for the orbit.
2	Orbit No.	–	B31	Readout orbit over which the standard deviation of the responsivity was calculated.
3	Spare			
.	Spare			
.	Spare			
.	Spare			
.	Spare			
29	Spare			
30	Noise Equivalent Radiance at given ν.	–	Fl. Pt.	NER at $\nu_1 \cong 250$ cm^{-1}.
.	"		"	"
.	"		"	"
.	"		"	"
.	"		"	"
.	"		"	"
1080	NER at given ν.	–	Fl. Pt.	NER at $\nu_{1051} \cong 2442$ cm^{-1}.

Table 5-9
Average Instrument Temperature

Word No.	Quantity	Units	Scaling	Remarks
1	Record Type	–	B31	Type = 6 indicates this record contains the average instrument temperature.
2	Orbit No.	–	B31	Readout orbit over which the average instrument temperature was calculated.
3	Spare			
.	Spare			
.	Spare			
.	Spare			
.	Spare			
.	Spare			
29	Spare			
30	Average Instrument Temperature at a given ν.	Degrees Kelvin	Fl. Pt.	Average instrument temperature at $\nu_1 \simeq 250$ cm^{-1}.
.	"	"	"	"
.	"	"	"	"
.	"	"	"	"
1080	Average Instrument Temperature at a given ν.	Degrees Kelvin	Fl. Pt.	Average instrument temperature at $\nu_{1051} \simeq$ 2442 cm^{-1}.

Table 5-10
Standard Deviation of the Instrument Temperature

Word No.	Quantity	Units	Scaling	Remarks
1	Record Type	–	B31	Type = 7 indicates this record contains the standard deviation of the instrument temperature.
2	Orbit No.	–	B31	Readout orbit over which the standard deviation of the instrument temperature was computed.
3	Spare			
.	Spare			
.	Spare			
.	Spare			
.	Spare			
29	Spare			
30	Standard Deviation of the instrument temperature at given ν_1	–	Fl. Pt.	Standard deviation of the instrument temperature at $\nu_1 = 250$ cm^{-1}.
.	"	"	"	"
.	"	"	"	"
.	"	"	"	"
1080	Standard Deviation of the instrument temperature at given ν_{1051}	–	Fl. Pt.	Standard deviation of instrument temperature at $\nu_{1051} = 2442$ cm^{-1}.

Table 5-11
Calibrated Atmospheric Spectrum

Word No.	Quantity	Units	Scaling	Remarks
1	Record Type	–	B31	Type = 8 indicates this record contains a calibrated atmospheric spectrum.
2	Orbit No.	–	B31	Readout orbit in which the calibrated spectrum was calculated.
3	Spectrum No.	–	B31	Sequential number assigned to a given spectrum in a given orbit.
4	Day	Days	B31	Time associated with this interferogram.
5	Hour	Z Hours	B31	
6	Minute	Z Minutes	B31	
7	Second	Z Seconds	B31	
8	Latitude	Degrees	Fl. Pt.	Latitude and Longitude of the center of the viewed area
9	Longitude	Degrees	Fl. Pt.	
10	Height of satellite	Kilometers	Fl. Pt.	Height of the satellite at the time stated in words 4-7.
11	Bolometer Temperature	Degrees K	Fl. Pt.	Bolometer temperature (average of two readings before and after interferograms).
12	Bolometer temperature redundant sensor	Degrees K	Fl. Pt.	Bolometer temperature from redundant sensor (average before and after interferogram).
13	Blackbody Temperature	Degrees K	Fl. Pt.	Blackbody temperature (average before and after interferogram).
14	Blackbody temperature from redundant sensor	Degrees K	Fl. Pt.	Blackbody temperature from redundant sensor (average before and after interferogram).
15	Beamsplitter Temperature	Degrees K	Fl. Pt.	Temperature of IRIS instrument beamsplitter.
16	Temperature of Michelson mirror drive motor	Degrees K	Fl. Pt.	IRIS Michelson mirror drive motor temperature.

Table 5-11
Calibrated Atmospheric Spectrum (Continued)

Word No.	Quantity	Units	Scaling	Remarks
17	IMCC Temperature	Degrees K	Fl. Pt.	IMCC Temperature
18	Temperature of cooling surface	Degrees K	Fl. Pt.	Cooling surface temperature
19	IMCC Position	–	B31	IMCC Position (2 bits digital) 0 = Cold Ref. 2 = Cold Ref. 1 = Earth 3 = Warm Ref.
20	+0.6 Volt Calibration	–	Fl. Pt.	+0.6 Volt Calibration
21	0 Volt Calibration	–	Fl. Pt.	0 Volt Calibration
22	-0.6 Volt Calibration	–	Fl. Pt.	-0.6 Volt Calibration
23	Calibration Transducer	–	–	Calibration Transducer
24	Solar Elevation Angle	Degrees	Fl. Pt.	Solar deviation angle at the viewed point.
25	Number of sync pulse errors	–	Fl. Pt.	Number of interferogram sync pulse errors.
26	Number of parity errors	–	Fl. Pt.	Number of instrument word parity errors.
27	Number of Gain Pulses Outside Center	–	Fl. Pt.	Number of gain pulses outside center region of the interferogram.
28	Spare Position	–	–	
29	Spare Position	–	–	
30	Specific Intensity	watts cm^{-1} $ster^{-1}$	Fl. Pt.	Specific intensity at $\nu_1 \simeq$ 250.
31	"	"	"	"
.	"	"	"	"
.	"	"	"	"
1080	Specific Intensity	watts cm^{-1} $ster^{-1}$	Fl. Pt.	Specific intensity at $\nu_{1051} \simeq$ 2442.

Table 5-12
Summary Record For the Orbit
(Last Record in File)

Word No.	Quantity	Units	Scaling	Remarks
1	Record Type	–	B31	Type = 9 indicates this record is a summary for the orbit.
2	Orbit Number	–	B31	Readout Orbit No.
3	Number of Spectra per orbit	–	Fl. Pt.	Number of calibrated spectra computed for the orbit.
4	Day	Day	B31	Time of the first calibrated spectrum computed for the orbit
5	Hour	Z Hour	B31	
6	Minute	Z Minute	B31	
7	Second	Z Second	B31	
8	Day	Day	B31	Time of the last calibrated spectrum computed for the orbit
9	Hour	Z Hour	B31	
10	Minute	Z Minute	B31	
11	Second	Z Second	B31	
12	Orbital Mean of Bolometer Temperature	Degrees K	Fl. Pt.	Mean bolometer temperature for the orbit
13	Sample Standard Deviation of Bolometer Temperature	–	Fl. Pt.	–
14	Orbital Mean of Blackbody Temperature	Degrees K	Fl. Pt.	–
15	Sample Standard Deviation of Blackbody Temperature	–	Fl. Pt.	–
16	Orbital Mean Beamsplitter Temperature	Degrees K	Fl. Pt.	–
17	Sample Standard Deviation of Beamsplitter Temperature	–	Fl. Pt.	–

Table 5-12
Summary Record For the Orbit
(Last Record in File) (Continued)

Word No.	Quantity	Units	Scaling	Remarks
18	Orbital Mean Temperature of Michelson mirror drive motor	Degrees K	Fl. Pt.	–
19	Sample Standard Deviation of Michelson mirror motor temperature	–	Fl. Pt.	–
20	Orbital Mean IMCC Temperature	Degrees K	Fl. Pt.	–
21	Sample Standard Deviation of IMCC Temperature	–	Fl. Pt.	–
22	Orbital Mean Temperature of Cooling Surface	Degrees K	Fl. Pt.	–
23	Sample Standard Deviation of Temperature of Cooling Surface	–	Fl. Pt.	–
24	Number of Interferograms containing sync pulse errors	–	Fl. Pt.	Number of interferograms in the orbit containing sync pulse errors.
25	Number of Interferograms containing word parity errors	–	Fl. Pt.	Number of interferograms in the orbit containing word parity errors.
26	Number of Interferograms containing gain switch pulses outside central region	–	Fl. Pt.	Number of interferograms in orbit containing gain pulses outside central region.

Table 5-12
Summary Record For the Orbit
(Last Record in File) (Continued)

Word No.	Quantity	Units	Scaling	Remarks
27	Number of warm calibration spectra used	—	Fl. Pt.	Number of warm calibration spectra used in the average to compute calibrated spectra.
28	Number of cold calibration used	—	Fl. Pt.	Number of cold calibration spectra used in the average to compute.
29	Spare	—	—	—
1080	Spare	—	—	—

REFERENCES

1. Wark, D. Q., and Fleming, H. E., Indirect Measurements of Atmospheric Temperature Profiles from Satellites: I, Introduction, Monthly Weather Review, 94, 35-362 (1966).

2. Conrath, B. J., Remote Sensing of Atmospheric Water Vapor and Ozone Using Interferometry in Proceedings of the Specialist Conference on Molecular Radiation and its Application to Diagnostic Techniques, ed. by Robert Goulard, Huntsville (1967).

3. Cooley & Tukey, Math. of Computation 19, 296 (1965).

4. Blackman, R. B., and J. W. Tukey, The Measurement of Power Spectra, Dover Publications, New York (1958).

5. Mertz, L., Transformations in Optics, John Wiley & Sons, Inc., New York - London - Sidney, (1965).

6. Wilson, 1952, An Introduction to Scientific Research, McGraw-Hill Book Company, Inc., New York, Chapter 8 and 9.

7. Forman, 1966, J. Opt. Soc. of Amer., Vol. 56, No. 7, July pp. 978-979.

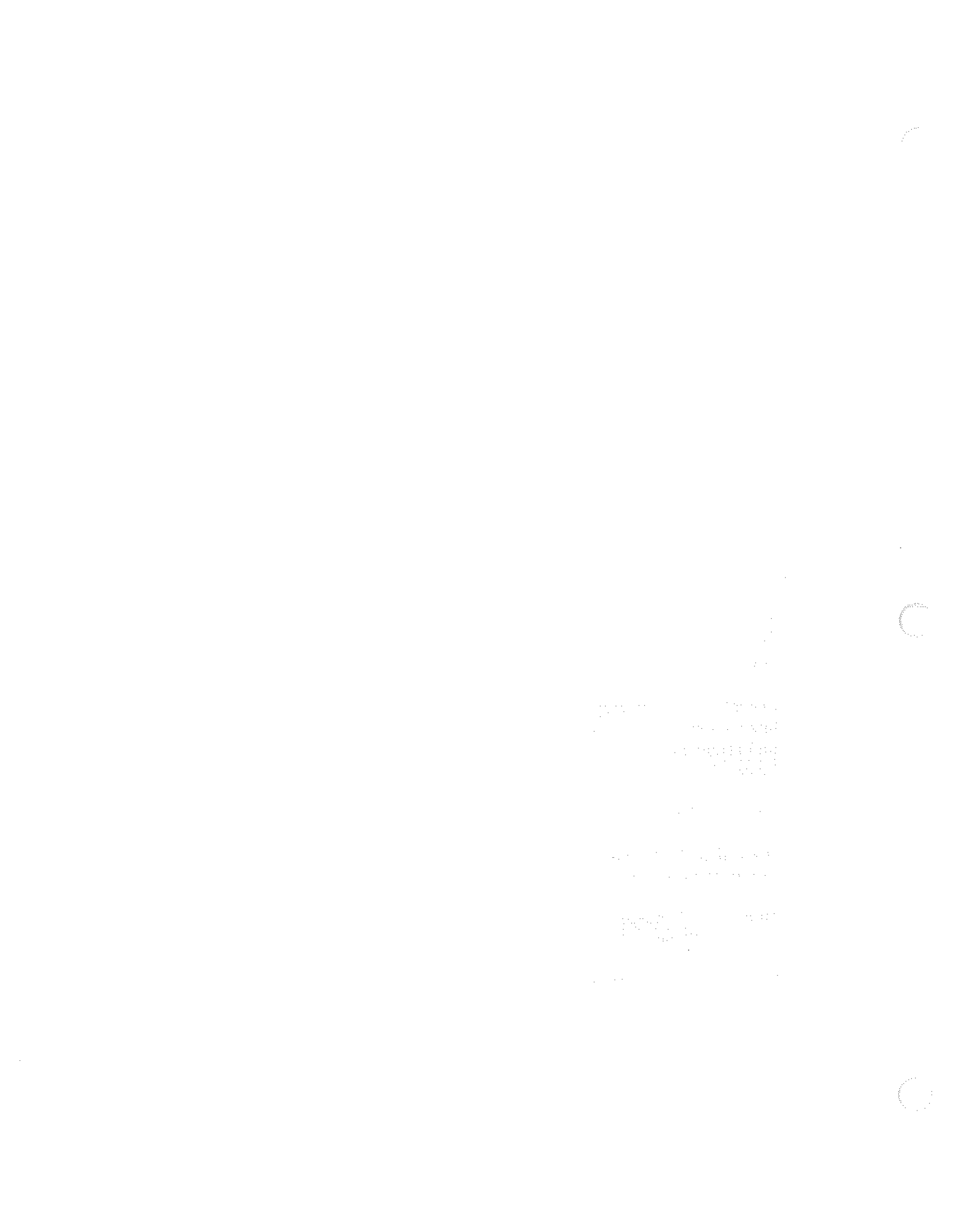

K02954

SECTION 6

THE SATELLITE INFRARED SPECTROMETER (SIRS) EXPERIMENT

by
D. Wark, D. Hilleary, J. Lienesch and P. Clark
National Environmental Satellite Center
Environmental Science Services Administration

6.1 Introduction

The Satellite Infrared Spectrometer (SIRS) has been developed for the purpose of indirect determinations of the vertical temperature profiles of the atmosphere. In its ultimate application, the results from this or a comparable instrument would be used to determine the three-dimensional temperature structure of the atmosphere to a height of 30 km or more.

The outputs of the Satellite Infrared Spectrometer are transformed to spectral radiances by the calibration procedure discussed in Section 6.3. The spectral radiances are then used ensemble to deduce the temperature profile within the field of view.

6.2 Description of the Experiment

A broad body of literature now exists on the methods of transforming spectral radiances to temperature profiles; most of these can be found in the bibliography.

Briefly, the procedures follow the same course. If the radiances in several spectral intervals are given, one can construct a set of integral equations,

$$I(\nu_i) = N\{B[\nu_i, T(p_c)]\,\tau(\nu_i, p_c) - \int_i^{\tau_c} B[\nu_i, T(p)]\, d\tau(\nu_i, p)\}$$

$$+ (1 - N)\{B[\nu_i, T(p_s)]\,\tau(\nu_i, p_s) - \int_1^{\tau_s} B[\nu_i, T(p)]\, d\tau(\nu_i, p)$$

$$i = 1, \ldots, M$$

$I(\nu_i)$ = spectral radiance at wavenumber ν_i

$B[\nu_i, T(p)]$ = Planck radiance at wavenumber ν_i and temperature T; in the atmosphere temperature is a function of the pressure level, p.

$\tau(\nu_i, p)$ = fractional transmittance of the atmosphere in the spectral interval centered at wavenumber ν_i and from pressure level p to the satellite.

Subscripts c and s refer to cloud-top and surface.

N = the product of the fraction of cloud cover within the field of view and the cloud emissivity; if the cloud is thick the emissivity is unity, whereas if the cloud is not opaque it is assumed to be geometrically thin.

These are the integral forms of the radiative transfer equation, with the following assumptions:

1. The spectral interval centered at ν_i lies in an absorption band of an atmospheric constituent whose mixture is known. The SIRS instrument makes use of several parts of the 15-micron carbon dioxide band; carbon dioxide is assumed to have a uniform mixture of about 0.0315 percent by volume.
2. The atmosphere is in local thermodynamic equilibrium, so that the source function is the Planck radiance, $B[\nu_i, T(p)]$.
3. The lower boundary, p_s, is a black surface at the wavelengths of interest.

The solution of the set of equations will generally follow procedures given in the bibliography:

1. Linearize the equations with respect to wavenumber, so that a single wavenumber, ν_r, appears in the source function.
2. Assume the transmittances, $\tau(\nu_i, p)$; these are weakly temperature dependent, and will require corrections.
3. Using characteristic patterns derived from radiosonde and rocketsonde measurements, solve for N, p_s, and $B[\nu_r, T(p)]$ by iterative techniques.

4. Transform $B[\nu_r, T(p)]$ to $T(p)$ from

$$B[\nu_r, T(p)] = \frac{2h \nu_r^3 c^2}{\exp [hc \nu_r / k T(p)] - 1}$$

where h, c, and k have their usual meanings.

5. Make corrections to $\tau(\nu_i, p)$ to satisfy the derived temperature profile, $T(p)$.

6. Repeat steps 3 and 4.

A single iteration for the transmittances should be adequate for a final solution of $T(p)$.

It is emphasized that suitable temperature profiles will result only when characteristic patterns of $B[\nu_r, T(p)]$ are used for the particular geographical locations and season of the observed spectral radiances.

Thus, the deduction of temperature profiles rests upon a large computer capability, an elaborate program, and an enormous body of data from radiosondes and rocketsondes.

The entire procedure would provide unusable soundings, however, if the instrument is not capable of meeting exacting standards of measurement. Experience has shown that the root mean square error of observation must not exceed one percent.

6.3 Description of the Instrument

The SIRS instrument is basically a Fastie-Ebert fixed-grating infrared spectrometer. The five basic components which compose the subsystem are:

SOUSE – SIRS Optics Unit and Sensing Electronics
SIPS – SIRS Instrument Power Supply
SOD – SIRS Output Demodulator
SOBADS – SIRS On-Board Analog-to-Digital System
SCUM – SIRS Control Unit Module

The SIRS subsystem measures the differences in infrared radiation between the earth and deep space in eight spectral bandpasses, each about 0.1 micron wide, between 11 microns and 15 microns. The eight spectral bandpasses are centered at 11.12, 13.33, 14.01, 14.16, 14.31, 14.45, 14.76, 14.95 microns. The instrument is pointed straight down at the subsatellite point for no satellite attitude error. The field-of-view is 11.5° on a side, giving a resolution of 120 nautical miles on a side square at the satellite height of 600 nautical miles. The eight bandpasses are isolated by a diffraction grating in the spectrometer and eight bolometer detectors placed on preselected fixed positions. Figure 6-1 shows a cut-away view of the SOUSE unit which contains the entire optics system. The signal flow diagram is shown in Figure 6-2.

The SOUSE unit contains: a plane, light-collecting mirror to provide a single earth-viewing beam fixed in the vertical; a balanced rotating chopper mirror; a spherical mirror of 25-inch focal length; a 5-inch diffraction grating; a set of 8 exit slits with a single interference filter at the entrance slit for order limitation; 8 wedge-immersed thermistor bolometers; and a blackbody radiation source for calibration. Also, the 8 preamplifiers and 8 operational amplifiers are located in the SOUSE unit.

The earth and space beams are received in the SOUSE unit and alternately directed to the bolometer detectors. This sequencing is accomplished by the chopper mirror which alternately passes earth radiation and space radiation to the detectors through the optics. The resultant signal is a 15 Hertz AC voltage, the amplitude of which is a measure of the difference in the radiant flux of the two beams. The infrared radiation from space is negligible. The chopped radiation is passed through the entrance slit to the spherical mirror, from which it is reflected as a collimated beam to the diffraction grating. The grating disperses the beam spectrally. The dispersed radiation is again collected by the spherical mirror and focused on the exit slits as a spectrum. The signals from the detectors are amplified by the preamplifiers and operational amplifiers.

Eight demodulators in the SOD provide eight DC analog voltages, each representative of the radiant energy difference between the earth and space beams for its associated bolometer detector. A lamp and photocell are employed in conjunction with the chopper mirror to generate the 15 Hertz pulses for use in the synchronous demodulation of the outputs from the SOUSE. A spare lamp is provided. Also contained in the SOD is the telemetry conversion circuitry required for all temperature monitoring thermistors and other function monitors.

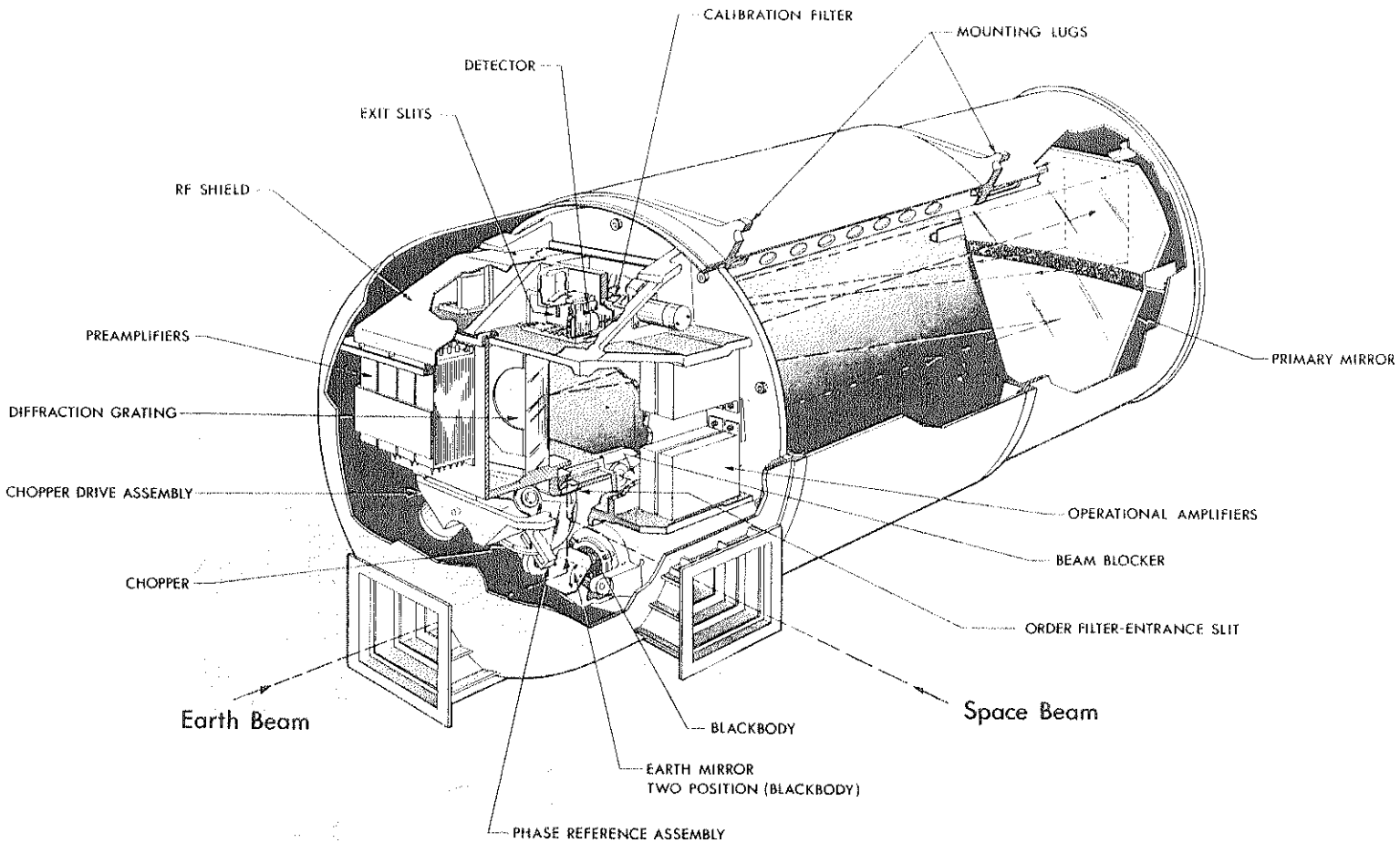

Figure 6-1—The Nimbus III Satellite Infrared Spectrometer (SIRS)

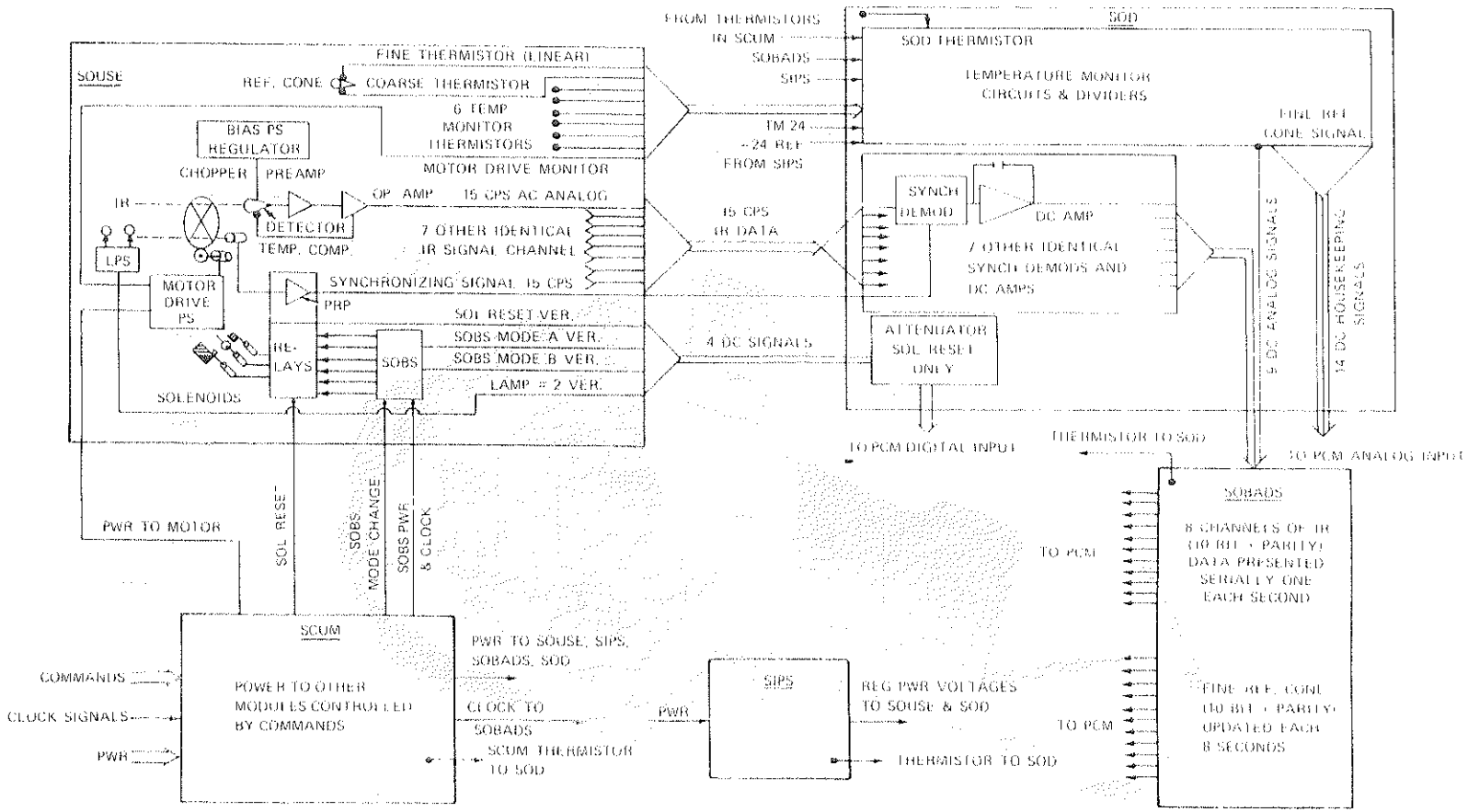

Figure 6-2-- SIRS Signal Flow Diagram

The demodulator outputs are inputs to the SOBADS, where the conversion to eleven bit (ten bit word, plus parity) digital words occurs. The eight channels of data are transferred to the PCM Subsystem in eight seconds, after which the cycle is repeated. The SOBADS samples the eight infrared outputs within 100 milliseconds. In addition to the eight infrared channels, the fine reference cone temperature data are also converted by the SOBADS to an eleven bit word for presentation to the PCM Subsystem every eight seconds. It is read by the PCM every sixteen seconds. The SOBADS uses the PCM synchronizing pulse for data synchronization. The SIRS is designed to operate in this repetitive manner continuously.

The SIPS converts the -24.5 VDC spacecraft bus voltage into highly regulated voltages of several levels and polarities for use in the SOUSE and the SOD.

The SCUM provides the power and command interface between the SIRS and the spacecraft. It contains set-reset relay circuits to command and control the distribution of the -24.5 VDC power for the various functions.

Under normal operating conditions, the only interruption to the continuous infrared data channel outputs will be a calibration cycle occurring at either of two predetermined intervals of time. The cycle is controlled by the SOBS (SIRS On-Board Sequencer) portion of the SOUSE unit. When operated in Mode A, the SOBS will commence the calibration sequence every 32 minutes. In Mode B, the calibration sequence occurs every 256 minutes. The mode is selected by spacecraft command.

The calibration cycle consists of the actuation of each of the three solenoids shown in Figure 6-2 and then resetting them to their original positions in a predetermined sequence. The set and reset pulses originate in the SOBS.

Step number one in the cycle actuates one solenoid which places a beam blocking shutter at the entrance slit to produce a "zero" signal at the infrared channel outputs. The "zero" level is also used to indicate the start of a calibration sequence. This condition is maintained for two minutes before the second step occurs.

The second step resets the beam blocking shutter solenoid and, by actuating a second solenoid, shifts the earth-viewing mirror to view the reference cone (internal blackbody target). In this position, the mirror reflects radiant energy from the reference cone (instead of earth) to the bolometer detectors. The infrared data channels now contain signals representative of the radiant energy differences between space and the reference cone. This condition is also maintained for two minutes.

Step number three actuates a third solenoid two minutes after the start of step number two to place a narrow band interference filter (calibration filter) in front of the detectors. The attenuations produced by the filter in the outputs of several of the infrared data channels are used as a wavelength calibration check. This condition is maintained for two minutes.

The fourth step is the application of a one second reset pulse to return the earth-mirror and calibration filter solenoids to their normal positions. This pulse is again applied two minutes later to insure their return to normal.

Thus, the calibration sequence consists of four two minute intervals. During three of these intervals, calibration data are generated and transmitted over the eight infrared channels. The fourth interval is the normal mode of operation of the SIRS between the solenoid reset pulses.

The laboratory tests of the SIRS instrument are accomplished by placing external blackbodies in the earth and space beams. The temperatures of these targets are precisely controlled and monitored by internal thermocouples. Since the SIRS measures the difference between earth and space radiation, the earth and space blackbody temperature difference is varied so that the difference in their radiances varies from 0 to 200 ergs/sec cm^2 steradian cm^{-1}. The outputs of the SOBADS are plotted as a function of the radiance differences. Figures 6-3 through 6-10 show typical calibration tests for the SIRS instrument at 26.0°C detector temperature. The orbital data will be processed on the basis of the instrument performance ascertained from the in-orbit calibration sequence data. Calculated Planck functions are used in the conversion of temperature to radiance and vice-versa. Figure 6-11 shows the temperature calibration of the reference cone (internal blackbody). Figure 6-12 shows the relationship between the calibration slopes and the temperature of the SIRS detectors. Figure 6-13 shows the relationship of the calibration filter transmissions and the temperature of the filter for the 4 channels affected.

There are 18 housekeeping data channels for monitoring the operation of the SIRS instrument. Four of the monitor channels are digital and fourteen are analog. The digital channels give an output signal for the "on" condition of the PRP back-up lamp, operation in SOBS Mode A, operation in SOBS Mode B, and for the solenoid reset condition.

Eleven of the fourteen analog channels are used for internal temperature monitors in the SIRS instrument. These include the temperature of the SIPS, SOD, SCUM, SOBADS, chopper mirror motor, order filter, detectors, calibration filter, reference cone, collimating mirror, and earth mirror. Figure 6-14 shows the thermistor calibration curve for the various temperature monitors in the SIRS instrument.

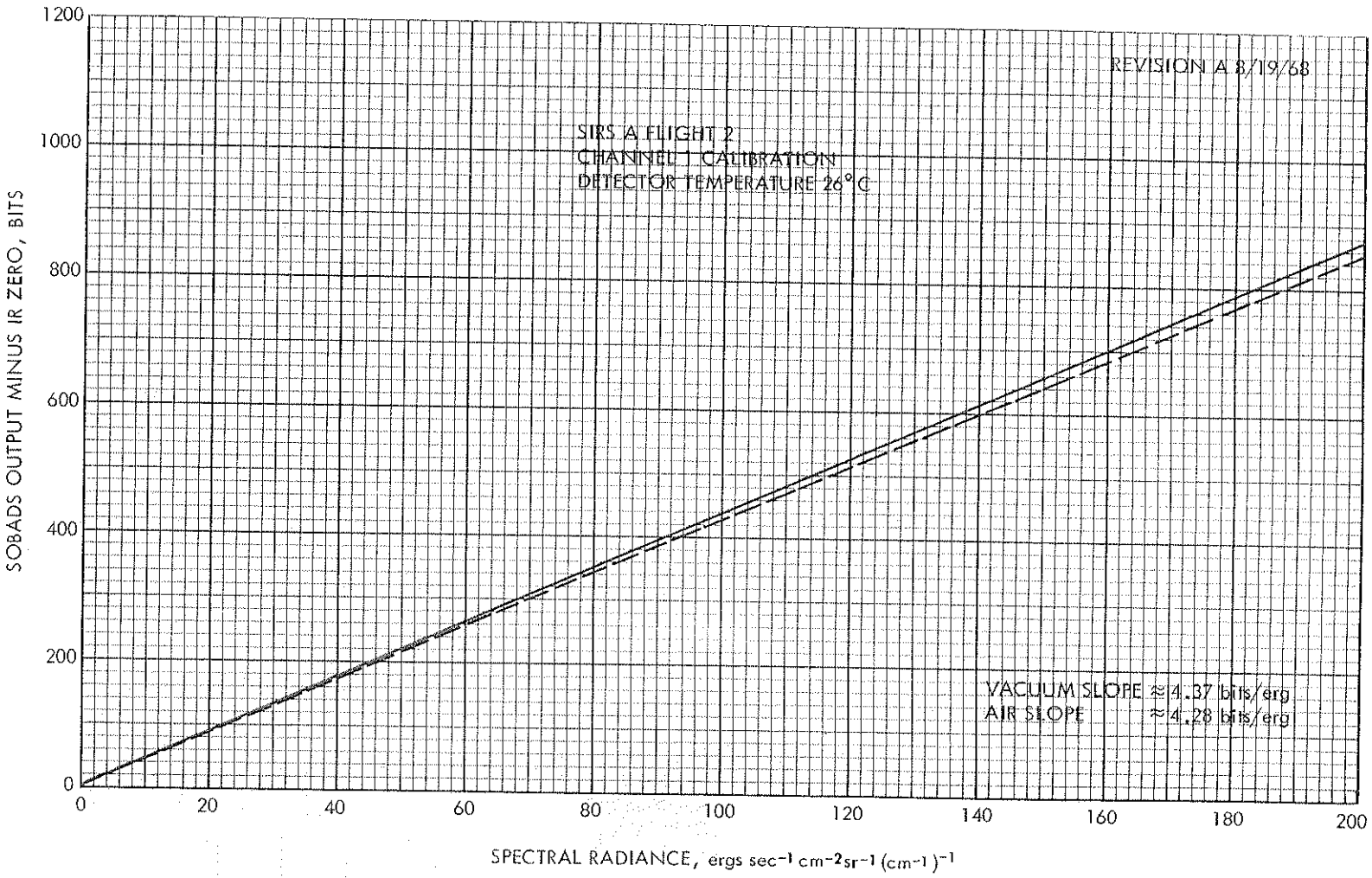

Figure 6-3–Channel 1 (899 cm^{-1}) Calibration Curve

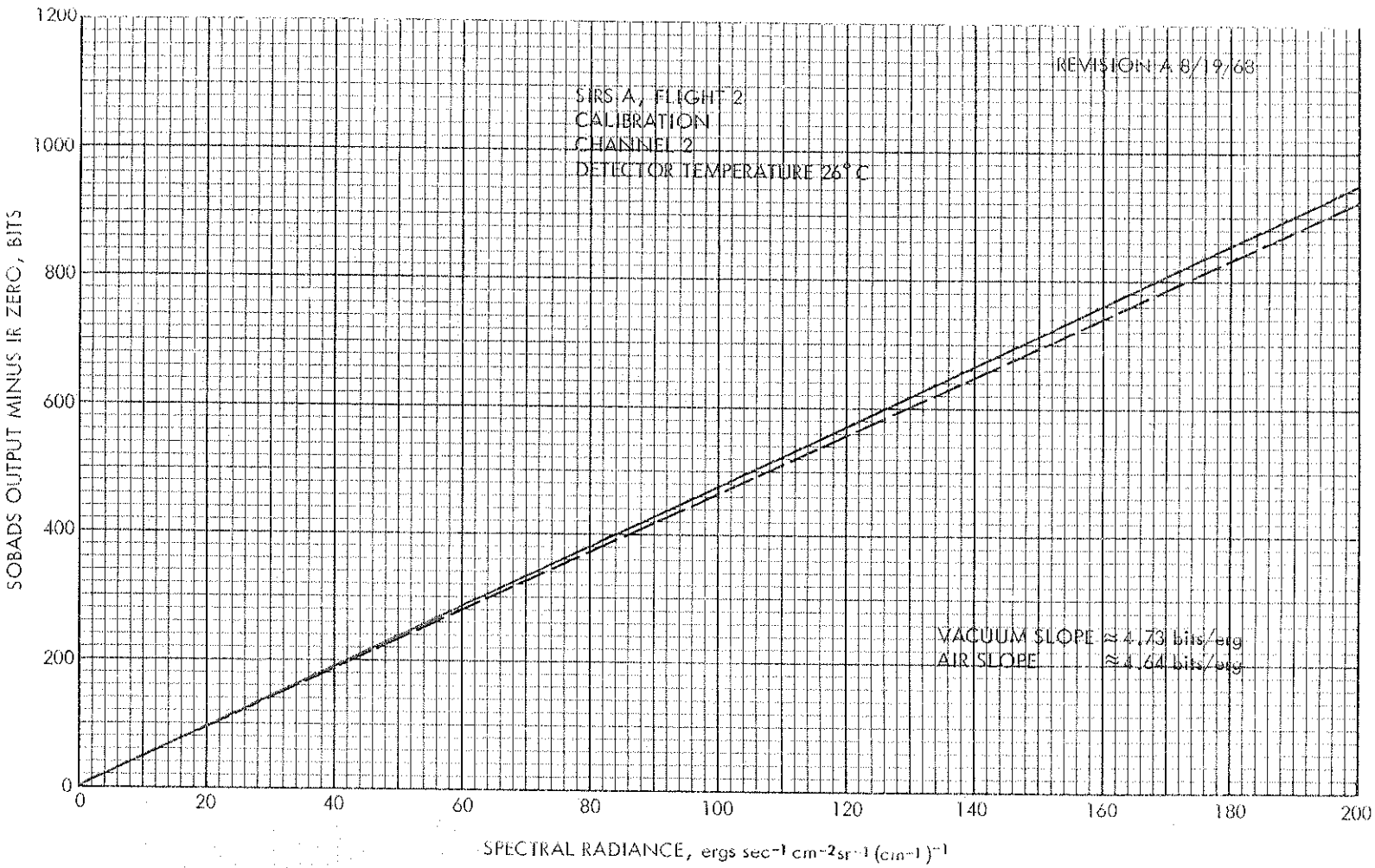

Figure 6-4-- Channel 2 (750 cm^{-1}) Calibration Curve

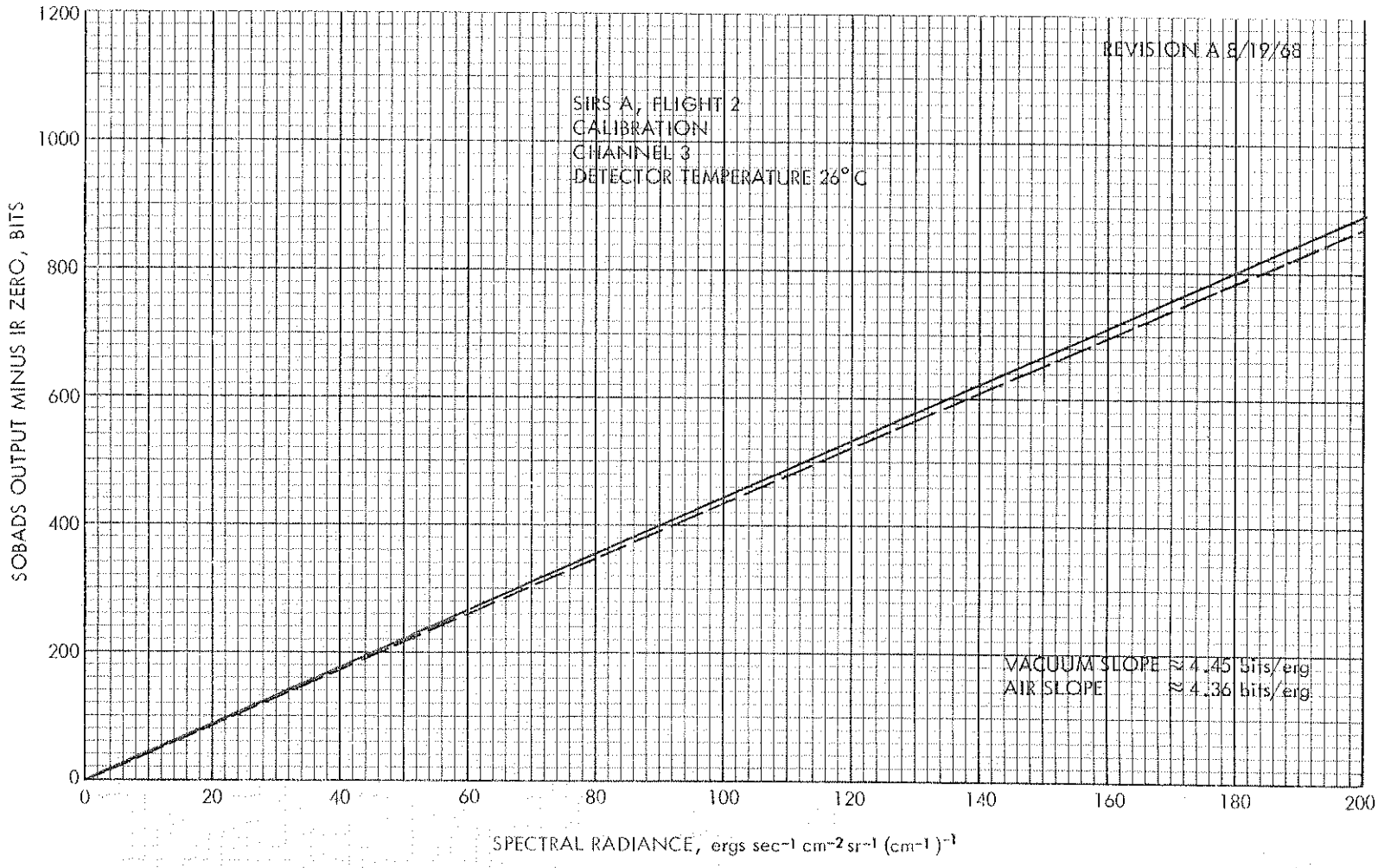

Figure 6-5–Channel 3 (714 cm^{-1}) Calibration Curve

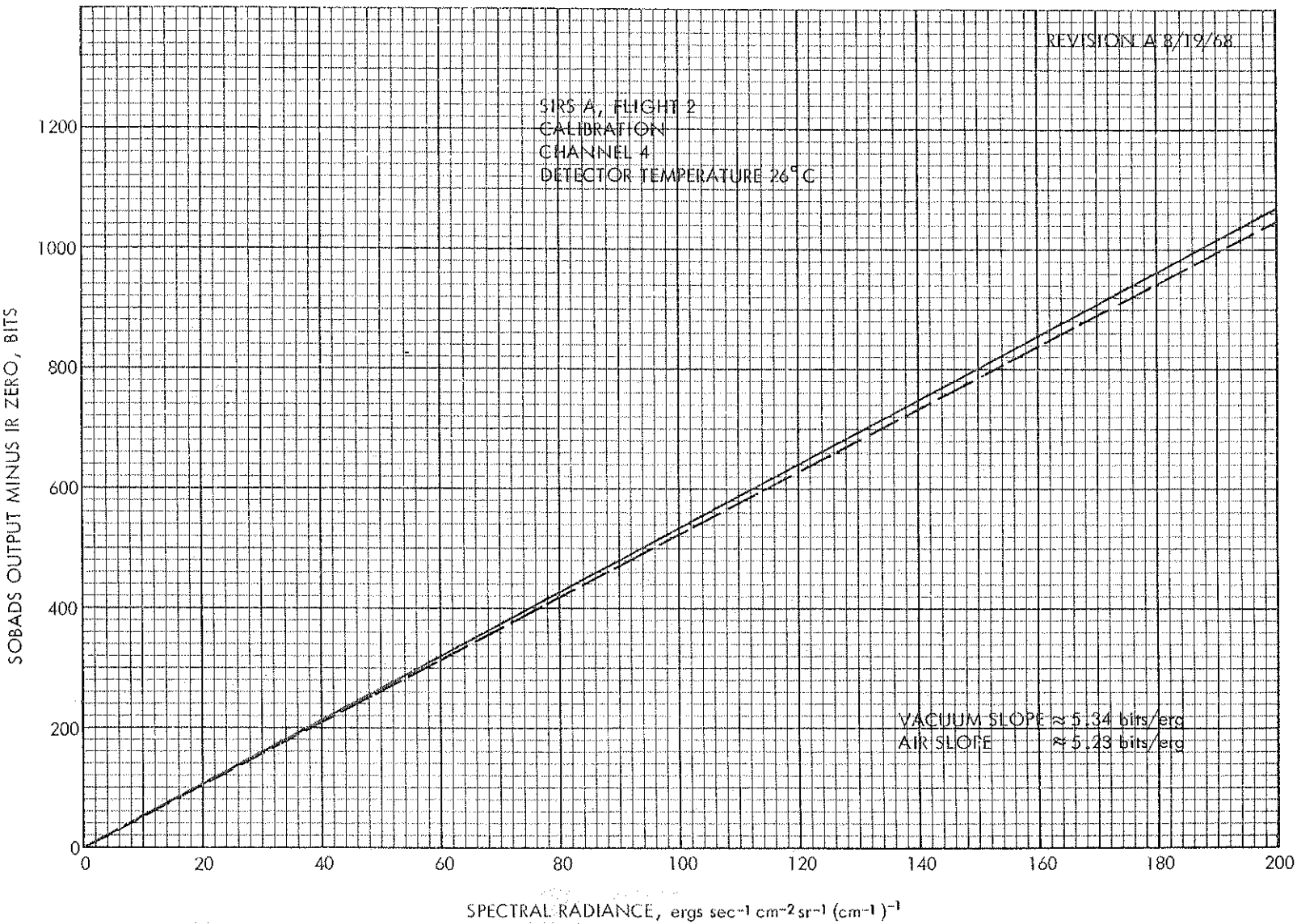

Figure 6-6--Channel 4 (706 cm^{-1}) Calibration Curve

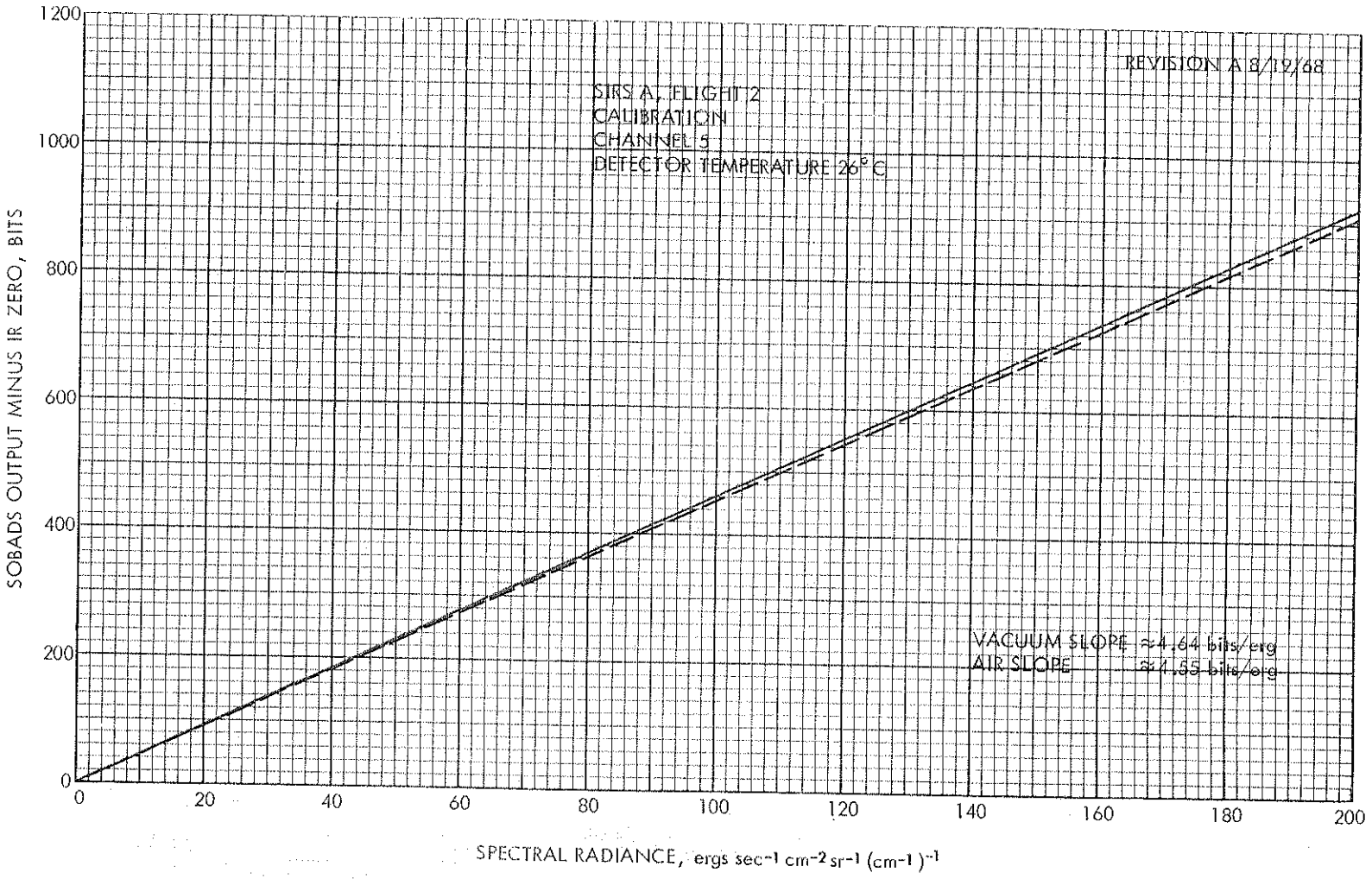

Figure 6-7--Channel 5 (699 cm^{-1}) Calibration Curve

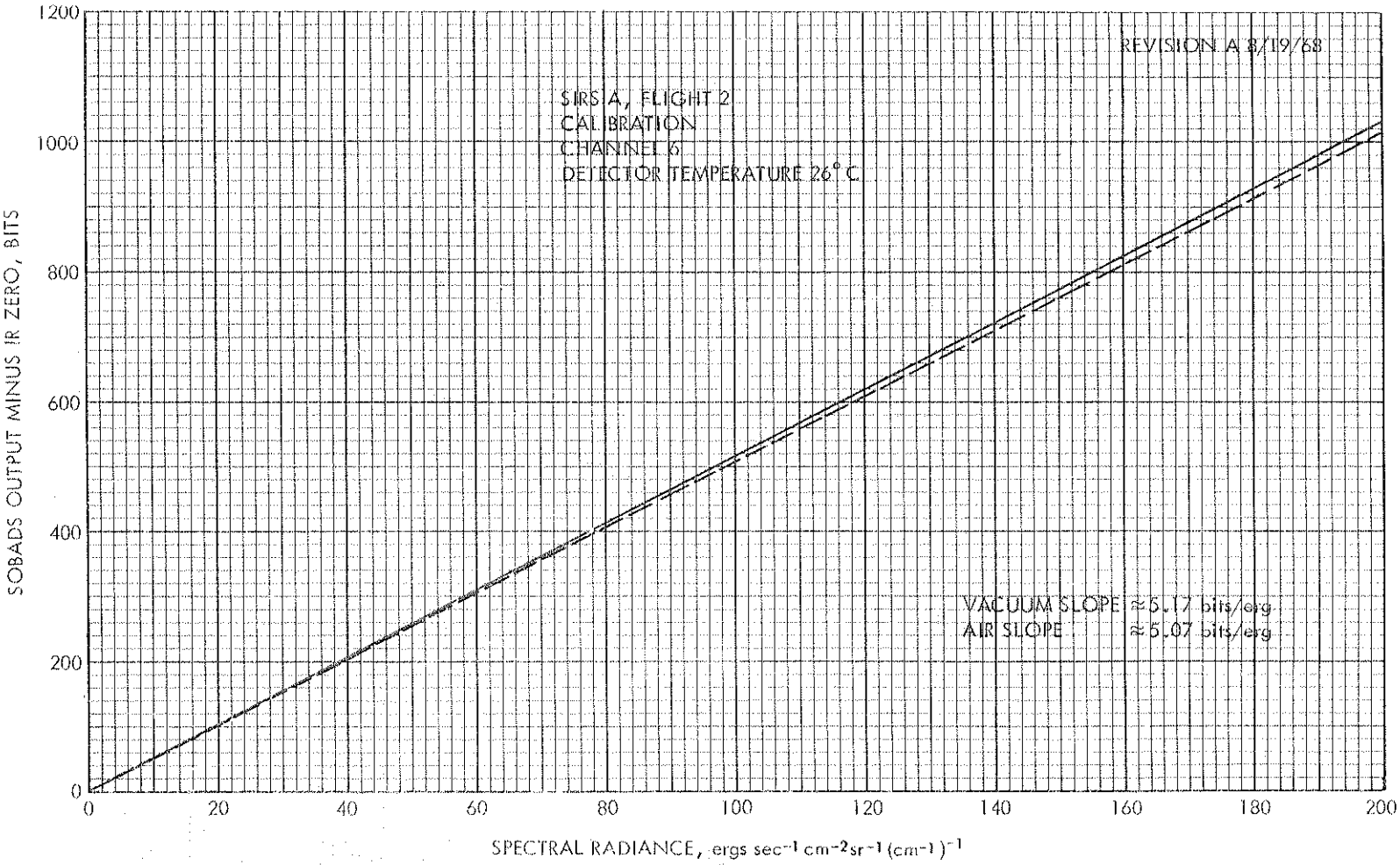

Figure 6-8 – Channel 6 (692 cm^{-1}) Calibration Curve

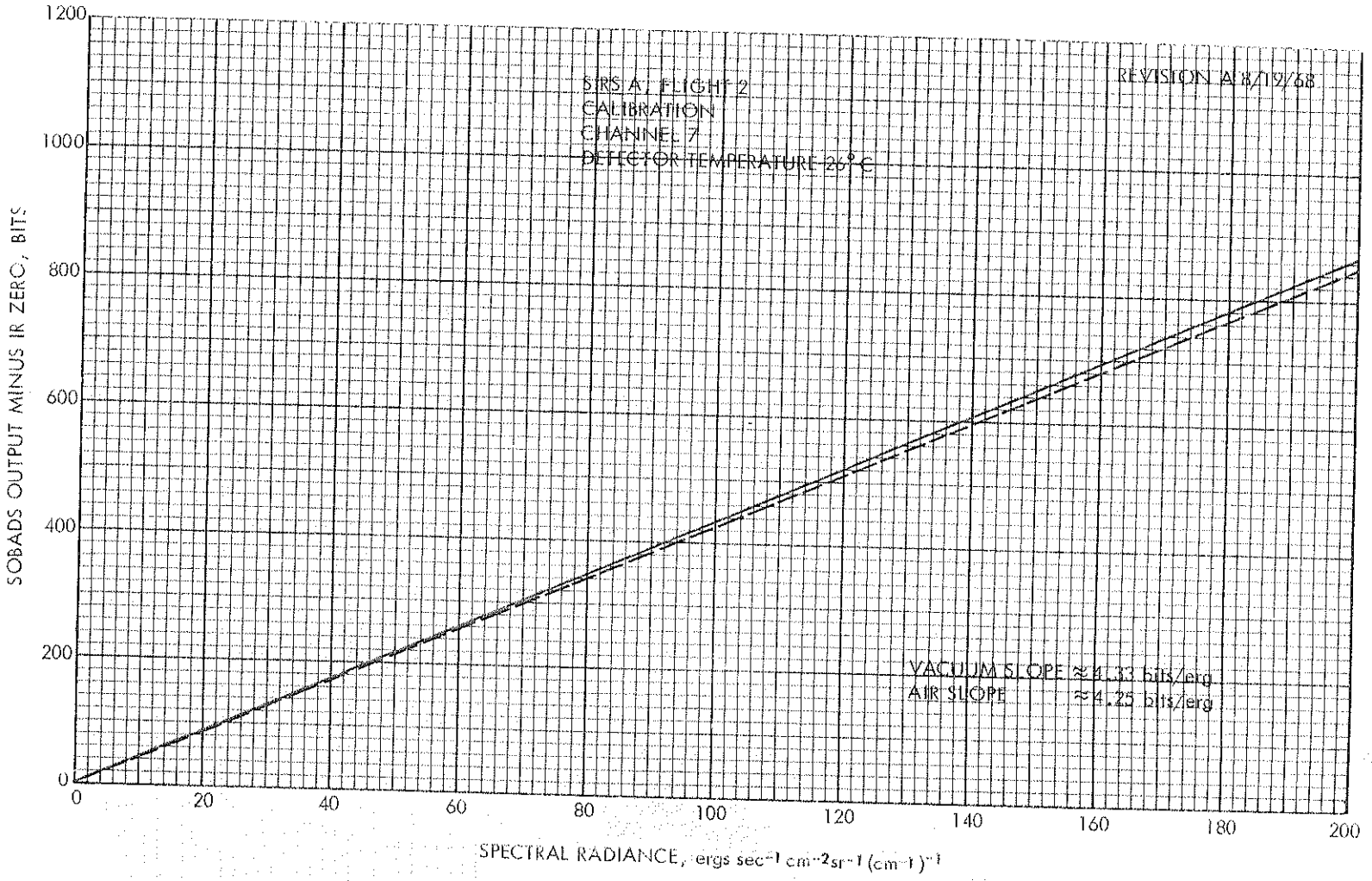

Figure 6-9—Channel 7 (677 cm^{-1}) Calibration Curve

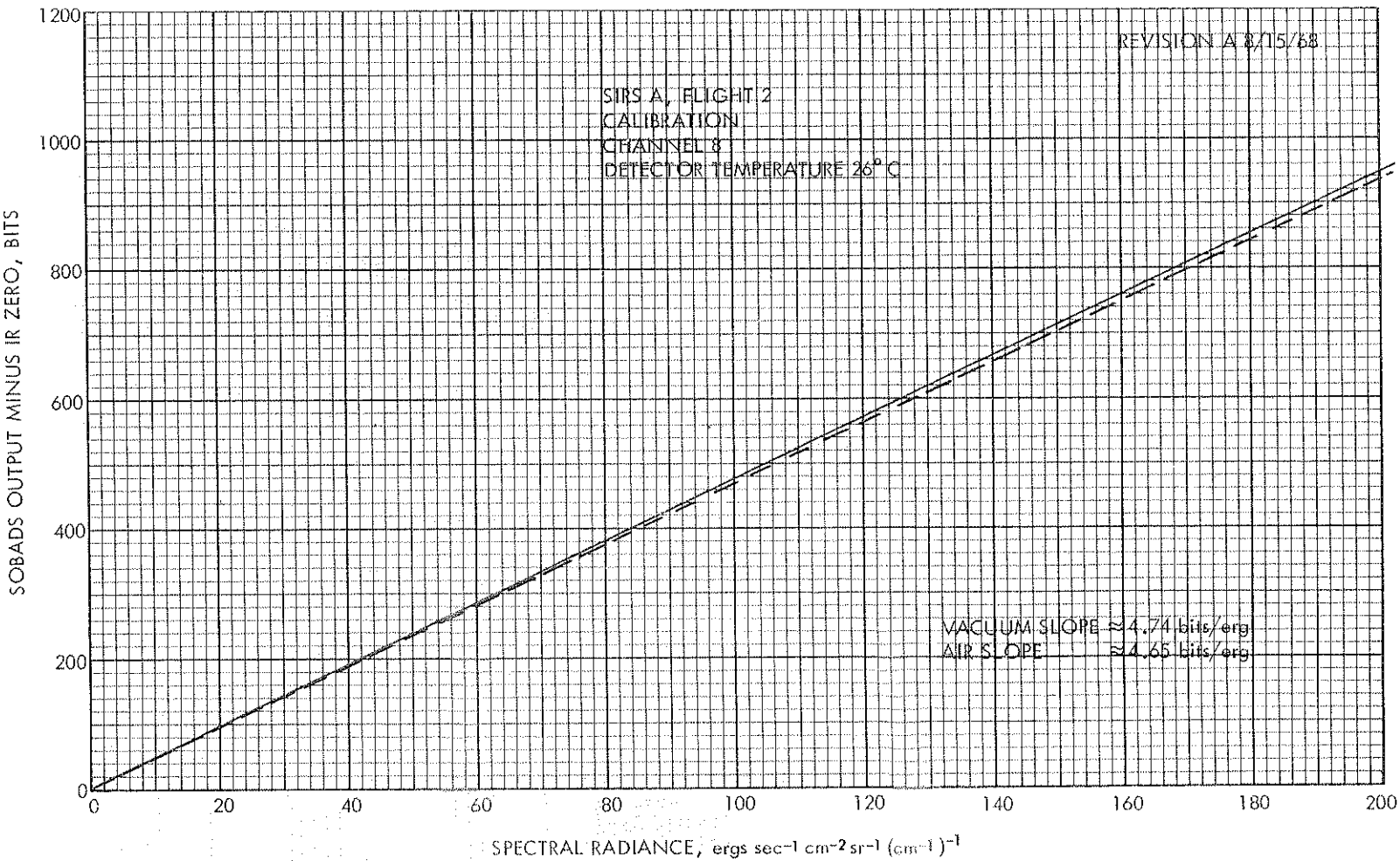

Figure 6-10– Channel 8 (669 cm^{-1}) Calibration Curve

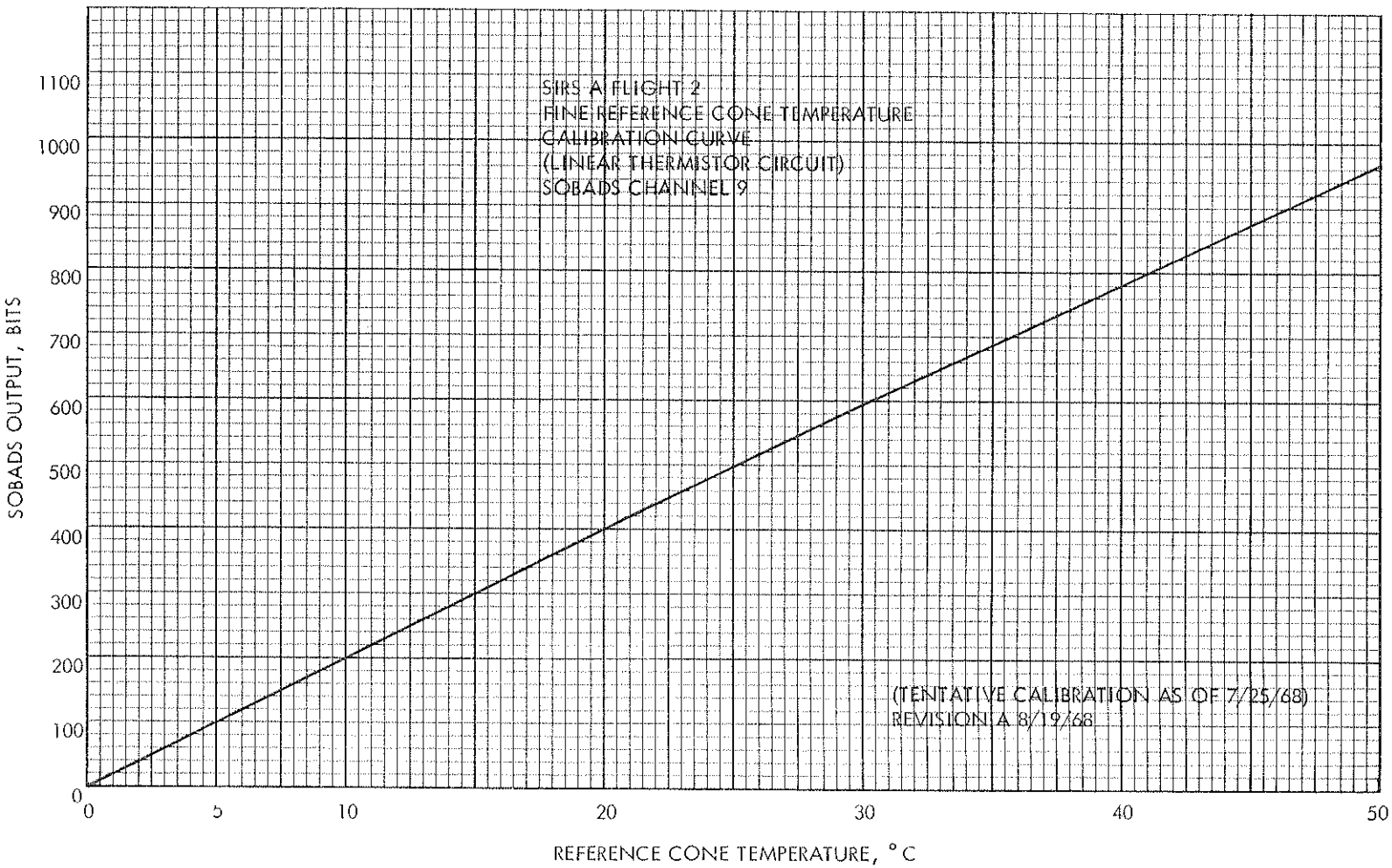

Figure 6-11– Reference Cone Calibration

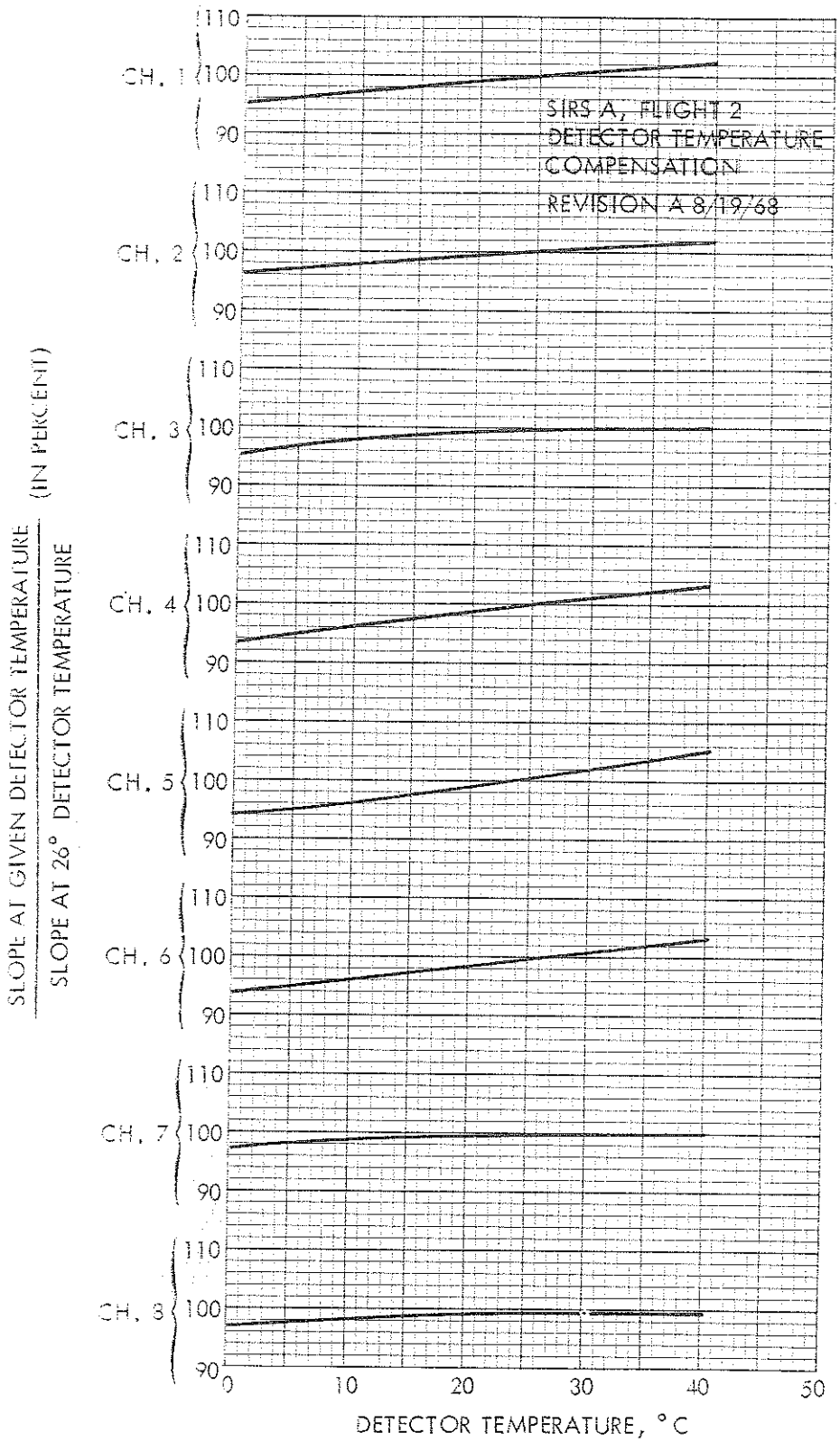

Figure 6-12– Calibration Curve Slopes vs. Detector Temperature

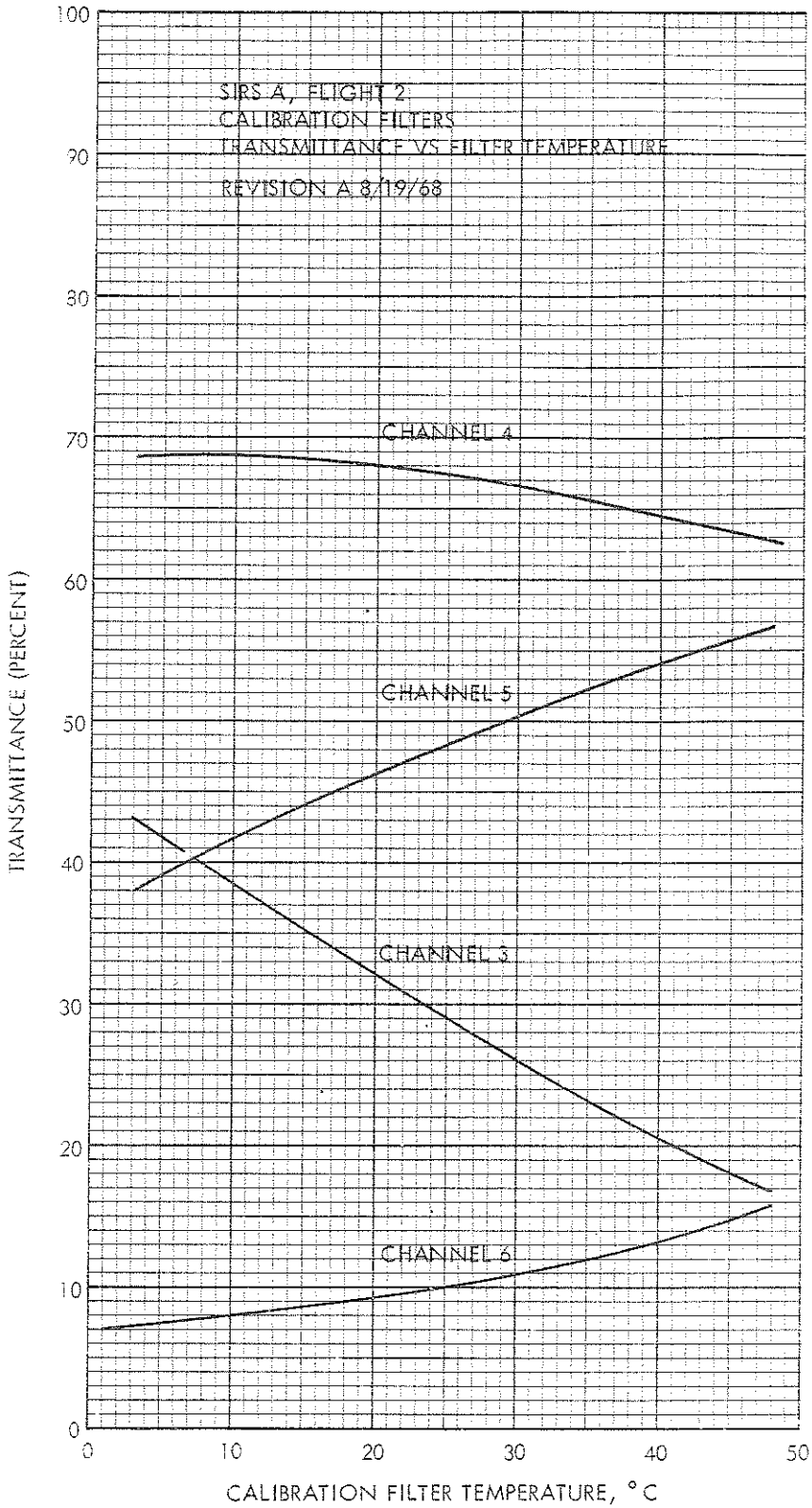

Figure 6-13– Calibration Filter Transmission vs. Temperature

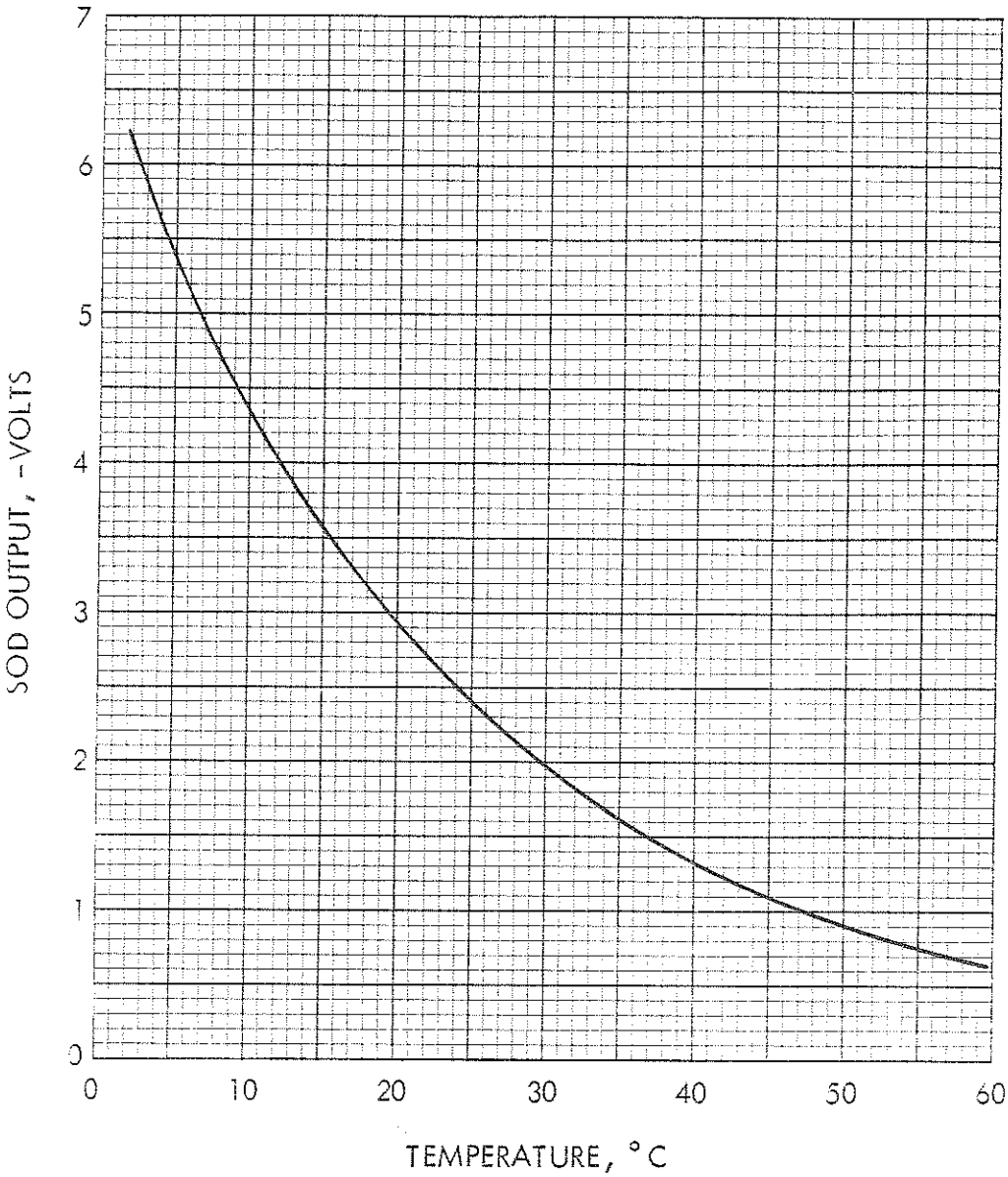

Figure 6-14–Temperature Monitor Thermistor Calibration

One analog channel is used to monitor the operation of the chopper motor. The operating levels are typically:

Motor off – 0 TMV

Motor one phase on – 4.250 ± .250 TMV

Motor two phases on – 5.750 ± .250 TMV.

The final two analog channels monitor the SIRS -24.0 volt supply and the Telemetry -24.5 volt supply. Figures 6-15 and 6-16 show the respective linear relationships between the telemetered voltage and the supply voltages. All of the housekeeping channels are sampled by the PCM system once every sixteen seconds.

All SIRS sensory and housekeeping data are handled by the Nimbus PCM telemetry system, recorded on the spacecraft tape recorder and transmitted to the STADAN Data Acquisition Facility and retransmitted to the NDHS at GSFC. The PCM telemetry ground station at the NDHS reduces the data in real time as they are received. Data are decommutated for processing on the CDC-924 computers. All SIRS sensory and housekeeping data are recorded on the computer generated Sensory Data Tape (SDT).

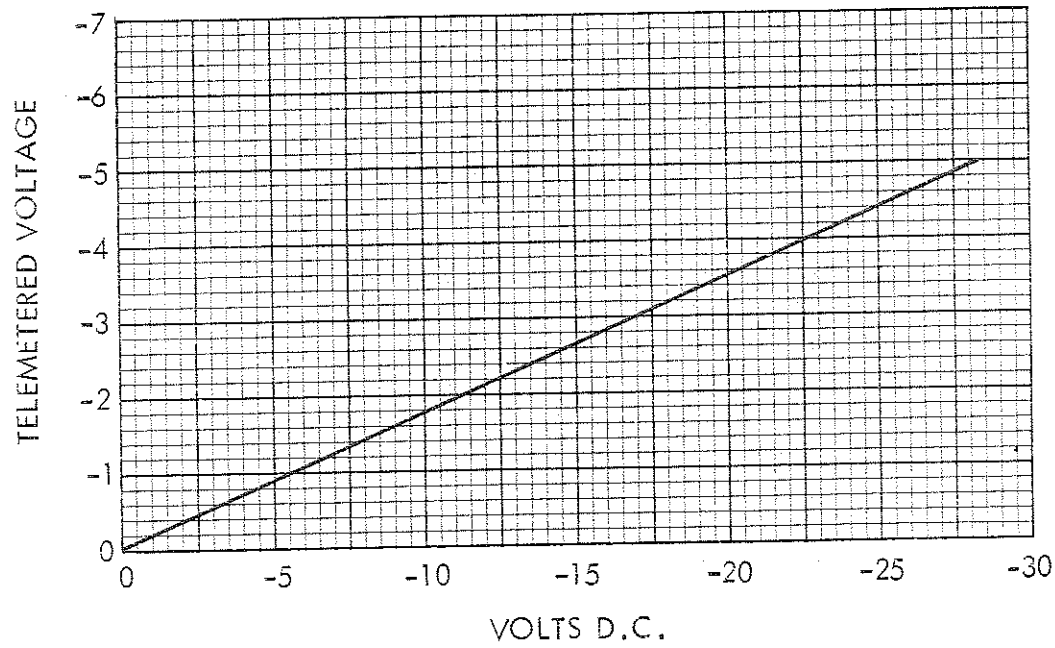

Figure 6-15– SIRS -24.0 Volt Supply Monitor

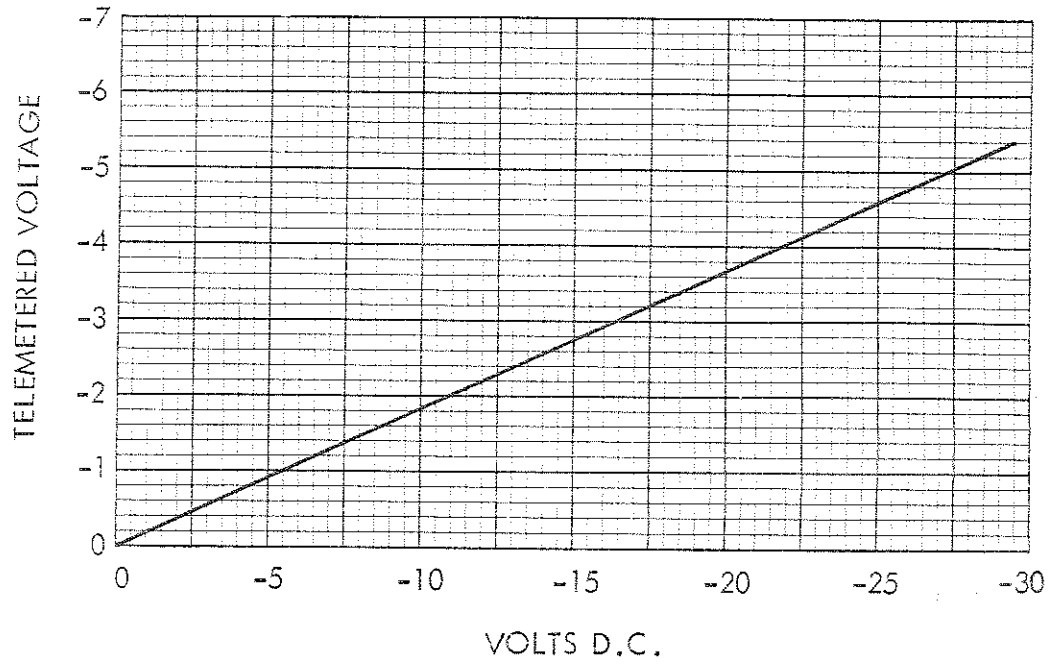

Figure 6-16—Telemetry -24.5 Volt Supply Monitor

6.4 SIRS Data Processing, Archiving, and Access

Sensory Data Tapes (SDT) containing all SIRS data will be delivered from the Nimbus Data Handling Facility to the National Environmental Satellite Center for further processing. Two types of SIRS archival tapes will be produced by the CDC 6600 computer at NESC: one will contain radiance values, the other will have derived atmospheric temperature profiles.

NESC will furnish SIRS archival tapes containing radiance values to the National Space Science Data Center at Goddard. These tapes will be formatted for compatibility with the IBM equipment at the NSSDC. (Section 6.5 shows a preliminary format for the SIRS archival tape furnished to NSSDC.) Changes to this format will undoubtedly be required after the experimental data become available and have been analyzed. There will be a period of time required for check-out of the instrument, verification of the experiment, and modifications of the computer programs before archival tapes will be made available to NSSDC. It is expected that this time interval will be no shorter than 3 months from Nimbus III launch. Any significant problems would, of course, extend this period of time.

NESC will archive tapes containing derived atmospheric temperature profiles at the National Weather Records Center. Each archived profile will have the associated space and time coordinates as well as the radiance values from which the profile has been derived. These archival tapes will be forwarded to NWRC when the procedures for the retrieval of temperature profiles have become well defined. A period of 6-12 months after Nimbus III launch appears to be a realistic estimate of the time required for defining the procedures adequately to allow for generation of NWRC archival tapes.

Final formats of any computer printouts obtainable from the archival tapes cannot be defined at present, and will be included in a future Nimbus III data catalog.

6.5 Preliminary Format of the SIRS Archival Tape

Tables 6-1 and 6-2 contain the preliminary format of the SIRS archival tape furnished to NSSDC. The first record of each orbit will contain information identifying the orbit and a summary of the instrument's status throughout the orbit. Basically, this information will be extracted from the history file of the SIRS data on the Sensory Data Tape. The second and all subsequent records of each orbit will contain the sensory and housekeeping data from each major frame. In addition, the computed values of radiance and the calibration data used in determining these values will be presented in each record. The latitude, longitude, time, and status of the instrument for each set of measurements will also be available.

Table 6-1
Header Record of the SIRS Archival Tape

Record Length: 450-24 BIT WORDS,
180-60 BIT WORDS

Word	Format	Event
1-30	BCD	Orbital description
31-399	SPEC2	SIRS Sybsystem Status Profile
400	F2	Fine Ref. Cone Temp.-Std. Dev.
401	"	-Min.
402	"	-Max.
403	"	-Mean
404	"	Coarse Ref. Cone Temp. - Std. Dev.
405	"	-Min.
406	"	-Max.
407	"	-Mean
408	"	Pcnt. Diff.
409-411	"	24VT - Min, Max, Mean
412-414	"	Motor P. S.
415-417	"	24VR - Min, Max, Mean
418-420	"	SCUM Temp. - Min, Max, Mean
421-423	"	SOBADS " - " " "
424-426	"	SOD " - " " "
427-429	"	SIPS " - " " "
430-432	"	Order Filter Temp. - Min, Max, Mean
433-435	"	Detector " " " "
436-438	"	Cal. Filter " " " "
439-441	"	Main Mirror " " " "
442-444	"	Motor " " " "
445-447	"	Earth Mirror Temp. - Min, Max, Mean
448-450	"	3-24 bit words of ZEROS
ALL TEMPERATURES IN °C.		

Table 6-2
Data Record of the SIRS Archival Tape

Record Length: 80 24 bit words,
32 60 bit words

Word II	Format	Event
1	I	Record Number
2	I	Major Frame Number
3-5	I	Time in hrs., min., sec.
6	I	Cal. Cycle Number
7-10	F2	Latitude, longitude, altitude, attitude
11-26	I	SIRS IR data (Bits), Chan 1-16
27-42	F2	" " " (Radiance), Chan 1-16
43-50	F3	Gain, chan 1-8
51-58	F3	Alpha, chan 1-8
59	I	Fine Ref. Cone (bits)
60	F2	Fine Ref. Cone (Temp)
61	"	SCUM Temp.
62	"	Order Filter Temp.
63	"	SOBADS Temp.
64	"	SOD Temp.
65	"	SIPS Temp.
66	"	Detector Temp.
67	"	Cal. Filter Temp.
68	"	Main Mirror Temp.
69	"	Motor Temp.
70	"	24VT (Voltage)
71	"	MOTOR P. S. (Voltage)
72	"	24VR (Voltage)
73	"	Earth Mirror Temp.
74	"	Course Ref. Cone Temp.
75	BCD	Status: SIRS
76	"	SOBS
77	"	SLMP
78	"	SICM
79	"	SAT
80	SPEC1	On/Off: SOLR, LAMP2, SOBSA, SOBSR

SPEC1 = last 4 bits of word; each bit (0 = off/1 = on) indicates status of SOLR, LAMP2, SOBSA, SOBSB respectively, i.e., 10_8 would indicate SOLR on all other events off. Bits 4-7 indicate good or bad data (0 = good/1 = bad), i.e., 104_8 would indicate LAMP2 on but the data is bad.

Table 6-2 (Continued)

SPEC2 = made up of following 9 word blocks:

Word	Format	Event
1	I	Major Frame Number
2-4	I	Time of Major Frame hrs., min., sec.
5	BCD	Status of SIRS
6	"	" " SOBS
7	"	" " SLMP
8	"	" " SICM
9	"	" " SAT

These 9 work blocks may or may not fill the entire 369 word block reserved for SIRS Subsystem Status Profile - if not filled then remainder of block will be filled with blanks.

I = right adjusted integer.

F2 = right adjusted integer - decimal point is understood to be between 2nd and 3rd decimal digits - i.e., 1.70 would be stored as 252_8 right adjusted - when read as 170 would multiply by 10^{-2} to retrieve original quantity 1.70

F3 = same as F2 except decimal point is understood to be between 3rd and 4th decimal digits.

BCD = 4 character BCD word (Note: CDC BCD format uses display code where 01_8 is A, etc.)

Display Code	Characters
00	zero
01	A
02	B
03	C
04	D
05	E
06	F
07	G
10	H
11	I
12	J
13	K
14	L
15	M
16	N
17	O

Table 6-2 (Continued)

Display Code	Characters
20	P
21	Q
22	R
23	S
24	T
25	U
26	V
27	W
30	X
31	Y
32	Z
33	0
34	1
35	2
36	3
37	4
40	5
41	6
42	7
43	8
44	9
45	+
46	-
47	*
50	/
51	(
52	)
53	$
54	=
55	blank
56	,
57	.

Table 6-2 (Continued)

Display Code	Characters
60	≡
61	[
62	]
63	:
64	≠
65	⌐
66	∨
67	∧
70	·
71	.
72	<
73	>
74	≤
75	≥
76	¬
77	;

The entire tape is written in binary mode with one orbit per file, i.e. (one history record of 180-60 bit words or 450-24 bit words followed by several data records of 480-60 bit words or 1200-24 bit words). Each data record contains data from 15 major frames.

BIBLIOGRAPHY

1. J. C. Alishouse, L. J. Crone, H. E. Fleming, F. L. Van Cleef, and D. Q. Wark, "A Discussion of Empirical Orthogonal Functions and Their Application to Vertical Temperature Profiles," Tellus, Vol. XIX, No. 3, 1967, pp. 477-482.

2. S. Chandrasekhar, Radiative Transfer, Clarendon Press, Oxford, 1950, 393 pp. Reprinted by Dover Publications, Inc., New York, 1960.

3. B. J. Conrath, "On a Mathematical Formulation of the Constituent Inversion Problem for Planetary Atmospheres," NASA, Goddard Space Flight Center Document X-622-66-542, October 1966.

4. S. R. Drayson and C. Young, "Theoretical Investigations of Carbon Dioxide Radiative Transfer," The University of Michigan High Altitude Engineering Laboratory Report No. 07349-1-F, Final Report of Weather Bureau Contract No. Cwb-11106, August 1966.

5. M. G. Dreyfus, "Wedge-Immersed Thermistor Bolometer," Applied Optics, Vol. 1, No. 5, Sept. 1962, pp. 615-618.

6. M. G. Dreyfus and D. T. Hilleary, "Satellite Infrared Spectrometer – Design and Development," Aerospace Engineering, Vol. 21, No. 2, Feb. 1962, pp. 42-45.

7. F. F. Fischbach, "A Satellite Method for Pressure and Temperature Below 24 km," Bulletin of the American Meteorological Society, Vol. 46, No. 9, Sept. 1965, pp. 528-532.

8. H. E. Fleming and D. Q. Wark, "A Numerical Method for Determining the Relative Spectral Response of the Vidicons in a Nimbus Satellite System," Applied Optics, Vol. 4, No. 3, March 1965, pp. 337-342.

9. H. E. Fleming and D. Q. Wark, "Further Remarks on a Numerical Method for Determining the Relative Spectral Response of the Vidicons in a Nimbus Satellite System," Applied Optics, Vol. 5, No. 2, Feb. 1966, pp. 352-353.

10. R. Fow, "Atmospheric Temperature Structure from the Microwave Emission of Oxygen," thesis, Massachusetts Institute of Technology, 1964.

11. R. Frith, "Meteorological Satellites," Weather, Vol. 16, No. 11, Nov. 1961, pp. 364-370.

12. D. Fryberger and E. F. Uretz, "Some Considerations Concerning the Measurement of the Atmospheric Temperature Field by Electromagnetic Means," IRE Transactions on Military Electronics, Vol. MIL-5, No. 4, Oct. 1961, pp. 279-285.

13. F. W. P. Götz, "Zum Strahlungsklima des Spitzbergensommers. Strahlungs- und Ozonmessungen in der Königsbucht 1929," Gerlands Beiträge zur Geophysik, Vol. 31, Nos. 1-3, 1931, pp. 119-154.

14. D. T. Hilleary, E. L. Heacock, W. A. Morgan, R. H. Moore, E. C. Mangold, and S. D. Soules, "Indirect Measurements of Atmospheric Temperature Profiles from Satellites: III. The Spectrometers and Experiments," Monthly Weather Review, Vol. 94, No. 6, June 1966, pp. 367-377.

15. J. T. Houghton, "Meteorological Significance of Remote Measurements of Infrared Emission from Atmospheric Carbon Dioxide," Quarterly Journal of the Royal Meteorological Society, Vol. 87, No. 371, Jan. 1961, pp. 102-104.

16. D. G. James, "Indirect Measurements of Atmospheric Temperature Profiles from Satellites: IV. Experiments with Phase 1 Satellite Infrared Spectrometer," Monthly Weather Review, Vol. 95, No. 7, July 1967, pp. 457-462.

17. L. D. Kaplan, "Inference of Atmospheric Structure from Remote Radiation Measurements," Journal of the Optical Society of America, Vol. 49, No. 10, Oct. 1959, pp. 1004-1007.

18. L. D. Kaplan, "The Spectroscope as a Tool for Atmospheric Sounding by Satellites," Journal of Quantitative Spectroscopy and Radiative Transfer, Vol. 1, No. 2, November 1961, pp. 89-95.

19. L. I. Koprova and M. S. Malkevich, "On the Empirical Orthogonal Functions for the Optimal Parameterization of Temperature and Humidity Profiles," Atmospheric and Oceanic Physics, Vol. 1, No. 1, January 1965, pp. 15-18. (English translation by the American Geophysical Union.)

20. Y. H. Katz (ed.), "The Application of Passive Microwave Technology to Satellite Meteorology: A Symposium, "The RAND Corporation Memorandum RM-3401-NASA; NASA NASr-21 (07), August 1963.

21. J. I. F. King, "The Radiative Heat Transfer of Planet Earth," Scientific Uses of Earth Satellites, Second Revised Edition, edited by J. A. Van Allen, University of Michigan Press, Ann Arbor, 1958, 316 pp.

22. J. I. F. King, "Meteorological Inferences from Satellite Radiometry. I," Journal of the Atmospheric Sciences, Vol. 20, No. 4, July 1963, pp. 245-256.

23. J. I. F. King, "Inversion by Slabs of Varying Thickness," Journal of the Atmospheric Sciences, Vol. 21, No. 3, May 1964, pp. 324-326.

24. V. P. Kozlov. "On the Estimation of the Vertical Temperature Profile from the Outgoing Radiation Spectrum," Atmospheric and Oceanic Physics, Vol. 2, No. 2, February 1966, pp. 80-86. (English translation by the American Geophysical Union.)

25. B. Krakow. "Spectroscopic Temperature Profile Measurements in Inhomogeneous Hot Gases," Applied Optics, Vol. 5, No. 2, Feb. 1966, pp. 201-209.

26. M. S. Malkevich, "Some Questions on the Interpretation of Radiation Measurements from Satellites," Kosmicheskie Issledovaniya, Vol. 2, No. 2, Mar.-Apr. 1964, pp. 246-256. (English Translation.)

27. M. S. Malkevich, V. P. Kozlov, and I. A. Gorchakova, "On Application of the Statistical Method for Determination of Atmospheric Temperature Profiles from Satellites," submitted to Tellus, 1967.

28. M. S. Malkevich and V. I. Tatarskii, "Determination of Vertical Atmospheric Temperature Profiles by Means of Outgoing Radiation in a CO_2 Absorption Band," Kosmicheskie Issledovaniya, Vol. 3, No. 3, May-June 1965, pp. 444-456. (English Translation.)

29. G. I. Marchuk, "Equation for the Value of Information from Weather Satellites and Formulation of Inverse Problems," Kosmicheskie Issledovaniya, Vol. 2, No. 3, May-June 1964, pp. 462-477. (English Translation.)

30. C. L. Mateer, "On the Information Content of Umkehr Observations," Journal of the Atmospheric Sciences, Vol. 22, No. 4, July 1965, pp. 370-381.

31. R. A. McClatchey, "The Use of the 4.3-Micron CO_2 Band to Sound the Temperature of a Planetary Atmosphere," in Proceedings of the Symposium on Electromagnetic Sensing of the Earth from Satellites, (R. Zirkind, ed.), Polytechnic Press of the Polytechnic Institute of Brooklyn, 1967.

32. M. L. Meeks and A. E. Lilly, "The Microwave Spectrum of Oxygen in the Earth's Atmosphere," Journal of Geophysical Research, Vol. 68, No. 6, Mar. 1963, pp. 1683-1703.

33. R. D. Rawcliffe, G. E. Meloy, R. M. Friedman, and E. H. Rogers, "Measurement of Vertical Distribution of Ozone from a Polar Orbiting Satellite," Journal of Geophysical Research, Vol. 68, No. 24, Dec. 1963, pp. 6425-6429.

34. S. F. Singer and R. C. Wentworth, "A Method for the Determination of the Vertical Ozone Distribution from a Satellite," Journal of Geophysical Research, Vol. 62, No. 2, June 1957, pp. 299-308.

35. S. D. Smith and C. R. Pidgeon, "Application of Multiple Beam Interferometric Methods to the Study of CO_2 Emission at 15μ," Mémoires de la Société Royale des Sciences de Liège, Ser. 5, Vol. 9, 1964, pp. 336-349.

36. W. L. Smith, "An Iterative Method for Deducing Tropospheric Temperature and Moisture Profiles from Satellite Radiation Measurements," Monthly Weather Review, Vol. 95, No. 6, June 1967, pp. 363-369.

37. W. L. Smith, "An Improved Method for Calculating Tropospheric Temperature and Moisture from Satellite Radiometer Measurements," Monthly Weather Review, Vol. 96, No. 6, June 1968, pp. 387-396.

38. O. N. Strand and E. R. Westwater, "Minimum-RMS Estimation of the Numerican Solution of a Fredholm Integral Equation of the First Kind," SIAM Journal on Numerical Analysis, Vol. 5, No. 2, June 1968, pp. 287-295.

39. O. N. Strand and E. R. Westwater, "The Statistical Estimation of the Numerical Solution of a Fredholm Integral Equation of the First Kind," Journal of the Association for Computing Machinery, Vol. 15, No. 1, January 1968, pp. 100-114.

40. S. Twomey, "On the Deduction of the Vertical Distribution of Ozone by Ultraviolet Spectral Measurements from a Satellite," Journal of Geophysical Research, Vol. 66, No. 7, July 1961, pp. 2153-2162.

41. S. Twomey, "The Application of Numerical Filtering to the Solution of Integral Equations Encountered in Indirect Sensing Measurements," Journal of the Franklin Institute, Vol. 279, No. 2, Feb. 1965, pp. 95-109.

42. S. Twomey, "Indirect Measurements of Atmospheric Temperature Profiles from Satellites: II. Mathematical Aspects of the Inversion Problem," Monthly Weather Review, Vol. 94, No. 6, June 1966, pp. 363-366.

43. S. Twomey and H. B. Howell, "A Discussion of Indirect Sounding Methods with Special Reference to the Deduction of Vertical Ozone Distribution from Light Scattering Measurements," Monthly Weather Review, Vol. 91, Nos. 10-12, Oct.-Dec. 1963, pp. 659-664.

44. D. Q. Wark, "On Indirect Temperature Soundings of the Stratosphere from Satellites," Journal of Geophysical Research, Vol. 66, No. 1, Jan. 1961, pp. 77-82.

45. D. Q. Wark and H. E. Fleming, "Indirect Measurements of Atmospheric Temperature Profiles from Satellites: I. Introduction," Monthly Weather Review, Vol. 94, No. 6, June 1966, pp. 351-362.

46. D. Q. Wark, F. Saiedy and D. G. James, "Indirect Measurements of Atmospheric Temperature Profiles from Satellites: VI. High-Altitude Balloon Testing," Monthly Weather Review, Vol. 95, No. 7, July 1967, pp. 468-479.

47. E. R. Westwater and O. N. Strand, "Application of Statistical Estimation Techniques to Ground-Based Passive Probing of the Tropospheric Temperature Structure," ESSA Technical Report IER 37-ITSA 37, April 1967.

48. E. R. Westwater and O. N. Strand, "Statistical Information Content of Radiation Measurements Used in Indirect Sensing," Journal of the Atmospheric Sciences, 1967. Vol. 25, No. 5, Sept. 1968, pp. 750-758.

49. M. Wolk, F. Van Cleef, and G. Yamamoto, "Indirect Measurements of Atmospheric Temperature Profiles from Satellites: V. Atmospheric Soundings from Infrared Spectrometer Measurements at the Ground," Monthly Weather Review, Vol. 95, No. 7, July 1967, pp. 463-467.

50. G. Yamamoto, "Numerical Method for Estimating the Stratospheric Temperature Distribution from Satellite Measurements in the CO_2 Band," Journal of Meteorology, Vol. 18, No. 5, Oct. 1961, pp. 581-588.

K02955

SECTION 7

THE MONITOR OF ULTRAVIOLET SOLAR ENERGY (MUSE) EXPERIMENT

by
Donald Heath and Raymond D. Westcott
National Aeronautics and Space Administration
Goddard Space Flight Center

7.1 Description of the Experiment

The purpose of the MUSE experiment is to look for changes with time in the ultraviolet solar flux in five broad bands from 1150 to 3000Å, to measure the solar flux in these regions, and to measure the atmospheric attenuation at these wavelengths as the sensors on board view the setting sun after the spacecraft has crossed the terminator in the northern hemisphere.

The sensors have their maximum response to solar radiation at 1216Å, 1600Å, 1800Å, 2000Å, and 2600Å. The solar flux from 1150 to 3000Å is the major source of energy input into the upper atmosphere.

An important part of this experiment is the monitoring of solar radiation which produces the photochemical equilibrium that governs the amount and distribution of ozone in the upper stratosphere. S. I. Rasool (Reference 1) has analyzed the effect on the ozone content, and the heating of the upper stratosphere which could result by changes in the solar flux at 2000Å and 2600Å.

The five nominal wavelength regions, each with a brief description of its purpose, are as follows:

1216Å – This channel monitors the solar hydrogen Lyman alpha radiation which plays a major role in the formation of the D-region of the ionosphere.

1600Å – Solar radiation at these wavelengths is responsible for the dissociation of O_2 in the upper atmosphere above 100 Km.

1800Å – Radiation in the vicinity of this wavelength causes the fluorescence of O_2, and is on the short wavelength side of the region where the sun changes from a 5500K to a 5000K blackbody.

2000Å – This solar radiation is responsible for the photodissociation of O_2 via the Herzberg Continuum at the level of the ozone layer.

2600Å – The photodissociation of ozone is caused by solar radiation at this wavelength which together with the 2000Å radiation determines the photochemical equilibrium of ozone.

The MUSE instrument is shown in Figure 7-1. The appropriate bands of ultraviolet flux enter the photodiodes, producing a current which is measured by an electrometer and digitized by the Nimbus PCM system. Simultaneously an Adcole solar aspect system measures the angle of incidence of the solar rays and transmits its digital information to the PCM system. The PCM data are stored on magnetic tape and transmitted on playback to the Data Acquisition Facility (DAF) and retransmitted to the Nimbus Data Handling Facility at GSFC. At the NDHF the PCM data are decommutated and selected housekeeping and MUSE sensory data are processed by a CDC 924 computer to create an IBM-360 compatible Sensory Data Tape (SDT) for final data processing. The MUSE instrument has only an in-flight electrical calibration sequence, as there are no known suitable ultraviolet sources capable of providing an in-flight optical calibration.

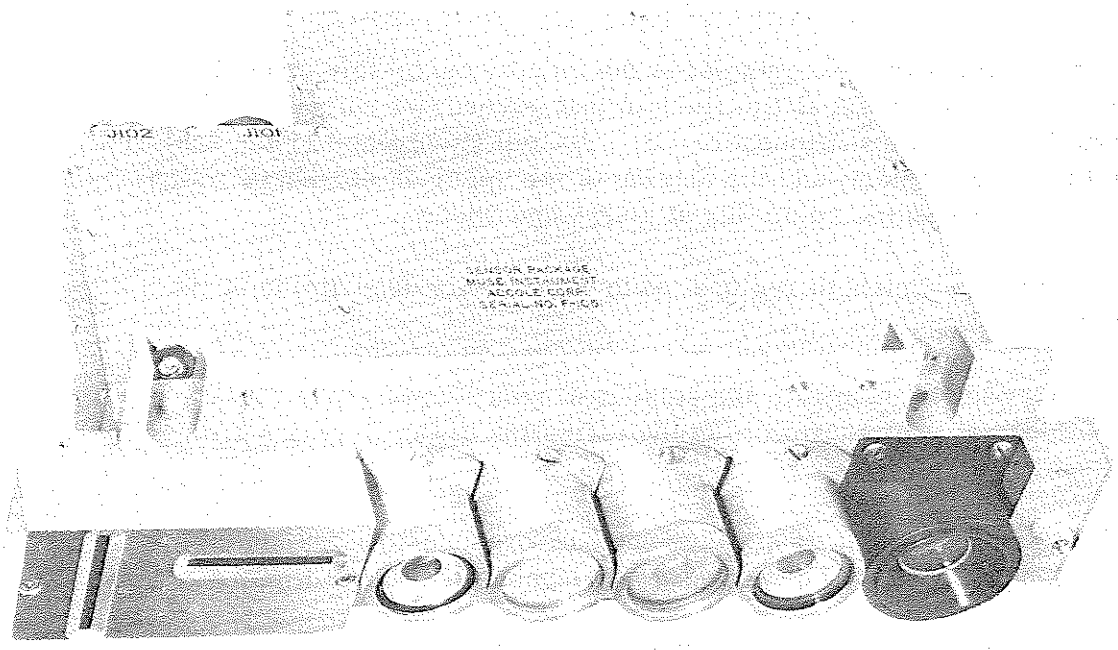

Figure 7-1–MUSE Sensor Package

7.2 Sensors

The sensors are vacuum photodiodes by EMR. All except the 1216Å sensor have semi-transparent photocathodes which are deposited on the windows. The 1216Å sensor consists of a solid tungsten cathode.

The five spectral regions are determined by the transmittances of the filter or window materials on the short wavelength side while the long wavelength cut-off is produced by the varying degrees of "solar blindness" of the different photocathode materials.

A summary of the characteristics of the five channels is given in Table 1. The effective wavelength ($\bar{\lambda}$) is defined as:

$$\bar{\lambda} = \sum_i R(\lambda_i)\,\lambda_i \Big/ \sum_i R(\lambda_i) \qquad (1)$$

Where $R(\lambda_i)$ = (Filter transmittance at λ_i) × (Quantum efficiency of photocathode at λ_i) × (Solar flux in specified interval centered at λ_i in quanta/cm^2-sec.)

The current output of a sensor is related to the solar flux incident normal to the photocathode by the formula:

$$I_{(amps)} = \sum_i f_0(\lambda_i)\,\Delta\lambda_i\,AS(\lambda_i)\,1.6 \times 10^{-19} \qquad (2)$$

Where $f_0(\lambda_i)$ is the solar flux at the top of the atmosphere in quanta/cm^2-sec-Å at λ_i

$\Delta\lambda_i$ is the wavelength interval centered at λ_i

A is the area of the photocathode which is illuminated

$S(\lambda_i)$ is filter transmittance × quantum efficiency at λ_i

One must assume a distribution of solar flux with wavelength. If the measured sensor current is different from that calculated with Eq. 2, one can determine the solar flux at the effective wavelength of the sensor by the relationship:

Table 7-1

Summary of MUSE Sensor Characteristics

Sensor	Photocathode		Window	Filters	Aperture	$\bar{\lambda}$	I^*_{calc}
1216	Tungsten		MgF_2	None	Note: This information will be included in a future Nimbus III Catalog		
1600	CuI		CaF_2	MgF_2 (G)			
1800	CuI		Al_2O_3	SiO_2 Al_2O_3			
2000	CsI		Al_2O_3	ADP SiO_2 Al_2O_3 (G)			
2600	CsTe		Al_2O_3	Neutral Density Calcite ($CaCO_3$) Al_2O_3 (G)			

*To determine solar flux at terminator at $\bar{\lambda}$, multiply $f(\bar{\lambda})$ from Ref. 2 by the ratio of I_{meas}/I_{calc}

$$f_0(\bar{\lambda}) = f(\bar{\lambda})_{assumed} I_{meas} / I_{calc} \text{ (quanta/cm}^2\text{-sec-Å)} \quad (3)$$

To convert Eq. 3 to (ergs/cm^2-sec-Å) multiply the above equation by the energy/quanta ($E = hc/\lambda$) at $\bar{\lambda}$.

A convenient compilation of the solar flux measurements of the Naval Research Laboratory and the Air Force Cambridge groups under the direction of Tousey and Hinteregger respectively has been made by Schultz and Holland (Reference 2).

Due to the high orbital altitude of the Nimbus spacecraft, considerable work was done to determine what effects the high energy particles in the Van Allen belts would have on the transmittance of the optical filters and the quantum efficiencies of the photocathodes. These results are contained in the papers of Heath and Sacher, Sacher, and Heath and McElaney (References 3, 4, 5).

7.3 Optical Calibration

The measurement of the quantum efficiencies of the photocathodes was made using the standard technique of calibrating a freshly deposited film of sodium salicylate in front of a photomultiplier against a calibrated nitric oxide ionization cell at H-Lyman alpha. The calibration was checked in the long wavelength region by calibrating the sodium salicylate – photomultiplier against a thermopile. It was assumed that the response of the sodium salicylate was uniform between 1216Å and 2537Å. This in turn was used to calibrate two standard diodes, tungsten and CsTe which are used as standard detectors for the calibration of the flight sensors.

The filters were calibrated by measuring their transmittances as a function of wavelength under vacuum.

The optical calibrations of the five sensors are shown in Figures 7-2 to 7-6 where the product of the Quantum Efficiency × Transmittances of the filters is given as a function of wavelength. Since no two sensors have the same quantum efficiency curve, one can assign only a nominal effective wavelength to each of the sensors. Hence, one should refer to Table 7-1 for the effective wavelengths of the sensors actually flown.

Calibration curve will be included in the first Nimbus III Monthly Catalog

Figure 7-2–Quantum Efficiency for 1216Å Sensor

Calibration curve will be included in the first Nimbus III Monthly Catalog

Figure 7-3—Quantum Efficiency × Transmittance of Filters for 1600Å Sensor

Calibration curve will be included in the first Nimbus III Monthly Catalog

Figure 7-4–Quantum Efficiency × Transmittance of Filters for 1800Å Sensor

Calibration curve will be included in the first Nimbus III Monthly Catalog

Figure 7-5–Quantum Efficiency - Transmittance of Filters for 2000Å Sensor

Calibration curve will be included in the first Nimbus III Monthly Catalog

Figure 7-6—Quantum Efficiency × Transmittance of Filters for 2600Å Sensor

The instrument is housed in an electronics package and a sensor package, located in the rear of the Nimbus spacecraft. The field of view of the sensors is about 90° with the center of the field of view parallel to the spacecraft velocity vector. Solar acquisition will, therefore, begin at 45° prior to the earth day/night terminator and completely cease at the satellite day/night transition. Just prior to the day/night transition, the solar flux will be partially occulted by the earth's atmosphere.

The instrument has a basic 48 second cycle and a one sample per second data rate. Figure 7-7 shows the MUSE analog data output resulting from the internal commutation of the sync pattern, electrometer calibration, and sensor outputs.

A block diagram of the instrument is shown in Figure 7-8. The five radioactive current sources and the five ultraviolet sensors are sequentially switched into a four decade automatic range switching electrometer. The analog output, along with 3 bits of range information, is sampled once per second by the PCM system.

The input current to the electrometer may be calculated using the following equation and Table 7-2:

$$I = M(V_{tm} - V_0 + V_b) - I_0 \qquad (4)$$

Where I = electrometer input current

M = slope of calibration curve for a particular decade

V_{tm} = electrometer output voltage

V_0 = 0.20 volts = electrometer output voltage with no input current (zero check)

V_b = 5.40 volts, which is a level removed from the analog output when the range falls in the upper half of a decade

I_0 = offset current due to ionizing radiation (assumed to be negligible).

During the first 8 seconds of the MUSE 48 second cycle, the electrometer is preprogrammed to the least sensitive decade (not indicated with range bits) and an automatic zero servo is enabled. Should the electrometer output voltage (zero check) exceed 0.250 volts or fall below 0.150 volts the zero will be digitally adjusted in 0.050 volt increments to bring the zero within these limits. If the range of adjustment is no longer sufficient for zero correction, a redundant electrometer will be automatically switched into the circuit and automatically rezeroed.

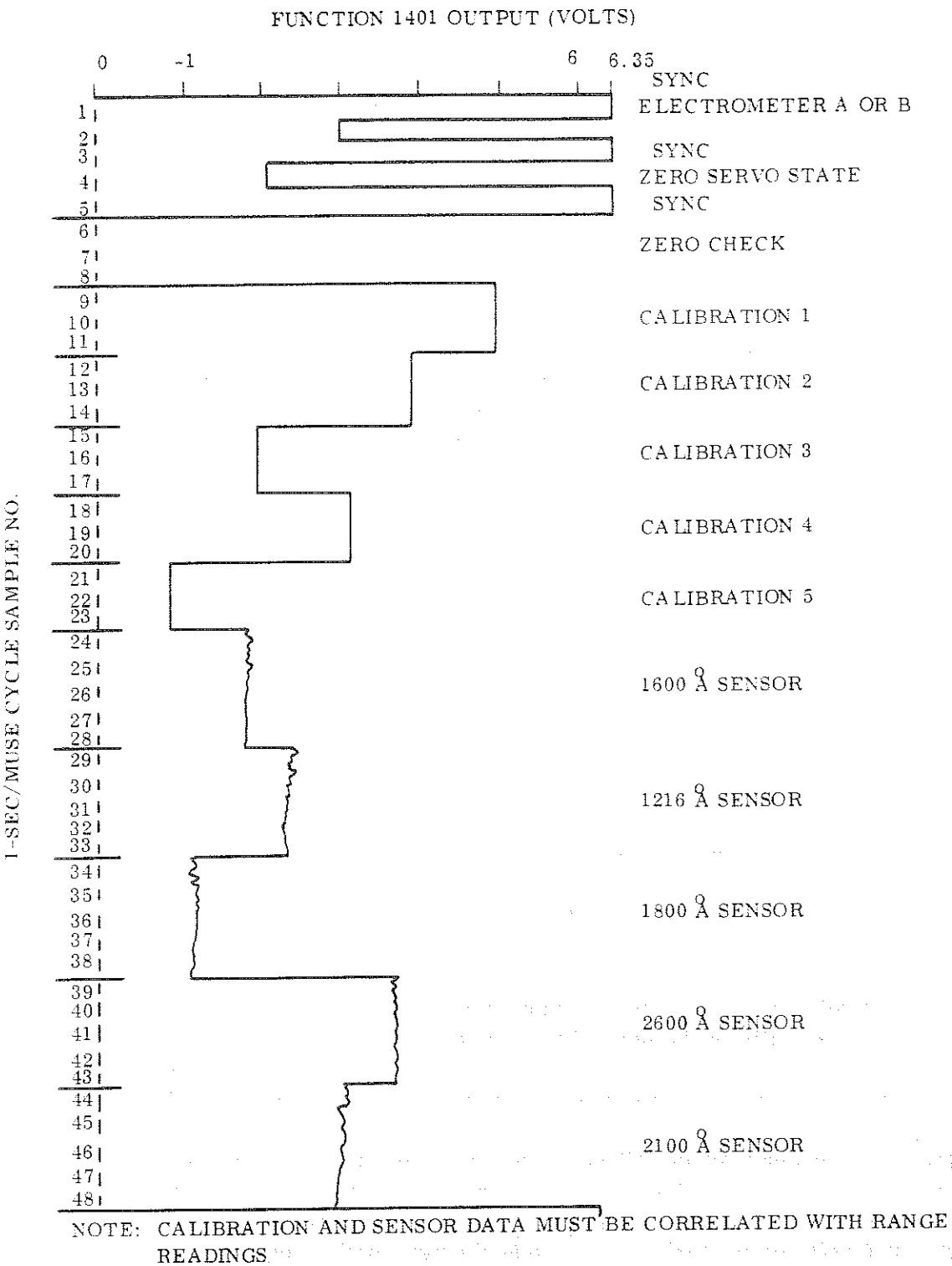

Figure 7-7–Analog Data Channel Output Voltage vs MUSE Cycle Sample Number

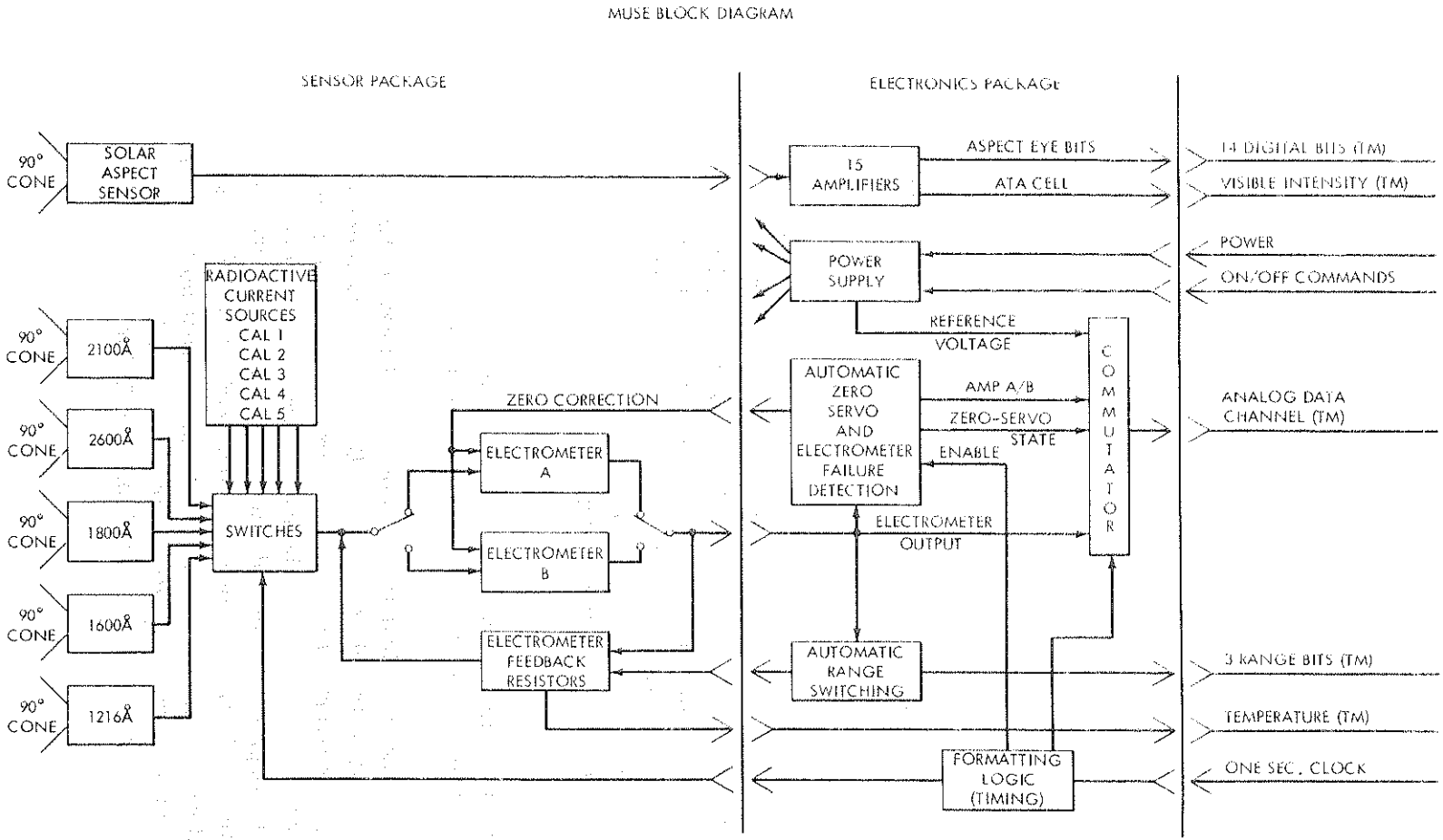

Figure 7-8–MUSE Block Diagram

Table 7-2
Conversion of Telemetry Voltage to Sensor Current

Range Bits	Vb (volts)	M (amps/volt)
This information will be included in a future Nimbus III Catalog		

The second sample of the 48 second cycle indicates which electrometer is in use. Electrometer A is represented by 5.90 ± 0.20 volts and electrometer B by 2.80 ± 0.15 volts.

The fourth sample of the 48 second cycle indicates the state of the zero servo. The zero servo corrects amplifier drift of the input MOS-FET's (Metal Oxide Field Effect Transistor) in 64 steps of 0.025 volts referred to the electrometer input. A step of 0.025 volts on the electrometer input will cause an 0.050 volt change in the electrometer output (verified by zero check). The zero servo state is indicated by a voltage of 0.10 to 6.3 volts in 64 levels corresponding to the 64 input levels available for adjustment. Initially, the zero servo is set at mid-range for launch (2.9 volts).

The sixth, seventh, and eighth samples of the cycle indicate the zero check. This value should be between 0.150 and 0.250 volts at all times.

The ninth sample through the 23rd sample contain calibration data for the gain settings of each decade of the electrometer. Because of the electrometer and current-source time constants, the first two samples of Cal. 1 do not indicate the final correct value and should not be used in gain corrections. The first sample of Cal. 2 through Cal. 5 should likewise be rejected. The statistically random variations in the calibration current are due to the low rate of alpha particle production within the Americium 241 constant current sources. It is, therefore, mandatory that one obtain a large number of samples and average them before attempting to correct the values of "M" found in Table 7-2.

The certified currents for these sources as of April 25, 1966 are as follows:

Table 7-3
Calibration Current Sources

Cal. 1	NM 7 - 7	3.97×10^{-11} amps.
Cal. 2	NN 1 - 7	2.99×10^{-10} amps.
Cal. 3	NM 9 - 4	5.93×10^{-10} amps.
Cal. 4	NM 5 - 4	1.97×10^{-9} amps.
Cal. 5	NN 4 - 5	1.04×10^{-8} amps.

The half life of AM-241 is about 475 years. The above currents should, therefore, be reduced (derated) by 0.003 for a measurement made in April 1969.

The electrometer decade resistors have a non-linear temperature coefficient. Since the temperature of the internal resistive element cannot be measured, no attempt will be made, at this time, to provide a temperature dependant gain correction factor.

The 24th through 48th samples indicate the sensor current outputs. Each sensor is switched into the electrometer for five seconds. The first and second samples of each sensor may be higher than the last three samples because of the electronics and sensory time constants. This will have to be determined by data inspection after launch. The sensors are commutated in the following order given in Table 7-4:

Table 7-4
Sensor Commutation

Samples 24 through 28	1600 Å Band
Samples 29 through 33	1216 Å Band
Samples 34 through 38	1800 Å Band
Samples 39 through 43	2600 Å Band
Samples 44 through 48	2600 Å Band

The MUSE instrument provides supporting measurements of the solar aspect angle, photodiode temperature and feedback resistor case temperature.

The solar aspect angle is measured using an Adcole Corporation solar aspect sensor. Essentially the aspect sensor measures two orthogonal angles between the sun and the normal vector of the MUSE optical axis. Assuming no spacecraft roll or pitch errors and assuming the MUSE optical axis coincides with the spacecraft velocity vector, the solar aspect pitch angle will indicate zero degrees at the

day/night terminator. The solar aspect yaw angle measured at the terminator will indicate the angle between the orbital plane and the high noon meridian. The quantization of these angles is 90/128 of a degree with an absolute accuracy of 50/128 of a degree. The aspect angle will be measured correctly only when the "ATA" voltage is below 6.35 volts. When this is the case, the data tapes will indicate "ATA" on.

The photodiode temperature (cathode temperature) is measured by a thermistor located in the 1800 Å sensor (middle sensor in Figure 1). The thermistor is fastened to the metal housing in the proximity of the photocathode surface of the photodiode.

The feedback resistor case temperature is measured by a thermistor embedded in the teflon block supporting the feedback resistors.

There are three anticipated sources of erroneous signal levels. These are:

1. Induced current resulting from ionizing radiation produced by the lower portion of the Van Allen belts, particularly near the poles.
2. Ultraviolet flux from the earth's albedo entering the field of view of the sensors.
3. Contamination of sensor surfaces during the launch process.

The level of induced current due to radiation produced by the Van Allen belts should not exceed 10^{-11} amperes or 10% of the most sensitive electrometer decade. In any event, a radiation field strength global pattern may be derived for correction purposes by observing sensor outputs while in darkness.

The contribution of the earth's albedo to the total ultraviolet flux is expected to be quite low. The extent of the albedo, if any, may be extrapolated by inspection of the curves of sensor outputs as a function of solar angle of incidence.

The contamination of sensor surfaces may be inferred if discrepancies arise between these data and those of a previously launched rocket carrying the same MUSE instrument. Should there be a reasonable discrepancy after the launch of Nimbus III as to possible contamination due to foreign material or radiation damage, a second MUSE instrument could be rocket launched for simultaneous measurements.

7.4 Format of the MUSE Archival Tape

The MUSE archival tape will be the basic repository for radiation data from the Nimbus Monitor of Ultraviolet Solar Energy (MUSE) experiment. This tape will be generated on the IBM 360 System with seven track recording in binary mode at 800 bytes per inch, and will be available to the scientific community through NSSDC within one year after launch. The format of the NMRT-MUSE is detailed in Tables 7-5 and 7-6.

The NMRT-MUSE will contain multiple files with each file representing one readout orbit of MUSE data. The End of File Mark will be recorded at the end of each playback orbit, and will be repeated at least twice following the last readout orbit on any reel of tape.

Each record in a file will consist of 360-32 bit words, 320-36 bit words, or 192-60 bit words. The first record of each file will contain a documentation and history summary for that orbit (Table 7-5), and all remaining records in a file will contain MUSE data (Table 7-6). All unused words in a record will contain binary zeroes.

Ninety degrees are added to all latitudes to eliminate negative signs. Final formats of any computer printouts obtainable from the archival tapes cannot be defined at present, and will be included in a future Nimbus III data catalog.

Table 7-5
Documentation and History Record of the MUSE Archival Tape

Word #	Quantity	Units	Scaling	Remarks
1	Satellite I.D.	–	Fx. Pt.	Nimbus III = 3
2	Orbit Number	–	Fx. Pt.	Readout orbit number
3	Day	Days	Fx. Pt.	Starting time for data in this file
4	Seconds	Z Seconds	Fx. Pt.	
5	Day	Days	Fx. Pt.	Ending time for data in this file
6	Seconds	Z Seconds	Fx. Pt.	
7	Day	Day	Fx. Pt.	Time of the terminator as measured in NTCC from PCM system
8	Seconds	Z Seconds	Fx. Pt.	
9	Day	Day	Fx. Pt.	Time of the terminator determined by theoretical calculations
10	Seconds	Z Seconds	Fx. Pt.	
11	Latitude	Degrees	Fl. Pt.	Latitude and longitude of terminator at time specified in words 9 & 10
12	Longitude	Degrees	Fl. Pt.	
13	Day	Day	Fx. Pt.	Time of ascending node for this orbit
14	Seconds	Z Seconds	Fx. Pt.	
15	Longitude	Degrees	Fl. Pt.	Longitude of ascending node for this orbit
16	GHAA	Degrees	Fl. Pt.	Greenwich hour angle of Aries at time specified in words 13 and 14
17	Right Ascension	Degrees	Fl. Pt.	Right ascension of sun at time specified in words 9 and 10
18	Declination	Degrees	Fl. Pt.	Declination of sun at time specified in words 9 and 10
19	MUSE	–	EBCDIC	"MUSE"
20	Initial Status of MUSE Subsystem	–	EBCDIC	Initial status of MUSE subsystem reported by NTCC ("OFF", "ON", "UNK")
21	Initial Status of ATA	–	EBCDIC	Initial status of ATA reported by NTCC ("OFF", "ON", "UNK")

Table 7-5
Documentation and History Record (Continued)

Word #	Quantity	Units	Scaling	Remarks
22	Initial Status of MUEL (Muse Electrometer Transistor)	–	EBCDIC	Initial status of MUEL reported by NTCC ("OFF", "A", "B")
23	Initial status of TERM (Terminator)	–	EBCDIC	Initial status of TERM reported by NTCC ("DAY", "NIT")
24	Initial Status of SAT (Satellite)	–	EBCDIC	Initial status of SAT reported by NTCC ("DAY", "NIT")
25	Initial Status of EAR (Earth)	–	EBCDIC	Initial status of EAR reported by NTCC ("DAY", "NIT", "IND")
26	Final status of MUSE	–	EBCDIC	Final status of MUSE reported by NTCC
27	Final status of ATA	–	EBCDIC	Final status of ATA reported by NTCC
28	Final status of MUEL	–	EBCDIC	Final status of MUEL reported by NTCC
29	Final status of TERM	–	EBCDIC	Final status of TERM reported by NTCC
30	Final status of SAT	–	EBCDIC	Final status of SAT reported by NTCC
31	Final status of EAR	–	EBCDIC	Final status of EAR reported by NTCC
32	Seconds	Z seconds	Fx. Pt.	Changes in status are described by the seconds of day, major frame number, event number (MUSE = 1, ATA = 2, MUEL = 3, TERM = 4, SAT = 5, EAR = 6) and new status of the event that changed
33	Major Frame No.	–	Fx. Pt.	
34	Event Number	–	Fx. Pt.	
35	Status Change	–	EBCDIC	

Table 7-5
Documentation and History Record (Continued)

Word #	Quantity	Units	Scaling	Remarks
36-111	–	–	–	Words 32-35 repeated 19 times to cover the first 20 event changes. In the case of less than 20 event changes, unused areas will contain binary zeroes
112	Number data cycles	–	Fx. Pt.	The number of data cycles counted by NTCC for this orbit
113	Normal data cycles	–	Fx. Pt.	The number of normal data cycles reported by NTCC for this orbit.
114	Bad Data Cycles	–	Fx. Pt.	The number of bad data cycles reported by NTCC for this orbit
115-124	Major Frame No.	–	Fx. Pt.	Major frame number reported by NTCC for ten bad data cycles
125-134	Cycle Number	–	Fx. Pt.	Cycle number reported by NTCC for the ten bad data cycles reported in words 115-124
135-144	Seconds	Seconds	Fx. Pt.	Seconds of day reported by NTCC for the ten bad data cycles reported in words 115-124
145-154	Type of Bad Cycle	–	EBCDIC	Type of bad data cycle reported by NTCC for the ten bad data cycles reported in words 115-124. (Normal = "NOR", Long = "LON", Short = "SHR")

Table 7-5
Documentation and History Record (Continued)

Word #	Quantity	Units	Scaling	Remarks
155-164	Seconds	–	Fx. Pt.	Length of bad data cycle in seconds reported by NTCC for the ten bad data cycles reported in words 115-124
165	Number of Samples	–	Fx. Pt.	
166	Std. Deviation	–	Fl. Pt.	Statistics for cathode temperature as reported by NTCC
167	Average Value	Deg. C	Fl. Pt.	
168	Minimum Value	Deg. C	Fl. Pt.	
169	Maximum Value	Deg. C	Fl. Pt.	
170-174	Statistics	–	–	Repeat of words 165-169 with statistics for feedback resistance temperature as reported by NTCC (Degrees C)
175-179	Statistics	–	–	Repeat of words 165-169 with statistics for Horizontal Solar Aspect as reported by NTCC (Degrees)
180-184	Statistics	–	–	Repeat of words 165-169 with statistics for Vertical Solar Aspect as reported by NTCC (Degrees)
185-189	Statistics	–	–	Repeat of words 165-169 with statistics for Zero Check as reported by NTCC (volts)
190-194	Statistics	–	–	Repeat of words 165-169 with statistics for Auto Servo as reported by NTCC (volts)

Table 7-5
Documentation and History Record (Continued)

Word #	Quantity	Units	Scaling	Remarks
195-199	Statistics	–	–	Repeat of words 165-169 with statistics for Calibration One as reported by NTCC (Amperes)
200-204	Statistics	–	–	Repeat of words 165-169 with statistics for Calibration Two as reported by NTCC (Amperes)
205-209	Statistics	–	–	Repeat of words 165-169 with statistics for Calibration Three as reported by NTCC (Amperes)
210-214	Statistics	–	–	Repeat of words 165-169 with statistics for Calibration Four as reported by NTCC (Amperes)
215-219	Statistics	–	–	Repeat of words 165-169 with statistics for Calibration Five as reported by NTCC (Amperes)
220-226	Histogram	–	Fx. Pt.	Frequency histogram of Zero Check for the following sequential intervals: 0-.05, .05-.10, .10-.15, .15-.20, .20-.25, .25-.30, greater than 0.30. These data include 3 samples per cycle as reported by NTCC
227	Major Frame Number	–	Fx. Pt.	Major frame number for day/night terminator as determined by NTCC

Table 7-5
Documentation and History Record (Continued)

Word #	Quantity	Units	Scaling	Remarks
228	Seconds	Seconds	Fx. Pt.	Start time of normal cycle nearest the day/night terminator as reported by NTCC. Day is specified in Word 7.
229	Cathode	Degrees C	Fl. Pt.	Cathode temperature at day/night terminator as reported by NTCC
230	Vertical Solar Aspect	Degrees	Fl. Pt.	Vertical Solar Aspect at day/night terminator as reported by NTCC
231	Horizontal Solar Aspect	Degrees	Fl. Pt.	Horizontal Solar Aspect at day/night terminator as reported by NTCC
232	Feedback Resistor Temperature	Degrees C	Fl. Pt.	Feedback Resistor Temperature at day/night terminator as reported by NTCC
233	Third Response	Amperes	Fl. Pt.	Third, fourth, fifth, and average measurements from 1600Å sensor at day/night terminator as reported by NTCC
234	Fourth Response	Amperes	Fl. Pt.	
235	Fifth Response	Amperes	Fl. Pt.	
236	Avg. Response	Amperes	Fl. Pt.	
237-240	Sensor Response	–	Fl. Pt.	Repeat of words 233-236 for 1216Å sensor as reported by NTCC
241-244	Sensor Response	–	Fl. Pt.	Repeat of words 233-236 for 1800Å sensor as reported by NTCC
245-248	Sensor Response	–	Fl. Pt.	Repeat of words 233-236 for 2600Å sensor as reported by NTCC
249-252	Sensor Response	–	Fl. Pt.	Repeat of words 233-236 for 2100Å sensor as reported by NTCC

Table 7-5
Documentation and History Record (Continued)

Word #	Quantity	Units	Scaling	Remarks
253	Number of Calibration Segments Averaged	–	Fx. Pt.	Number of ten minute calibration segments averaged by NTCC. (Maximum = 10)
254	Frame Number	–	Fx. Pt.	Starting frame number for first segment of calibration data averaged by NTCC
255	Frame Number	–	Fx. Pt.	Ending frame number for first segment of calibration data averaged by NTCC
256-273	Frame Number	–	Fx. Pt.	Repeat of words 254-255 for second thru tenth segment of calibration data averaged by NTCC
274-283	Calibration I	Amperes	Fl. Pt.	Average values of calibration one for segments 1-10 processed by NTCC
284-293	Calibration II	Amperes	Fl. Pt.	Average values of calibration two for segments 1-10 processed by NTCC
294-303	Calibration III	Amperes	Fl. Pt.	Average values of calibration Three for segments 1-10 processed by NTCC
304-313	Calibration IV	Amperes	Fl. Pt.	Average values of calibration Four for segments 1-10 processed by NTCC
314-323	Calibration V	Amperes	Fl. Pt.	Average values of calibration Five for segments 1-10 processed by NTCC
324-360	–	–	–	Spare locations

Table 7-6
Data Record Format of the MUSE Archival Tape

Word #	Quantity	Units	Scaling	Remarks
1	Day	–	Fx. Pt.	Day at beginning of MUSE cycles
2	Seconds	Seconds	Fx. Pt.	Seconds of day at beginning of MUSE cycle as determined by NTCC
3	Cycle Number	–	Fx. Pt.	MUSE Cycle number for this record as determined by NTCC
4	Minor Frame No.	–	Fx. Pt.	Minor frame number at start of cycle as reported by NTCC
5	Major Frame No.	–	Fx. Pt.	Major frame number at start of cycle as reported by NTCC
6	Cycle Length	Seconds	Fx. Pt.	Length in seconds of this cycle as determined by NTCC
7	Status	–	–	The rightmost 18 bits of this word contain the six events for the MUSE subsystem with each octal position from left to right representing MUSE, ATA, MUEL, TERM, SAT, EAR. The values assigned to each octal position are the following: 0 = OFF, 1 = ON, 2 = A, or DAY, 3 = B or NIT, 4 = unused, 5 = unused, 6 = IND, 7 = UNK
8	Cathode Temperature	Degrees C	Fl. Pt.	Cathode temperature for this MUSE cycle (Average)

Table 7-6
Data Record Format (Continued)

Word #	Quantity	Units	Scaling	Remarks
9	Feedback Resistor Temperature	Degrees C	Fl. Pt.	Feedback resistor temperature for this MUSE cycle (Average)
10-12	ATA	Tel. Volts	Fl. Pt.	ATA value for this MUSE cycle (Three values)
13	MUSE power	–	Fx. Pt.	MUSE power status for this cycle (1 = ON, 0 = OFF) as reported by NTCC
14	Day/Night/ Twilight	–	Fx. Pt.	Day/Night/Twilight Code at time given in words 1 and 2 0 = DAY 1 = TWILIGHT 2 = NIGHT
15	Latitude	Degrees	Fl. Pt.	Latitude of subsatellite point at beginning of cycle (time specified in words 1 & 2) Ninety degrees added to eliminate negative sign
16	Longitude	Degrees	Fl. Pt.	Longitude (0-360 West) of subsatellite point at beginning of cycle (time specified in words 1 & 2)
17	Height	Kilometers	Fl. Pt.	Height of satellite at beginning of cycle (time specified in words 1 & 2)
18	Latitude	Degrees	Fl. Pt.	Latitude of subsatellite point at end of cycle. (time specified in words 1 & 2 plus 48 seconds). Ninety degrees added to eliminate negative signs.

Table 7-6
Data Record Format (Continued)

Word #	Quantity	Units	Scaling	Remarks
19	Longitude	Degrees	Fl. Pt.	Longitude (0-360 West) of subsatellite point at end of cycle (time specified in words 1 & 2 plus 48 seconds)
20	Height	Kilometers	Fl. Pt.	Height of satellite at end of cycle (time specified in words 1 & 2 plus 48 seconds)
21	Right Ascension	Degrees	Fl. Pt.	Right ascension of sun at beginning of cycle (time specified in words 1 & 2)
22	Declination	Degrees	Fl. Pt.	Declination of sun at beginning of cycle (time specified in words 1 & 2). Ninety degrees added to eliminate negative signs.
23	GHAA	Degrees	Fl. Pt.	Greenwich hour angle of Aries at time specified in words 1 & 2
24-71	Horizontal Solar Aspect Segment No.	(0-127)	Fx. Pt.	Horizontal Solar Aspect. One word for each second of MUSE cycle
72-119	Vertical Solar Aspect Segment No.	(0-127)	Fx. Pt.	Vertical Solar Aspect. One word for each second of MUSE cycle.
120-167	Horizontal Solar Aspect (ALPHA)	Degrees	Fl. Pt.	Horizontal Solar Aspect expressed as angle ALPHA and calculated by NTCC. One word for each second of MUSE cycle.

Table 7-6
Data Record Format (Continued)

Word #	Quantity	Units	Scaling	Remarks
168-215	Vertical Solar Aspect (BETA)	Degrees	Fl. Pt.	Vertical Solar Aspect expressed as angle BETA and calculated by NTCC. One word for each second of MUSE cycle.
216-235	Range Setting	(0-7)	Fx. Pt.	Forty half-words of range setting bits corresponding to last forty seconds of MUSE cycle.
236-283	Raw Data	Tel. Volts	Fl. Pt.	Raw data for this MUSE cycle. One data word for each second in cycle.
284-323	Calibrated Data	Amps	Fl. Pt.	Forty measurements corresponding to the last forty seconds of cycle. Telemetry volts are converted to Amps
324-348	Calibrated Data	Quanta cm^{-2} sec^{-1}	Fl. Pt.	Twenty five measurements corresponding to the last 25 seconds of cycle. Response from five sensors calibrated in Quanta cm^{-2} sec^{-1}
349-360	Spare	–	–	Spare locations

REFERENCES

1. S. I. Rasool, "Effects of Assumed Changes in the Near Ultraviolet Radiation on the Photochemical Distribution of Atmospheric Ozone and on Heating Rates in the Stratosphere," XII General Assembly of IUGG, August 19-31, 1963.

2. E. D. Schultz and A. C. Holland, "The Solar Flux Incident at the Top of the Atmospheres of Earth and Neighboring Planets for the Spectral Region 50Å to 3000Å," GCA Technical Report 62-14-N, GCA, Bedford, Mass.

3. D. F. Heath and P. A. Sacher, "Effects of a Simulated High Energy Electron Space Environment on the Ultraviolet Transmittance of Optical Materials Between 1050 and 3000Å," Applied Optics, 5, 937 (1966).

4. P. A. Sacher, "The Effects of a Simulated Proton Space Environment on the Ultraviolet Transmittance of Optical Materials Between 3000Å and 1050Å," NASA, X-622-G7-416, August 1967.

5. D. F. Heath and J. H. McElaney, "Effects of a High Energy Particle Environment on the Quantum Efficiency of Spectrally Selective Photocathodes for the Middle and Vacuum Ultraviolet," Applied Optics, 7, 2049 (1968).

SECTION 8

THE INTERROGATION, RECORDING AND LOCATION SYSTEM (IRLS) EXPERIMENT

by
Charles E. Cote
National Aeronautics and Space Administration
Goddard Space Flight Center

8.1 IRLS General Description

8.1.1 IRLS System Objectives

The IRLS (Interrogation, Recording, and Location System) is designed to collect geophysical, meteorological and other experimental data from remote unmanned data collection stations (platforms), to determine the location of the platforms and track mobile platforms such as on balloons, buoys, and ships. Figure 8-1 shows the IRLS concept.

Objectives of IRLS are:

1. To provide a radio relay and location system for remote platforms.
2. To prove feasibility of selective interrogations of a remote platform from a satellite and receipt of an automatic response.
3. To obtain data collection from platforms on a global scale.
4. To determine system accuracy of platform location on a global scale for both fixed and moving platforms.
5. To determine system performance in resolving platform location.
6. To demonstrate the dissemination of the data collected and the locations determined within an orbital period.

8.1.2 System Description

The elements making up the IRLS system are a set of remote platforms, a satellite, and a ground station. The platforms accept analog data from various sensors, convert the measurements to digital form, and transmit

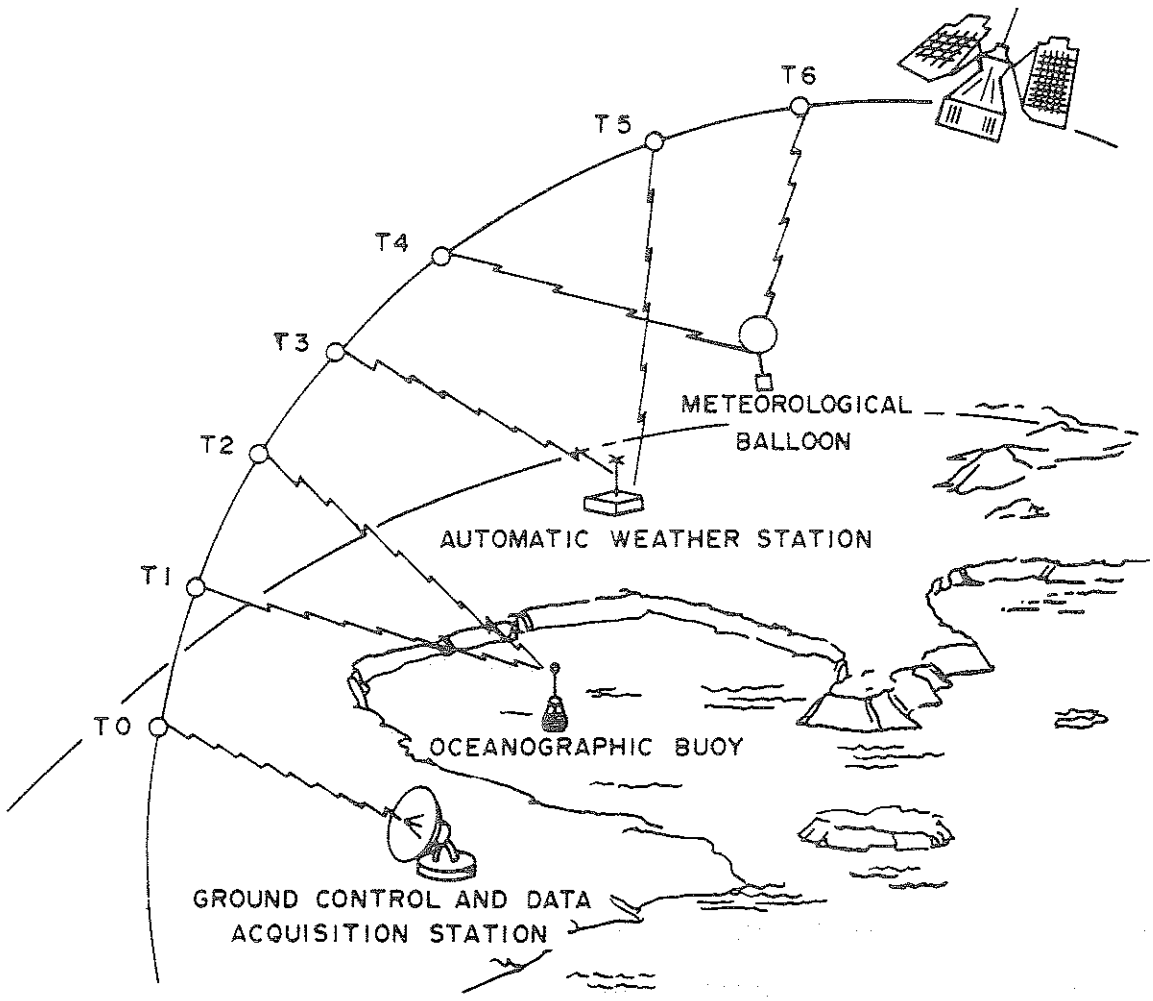

Figure 8-1–Interrogation, Recording and Location System

these data to the satellite via a PCM communication link. On each orbital pass, when in the vicinity of an IRLS ground station (located at ALASKA and GSFC), the satellite command memory is programmed by the IRLS Ground Acquisition and Command Station (GACS) to communicate with selected platforms during the coming orbit. The satellite stores both the address (number) of each platform and the desired time each should be contacted. At the designated times in orbit, the satellite interrogates each platform, measures the satellite-to-platform distance by determining the propagation time of the RF signal, and receives and stores the platform data. Upon return to the locale of the ground stations, the station commands the satellite to transmit all stored data and to accept new commands for use during the next orbit.

The system uses a coded digital message for transmission of all data, for timing synchronization between satellite and platforms or ground station, and for measurement of satellite-to-platform range.

The system employs a 20,000 bit satellite data memory capable of storing data measurements during each orbit for up to 20 different interrogations stored in the command memory. Two interrogations are required per platform if a location computation is to be made. The range measurements between satellite and platform are made to an accuracy of ±500 meters.

With a knowledge of satellite orbit parameters and past platform locations, two such range measurements are sufficient to establish the position of a moving platform, such as a buoy or balloon.

The analog sensor data are converted by the platform electronics into a digital format. In transmitting data to and from the IRLS subsystem via the IRLS RF link, all bits of data are treated as twelve minor bits in a manner that provides noise protection in communication and the sensitivity to perform an accurate range determination.

Major characteristics of the IRLS system are tabulated below:

Data Capacity:	2044 scientific data measurements (Channels), 20 range measurements, 20 time measurements.
Range Measurement Accuracy:	±500 meters (±0.27 nautical miles)
Accuracy of Data:	1% maximum error, 0.2% linearity and repeatability, 0.8% resolution.
Number of Interrogations:	20 Maximum
Data Measurements per Platform:	168 Maximum (28 per frame, 1 to 6 frames per platform)
Available Orbit Time for Data Collection:	3.64 hours maximum (can be extended for blind orbits).
Data Transfer Time:	Platform to Satellite - 4 frames per second Satellite to Ground - 30 second maximum for completed data dump and new command entry. (1.041 Kilobits/second major bit rate) (12.5 Kilobits/ second minor bit rate)

8.2 Platform Elements

The remote data stations from which the IRLS spacecraft equipment collects its data consist of three main elements: the sensor, the platform electronics, and the antenna.

8.2.1 Sensor

The source of the data collected from the individual platform is a sensor provided by the individual platform experimenter. The output of the sensor is generally an analogue voltage although the platforms are also equipped to handle digital inputs.

8.2.2 Platform Electronics

The platform consists of the data conditioning equipment, the synchronizing equipment and the communication equipment including the transmitter and receiver. A standard "all weather" platform has been designed as part of the IRLS program.

The data inputs are quantized into 7 bit digital words. On the 9 technological evaluation platforms, 6 out of the 28 data words placed into each frame are reserved for platform housekeeping telemetry utilized in the technical evaluation of the platform performance under extreme enviromental conditions.

They are:

data word	1	transmitter power amplifier temperature
	2	transmitter plate current
	3	receiver module temperature
	4	data and range module temperature
	5	data and range module 3.4v logic level
	6	power control and dist. module 24v input level

The transmitter in the platform radiates 25 watts at 466.0 MHz. The receiver operates at 401.5 MHz.

8.2.3 Antennas

There are two types of antennas developed for the IRLS application, each having about 6db peak gain. The general purpose antenna is a loop vee type having a bifolium pattern. This overhead has reduced gain for arc pass but has improved performance at lower elevation angles at which interrogations are generally contemplated. The other antenna is a cavity-backed spiral with a cardioid pattern. It has higher gain overhead than at the lower angles but has the advantage of not having its pattern affected by the bobbing action of ocean activity and therefore is more suitable for buoy applications than the loop vee.

8.3 Interrogation of Nimbus from IRLS Ground Acquisition and Command Stations and Unloading Data

The Nimbus satellite is interrogated each orbital pass over the Alaska and Rosman Data Acquisition facility (DAF) stations. The DAF stations transmit a command through the normal spacecraft command system to place the IRLS system on the satellite in a readout mode allowing data readout to be initiated. The data output from the satellite is shown in Figure 8-2 for one frame of platform data when the IRLS to GACS RF communication line is established. This is composed of a barker code for synchronization, the address complement of the platform, 28 data words of seven major bits each, two words containing ranging vernier time, plus parity and range data information. Data transfer is accomplished at 1041 bits per second until the entire contents of the 20,000 bit data memory have been transmitted. The memory content is destroyed after each data readout cycle.

Following the receipt of the spacecraft data, the IRLS GACS Station transmits twenty 31 bit command words which the satellite loads into the IRLS command memory. Each command word contains a platform address and a time of interrogation. This entire cycle of data dump and command load takes less than 35 seconds.

8.4 Interrogation of Platform

The 31 bit command word is composed of a 16 bit platform address and a 15 bit time code. The time code is a count of .4 second units that establishes when the platform is to be interrogated. The time code count is continuously being compared to a counter driven by the Nimbus spacecraft clock 10 cps reference frequency. The counter is reset to zero at the beginning of the command load cycle. When count coincidence occurs, the interrogation cycle

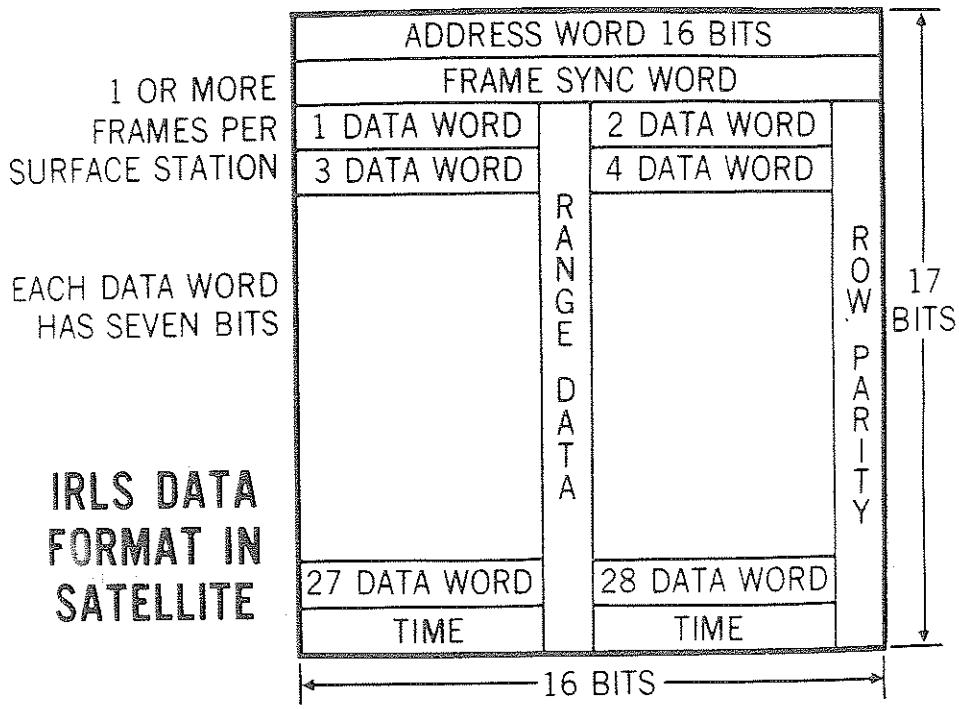

Figure 8-2–Data Output from the Satellite to DAF for One Frame of Platform Data

is initiated by continuously transmitting the platform address portion of the command word and placing the data memory into the write mode. Receipt of this address by the platform causes it to continuously transmit its own address to the satellite. After the address is received by the spacecraft, the complement of the address is transmitted by the spacecraft for the duration of the interrogation. A timer in the IRLS spacecraft equipment limits each platform interrogation to 3 seconds. At the end of the 3 second interval, the transmitter is turned off, the data memory is placed in a static mode and if the command was not the 20th, the next command is placed in the command register. After the 20th command, the command memory is empty and goes into a static mode.

8.5 Receipt of Platform Data and Ranging

When the platform receives its address complement, it transmits its address complement twice followed by a 28 word frame followed by its address complement. Up to six frames of data may be transmitted.

At the satellite, the platform address complement is decoded, the data memory placed in the write mode, and data, range and barker code

(synchronization) are written into the data memory. At completion of transmission, the data memory is returned to static condition.

The ranging vernier time (line 17 of Figure 8-2) are units of time used to accurately establish the time when ranging function was actually performed. Ranging is accomplished by measuring time between transmission and reception of the signal. The ranging word is the eighth column of the frame. See Figure 8-2.

Geometry of the ranging measurement is shown in Figure 8-3. If a measurement is made from the satellite at time T_1, the propagation time may be converted to a radial distance R_1. As the height of the satellite is known above point 1 on the earth's surface (dashed line), this signal measurement would essentially indicate that the platform is somewhere on the circumference of a circle of radius r_1. A similar measurement at time T_2 would indicate location on the circumference of a circle of radius r_2. Knowing the locations of the two subsatellite points from the spacecraft Ephemeris and the time of interrogation, the location of the platform is found by determining the intersection of the two circumferences. Two solutions are obtained by this procedure: a correct one and a mirror image on the opposite side of the subsatellite track. Utilizing either the knowledge of the previous general location or when data are available from two successive satellite passes, the unique location can be determined. To optimize the calculations, the interrogations are scheduled for the included angle between R_1 and R_2 to be approximately 90°. For nominal spacecraft orbit, this varies from 2 to 4 minutes, depending on the platform offset from the satellite sub-point track.

8.6 IRLS Platforms

The platforms of the IRLS experiment are classified into two main groups; a fixed number of platforms utilized for the technological evaluation of the experiment, and other platforms utilized by co-operating government agencies and non-profit organizations to evaluate the usefulness of IRLS in their scientific programs. The technological evaluation group is further subdivided into the Integration Support Equipment (ISE) platforms which are under direct NASA Goddard supervision and the Field Test platforms which are installed and maintained by supporting organizations at a variety of global locations. All participants provide their own sensors for obtaining the data to be collected. All IRLS platform addresses are assigned by the National Aeronautics and Space Administration.

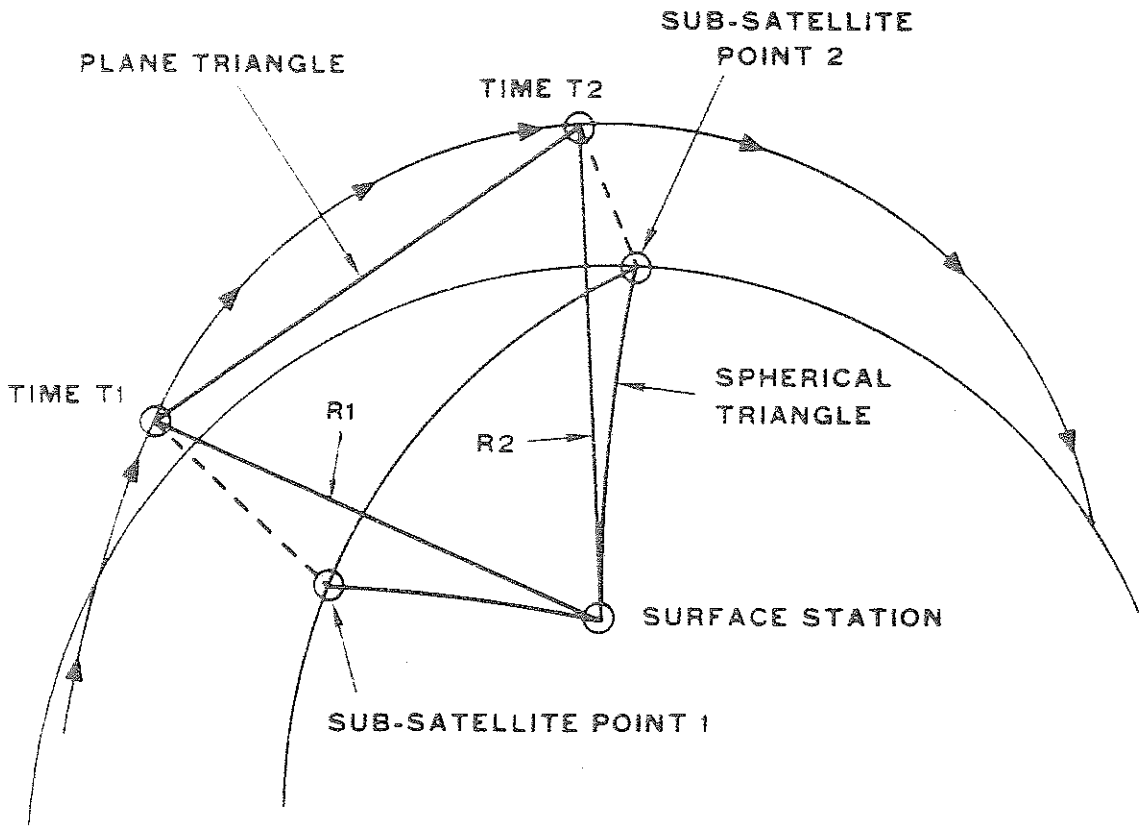

Figure 8-3–Platform Positioning Geometry

8.6.1 Technological Evaluation Platforms

These platforms are supplied to the installing organizations by the IRLS project office.

8.6.1.1 Integration Support Equipment Platforms

Two of these platforms are precisely located at Goddard Space Flight Center. Data transmitted to the spacecraft consist of: a) Calibrated reference voltages and b) typical sensory measurements such as temperature and/or pressure.

These platforms are used to evaluate system parameters over the expected lifetime of the satellite and to determine the accuracy of the platform location techniques and the data coding and transmission system.

A third ISE platform is installed in the NASA/GSFC van for use at the Western Test Range in the prelaunch countdown. After launch it will be utilized in a vehicle tracking experiment as it returns to G.E., Valley Forge, Pa.

8.6.1.2 Air er Service Platform

This platform is installed in an AWS weather reconnaissance aircraft. The AWS uses the international weather code for data inputs consisting of location, time, air temperature, pressure, cloud information, turbulence, wind direction, etc.

The purpose of the AWS participation is to demonstrate the technological capability (interfacing of AWS aircraft with meteorological and communication satellites) for future routine collection and rapid dissemination of perishable meteorological operational data to appropriate world weather centers. The demonstration and evaluation of the IRLS positioning capability is also an object of the AWS participation.

8.6.1.3 National Center for Atmospheric Research Platforms

Two platforms are installed on NCAR balloons. Data gathered by the platforms are air temperature, ambient pressure, IRLS package temperature, battery temperature and voltage.

The purpose of NCAR's participation in the NIMBUS IRLS experiment is to demonstrate and evaluate the IRLS positioning capability and the capability to relay meteorological data from a balloon to the ground via a satellite. Integration of the balloon position over a period of days will provide a new technique in the measurement of upper atmospheric wind velocities. Both these capabilities will be compared with other techniques i.e., positioning - photography and radar; data relay - via telemetry system.

8.6.1.4 National Science Foundation Platform

The platform is located on the U.S.N.S. Eltanin cruising in the Antarctic region.

The following data will be input manually by an ESSA meteorologist aboard the U.S.N.S. Eltanin:

1. time and position of the ship as determined by TRANSIT
2. cloud cover at 0000 and 1200 GMT
3. position of ship for 0000 and 1200 GMT weather report
4. surface report - wind direction and velocity, air temperature, pressure, and sea surface temperature at 0000 and 1200 GMT
5. air temperature, wind direction and velocity and height at 1000, 850, 700, 500, 300, 200, 100 and 50 mb.
6. tropopause pressure, air temperature, wind direction and velocity.

The purpose is to demonstrate the capability of relaying weather data from the ship to the Weather Bureau in 2 to 3 hours instead of the usual 2 to 3 days. Speedy delivery of these perishable data will make them useable in weather charts.

8.6.1.5 Office of Naval Research, Naval Oceanographic Office and Naval Research Laboratory Platform.

The platform is located on the floating ice island, T_3, in the Arctic region.

Data will consist initially of reference voltages to enable Navoceano and NRL to verify the accuracy of the IRLS data transmission system. These data will be replaced within a short time (a week) by data obtained for Lamont Geological Observatory on fracturing of the sea ice as a function of environmental factors. These will include a count of the number of events detected by a seismometer (separated onto 5 energy bands), water velocity (direction) and temperature in the air above the ice at two different depths in the ice. Position of the IRLS installation as determined by TRANSIT and the time of position determination will also be inputted to the IRLS data channels.

The objective of ONR's participation in the IRLS experiment is to enable Navoceano-NRL to evaluate the position determination capability of IRLS and to demonstrate the capability of IRLS to transmit seismometer data from the arctic region to the U.S. in 2 to 3 hours instead of the usual weeks or months.

8.6.1.6 U.S. Naval Oceanographic Office Platform

This platform is on a moored buoy off the coast of Puerto Rico. The following data are collected:

1. direction of buoy inclination
2. degree of buoy inclination
3. wave height
4. surface current speed
5. sub surface buoy depth
6. battery voltage
7. sub surface buoy leak detection
8. surface cable rupture
9. surface buoy leak detection.

The objective of Navoceano's participation is to evaluate the position determination capability of IRLS for future application to drifting buoys and to evaluate the data transmission capability of IRLS as influenced by the buoy's environmental characteristics.

8.6.2 Co-operative Scientific Experimenter Platforms

These platforms are supplied by the participating scientific experimenters.

8.6.2.1 U.S. Naval Oceanographic Office Platform

The platform is located on Argus Island (a Texas Tower) near Bermuda.

This platform sends five frames of data.

1. inputs one thru 112 will consist of binary numbers 001 thru 112.
2. wave height
3. surface temperature
4. current meter (water velocity)
5. sub surface temperature
6. remaining channel inputs of the fifth frame are calibrated reference voltages.

The purpose of this platform is to enable Navoceano to evaluate the capability and reliability of the IRLS data transmission system. Since the location of the platform is fixed, the positioning feature of IRLS is of secondary importance.

8.6.2.2 Woods Hole Oceanographic Institution Platforms

One or two platforms are located in the Gulf Stream off Cape Hatteras and one on Georges Bank (off Cape Cod).

Data Content on all platforms:

1. temperature at 300 meters
2. temperature at 150 meters
3. temperature at surface
4. temperature of air above the surface.

The purpose of the platforms in the Gulf Stream is to determine the location and characteristics of eddies. The purpose of platform on George's Bank is to determine the characteristics of current flow. The use of the positioning feature of IRLS is of primary importance to the Woods Hole Oceanographic Institute.

8.6.2.3 Bureau of Commercial Fisheries Platform

Platform is on a drifting buoy in the North Pacific south of Alaska.

Data Contents:

1. temperature of the water at the surface
2. temperature of the water at a depth of 50 meters
3. pressure at a depth of 50 meters
4. salinity of sea water at depth of 2 meters.

The primary purpose of the Bureau of Commercial Fisheries' participation in the IRLS program is in the utilization of the positioning feature of IRLS in order to determine current flow (rate and direction) in the North Pacific. The secondary purpose of this experiment will be to utilize the data received from the platform in a scientific program.

8.6.2.4 Naval Air Systems Command Platforms

Two platforms are used in conjunction with Air-Sea Rescue beacons.

Only one channel is used to indicate the presence or absence of signal on an Air-Sea Rescue receiver from an Air-Sea Rescue beacon.

The purpose of the Naval Air System Command's participation is to demonstrate the use of a satellite system (IRLS) in the Air-Sea Rescue Program.

3.7 Data Dissemination, Archiving and Access

The IRLS Ground Acquisition and Command Station transmits the IRLS data collected from the spacecraft to a CDC 924 computer in the Nimbus Data Handling Facility at GSFC. The CDC 924 computer performs the location calculations for the various platforms, and separates the data for the individual platform experimenters on printed computer outputs. The computer outputs will be mailed to the IRLS platform experimenters, and copies will be retained in the Nimbus/ATS Data Utilization Center, NASA, Goddard. During a special test period the output data will also be punched on paper tape in teletype format for dissemination to the experimenters within the orbital time period.

The computer printouts will show platform location at given times. Any geophysical data collected will be expressed in voltages. Calibration charts and tables necessary to translate these voltage measurements into corresponding measurements of temperature, wind velocity, etc., are available through the individual platform experimenters listed in 3.6.1 and 3.6.2.

REFERENCES

1. Hogan, G. and Cressey, J., The Interrogation Recording and Location System, National Telemetry Conference, November 1965.

2. Survey of Requirements for a Geophysical Data Collection Satellite System, Contract No. NAS r 49(12), Stanford Research Institute, August 1963.

3. The Feasibility of a Global Observation and Analysis Experiment, National Academy of Sciences, National Research Council, Publication 1290, March 1966.

4. Operations Analysis of the IRLS Experiment, Contract No. NAS 5 3747, Operations Research Inc., Phase I - Simulation Modes and Error Analysis, March 1966, Phase II - Composite Error Analysis, August 1966.

5. Final Engineering Report for IRLS, Contract No. NAS 5 9559, Radiation Inc., June 1967.

SECTION 9

THE REAL TIME TRANSMISSION SYSTEMS EXPERIMENT

by
Staff Members, Allied Research Associates

9.1 General

A detailed discussion of the Real Time Transmission System will not be presented here. The reader interested in detailed information for APT station operational usage, including gridding techniques is referred to the "Nimbus III Real Time Transmission System (DRID and DRIR)" (Reference 1).

The HRIR and IDCS data can be instantaneously transmitted by the spacecraft to APT stations within satellite acquisition range while being simultaneously stored on tape for subsequent transmission to a central Data Acquisition Facility. The instantaneous transmission modes of the IDCS and the HRIR are referred to, respectively, as the DRID and the DRIR system. The DRID system is the new IDCS camera experiment providing daytime meteorological data while the DRIR system is essentially the same as the experiment initially tested on Nimbus II to provide nighttime meteorological data. Both produce data in pictorial format.

DRID and DRIR data are transmitted from the satellite at a frequency of 136.95 MHz. Automatic Picture Transmission (APT) ground stations (References 1, 2 and 3) throughout the world can acquire the direct readout data when the satellite is within line of sight of the local antenna. However, some modifications to the APT ground equipment are necessary to properly acquire the DRIR data (References 4,5 and 6). Nimbus III DRID picture reception requires no modification of fascimile equipment presently set up to receive Nimbus II APT pictures, although adjustment of the receiver may be required to derive full 1/1 aspect ratio.

The Data Code Experiment employed on Nimbus II APT pictures (Reference 7) will be discontinued. Those participating APT stations not routinely receiving the transmitted daily APT Predict messages will if requested receive Nimbus APT Ephemeris messages twice each month to aid them in tracking the Nimbus Satellite. Daily APT Predict messages (TBUS-2) giving both day and night Nimbus ephemeris information will be furnished over the National and International Radio teletypewriter weather circuits.

Request for routine information, documentation, guidance, assistance and grids relating to the Nimbus III Real Time Transmission Systems (both DRID and DRIR) should be directed to:

Nimbus Project, Code 450
National Aeronautics and Space Administration
Goddard Space Flight Center
Greenbelt, Maryland 20771 U.S.A.
Attn: NADUC Manager.

DRID and DRIR data are not intended for distribution beyond the local acquisition facilities. Should potential users desire information concerning these data for specific applications, they should contact the agencies responsible for the various receiving stations. However, the same DRID and DRIR data as recorded on board the spacecraft, can be obtained in the higher quality IDCS and HRIR film formats from the appropriate archival source.

9.2 Direct Readout Image Dissector Camera System (DRID)

Although the Image Dissector Camera differs from the APT cameras flown on previous TIROS, TOS, ESSA and Nimbus satellites, the real time operation of the system is almost identical to the Nimbus I and II APT. Previous APT cameras consisted of a wide angle lens, a mechanical shutter, and a storage vidicon on which the complete scene was exposed, slowly scanned, and then erased. Thus, all the pictorial information contained in a single frame was exposed instantaneously from a fixed position in space. The image dissector is a shutterless electronic scan and step tube mounted behind a wide angle lens. Scanning and stepping functions occur continuously while the satellite is progressing along its orbital path, i.e., the earth scene is not exposed instantaneously from a fixed location in space. The 108° lens used on the camera is identical to the lenses used on the Nimbus I and II APT systems. The side to side camera field of view is 98.2° (nominal) providing a ground coverage of about 1600 x 1600 nautical miles from a 600 nautical mile altitude.

The video presentation contains no fiducial marks as in the Nimbus I and II APT picture and the line sync pulse consists of seven black to white pulses instead of the conventional APT type of black sync pulses. The 3 second start time, 5 second phasing period, and 5 per cent line blanking are identical to those of previous Nimbus APT, as are the 4 hz line rate and 200 second active picture period.

A more detailed description of the IDCS may be found in Section 2 of this Guide.

9.3 Direct Readout High Resolution Infrared Radiometer (DRIR)

DRIR data can be acquired by APT ground stations provided that suitable modifications are made to the facsimile equipment. Modifications are needed to accomodate the new 48 rpm of the HRIR scan mirror. Details of the modifications are outlined in References 4, 5, 6. These documents can be obtained from the source provided in 9.1.

The DRIR data will be presented as gray scales from white through gray to black (corresponding to cold, cool and warm radiating surfaces, respectively) on the facsimile paper. For the Fairchild facsimile recorder, the total width of the data is 21.5 cm (8.45 inches). Within this width, the data from earth and atmosphere (from horizon to horizon) will occupy approximately seven cm (2.75 inches), the remainder representing space and the interior of the radiometer housing. The APT facsimile scan rate must be modified to synchronize with the 48 rpm scan rate of the HRIR.

The facsimile stylus moves across the paper at a constant rate, so distance across the paper is directly proportional to angular rotation of the HRIR scanning mirror. The line width (in the direction of paper feed) of the Fairchild facsimile scan is nominally 0.0254 cm (0.01 inch), and the rate of data (paper) advance is 1.22 cm min^{-1} (0.48 inch min^{-1}).

The DRIR data are of slight value until they are geographically referenced. While this might be done by reference to coastlines or other identifiable geographical features, or crudely by reference to cloud features which can be associated with those on a recent weather map, these are special causes and are usually of marginal utility. For example, they are seldom if ever applicable over oceans.

Section 3 of this document describes the HRIR sensory system.

REFERENCES AND BIBLIOGRAPHY

1. Goldshlak, L., Nimbus III Real Time Transmission Systems DRID and DRIR, Technical Report No. 5, Contract No. NAS 5-10343, Allied Research Associates, Inc. 1968.

2. Goldshlak, Leon, APT Users' Guide, Scientific Report No. 1, Contract No. AF 19 (628)-2471, Allied Research Associates, Inc., 1963 (Out of print. May be available through the Defense Document Center or Federal Clearing House for Scientific and Technical Information).

3. National Weather Satellite Center, APT Users' Guide, Environmental Science Services Administration, Washington, D.C., 1965. For sale by the Superintendent of Documents, Government Printing Office, Washington, D.C., 20402. Price: $1.00.

4. User Guide for HRIR Modifications to the APTS Ground Stations, Contract No. NAS 5-667, Astro-Electronics Division, Defense Electronic Products, Radio Corporation of America, Issued 23 November 1965, changed 4 November 1966, changed 31 March 1967.

5. Instruction Manual for HRIR Modifications to the APTS Ground Stations Using Fairchild Facsimile Recorders, Contract No. NAS 5-667, Astro-Electronics Division Defense Electronic Products, Radio Corporation of America, Issued 10 January 1966, Revision 1 issued 18 November 1966, change 1 issued 6 January 1967.

6. Instruction Manual for HRIR Modification to the APTS Ground Stations Using Muirhead Facsimile Recorders, Contract No. NAS 5-667, Astro Electronics Division, Defense Electronic Products, Radio Corporation of America, Issued 22 February 1962, change 1 issued 22 November 1966.

7. Goldshlak, Leon and William K. Widger, Jr., The Nimbus Data Code Experiment, Technical Note No. 1. Contract No. NAS 5-10114, Allied Research Associates, Inc., January 1966.

8. Smith, Robert B., Manual Gridding of DRIR Facsimile Pictures, Technical Note No. 7, Contract No. NAS 5-3253, ARACON Geophysics, A Division of Allied Research Associates, Inc., Concord, Massachusetts, November 1965.

9. Widger, W. K., Jr., J.C. Barnes, E.S. Merritt and R.B. Smith, 1965: Meteorological Interpretation of Nimbus High Resolution Infrared (HRIR) Data, Final Report, Contract No. NAS 5-9554, ARACON Geophysics Company. (To be republished in the NASA Contractor Report (CR) series).

10. Vermillion, Charles, H., 1968. Constructing Inexpensive Automatic Picture Transmission Ground Station, A Report, NASA SP-5079. For sale by the Clearinghouse for Federal Scientific and Technical Information, Springfield, Virginia, 22151. Price: $0.50.

SECTION 10

THE NIMBUS III CATALOG

by
Staff Members, Allied Research Associates

10.1 General

The Nimbus III Catalog, to be published in monthly Volumes of 2 parts, will provide a relatively current source of information required for obtaining Nimbus III data. There will be six sections in Part 1. Part 2 will contain the MRIR pictorial data only.

10.2 Nimbus III Catalog, Part 1

10.2.1 Section I - Introductory Remarks

Section I will contain significant highlights of the satellite operation during the month including any required post launch changes in experimental calibration data as contained in preceding sections of this Guide. For example, unusual or major meteorological events may be noted. Also, performance of the various sensory systems and of the spacecraft will be described, particularly when significant deviations from normal operations have been experienced.

10.2.2 Section II - Daily Sensor "On" Status Charts

Section II will show schematically the locations over which the IDCS, MRIR, HRIR, IRIS, SIRS, MUSE sensors were on. A modified Miller Mercator cylindrical projection is used as the base map. The map extends from 85°S to 85° N latitude and spans 900 degrees of longitude. Ten degree latitude-longitude lines are shown - each third (30 degree) line being accentuated.

Superimposed on the maps are representations of those segments of the subpoint track during which the appropriate sensor was on. Swath numbers are labelled at the ascending or descending nodes. Time of ascending node defines the date of the entire swath. Each map will contain daytime or nighttime data for one day (Universal Time).

Ascending nodes and swath numbers are shown on each map representing daytime data. Descending nodes are substituted on maps which contain nighttime data.

To assist the user in relating an orbital segment on the map with the correct swath number a complete orbital track transparent overlay (Figure 10-1) will be included as one insert in the first volume of the Nimbus III catalog. Tick marks indicate number of minutes before and after ascending and descending modes, so that the approximate time of data coverage can be determined for any location.

Figure 10-2 depicts the coverage obtained from the IDCS, HRIR and MRIR systems at a 600 nautical mile altitude. The coverage swaths are drawn on the same projection on that used to show sensor "On" tracks in Section II of the monthly catalogs. This display is provided to permit the user to estimate the extent of sensor coverage from the subpoint track segments shown in the catalogs.

The user may, if he wishes, trace the swath widths in Figure 10-1 on transparent or transluscent paper and overlay this on the subpoint tracks to obtain actual sensor coverage on the earth.

Equations (1) and)2) can be used to calculate sensor coverage if higher accuracies are desired.

For IDCS:

$$\phi = \sin^{-1}\left(\frac{R+h}{R}\sin n\right) - n \qquad (1)$$

For HRIR and MRIR:

The altitude is sufficiently high so that the horizons show in the data and

$$\phi = \cos^{-1}\left(\frac{R}{R+h}\right) \qquad (2)$$

Where ϕ = geocentric angle between satellite subpoint and edge of sensor coverage, measured in a plane perpendicular to the orbit plane, in degrees.

VALIDITY PERIOD

FROM _____ ORBIT _____
TO _____ ORBIT _____

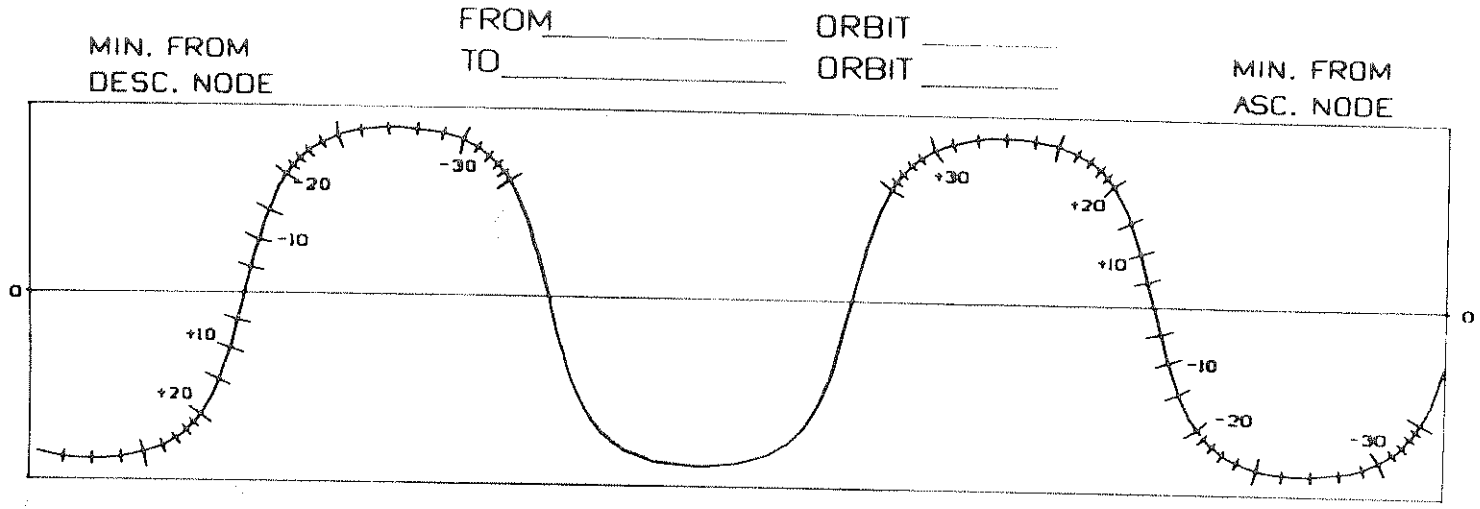

FROM _____ ORBIT _____
TO _____ ORBIT _____

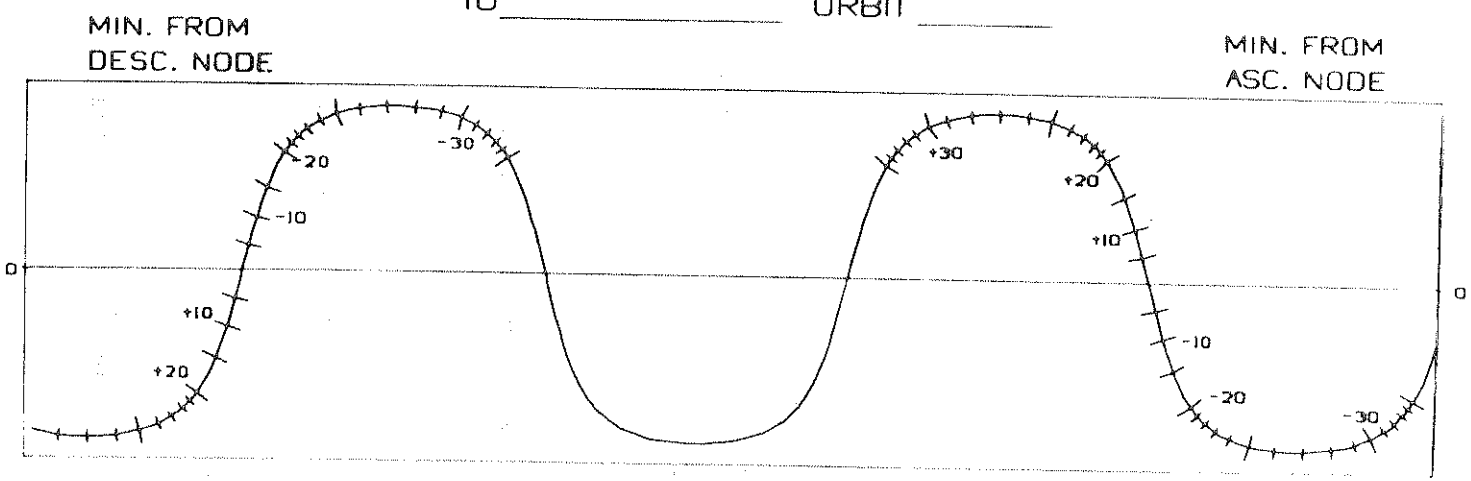

Figure 10-1–Nimbus III Subpoint Track

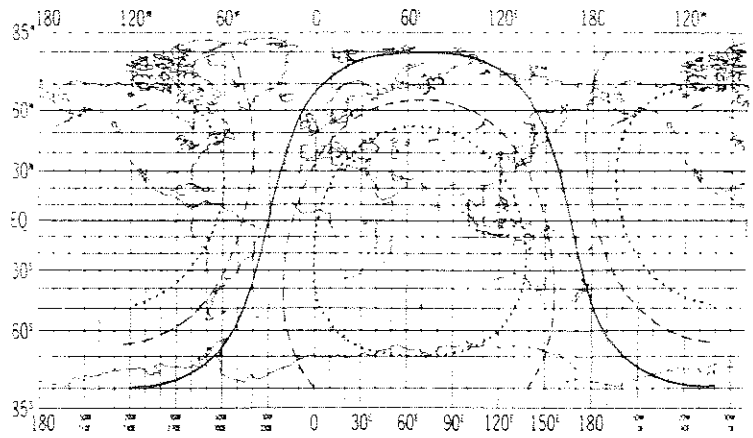

Figure 10-2–Coverage of IDCS (dashed), and MRIR and HRIR (dotted)

R = earth radius in nautical miles
h = satellite height in nautical miles
n = angle, measured at the satellite, between local vertical and extreme coverage limit of IDCS a plane perpendicular to the orbital plane.

The angle is 45.2° to the right edge, and 46.8° to the left edge of the picture (See Figure 2-6, Section 2).

10.2.3 Section III – Real Time Transmission System (DRIR and DRID)

Section III is a summary of DRID and DRIR operations and performance.

10.2.4 Section IV – Orbital Data

Section IV is a listing of Nimbus III orbital elements and ascending and descending nodes.

10.2.5 Section V – IDCS Montages

Section V contains the IDCS daily montages. Each montage is constructed from positive photographic paper prints in data orbit sequence for a 24 hour period.

A montage displays daily IDCS coverage of the entire earth. There will be one IDCS montage (approximately 200 pictures) displayed per page.

10.2.6 Section VI - HRIR Montages

Section VI contains the nighttime and daytime HRIR montages. Each montage is constructed from positive photographic paper prints in data orbit sequence for a 24 hours period. Nighttime and daytime data are separated into different montages. There will be one HRIR montage (12-14 data strips) displayed per page.

10.3 Nimbus III Catalog, Part 2, MRIR Pictorial Data

Part 2 of the Nimbus III monthly catalog will contain the MRIR pictorial data, one readout orbit per page. Part 2 will have approximately 400 MRIR pictures reproduced per each monthly volume.

REFERENCES AND BIBLIOGRAPHY

1. Aeronomy and Meteorology Division, 1965: Nimbus I User's Catalog: AVCS and APT, NASA, Goddard Space Flight Center, Greenbelt, Maryland.

2. Aeronomy and Meteorology Division, 1965: Nimbus I High Resolution Radiation Data Catalog and User's Manual, NASA, Goddard Space Flight Center, Greenbelt, Maryland.

3. Nimbus Project, 1966: Nimbus II User's Guide, NASA, Goddard Space Flight Center, Greenbelt, Maryland.

4. Nimbus Project, 1966: Nimbus II Data Catalog, Vols 1-5, Goddard Space Flight Center, Greenbelt, Maryland.

5. Nimbus Project, 1966: Nimbus II HRIR Montage Catalog, Goddard Space Flight Center, Greenbelt, Maryland.

6. Nimbus Project, 1966: Nimbus II MRIR Catalog, Vols 1-2, Goddard Space Flight Center, Greenbelt, Maryland.

7. Nimbus Project, 1966: Nimbus II AVCS Montage Catalog, Goddard Space Flight Center, Greenbelt, Maryland.

APPENDIX A

ABBREVIATIONS

AFCRL	Air Force Cambridge Research Laboratory
APT	Automatic Picture Transmission
ATS	Applications Technology Satellite
AVCS	Advanced Vidicon Camera System
A/D	Analog to Digital
AWS	Air Weather Service
BCD	Binary Coded Decimal
CDA	Command Data Acquisition
DAF	Data Acquisition Facility
DEMOD	Demodulator
DRID	Direct Readout Image Dissector
DRIR	Direct Readout Infrared Radiometer
ESSA	Environmental Science Services Administration
GACS	Ground Acquisition and Command Station
GMT	Greenwich Mean Time
GSFC	Goddard Space Flight Center
HAX	HRIR APT Switching
HDRSS	High Data Rate Storage System
HRIR	High Resolution Infrared Radiometer
IDCS	Image Dissector Camera System
IMCC	Image Motion Compensation and Calibration (a subsystem of IRIS)
IRIS	Infrared Interferometer Spectrometer
IRLS	Interrogation Recording and Location System
ISE	Integration Support Equipment (Platforms)
LABS	Laboratory for Atmospheric and Biological Sciences
MRIR	Medium Resolution Infrared Radiometer
MSL	Meteorological Satellite Laboratory
MUSE	Monitor of Ultraviolet Solar Energy
NDUC	Nimbus Data Utilization Center
NASA	National Aeronautics and Space Administration
NASCOM	NASA Communications
NAVOCEANO	Naval Oceanographic Office
NCAR	National Center for Atmospheric Research
NDHS	Nimbus Data Handling System
NDUC	Nimbus Data Utilization Center

NER	Noise Equivalent Radiance
NESC	National Environmental Satellite Center
NMC	National Meteorological Center
NMRT	Nimbus Meteorological Radiation Tape
NRL	Naval Research Laboratory
NSSDC	National Space Science Data Center
NTCC	Nimbus Technical Control Center
NWRC	National Weather Records Center
ONR	Office of Naval Research
PCM	Pulse Code Modulation
RTG	Radioisotope Thermoelectric Generator
RTTS	Real Time Transmission System
SDT	Sensory Data Tape
SCUM	SIRS Control Unit Module
SIPS	SIRS Instrument Power Supply
SOBADS	SIRS On-Board Analog-to-Digital System
SOD	SIRS Output Demodulator
SOUSE	SIRS Optics Unit and Sensing Electronics
STADAN	Station Data Acquisition Network
T&DS	Tracking and Data Systems
UT	Universal Time
WMSAD	World Map Predicts and Station Acquisition Data
XMTR	Transmitter